Viscous Dark Matter and its Astrophysical and Cosmological Signatures

A thesis submitted in partial fulfilment of

the requirements for the degree of

Doctor of Philosophy

by

Arvind Kumar Mishra

(Roll No. 15330017)

Under the supervision of

Prof. Jitesh R. Bhatt

Professor

Theoretical Physics Division

Physical Research Laboratory, Ahmedabad, India.

DISCIPLINE OF PHYSICS

INDIAN INSTITUTE OF TECHNOLOGY GANDHINAGAR

2020

to

My Family

Declaration

I declare that this written submission represents my ideas in my own words and where others' ideas or words have been included, I have adequately cited and referenced the original sources. I also declare that I have adhered to all principles of academic honesty and integrity and have not misrepresented or fabricated or falsified any idea/data/fact/source in my submission. I understand that any violation of the above will be cause for disciplinary action by the Institute and can also evoke penal action from the sources which have thus not been properly cited or from whom proper permission has not been taken when needed.

Signature

Name: Arvind Kumar Mishra

(Roll No: 15330017)

Date:

CERTIFICATE

It is certified that the work contained in the thesis titled **"Viscous Dark Matter and its Astrophysical and Cosmological Signatures"** by Mr. Arvind Kumar Mishra (Roll No. 15330017), has been carried out under my supervision and that this work has not been submitted elsewhere for a degree.

Prof. Jitesh R. Bhatt
Theoretical Physics Division,
Physical Research Laboratory,
Ahmedabad, India.

(Thesis Supervisor)

Date:

Thesis Approval

The thesis entitled

Viscous Dark Matter and its Astrophysical and Cosmological Signatures

by

Arvind Kumar Mishra
(Roll No. 15330017)

is approved for the degree of

Doctor of Philosophy

Examiner	Examiner
Supervisor	Chairman

Date: _____

Place: _____

Acknowledgments

The journey of my Ph.D. could not be accomplished without the motivation, blessings, and continuous support of many people who gave me new energy and inspiration at every moment of my life. Here I take the opportunity to thank everyone who made it possible.

Firstly, I am grateful to my supervisor, Prof. Jitesh R. Bhatt, for his continuous support, encouragement, help, and advice throughout my Ph.D. I have learned a lot while discussing different aspects of science with him. I am very thankful to him for correcting my mistakes and improving me for being so understanding and cooperative always.

I am very thankful to my doctoral committee members Prof. Subhendru Mohanty and Dr. Namit Mahajan, for their useful suggestions, comments, and encouragement. Their insightful comments and discussions have benefited greatly in my research. I am especially thankful to Prof. Srubabati Goswami for inviting me to PRL during my thesis defense.

I express my sincere gratitude to all the faculty members who had taught me during the course work, including Prof. R. Rangarajan, Prof. Subhendra Mohanty, Prof. Srubabati Goswami, Prof. Jitesh R. Bhatt, Prof. H. Mishra, Prof. B. K. Sahoo, Prof. J. Banerji, Prof. D. Angom, Dr. Namit Mahajan, Dr. Partha Konar, Dr. K. Patel, Dr. N. Singh.

I express my immense gratitude to my Professors who taught me Mathematics during my B.Sc., especially Prof. Matamber Tiwari, Prof. Satya Dev, Prof. Siv Sharma Shukla. I am highly obliged to Prof. R.P. Malik to teach me General Relativity and introduce different dimensions of science during my M.Sc. I am also thankful to Prof. Dr. Sanjay Siwach for his guidance whenever required in my Ph.D. life.

I am thankful to my collaborators Dr. Abhishek Atreya, Dr. Alekha Nayak. I have learned many new things while discussing different aspects of cosmology and particle physics with them. I am also very thankful to Raghu sir for organizing the journal group discussion meeting. I am thankful to all group members, Raghu sir, Arnab, Richa, Gaurav, Mansi, Bhavesh, for fruitful discussions, which helped me during my research.

I am also grateful to all my seniors, especially Anjali didi, Luxmi didi, Ikshu didi, Niharika didi, Shradha Didi, Lata didi, Navpreet didi, Avdhesh bhaiya, Arun bhaiya, Manu bhaiya, Guru bhaiya, Prahlad bhaiya, Arpan bhaiya, Uday bhaiya, Krishna bhaiya, Deepak bhaiya, Venkatesh bhaiya, Soumya bhiya, Bhavesh, Aman, for their support, and encouragement.

I am thankful for all my batchmates- Naman, Richa, Balbeer, Ritika, Ashish, Harsh Oza, Harsh Raj, Subir, Archita, Aarthy, Rahul, Akanksha, Ranadeep, Nidhi, Shefali, Shivangi, Varun, Kaustav.

I am also grateful to all the fellow researchers from PRL for the numerous help and the support that they have given at various times. Especially, I would like to mention Komal, Tanmoy, Abhaya, Girish, Chandan, Selva, Prasanna, Rupa, Kuldeep, Ashim, Alekha, Tripurari, Nimmala Narendra, Golam Sarwar, Oindrila, Sukanya, Surya, Ayon, Priyank, Anshika, Vishal, Deepak, Sudipta, Pravin, and Hrushikesh. Kindly forgive me if I have left out anyone's name, and please know that I am thankful to all of you.

A special thanks to my best friends, Amit Soni, Susheel Kumar Mishra, Sachin, for supporting and inspiring me at all times.

I am very thankful to my best friends - Richa Arya and Naman Deep Singh, for their help, support, and motivation. We have many memorable things, including the cooking, journey, and driving practice.

Above all, I am immensely grateful to my parents and my family for their blessings, encouragement, and belief in me throughout my life. Thank you so much for your patience and the support you have given me to accomplish this.

Arvind Kumar Mishra

Abstract

The Standard Model (SM) of cosmology (Lambda Cold Dark Matter (ΛCDM)) successfully explains the large-scale structure and the cosmic microwave background radiation observations. However, it encounters some theoretical and observational challenges, which demand a modification from the standard behavior. The drawbacks of SM include an interpretation of the cosmological constant, small-scale structures observations, and anomaly in the 21-cm signal observed by the Experiment to Detect the Global Epoch of reionization Signature (EGDES) collaboration. The ΛCDM model assumes that the Dark Matter (DM) is a cold, collisionless, and dissipationless fluid. However, as the real Universe contains non-ideal species, one needs to explore beyond the ideal behavior and study the effects of imperfections in the cosmic fluid. In this thesis, we study the Viscous Dark Matter (VDM) and explore some of its possible signatures in the Universe.

The Self-Interacting Dark Matter (SIDM) is a possible candidate to address the small-scale problems faced by the ΛCDM model. We calculate the mean free path of dark matter particles and argue that for SIDM particles, the hydrodynamic description is valid from galactic to large scale. We propose that the self-interaction between the DM particles may lead to viscosity in the DM fluid. We estimate the shear and bulk viscosity of the Viscous Self Interacting Dark Matter (VSIDM) fluid using the kinetic theory in relaxation time approximation. The astrophysical constraint on the ratio of DM self-interaction cross-section to its mass (σ/m) indicates that the viscosity is large at present and increases by two orders of magnitude from the galactic to cluster scale. Therefore, one may expect interesting cosmological consequences from such a large DM viscosity. Our calculation found that the SIDM viscosity is sufficiently large to account for the present accelerated expansion and hence mimic the Dark Energy (DE). Thus, the viscous SIDM model provides a unified description of the DM and DE.

Further, we explore the effects of the VSIDM dissipation at a low redshift interval, $0 \leq z \leq 2.5$. For this, we assume the viscosities as a constant with the redshift and parameterize the fluid velocity gradients as a power-law form. Using the χ^2 minimization techniques, we obtain the averaging length scale is $\approx$ 20 Mpc, which is larger than a typical cluster scale. The best value of the model parameters indicates that the

cosmic dissipation is large at present, $z = 0$, and decreases on the redshifts $0 \leq z \leq 2.5$. We report that the decreasing dissipation (as redshift increases) explains the late-time observations, whereas the constant dissipation fails to do so.

Furthermore, String theory provides a lower bound, called KSS bound, on the shear viscosity to the entropy density ratio as $\eta/\mathfrak{s} = 1/4\pi$. Using the cluster scale constraint on σ/m, we find that the SIDM fluid violates the KSS bound if the SIDM mass is above a GeV scale. Assuming that VSIDM respects the KSS bound, we constrain the DM mass and report that the DM mass should be sub-GeV. Our result provides a new DM mass range, which can be explored in the DM detection experiment. Further, we also explore the evolution of the bulk and shear viscosity in the SIDM fluid, parameterizing them as redshift dependent. We find that the SIDM viscosities are large at present and decrease on large redshift, supported by the late-time observations.

We also study the evolution of the DM temperature in the presence of viscosity. The DM viscosity causes energy dissipation and hence increases its temperature. For a large DM viscosity, its temperature will be high, and so the DM may no longer be a cold fluid. Therefore it will affect the large scale and the CMB observation. We derive a condition on the DM viscosity parameters which is consistent with the CMB observation.

Further, we propose a possibility of photon production from viscous dark matter energy dissipation. The photon generation has been considered in two ways: first, when the DM directly dissipates into the photons, and second when the DM firstly dissipates into dark radiation and then generates the visible photons via kinetic mixing between the dark radiation and photons. We find that the photons obtained from the kinetic mixing increase the number density in the Rayleigh-Jeans limit of the cosmic microwave background radiation. As a consequence, it can explain the EDGES anomaly observed in the 21-cm signal. Further, using the EDGES observation, we explore the DM model parameters such as its mass, kinetic mixing parameter, and dark radiation mass, whose information is crucial for the DM viscosity estimation and dark radiation searches.

After that, we investigate the DM microphysics using the interacting viscous dark matter-gas formalism in light of the reported EDGES anomaly. The DM viscosity heats

the DM and also the gas via its interaction with the gas. The gas heating increases as the mass and viscosity of the DM increases. Therefore, to explain the EDGES 21-cm signal, the DM mass should be small, but the DM-gas interaction cross-section ($\hat{\sigma}$) should be large in comparison with the ideal DM case. Further, using the CMB constraint on the DM-gas interaction cross-section, we report that the EDGES 21-cm signal allows a large viscosity compared to the bounds from structure formation. We find that the DM coldness condition provides a stringent limit on the dark matter viscosity.

Keywords: Dark matter, dark energy, self-interacting dark matter, dark matter viscosity, 21-cm line, CMB, EDGES.

Abbreviations

DM	Dark matter
CDM	Cold dark matter
SIDM	Self-interacting dark matter
VSIDM	Viscous self-interacting dark matter
VDM	Viscous dark matter
CMB	Cosmic Microwave Background
KSS	Kovtun-Son-Starinets
LSB	Least Surface Brightness
RJ	Rayleigh-Jeans
EDGES	Experiment to detect global epoch of reionization

Contents

List of Figures

Chapter 1

Introduction

The study of the origin, evolution, and fate of our Universe has been one of the most fascinating subjects in the history of humankind. Our present understanding of the Universe is a result of the continuous effort of observations and building the fundamental theory that governs it. Cosmology describes the evolution of the Universe as a whole. The actual size of the Universe is very large, but the Universe, which is visible to us today, is close to $\sim$ 14000 Mpc. On scales larger than $\sim$ 100 Mpc, the Universe is homogeneous and isotropic, but on the smaller scales, the Universe is inhomogeneous and dominated by the structures such as a galaxy, clusters, superclusters, etc.

The force of gravity is the weakest amongst all the other fundamental forces-electromagnetic, weak, and strong find in nature. However, the gravitational force becomes dominant on the cosmological scales and is responsible for large-scale structure formation. Therefore, the dynamics of the Universe crucially depend on our knowledge about the gravitational interaction.

1.1 General theory of relativity (GTR)

In this Section, we briefly discuss the GTR, but a broader discussion can be found in Refs. [12][13]. According to the general theory of relativity, gravity is not a force, but it is the curvature of space-time. Matter curves the space-time, and the curvature decides the trajectory. GTR relies on the assumption of *Equivalence principle*, which states that there is no difference between a uniform gravitational field and a uniformly

accelerated frame in the absence of gravity.

The Einstein equations are obtained by varying the Einstein-Hilbert (EH) action with the matter field, which is defined as

$$S_{E-H} = \int \left(\frac{1}{16\pi G} R + \mathcal{L}_m \right) \sqrt{-g}\, d^4x \tag{1.1}$$

where R and $\mathcal{L}_m$ represent the Ricci scalar and the matter field, respectively, g represent the determinant of the metric tensor, $g_{\mu\nu}$. After varying the EH action w.r.t. metric tensor $g_{\mu\nu}$ we get

$$R_{\mu\nu} - \frac{1}{2} g_{\mu\nu} R = -8\pi G T_{\mu\nu} \,, \tag{1.2}$$

where

$$R^{\mu\nu} = \frac{\delta R}{\delta g^{\mu\nu}} \quad \text{and} \quad T_{\mu\nu} = \frac{1}{\sqrt{-g}} \frac{\delta \left(\sqrt{-g} \mathcal{L}_m \right)}{\delta g^{\mu\nu}} \,. \tag{1.3}$$

The above equations are Einstein equations, which can be rewritten in shorthand notation as

$$G_{\mu\nu} = -8\pi G T_{\mu\nu}, \tag{1.4}$$

where, $G_{\mu\nu}$ is Einstein tensor, defined as $G_{\mu\nu} = R_{\mu\nu} - \frac{1}{2}\, g_{\mu\nu}\, R$. In the above equations, the LHS describe about the geometry of the space-time and RHS tells about the energy-momentum of the particles present in the Universe. These equations are in tensorial forms, in which $R_{\mu\nu}$ and R represents the Riemann tensor and the curvature scalar, respectively. The Ricci tensor is related with the Riemann tensor $R_{\mu\kappa} = R^{\lambda}_{\mu\lambda\kappa}$, where the Riemann tensor is defined as

$$R^{\lambda}_{\mu\nu\kappa} \equiv \frac{\partial \Gamma^{\lambda}_{\mu\nu}}{\partial x^{\kappa}} - \frac{\partial \Gamma^{\lambda}_{\mu\kappa}}{\partial x^{\nu}} + \Gamma^{\eta}_{\mu\nu} \Gamma^{\lambda}_{\kappa\eta} - \Gamma^{\eta}_{\mu\kappa} \Gamma^{\lambda}_{\nu\eta} \,. \tag{1.5}$$

Here $\Gamma^{\lambda}_{\mu\nu}$ is the Affine connection which is related with the first order derivative of the metric tensor as

$$\Gamma^{\lambda}{}_{\mu\nu} = \frac{1}{2} g^{\lambda\sigma} \left(\frac{\partial g_{\sigma\nu}}{\partial x^{\mu}} + \frac{\partial g_{\sigma\mu}}{\partial x^{\nu}} - \frac{\partial g_{\mu\nu}}{\partial x^{\sigma}} \right) \tag{1.6}$$

The curvature scalar is obtained as $R = g^{\mu\lambda} R_{\mu\lambda}$. Further, the Einstein equations given by Eq. (1.4) are symmetrical; thus, there are ten independent equations.

In absence of any source or sink, the energy momentum tensor follows the conservation equations

$$\Delta_{\mu} T^{\mu\nu} = 0 \tag{1.7}$$

In above equation, the 0-th component, i.e., $\nu = 0$ tells about the evolution of the energy density and i-th components i.e., $\nu = i$ tells about the evolution of velocity of the fluid. We also see that Eq. (1.7) have 4 independent equations. Thus using equations (1.4) and (1.7) simultanously there are only 6 independent equations.

The Einstein equations are nonlinear in nature and hence in general complicated to solve even for the simple systems. However, if the symmetries are present in the system, they can be solved analytically.

1.2 Background cosmology

In the standard cosmology, the evolution history of the Universe is studied using Einstein's equation. To understand the dynamics of the space-time, we need to provide the metric and energy-momentum tensor. The space-time which respects the cosmological principle (homogeneous and isotropic) is given by FLRW metric. Using the FLRW metric, the distance between the two-point in space-time is written as

$$ds^2 = g_{\mu\nu}\, dx^\mu dx^\nu = -dt^2 + a^2(t)\left[\frac{dr^2}{1-kr^2} + r^2(\sin^2\theta + d\phi^2)\right] \ , \tag{1.8}$$

where $a(t)$ is the scale factor. The value of the k can be $-1, 0$, or $+1$ depending upon the negative, zero, and positive spatial curvature of the Universe. Further to simplify our discussion, we assume cosmic fluid as perfect fluid, for which the energy-momentum tensor is given by

$$T^{\mu\nu} = \rho u^\mu u^\nu + P\,(u^\mu u^\nu + g^{\mu\nu}) \ . \tag{1.9}$$

Further, 00-component of the Einstein equation provides us

$$H^2 + \frac{k}{a^2} = \frac{8\pi G}{3}\rho \ , \tag{1.10}$$

where $H = \dfrac{\dot{a}}{a}$ is the Hubble expansion rate of the Universe. The above equation (1.10) tells about the rate of the cosmic expansion, which depends on the energy density and curvature of the Universe. Further, using the ii-component of the Einstein equation, we get

$$2\frac{\ddot{a}}{a} + H^2 + \frac{k}{a^2} = -8\pi G P \ . \tag{1.11}$$

Here $\frac{\ddot{a}}{a} = \dot{H} + H^2$. After substracting Eq. (1.10) from Eq. (1.11), we have

$$\frac{\ddot{a}}{a} = -\frac{4\pi G}{3}(\rho + 3P) \ . \tag{1.12}$$

This equation tells about the rate of the change in the expansion rate of the Universe, which depends on the pressure and energy density of the cosmic fluid.

- For a normal matter or energy, $\rho > 0$, $P \geq 0$, so $\ddot{a} \leq 0$. Therefore in the presence of normal matter or energy, the Universe cannot be static and decelerate throughout its evolution.
- When $P < -\frac{\rho}{3}$, $\ddot{a} > 0$, in this case the Universe will accelerate. Therefore, the accelerated expansion can only be fuelled by an exotic form of matter which has a large negative pressure.

Evolution of the cosmic energy density

Using Eq. (1.7), the energy evolution is given by

$$\frac{d\rho}{dt} + 3H(p + \rho) = 0 \ . \tag{1.13}$$

To solve the above equation, let us consider $P = w\rho$, where w is constant and depends on the type of the species considered. After integrating the above equation, we get

$$\rho(t) = \rho_0 \, a^{-3(1+w)} \ , \tag{1.14}$$

where $\rho_0 = \rho(t = t_0)$ is the energy density at present. In the flat Universe $k = 0$, using Eq.(1.10), one can find the scale factor as

$$a(t) \propto (t - t_0)^{\frac{2}{3(1+w)}} \ , \tag{1.15}$$

where $t_0 = t(0)$ corresponds for the present value of time.

1. For a dust or matter, $w = 0$, so

$$\rho \propto a^{-3}, a(t) \propto (t - t_0)^{2/3} \ . \tag{1.16}$$

2. For a relativistic particle or radiation, $w = 1/3$, so

$$\rho \propto a^{-4}, a(t) \propto (t - t_0)^{1/2} \ . \tag{1.17}$$

1.3 Dark side of the Universe

The structure we see in the Universe is made from visible matter, and its properties are well described by the standard model of particle physics. However, many observations suggest the presence of the mysterious matter and energy called dark matter (DM) and dark energy (DE), which contribute a major fraction to the Universe's energy budget. They can not be described using the SM particle physics model and but their information is important to understanding the evolutionary history of the cosmos. Here we will briefly discuss their properties and possible candidates.

1.3.1 Dark Matter

There are many cosmological and astronomical which indicate the presence of an unknown kind of matter. In 1923 using the measurement of radial velocity dispersion of the galaxies in the Coma cluster, Zwicky [14] argued the presence of a large amount of the non-luminous matter is required. This result was further confirmed by measurement of the radial velocities of 30 galaxies in Virgo cluster [15], and also the galaxies and cluster masses [16]. The observations also suggest that dark matter is persuaded over all scales, from galactic to large cosmological scales, like cluster and supercluster scales.

Galaxy rotation curves

The evidence of DM comes from the observation of the rotation curve of the M31 galaxy [17]. In Fig. 1.1, we have shown a typical rotation of the galaxies. On the x-axis, we plot the distance from the galactic center, and on the y-axis, we plot the orbital velocity of the particles. If the orbital velocity follow the Newtonian physics, then

$$v(r) = \sqrt{\frac{GM(< r)}{r}} \ , \tag{1.18}$$

where r is the distance of the particles from the center of the galaxy. Here $v(r)$ is the velocity, $M(< r)$ is the mass enclosed in the radius smaller than r. If we assume that

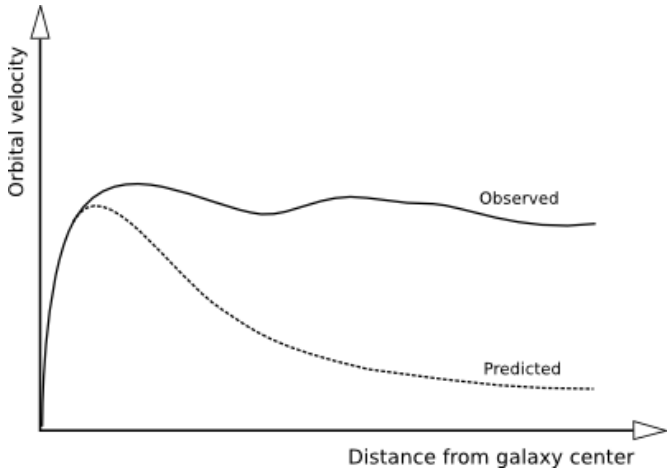

Figure 1.1: Typical rotation curve of galaxies. Image source [1]

all the galaxy mass is distributed up to the galactic disc with radius r_{disc}, then

$$v(r) = \begin{cases} \sqrt{\dfrac{GM(<r)}{r}} & \text{if } r < r_{\text{disc}} \ , \\ \sqrt{\dfrac{GM_g}{r}} & \text{if } r > r_{\text{disc}} \ , \end{cases} \tag{1.19}$$

where M_g is the total mass of the visible galaxy. So an assumption of constant energy density $v(r) \propto r$ for $r < r_{\text{disc}}$ and $v(r) \propto r^{-\frac{1}{2}}$ for $r > r_{\text{disc}}$. Thus according to the Newtonian dynamics prediction, velocity outside the disc radius should decrease. Nevertheless, the observation indicates that the velocity does not decrease after the galactic disc but becomes constant. To match the predicted velocity with the observational data, a new kind of matter is required, which is present outside the disc. The mass of the matter will be such that outside the disc, the ratio of its mass with the radius, M/r must be constant so that the velocity becomes constant. This matter certainly will not be visible; otherwise, it must be observed in the experiment.

Bullet cluster

The collision between the galaxy clusters (Bullet cluster) is another observation that provides strong evidence for the presence of the DM in the Universe [18]. The galaxy cluster is one of the largest gravitational bound objects of the Universe. When two galaxy clusters collide, then the normal matter between the clusters will interact and lie in the central part of the collision, see Fig. 1.2. X-ray observation suggests a signature of the X-rays in the collision's central part (pink color). Further, the weak gravitational

Figure 1.2: Observation of Bullet cluster as an evidence of DM. Image source [2]

lens measurements (blue region), which provide information about the mass, indicate the large mass concentrated outside the central part. This mass corresponds to the DM because, during the collision, the DM does not interact with the visible particles and hence goes away from the central regions.

Evidence from the structure formation

The structures we see today also indicate the presence of cold dark matter. The CMB anisotropy in the temperature also suggest the density perturbation of the baryon at the time of decoupling $z \sim 1100$ to be [19]

$$\delta_B = \frac{\delta\rho_B}{\rho_B} \leq 10^{-4} \ , \tag{1.20}$$

where $\delta\rho_B$ and ρ_B represents the perturbation and the background value of the baryon energy density. If one assumes that Universe is only dominated by the baryons, then since $\delta_B \propto a$ in the matter-dominated era, so we expect at present, $\delta_B \sim 10^{-1}$. However, at present, we see the structures are in nonlinear regimes. This implies that there is a pressureless species that should be present, which decouples in the early Universe and grow fastly in compared with the baryons, and becomes nonlinear by the present time.

Furthermore, CMB observation also confirms the existence of the large mass in comparison with the baryonic mass [20]. The other possible evidence of DM can be found in a review [21].

Properties of the dark matter

The dark matter candidates must satisfy all the constraints obtained from the astrophysical, cosmological, and laboratory experiments. The different results indicate the following properties of the DM particles.

- The DM contributes $\sim 26.8\%$ energy content of the total energy budget of the Universe.
- The DM is non-baryonic in nature. The conclusion is based on the constraint on the Big-Bang Nucleosynthesis (BBN), which demands that the baryonic energy density should not be larger than the ≈ 0.04 times of the critical energy density of the Universe [22].
- The DM particle is stable on the cosmological times scale , i.e. the lifetimes ($t_{\rm DM}$) should be smaller than the age of the Universe ($t_{\rm U}$), i.e., $t_{\rm DM} < t_{\rm U}$. Otherwise, the DM should have been decayed until today.
- The DM particles are chargeless (neutral), colorless, and interact with the SM particles only with the gravitational interaction. Present observations have not indicated any non-gravitational interaction of the DM particles on large scales.
- Recent astrophysical observations suggest a possibility of small self-interactions between the DM particles. It may be needed to solve some of the discrepancies indicated by the small scale structures [23].

Dark matter candidates

There are a plethora of models for the DM discussed in the literature. The WIMP is one of the popular candidates for dark matter. The interaction of this class of particles is the order of the weak interaction and provides a natural explanation of the correct relic density of the DM. This property is called the WIMP miracle. The most of the WIMP belongs to the lightest supersymmetry particles such as neutralino, gravitino, see a review [24]. The other possible DM candidates include the Axions [25], Sterile neutrinos [26], Massive Astrophysical Compact Halo Objects (MACHOs), Primordial

Black Holes (PBHs)[27], Mirror dark matter [28] etc. For the detail introduction of the possible DM candidates, see Refs. [29][30][31][32] [33] [34] [35].

The dark matter may be categorized as cold, warm, or hot, depending on its velocity dispersion when they decoupled with the rest of thermal plasma [36].

Cold dark matter (CDM) : They have non-relativistic velocities, so their free streaming length (FSL) is small (less than the galaxy scale). Hence they follow the bottom-up scheme, which states that small structures like galaxies form first and then by their self gravitational interactions larger structure of the Universe like cluster and supercluster form. The examples of CDM are WIMP, MACHO, etc. [29]

Warm dark matter (WDM) : They have a moderately relativistic velocity at decoupling, and their free streaming is smaller than the hot dark matter but larger than the CDM (approximately equal to the galaxy scale). They behave like a CDM on large scales. An example of WDM is the sterile neutrino. For a nice introduction of WDM, see Refs. [37] [38].

Hot dark matter (HDM): The DM particles are relativistic at the time of decoupling, so their FSL is very large (greater than galaxy scale). The HDM particles can freely stream through the overdense region (density greater than the critical density of the Universe) and could tend to smooth the density fluctuations of matter on small scales. As a consequence, only the fluctuations on scales larger than the product of velocity and age of the Universe survive. The HDM follows the top-down scheme, which states that large-scale structure forms first, and then it fragments into smaller scales like the galaxy. The popular candidates for HDM are neutrinos. A more discussion on HDM can be found in a review [39].

DM detection

The unknown nature of the DM leads to the many possible mechanisms for its detection. The detection will shed light on the DM properties and also provide an information of the large-scale structure formation of the Universe. Here we will discuss the detection techniques used for dark particle matter. The detection experiments are based on the DM properties and the way they show their possible signatures in the experiment. Fig. 1.3 provides a cartoonist picture of the ongoing and future DM searches.

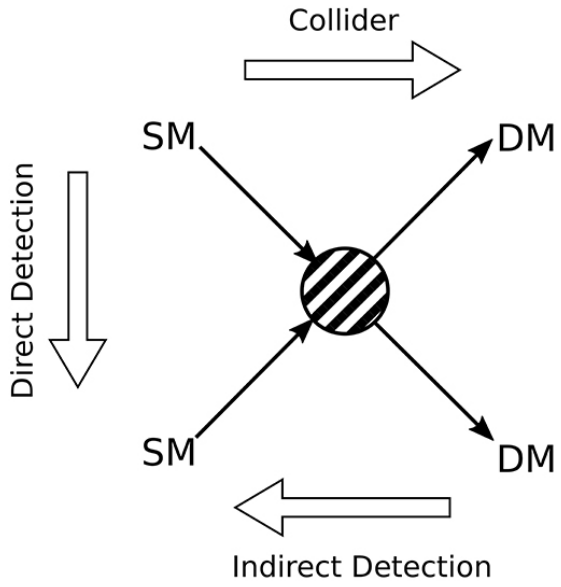

Figure 1.3: Different techniques for detecting dark matter. Image source [3]

Direct detection

The DM is omnipresent at all scales. It contributes largely to the central region of the DM halo and decreases towards the outer region of the halo. Since the DM particles pass through our earth, therefore the DM particles will collide with the detector materials. Therefore, it can provides the signal due to nuclear recoils with the DM scattering [40][41]. If the nuclear mass is m_N, then nuclear recoil energy, E_R is given as [42]

$$E_R = \frac{q^2}{2m_N} = \frac{\mu^2 v^2}{m_N}(1 - \cos\theta) \ , \tag{1.21}$$

where, q, θ and v corresponds for the momentum transfer, angle in the center of mass frame, and the DM particles' velocity with respect to the target nuclei, respectively. Here $\mu = m_\chi m_N/(m_\chi + m_N)$ is the reduced mass. For example, in LUX [43], Xenon [44] detectors, $m_N = 120$ GeV, and for this the energy threshold is $\sim$ few KeV. It is clear that the threshold value is smaller than the binding energy of the Xenon $\sim$ few GeV; therefore, DM interacts with the nucleus as a whole. For more details of the direct DM experiments, see Refs. [45, 46].

Indirect detection

If WIMP particles annihilate or decay into Standard Model particles like photons, charged leptons, or neutrinos, then their detection will give an indirect signature for

dark matter. The favored sources for direct signals are galactic center and halo, dwarf galaxies, etc., because a large dark matter density increases annihilation and decay rates of dark matter particles into SM particles. This DM annihilation product may cause deformation in the cosmic ray spectral distribution. Indirect detection can be made from ground and space based detectors. For a more information about the indirect searches, see Refs. [47][48][45].

Collider searches

There is also a possibility that the DM particles may be created in the collider experiments such as the Large Hedron Collider (LHC) [49]. However, in the case of the WIMP, due to weak interaction with the SM particles, the detector may not be able to detect the DM particles. In this situation, the measurement can be quantified in terms of the missing energy that one would expect from the kinematic estimation. At LHC, the missing energy can be determined from jets, top quarks, and leptons in detectors [49]. A more detail discussion of collider searches, see Refs. [50][51] [52].

1.3.2 Dark Energy

The Hubble law suggests that the Universe is expanding. It is expected that if the Universe is dominated by the known matter source, then the speed of the cosmic evolution should decrease with time, and the Universe must be in the decelerating phase. However, recent observations indicate indicate that at present, the Universe is undergoing an accelerated expansion. For a review on the cosmic acceleration, see Refs. [53–56] .

Type Ia Supernovae (SNe) data

The first direct observations are provided by the measurements of the high redshift Type Ia Supernovae (SNe) data [57][58]. SNe Ia is the product of the stellar evolutions and forms when the star mass becomes larger than the Chandrashekhar limit, and a further explosion takes place. It is believed that the SNe Ia forms in a similar manner and their absolute luminosity is the same irrespective of the surrounding (the time when they exist).

Using the observations of the large redshifts SNe Ia, two different groups Purlmeter et al. [57] ($0.18 < z < 0.83$) and Riess et al. [58] ($0.16 \leq z \leq 0.62$) have estimated the corresponding luminosity distances. They reported the dimmed SNe Ia in comparison with what they would have expected when the Universe is filled with normal matter. Their estimation showed that the Universe consists of more energy with negative pressure and is also in an accelerating phase.

Age of the Universe

The comparison between the age of the Universe, t_U with the old globular cluster age is also another evidence of the present accelerated expansion of the Universe. The age argument is based on the fact that the age of the Universe should be larger than the age of any species that reside in the Universe. The age of the Globular cluster of the MW and M4 corresponds for the $t_G = 13.7 \pm 2$ Gyr [59] and $t_G = 12.7 \pm 0.7$ Gyr [60], therefore the lowest bound on the Universe age, $t_U > 11 - 12$ Gyr. This problem is reflected in the pure matter-dominated era, but this discrepancy can be resolved if one assumes the cosmological constant in theory [53].

Furthermore, several other independent observations such as Large Scale Structures (LSS) [61], Cosmic Microwave Background Radiation (CMBR) [62] etc. provide the concrete support to the late time cosmic acceleration.

Model for the dark energy

To explain the observations, a hypothetical new form of energy, called dark energy (DE), is required, which generates negative pressure. This contributes $\sim 68.3\%$ of the total energy budget of the Universe. The theoretical attempts to explain dark energy have been majorly devoted in three different ways; (1) by modifying the gravity sector, (2) by changing the energy-momentum content of the Einstein's field equation, (3) by the inclusion of gravity beyond the Einstein's general relativity, see review [53].

Modifying matter properties

The inclusion of the extra scalar field that couples minimally with the gravity can cause to accelerate the Universe (same as in inflationary scenario) and act as a dark

energy candidate. The scalar fields naturally arise in the standard model and String theory. There are many models such as Quintessence model [63–65], K-essence [66–68], Techyonic field [69–72], Phantom field etc.[73]. However, this explanation of the cosmic acceleration demands a new scalar field in the Universe.

Another possible candidate is a Chaplygin gas model, which have negative equation of state, $P = -A/\rho^B$, where $A > 0$ and $0 < B \leq 1$ [74][75]. It is inspired from the String theory [76]. However this model is saverly constraint from the cosmological observations [77][78], also see (Ref.[199] of Ref. [53]) .

An interesting possibility for cosmic acceleration suggests that the Universe is dominated by the bulk viscous fluid. The viscosity provides a negative pressure and for large viscosity in cosmic medium may causes to accelerate the Universe [79–92]. Since cosmic viscosity is a central issue of the thesis, we will present a detailed discussion of how the bulk viscosity causes a cosmic acceleration in chapter 2.

Backreaction effect

At the late time of cosmic history, the Universe is dominated by inhomogeneities due to the small-scale structures. It has been argued that the backreaction generated from the local inhomogeneities are large enough to modify the background expansion and lead to the present accelerated expansion [93][94]. However, whether the backreaction can account for the present cosmic acceleration is under debate, see Refs. [95][96]. We will discuss this issue in some more detail in chapter 3.

Modified gravity

In the above discussion, it was assumed that Einstein's equation correctly explains the cosmic evolution and modification in the energy-momentum tensor causes accelerated expansion. However, it is possible that Einstein's theory fails on large scales, and the law of gravitation is governed through some other theory. The new theory of gravity should be able to explain the cosmic acceleration at very large scales and must be compatible with the general relativity on small scales. This kind of gravity theory is called *Modified gravity*, which includes $f(R)$ theory, massive gravity, etc. For a detail discussions of the modified gravity theories and its implications in cosmology, see Ref. [97] [98] and a a review [99].

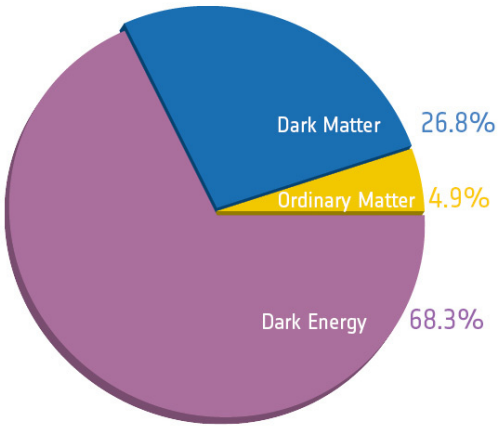

Figure 1.4: Present energy budget of the Universe. Image source [4]

1.4 The standard model of cosmology

The standard model of cosmology, also known as a ΛCDM model, is a mathematical formulation of the outcome of different cosmological and astrophysical observations. The fundamental equations which provide the information on how the Universe evolves with time are Einstein's equation and energy-momentum conservation equations. Below we will briefly discuss the ΛCDM model and the cosmic evolution, but for more details, see Refs. [12][36] [100].

The ΛCDM Model of cosmology assumes that the major amount of the Universe is made of the cosmological constant, DM (χ), baryonic matter (B), and radiation component (R). Fig.1.4 presents the contribution of the different components of the Universe based on the astronomical and cosmological observations. It indicates that the major part of the Universe is dark, which is made of the DM $\sim$ 26.8% and DE $\sim$ 68.3%. Rest 4.9% Universe is made of visible, baryonic matter. Thus study the evolution and fate of the Universe, we need to understand the properties of dark matter and dark energy.

Further, using the Einstein equations, get

$$H^2 = \frac{8\pi G}{3}\left[\rho_R + \rho_B + \rho_\chi + \rho_k + \rho_\Lambda\right] = \frac{8\pi G}{3}\,\rho_T\ , \tag{1.22}$$

where, $\rho_T = \rho_R + \rho_B + \rho_\chi + \rho_k + \rho_\Lambda$ is the total energy density of the Universe, contributed from the radiation (ρ_R), baryonic matter (ρ_B), dark matter (ρ_χ), curvature (ρ_k)

and the cosmological constant, (ρ_Λ). Here $\rho_k = -3k/8\pi G a^2$ and $\rho_\Lambda = \Lambda/8\pi G$. In case, when the component of cosmic fluid do not interact, then the evolution of their energy density is obtained from Eq. (1.13). Therefore, using Eq.(1.13), above equation can be rewritten as

$$H^2 = H_0^2 \left[\Omega_{R0}(1+z)^4 + \Big(\Omega_{B0} + \Omega_{\chi 0}\Big)(1+z)^3 + \Omega_{k0}(1+z)^2 + \Omega_\Lambda\right] , \tag{1.23}$$

where subscript, 0 corresponds for the present value of the quantites. Furthermore,

$$\Omega_i = \rho_i/\rho_c \quad \text{and} \quad \rho_c = 3H_0^2/8\pi G \ . \tag{1.24}$$

where $i = B, R, \chi, k, \Lambda$ and ρ_c is the present critical energy density of the Universe. The Planck 2018 data (using *TT+TE+EE+LowP+lensing+ ext*) provides [20]

$$\Omega_{B0}\, h^2 = 0.02242 \pm 0.00014 \quad \text{and} \quad \Omega_{\chi 0}\, h^2 = 0.11933 \pm 0.00091 \ . \tag{1.25}$$

The Hubble expansion rate $H_0 = (67.66 \pm 0.42)$ km-sec^{-1} Mpc^{-1}, also $h = H_0/100$km-sec^{-1} Mpc^{-1}. Further the second Freedmann equation is written as

$$\frac{\ddot{a}}{a} = -\frac{4\pi G}{3}\left[\rho_T + 3\Big(P_R + P_B + P_\chi + P_k + P_\Lambda\Big)\right] , \tag{1.26}$$

where, P_R , P_B , P_χ , P_k and P_Λ represent the pressure of radiation, baryonic matter, dark matter, curvature and the cosmological constant, respectively. The pressure of cosmological constant is negative, given by $P_\Lambda = -\rho_\Lambda = -\Lambda/8\pi G$.

1.5 Large scale structure of Universe

The present Universe consists of the star, galaxies (collection of large numbers of stars), clusters (consists of the many galaxies), superclusters (collections of the clusters), filaments, and voids. The question arises, how do these structures forms, and why the way they are?

1.5.1 Linear structure formation

To form the structure, a small inhomogeneity should be present at early times, which was further amplified in subsequent cosmological phases. In the very early Universe,

inflation possibly provides the initial seeds for the growth of the density inhomogeneities. *These perturbations are assumed to be gaussian, scale-dependent and amplified in radiation and matter-dominated Universe* [36] [100]. Here we discuss the Newtonian description for the structure formation, which is valid for the mode exists inside the Hubble radius. For the modes lie outside the Hubble radiusthe full general relativistic calculation required. For a detailed discussion of the large scale structure formation, see Refs. [101] [102]. The basic equation of the are given as [103][104]

$$\frac{\partial \rho}{\partial t} + \nabla_r.(\rho \mathbf{v}) = 0 \quad \text{(continuity equation)} \ . \tag{1.27}$$

Euler equation

$$\frac{\partial \mathbf{v}}{\partial t} + (\mathbf{v}.\nabla_r)\mathbf{v} = \nabla_r \psi - \frac{\nabla_r P}{\rho} \ . \tag{1.28}$$

Poisson's equation

$$\nabla_r^2 \psi = 4\pi G \rho \ . \tag{1.29}$$

Where ρ, $\mathbf{v}$, P and ψ represents the energy density, fluid velocity, pressure and the gravitational potential. To complete the equations we need to provide the pressure expression,

$$P = P(\rho, s) \ . \tag{1.30}$$

The entropy conservation equation is given by

$$\dot{s} + \nabla_r.(s\mathbf{v}) = 0 \ , \tag{1.31}$$

where s is the entropy per unit fluid mass.

To study the evolution of the perturbation, we decompose all quantities into its smooth background value and perturbations, i.e.,

$$\rho(t, \vec{r}) = \bar{\rho}(t) + \delta\rho(t, \vec{r}) \ , \tag{1.32}$$

$$\mathbf{v}(t, \vec{r}) = \bar{\mathbf{v}}(t) + \delta\mathbf{v}(t, \vec{r}) \ , \tag{1.33}$$

$$\psi(t, \vec{r}) = \bar{\psi}(t) + \delta\psi(t, \vec{r}) \ , \tag{1.34}$$

$$P(t, \vec{r}) = \bar{P}(t) + \delta P(t, \vec{r}) \ . \tag{1.35}$$

Here $\vec{r}$ is a physical coordinates and $\bar{\mathbf{v}} = H\vec{r}$ is the homeogenous velocity field. However here we will discuss the isoentropic process, therefore, do not consider the perturbation in the entropy. We work in the comoving coordinate, $\vec{r} = a\vec{x}$. then

$$\vec{\nabla}_r = \frac{1}{a}\vec{\nabla}_x \quad \text{and} \quad \left.\frac{\partial}{\partial t}\right|_r = \left.\frac{\partial}{\partial t}\right|_x - H\vec{x}\cdot\vec{\nabla}_x \ . \tag{1.36}$$

Furthermore, tranfering the perturbation mode from real space to k-space, via Fourior transform as

$$\delta A(t,\vec{r}) = \int \delta A(t,\vec{k})\, e^{-i\vec{k}\cdot\vec{x}}\, d^3x \ , \quad \delta A(t,\vec{k}) = \frac{1}{(2\pi)^3}\int \delta A(t,\vec{x})\, e^{i\vec{k}\cdot\vec{x}}\, d^3k \ , \tag{1.37}$$

where $\delta A(t,\vec{r})$ represents any type of the perturbations. Further keeping only the first order of perturbation, equations (1.27),(1.28), and (1.29) becomes

$$\frac{\partial\delta\rho}{\partial t} + 3H\delta\rho + i\frac{\bar{\rho}}{a}\vec{k}\cdot\delta\mathbf{v} = 0 \ , \tag{1.38}$$

$$\frac{\partial\delta\mathbf{v}}{\partial t} + H\delta\mathbf{v} = -i\frac{\vec{k}}{a\bar{\rho}}c_s^2\delta\rho - i\frac{\vec{k}}{a}\delta\psi \ , \tag{1.39}$$

$$k^2\delta\psi = 4\pi G\delta\rho \ , \tag{1.40}$$

where $k = |\vec{k}|$ and $\vec{\nabla}\cdot\vec{v} = 3H$. Furthermore assuming the energy density contrast as , $\delta(t,k) = \left[\rho(t,k) - \bar{\rho}(t)\right]/\bar{\rho}(t)$ and using equations (1.38), (1.39) and (1.40), we get

$$\frac{\partial^2\delta}{\partial t^2} + 2H\frac{\partial\delta}{\partial t} + \left(c_s^2\frac{k^2}{a^2} - 4\pi G\bar{\rho}\right)\delta = 0 \ , \tag{1.41}$$

where, we define $\delta(t,k) \equiv \delta$. In above equation, the second term corresponds to the dilution term.

To understand the solution, we fistly assume tha static Universe, $H = 0$. In this case the solution depends on the sign of the δ proportional term. For positive sign case, both the density solution will be oscillating. However, if the sign is negative, the one solution is exponentially growing and the other is exponentially decaying. In order to study the scale over which the density growth (decay) becomes effective, one define Jeans Scale (JS) as

$$k_J = \sqrt{\frac{4\pi a^2 G\bar{\rho}}{c_s^2}} \ , \quad \lambda_J = \frac{2\pi a}{k_J} = c_s\sqrt{\frac{\pi}{G\bar{\rho}}} \ , \tag{1.42}$$

Therefore we see that for the length scale (L) larger than JS, i.e, $L > \lambda_J$, the δ can grow (decay) exponentially. This case is interesting for understanding how pressure and gravity affect the growth of density perturbation.

Actual Universe is expanding in nature. The structure formation is mainly governed by the DM (large amount in compared with the baryons in the matter dominated era also DE contribution is also very small), which is assumed to be pressureless. Therefore in this case, $c_s = 0$. So the Eq. becomes

$$\frac{\partial^2\delta}{\partial t^2} + 2H\frac{\partial\delta}{\partial t} - 4\pi G\bar{\rho}\delta = 0 \ . \tag{1.43}$$

In the matter dominated era, $H = 2/3t$, therefore the solution of the above equation is given as

$$\delta(t,\vec{k}) = \delta_+(\vec{k})D_+(t) + \delta_-(\vec{k})D_-(t) \ , \tag{1.44}$$

where $D_+(t) = \exp(kt)$ and $D_-(t) = \exp(-kt)$, corresponds for the growing mode and decaying mode, respectively. Their coefficients δ_+ and δ_- can be found by using the intial conditions. Since we are interested in the structure formation, therefore we will consider only the growing solution, i.e., $\delta(t,\vec{k}) = \delta_+(\vec{k})D_+(t)$.

Initially the structure were in linear regime ($\delta = \delta\rho/\rho << 1$) but as the time proceeds, the density perturbation grows and in deep matter-dominated era, the growth becomes non-linear in nature ($\delta \sim 1$).

1.5.2 Non-linear structure formation

The linear theory of cosmological perturbations works very well for the large scales and early Universe. However, when the density perturbations become an order of the background density, then the linear perturbation theory fails. To understand the non-linear theory, one has to rely on the higher-order perturbation theory, Press-Schechter theory, or the numerical gravity solvers. The analytic expression in these regions is very difficult, so the correct dynamics of the density perturbation can be described by the numerical simulation. However, for a very simple case, one can obtain the analytic solution and study the evolution of the density in the nonlinear region.

Spherical top hat collapse model

The simplistic description is a spherical top hat collapse model, which assumes the isolated spherical halo on the homogeneous background of the Universe. As time passes, the perturbation grows; however, after some time, the perturbation stops growing. The

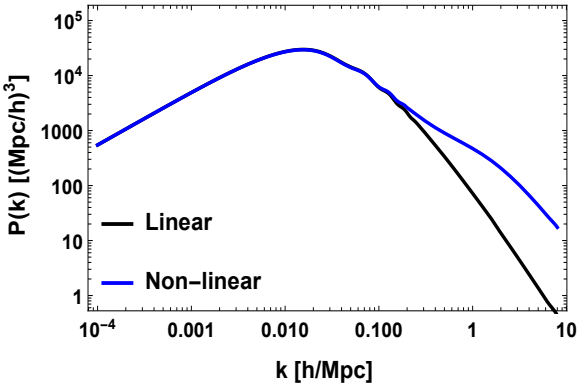

Figure 1.5: A linear and nonlinear matter power spectrum obtained from CDM using the CLASS code [5].

radius at which this happens is called the turnaround radius. After the turnaround, the density again starts growing, and the radius starts decreasing. After some time, the system becomes virialized and forms a halo. At time of the virialization, the density becomes $\approx$ 178 times the background energy density and the linear density grows to, $\delta \simeq 1.69$. This suggests that if the linear density exceeds $\delta \simeq 1.69$, halo formation occurs, which is typically 178 times larger than the background density. After being equipped with the linear structure formation input, one can estimate the number density of the halo for a given mass by the *Press-Schechter mass function* [105]. This model is very successful in explaining the CMB and large-scale structure of the Universe.

N-body simulations and Halofit model

The cosmological N-body simulation provides the correct picture of the nonlinear gravitational evolution on a small scale. The result obtained from the N-body simulation has been further used to develop a fitting formula or the halo model to study gravitational clustering.

The halofit model, as suggested in Ref. [106], has been used to predict the nonlinear matter power spectrum, which fits the result of N-body simulations. However, it has been further reported that on the small scales ($k < 0.65h$ Mpc^{-1} (or $L > 9.6h^{-1}$Mpc)), the halofit model underestimates the matter power spectrum as suggested by recent precise simulation. An accurate fitting of the simulation results for the scale, $k \leq 30h$Mpc^{-1} (or $L \geq 0.2h^{-1}$Mpc) is given by the modified halofit model,

which is discussed in Ref.[107].

In Fig. 1.5, we plot both the linear matter power spectrum (LMPS) and nonlinear matter power spectrum (NLMPS) $P_{\delta\delta}(k)$ obtained from the modified halofit model [107], using the CLASS code [5] as a function of the scale at present. We find that the LMPS matches the NLMPS on a large scale, but they differ on a small scales.

1.6 Problems of the standard cosmology

The ΛCDM model explain the large scale (scale larger than $\sim O$ (Mpc)) observational data (where the structures are in linear regime of the density perturbations) very well. However, this model faces some serious challenges from both theoretical construction and cosmological observations. Some of the problems are as follows;

1.6.1 Cosmological constant problem

The cosmological constant (Λ) is a candidate for the dark energy in this model. The dark energy has a constant and negative equation of state, $w = -1$, which indicates the constant energy density throughout the cosmic evolution. The origin of Λ is considered as the vacuum energy density of the Universe. However, the quantum field theory calculation suggests that the vacuum energy of the quantum fields is $\sim 10^{121}$ times larger than the energy density associated with the present dark energy density [108]. The difference between the energy density of the above two suggests that the vacuum energy may not be the correct explanation of the Λ.

However, to solve the cosmological constant problem, many theories have been proposed. Since the issue is related to the zero-point energy, therefore one may expect that incorporating the supersymmetry (SUSY) may possibly resolve the problems. The idea is based on the supersymmetric construction that there will be a fermion superpartner with the same mass for every boson. Since the ground state energy of the fermions and bosons is negative and positive, the overall effect will be completely canceling the ground state energy. However, the SUSY is broken, so we do not know how the SUSY breaking scale is related to the observed Λ value [53]. The other possible methods to solve the Λ can be found in the reviews [53][109].

1.6.2 Problems on the small scale

On a small scale, where the Universe is dominated by the structures (in nonlinear regimes), the linear theory fails, and the Universe is well described by N-body simulations. However, it was realized that the results obtained from the N-body dark matter only simulations show some discrepancy with the observations. The disagreement between the observations and CDM simulations on the small scales is mainly related to the following problems;

Core-cusp problem

N-body simulations based on the collisionless CDM shows the cuspy density profile given as $\rho \propto r^{-1}$ (where ρ is the density and r is the distance away from the center), towards the center of the galaxy [110]. This kind of halo is described by the universal Navarro-Frenk-White (NFW) profile [111, 112]. But the observations of the rotation curve of the dwarf and the Least Surface Brightness (LSB) galaxies indicate the linearly increasing velocity towards the center of halo, which suggest that the DM density profile is the core, i.e., $\rho \propto r^{0}$ [113–118]. The difference between the slope of density profile predicted from CDM simulations and observations is termed as the core-cusp problem, for an overview, see [119]. This problem is not limited on the small galactic scale but also reflected in the cluster scale [120–122].

Missing satellite problem (MSP)

This problem is related to the number of satellite galaxies around the host galaxies. These satellites have their own halo and orbit around the most massive nearby halo. Numerical simulations using CDM predicts large number of subhalos around the host halos, since the halo mass function diverges for small halo masses as $\frac{dN}{dM_{\rm halo}} \propto M_{\rm halo}^{-1.9}$ [123]. However, it has been revealed that the number of subhalos predicted in the simulation is much higher than the observed satellite galaxies. For the Milky way size of halo, the simulation provides a few hundred halos [124, 125], but only a few galaxies are reported so far, see also a review [126].

Too-big-to-fail (TBTF) problem

This problem relates to the inconsistency between the dynamics of brightest dwarf spheroidal (dSph) galaxies (which is DM dominated) found in the Milky Way (MW) and the most massive subhalo obtained from ΛCDM simulations. In Refs. [127][128], it is found that dSph galaxies in the Milky Way have a large velocity dispersion; therefore, these galaxies should be lie in the most massive subhalo around the MW. However, the massive subhalos found in ΛCDM simulations are too dense to host the observed satellites. In other words, the massive halo in MW is too dense to allow the baryonic structure. For more reference on this issue, see Refs.[129, 130].

Diversity problem

In the ΛCDM model, the DM density follows the universal NFW profile. For a fixed DM halo parameter, the NFW profile is fixed, so one expects the same kind of behavior for a similar halo. However, the observations of the velocity rotation curve of spiral galaxies show considerable diversity in the interior properties (e.g., velocity dispersion) of halo [131][132][133]. This is called the diversity problem.

It is important to note that all the above-discussed problems are not independent in nature; instead, some of them are common in origin. For example, any mechanism that solves the core-cusp problem by reducing the density at the DM halo's inner regions will also address the too big to fail problem and diversity problems.

A possible solutions of the small scale issues

The resolution of the abovementioned problems can be obtained as follows: the central density profile of the DM host halo solves the core-cusp problem. The subhalo mass function becomes divergent for low halo mass; therefore, reduction in halo mass ameliorates the missing satellite problem [124][125]. Further decreasing the large subhalo central density profile of the DM addresses the TBTF problem [127][128].

Furthermore, the possible methods to address the small scale issues are broadly categorized into two following ways;

Baryonic dissipation mechanism

We emphasize that the small-scale issues discussed above are based on the CDM-only simulations results. Since the baryons contribute predominantly to the energy density of the inner region of the DM halo, therefore, one may expect that once the CDM, along with the baryonic matter is taken into account in the numerical simulations then some of the problems may be ameliorated. The baryonic dissipation mechanism, such as the supernovae feedback, star formation takes away baryons from the DM halo, modifies the gravitational potential, and can convert cuspy into core profile in dwarf DM halo [134–139]. In Ref. [140] it has been shown that the baryonic mechanism is also able to solve the missing satellite problems. However, the core formation requires large star creation efficiency, and suppressing the galaxy formation needs low star generation, which is opposite in nature [141]. Therefore whether the baryonic mechanism will solve the small scale issues or not is still unclear [23].

The dark matter microphysics

The nature of the DM affects the structure formation history; hence its complex physics may be a possible root of the small scale problems. In the ΛCDM simulations, the dark matter is assumed to be cold, collisionless, and interacting themselves via gravity. However, instead of the DM is cold if the DM is warm (velocity dispersion is large but less than the hot dark matter), then due to free streaming, warm dark matter (WDM) can damp the matter power spectrum [142][143]. Hence, in contrast with the CDM halo, WDM reduces the number of subhalos, and due to the late time formation of these haloes (in comparison with the CDM counterpart), the DM halo is less concentrated [37, 144]. Numerical simulations using the warm dark matter suggest that it can solve the TBTF and missing satellite problem [145–147].

Although, unlike the CDM, WDM produces the core density profile, but the core length is too small to ameliorate the core-cusp problem [148]. Furthermore, WDM also shows disagreement with the Lyman-alpha observations (which provides the information about the power spectrum on the small scales) [38, 149] and hence using this, the constraint on the WDM mass has been derived [150]. In other work, it is shown that the relativistic WDM corresponds to 4 KeV mass explain the Lyman-alpha and Slogan

Digital Sky Survey (SDSS) data but fails to address major small scale issues [151]. For a comparison with the CDM and WDM in the light of the small scale cosmology, see also Ref. [152].

Further, it has been found that the decaying dark matter (DDM) can address TBTF, and MSP also does not violate the Lyman-alpha limit [153, 154]. The DDM, which decays into dark radiation and WDM, can address the effective relativistic degree of freedom and small scale constraint faced by the ΛCDM model [155]. Another interesting solution to the small scales problems is the presence of self-interaction between the dark matter particles [156]. We will discuss this possibility in great in chapter 3.

1.6.3 Anomaly in 21-cm cosmological signal observed by EDGES

The problem is related to the measurement of the 21-cm cosmological signal. Here, we will briefly review the basics of the 21-cm signal and its cosmological evolution. Later, we also discuss the anomaly observed in the 21-cm global absorption signal reported by the EDGES collaboration.

The 21-cm absorption or emission line emits from the ground level of the neutral hydrogen atom. This signal comes from the spin-flip transition between the singlet ($F = 0$) and triplet ($F = 1$) hyperfine states. After CMB decoupling, the proton and electron combine and form the hydrogen atom, which dominantly contributes to the gas. Therefore, for the cosmological context, a 21-cm signal is a useful tool to study the properties of the gas and provides valuable information about the first-star formation and the reionization phase [6].

In the cosmological context, the 21-cm signal has been applied to study the gas properties on some background radiation (CMB radiation). The intensity of the observed 21-cm signal is quantified in terms of the differential brightness temperature, T_{21} given by [157–159]

$$T_{21} = \frac{1}{1+z}(T_S - T_{\rm CMB})(1 - \exp^{-\tau}) \ , \tag{1.45}$$

where $(1 + z)$ factor in denominator corresponds to the dilution of temperature due to expansion of the Universe. In above equation, $T_{\rm CMB}$ is the temperature of black body radiation, which emits during the fromation of atom via recombination of proton

and electron. Further, T_S represnets the spin temperature, which defines the relative population of the triplet (n_1) and singlet (n_0) states due to the hyperfine splitting in neutral hydrogen atom. The T_S is given by [160]

$$\frac{n_1}{n_0} = \frac{g_1}{g_0}\, e^{-\frac{E_{21}}{T_S}} \simeq 3\left(1 - \frac{E_{21}}{T_S}\right) \ , \tag{1.46}$$

where E_{21} is the energy of the 21 cm line. Here τ is the optical depth of the cosmic medium, which is defined as

$$\tau \approx \frac{3\lambda_{21}^2 n_H A_{10}}{16 T_S H(z)} \ , \tag{1.47}$$

where, λ_{21} is the wavelength of 21 cm-line at rest and n_H is the number density of the neutral hydrogen atom. For a optical thin case, $\exp^{-\tau} \approx 1 - \tau$, so using Eq. (1.45) and Eq. (1.47), one can get

$$T_{21} \approx \frac{3\lambda_{21}^2 A_{10}}{16(1+z)}\left(1 - \frac{T_{\rm CMB}}{T_S}\right)\left(\frac{n_H}{H(z)}\right) \ . \tag{1.48}$$

It is clear from the above equation that whenever the spin temperature becomes different from the CMB, the absorption or emission of the 21-cm line takes place.

In the evolutionary history of the Universe, the spin temperature is determined by three competing mechanisms: CMB radiation, collisions, and Lyman-α radiation. In the local equilibrium and using the argument of detailed balance, one can obtain the spin temperature as [160]

$$T_S = \frac{T_{\rm CMB} + y_c T_G + y_w T_{Ly\alpha}}{1 + y_c + y_w} \ , \tag{1.49}$$

where, T_G and $T_{Ly\alpha}$ represents the kinetic temperature of gas and Lymann-alpha temperature. The temperature, $T_{Ly\alpha}$ is defined through the detailed balance equation. The other quantities y_c and y_w are defined as [160]

$$y_c = \frac{T_S}{T_G}\left(\frac{P_{01}^c}{A_{10}}\right), \quad y_w = \frac{T_S}{T_{Ly\alpha}}\left(\frac{P_{01}^w}{A_{10}}\right) \ . \tag{1.50}$$

Here P_{01}^c and P_{01}^w are the probabilities of the ground and excited state of the Hydrogen through the collisions and Lyman-alpha radiation.

Standard model of 21-cm cosmology

Figure 1.6 provides the evolution of the brightness temperature as a function of the redshift (also in frequency) during the cosmic evolution in the context of the ΛCDM

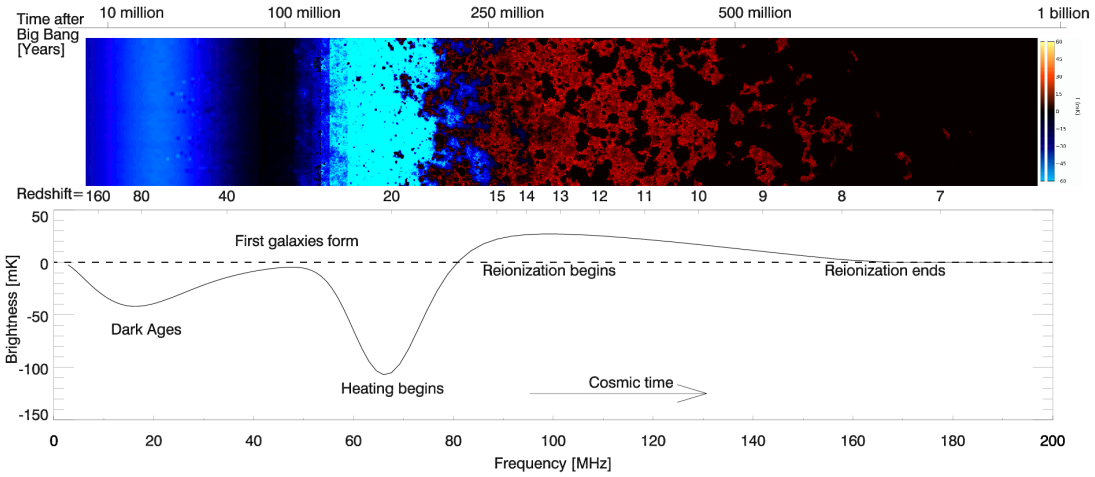

Figure 1.6: 21-cm signal in the standard cosmological model. Image source [6]

model. In the standard cosmological description, the gas remains thermally couple with CMB via the Compton scattering off the residual electrons, i.e., $T_G = T_{\rm CMB}$ and consequently, the collisions drives, $T_S = T_G$. Below the redshift 150, due to decreasing electron fraction, the Thomson scattering between the CMB and free-electron becomes ineffective, and gas gets thermally decoupled from the CMB radiation and cools adiabatically for the rest of the cosmic evolution. Therefore the gas temperature does no longer follows the CMB temperature. However, the collisions between the Hydrogen-Hydrogen, Hydrogen-electron is sufficient enough so that the spin temperature couples to the gas temperature, i.e., $T_S = T_G$. Since $T_S < T_{\rm CMB}$, therefore the first time the 21-cm absorption signal is produced. Nevertheless, as time proceeds, the number density of the particles decreases; therefore, the collisions between the gas become less effective, and hence T_S will no longer hold the gas temperature T_G. At this time, gas absorbed or emitted the CMB radiation efficiently, and the spin temperature becomes CMB temperature; therefore, the 21-cm signal vanishes.

Further, at $z < 20$, the first-star formation took place and emitted ultraviolet radiation. As a consequence, the stellar Lyman α couples the spin temperature with the gas via the Wouthuysen-Field effect [160, 161] such that $T_S = T_G$. Therefore due to the difference between the spin and the CMB temperature, the 21-cm absorption signal occurs. However, at later, $z \leq 15$, the starlight reionized the thermal plasma, and it increases the spin temperature over the CMB; therefore, the emission of the 21-cm signal takes place. At the end of the reionization $z \leq 6$, the Universe again becomes

neutral and $T_S = T_{\rm CMB}$, therefore no absorption or the emission signal of the 21-cm be produced.

As discussed above assuming $T_S = T_G$, the standard cosmological prediction for the brightness temperature at $z \simeq 17$ is

$$T_{21} \geq -220 \text{ mK} \ , \tag{1.51}$$

and for which the gas temperature is equal to 6.8 K [158].

Anomaly in 21-cm cosmological signal reported by EDGES

The EDGES [162] measured a global average of 21-cm absorption signal which is centered around frequency $\nu \approx 78$ MHz (redshift $z \approx 17$). The EDGES brightness measurement at $z \simeq 17$ with 99% confidence interval is given by

$$T_{21}^{EDGES} \approx -500^{+200}_{-300} \text{ mK} \ . \tag{1.52}$$

In the optimal condition, this corresponds to the gas temperature: $3.26^{+1.94}_{-1.58}$ K [158]. The amplitude of the absorption signal is approximately two times larger than the standard cosmological prediction. This signal was reported in the cosmic dawn era $15 \leq z \leq 20$, where the Universe was in its coolest phase, and the star formation started for the first time in cosmic history. Later, as the star formation proceeds, the ultraviolet radiation emitted from the stars heat the baryonic matter, and the spin temperature increases and which reduces the strength of the signal.

Possible resolution of the EDGES anomaly

From Eq.(1.45), it is evident that any mechanism that reduces the brightness temperature can explain the EDGES signal.

The one possibility is the decreasing gas temperature. Since the DM temperature is small in comparison with the gas, therefore the elastic scattering of the dark matter with the gas can transfer the heat energy from gas to DM and reduce the gas temperature [157, 158, 163].

The other method to address the EDGES anomaly is to increase the photon number density in the Rayleigh-Jeans limit of the CMB radiation. It may occur due to the

excess of early radio background [164–166], resonant scattering of a dark photon in standard photons [11], resonant conversion of axions into photons under the magnetic fields [167].

The other possible alternative explanations of EDGES observation include the emission of 21-cm axion [168–170], early dark energy [171].

1.7 Thesis overview

In this thesis, I have attempted to address some major problems of the CDM model, such as the dark energy, EDGES anomaly in the framework of the viscous dark matter. Further, I have also discussed the possible signals from the viscous dark matter (visible photon production) and explored the DM properties such as its mass (sub-GeV), which is relevant for future DM searches.

In chapter 2 we present a brief introduction of the relativistic viscous hydrodynamics and relativistic kinetic theory.

In chapter 3, we propose the viscous self-interacting dark matter. We calculate the shear and bulk viscosity of SIDM using kinetic theory and the relaxation time approximation. It is found that at present, $z = 0$, due to the large velocity dispersion of the DM particles, the SIDM viscosity (both shear and bulk) is large and significantly contributes to cosmic dissipation. We check the effect of this on the cosmic evolution and find that the SIDM viscosity is large enough to account for the present accelerated expansion of the Universe, hence mimic the dark energy.

Further, in chapter 4, we study the evolution of the SIDM dissipation at the late time of the cosmic evolution. Considering the variation of the velocity gradient of cosmic fluid at a small redshift interval ($0 \leq z \leq 2.5$), we find that VSIDM can also explain the low redshift observations such as supernovae data, cosmic chronometer data very well.

In chapter 5, we study the SIDM properties such as DM mass, viscosity evolution, in the light of the KSS bound, and the low energy observations ($0 \leq z \leq 2.5$). We see that the VSIDM fluid violates the KSS bound. Further in the assumption that the VSIDM obeys the KSS bound, we find that the mass of the SIDM particles should be sub-GeV. Further, assuming a power-law form of SIDM viscosity, we investigate its evolution in the light of late-time observations. We report that the shear and bulk viscosity are large at present and decrease at an earlier time.

In chapter 6, we explore the effect of DM viscosity at large redshift interval ($15 \leq z \leq 1100$). The viscosity in the DM cause to produce energy dissipation and hence heats the DM fluid. We propose that viscous energy dissipation can produce visible photons. Our calculation indicates that these generated photons can increase the CMB

photons in the RJ limit and are sufficient enough to explain the anomaly in the 21-cm cosmological signal observed by the EDGES collaboration.

In chapter 7, we study the DM microphysics using the viscous DM-gas interactions and recent anomaly observed in the global 21-cm signal anomaly observed by the EDGES. For large DM viscosity, the DM transfers heat energy to the gas and increases its temperature. Therefore one of the possible explanations of EDGES anomaly demands low gas temperature constraint the DM properties such as its interaction with the gas, viscosity.

In the last Chapter 7, we have summarized our results and discussed our future directions.

Chapter 2

Introduction of viscous cosmology

2.1 Introduction

Cosmology is a description of the Universe as a whole. The Universe is made from different species, such as the DM, DE, baryons, and relativistic particles (photons and neutrinos). The particles interact with each other in a specific manner. The large-scale property of the cosmos results from the individual particle dynamics that reside in the Universe.

To study cosmic evolution using the interaction of the individual particles is a challenging task. Therefore the many-body description will be needed to understand the dynamics of cosmic evolution. Hydrodynamics is one of the simplest description of many-body interacting systems. We focus our study on dark matter, so for simplicity, we use the hydrodynamic picture for the dark matter particles. We assume a system of dark matter particles as a viscous fluid and apply the fluid equations to study its properties. In order to calculate the transport coefficient (such as bulk and shear viscosity), we need microscopic theory such as kinetic theory or field theory. We calculate the viscosity using the kinetic theory framework.

The organization of this chapter is as follows. In Section 2.2, we briefly discuss about non-relativistic and relativistic hydrodynamics. In Section 2.3, we present the relativistic kinetic equation. Having equipped with both the picture, we calculate the transport coefficient, i.e., bulk and shear viscosity using relaxation time approximation in Section 2.4. Further, in Section 2.5, we present a brief introduction of viscous

cosmology. Finally, in Section 2.6, we discuss the validity of hydrodynamics for the dark matter particles.

2.2 Introduction to hydrodynamics

Hydrodynamics is the simplest description to study the many-body interacting system. Validity of hydrodynamic approximation would require the following hierarchy of length scales

$$L_{\rm mfp} << L_f < L_{\rm s} \,, \tag{2.1}$$

where $L_{\rm mfp}$ is the mean free path, L_f denote scale of the fluid element and $L_{\rm s}$ describes the system size.

2.2.1 Non-relativistic hydrodynamics

The properties of the non-relativistic, ideal and neutral fluid is defined by its energy density (ρ), velocity (u^i), and pressure (P). The evolution of energy density, and pressure are studied by using the continuity equation [172]

$$\frac{\partial \rho}{\partial t} + \frac{\partial}{\partial x^i}(\rho u^i) = 0 \,, \tag{2.2}$$

and Euler equation

$$\rho \frac{\partial u^i}{\partial t} + \rho\, u^j \frac{\partial u^i}{\partial x^j} = -\frac{\partial P}{\partial x^i} \,. \tag{2.3}$$

In the above four equations (three in velocity and one in energy density), there are five variables (ρ, u^i and P). Therefore to close the equations, one needs to provide the equation of state, which relates the pressure to energy density, i.e., $P = P(\rho)$.

However, when the fluid is non-ideal, then the dissipation can occure. For example, if two layers of fluid have velocity gradient, then the viscosity, if a gradient in the number density, then the number diffusion, and if gradient in the temperature, then the heat diffusion phenomena. In that case, when the fluid is viscous, the Euler euation is replaced by Navior-Stokes equation, given by

$$\rho \frac{\partial u^i}{\partial t} + \rho\, u^j \frac{\partial u^i}{\partial x^j} = -\frac{\partial P}{\partial x^i} - \frac{\partial \Pi^{ji}}{\partial x^j} \tag{2.4}$$

$$\text{where,} \quad \Pi^{ji} = -\eta\left(\frac{\partial u^i}{\partial x^j} + \frac{\partial u^j}{\partial x^i} - \frac{2}{3}\frac{\partial u^k}{\partial x^k}\delta^{ij}\right) - \zeta \frac{\partial u^k}{\partial x^k}\delta^{ij}, \tag{2.5}$$

The non-relativistic fluid equation has been a successful theory and tested in many applications. So any relativistic fluid equation should reduce in the above equation in the non-relativistic limit.

2.2.2 Relativistic hydrodynamics

In relativistic hydrodynamics, the energy density and the velocity are not the relevant quantity because the energy density does not provide information about the kinetic energy, and the velocity vector is not a Lorentz invariant. Therefore for the relativistic version, we consider energy as total energy (ϵ), and velocity is replaced by the four-velocity. In relativistic theory, the definition of the four-velocity is unambiguous. The velocity can be defined as either the energy frame (Landau-Lifshitz frame [172]) or the flow of the particle frame (Ecart frame [173]). As the physics should not depend on the specific choice of velocity defining a frame, so these two frames are related. For a good review of the viscous hydrodynamics, see Refs. [174] [175] [176].

Relativistic ideal hydrodynamics

In relativistic hydrodynamics, the energy-momentum tensor and the charge four-vector of the ideal fluid is written as

$$T^{\mu\nu}_{\text{ideal}} = \epsilon u^\mu u^\nu + P\Delta^{\mu\nu} \quad \text{and} \quad N^\mu = nu^\mu \ . \tag{2.6}$$

In the above equations, u^μ represents the four velocity time like vector, which is normalized as, $u^\mu u_\mu = -1$. $\Delta^{\mu\nu} = u^\mu u^\nu + g^{\mu\nu}$ is the orthogonal projection operator to the velocity, i.e., $u_\mu \Delta^{\mu\nu} = \Delta^{\mu\nu} u_\nu = 0$. In absence of any source or sink,

$$\nabla_\mu T^{\mu\nu}_{\text{ideal}} = 0 \quad \text{and} \quad \nabla_\mu N^\mu = 0 \ . \tag{2.7}$$

So the energy and velocity of the fluid evolves as

$$u^\mu \partial_\mu \epsilon + (\epsilon + P)\, \nabla_\mu u^\mu = 0 \ , \tag{2.8}$$

$$\text{and} \ , \quad (\epsilon + P)\, u^\mu \nabla_\mu u^\nu + \Delta^{\mu\nu} \partial_\mu P = 0 \ . \tag{2.9}$$

In the non-relativistic limit, $P \ll \epsilon$ and $u^\mu \partial_\mu \approx \partial_t + u^i \partial_i$. Therefore the energy is replaced by the rest mass energy density, $\epsilon + P \simeq mn = \rho$ [172], where m and n

corresponds for the mass and number density of the particles. For non-relativistic regime, Eq. (2.8) and Eq. (2.9) reduces in its non-relativistic version of continuity and the Euler equation, as given in Eq. (2.2) and Eq. (2.3).

Relativistic viscous hydrodynamics

In the Landau-Lifshitz frame ($u_\mu T^{\mu\nu} = -\epsilon u^\nu$ [172]), the total energy momentum tensor for a dissipative fluid can be given by

$$T^{\mu\nu} = T^{\mu\nu}_{\text{ideal}} + T^{\mu\nu}_{\text{visc}} \tag{2.10}$$

where, the viscous terms is given by

$$T^{\mu\nu}_{\text{visc}} = \Pi_B \Delta^{\mu\nu} + \Pi^{\mu\nu} \, . \tag{2.11}$$

Here, Π_B, and $\Pi^{\mu\nu}$ represent the bulk stress and shear stress tensor, respectively. In the first order of gradient expansion, these coefficients are defined as

$$\Pi_B = -\zeta \nabla_\mu u^\mu \ , \tag{2.12}$$

$$\text{and} \quad \Pi^{\mu\nu} = -2\eta\sigma^{\mu\nu} = -\eta \left[\Delta^{\mu\alpha}\Delta^{\nu\beta} + \Delta^{\mu\beta}\Delta^{\nu\alpha} - \frac{2}{3}\Delta^{\mu\nu}\Delta^{\alpha\beta} \right] \nabla_\alpha u_\beta \, , \tag{2.13}$$

where, η and ζ represents the shear and bulk viscosity. The shear stress is orthonormal to the velocity, $u_\mu \Pi^{\mu\nu} = 0$, and traceless, $\Pi^\mu_\mu = 0$. It is important point to note that the viscous contribution in the energy-momentum tensor is a small perturbation on the ideal part, therefore $T^{\mu\nu}_{\text{visc}} \ll T^{\mu\nu}_{\text{ideal}}$. In absence of the extra energy source, the covariant form of the energy-momentum conservation equation can be written as

$$\nabla_\mu T^{\mu\nu} = 0 \, . \tag{2.14}$$

So, using the above equations, one can write the evolution equation of fluid energy as

$$u^\mu \partial_\mu \epsilon + (\epsilon + P) \nabla_\mu u^\mu - \zeta \left(\nabla_\mu u^\mu \right)^2 - 2\eta\sigma^{\mu\nu}\sigma_{\mu\nu} = 0 \, , \tag{2.15}$$

and the fluid velocity as

$$(\epsilon + P + \Pi_B) u^\mu \nabla_\mu u^\nu + \Delta^{\mu\nu} \partial_\mu (P + \Pi_B) + \Delta^\nu_\mu \nabla_\alpha \Pi^{\alpha\mu} = 0 \, . \tag{2.16}$$

Along with this there may be conserved charges (for example, dark matter or the baryons). In the first order gradient expansion, the four current vector, N^μ is written as

$$N^\mu = nu^\mu + \nu_d^\mu \tag{2.17}$$

where, ν_d^μ is the diffusion four vector, given by

$$\nu_d^\mu = -\kappa\left(\frac{nT}{\epsilon + P}\right)^2 \Delta^{\mu\nu}\partial_\nu\left(\frac{\mu_c}{T}\right). \tag{2.18}$$

Here κ, μ_c, T represents the thermal conductivity, chemical potential and temperature, respectively. The component of N^μ along the u^μ at rest frame represents the total charge, $n = -u_\mu N^\mu$ and perpendicular on u^μ corresponds for the diffusion four-vector $\nu_d^\mu = -\Delta^{\mu\alpha}N_\alpha$. The ν_d^μ is also perpendicular to u^μ by construction, $u_\mu\nu_d^\mu = 0$. The covarient form of the number density evolution equation is given by

$$\nabla_\mu N^\mu = u^\mu\partial_\mu n + n\nabla_\mu u^\mu + \nabla_\mu\nu_d^\mu = 0 \ . \tag{2.19}$$

In equilibrium condition, the velocity gradient vanishes, therefore the non-equilibrium transport coefficient, Π_B, $\Pi^{\mu\nu}$ and ν_d^μ vanishes.

In the non-relativistic limit, the dissipative part of the relativistic energy momentum tensor (Eq.(2.11)) is approximated as

$$T^{ij}_{\text{visc}} = -\eta\left(\frac{\partial u^i}{\partial x^j} + \frac{\partial u^j}{\partial x^i} - \frac{2}{3}\frac{\partial u^k}{\partial x^k}\delta^{ij}\right) - \zeta\frac{\partial u^k}{\partial x^k}\delta^{ij}, \tag{2.20}$$

We stress that in non-relativistic limit, Eq. (2.15) and Eq. (2.16) reduces in its non-relativistic version of continuity and the Navier-Stokes equation, given in Eq. (2.2) and Eq. (2.4). For a discussion related with the conserved charges, see Refs. [177] [174].

2.2.3 Entropy generation

The entropy is a thermodynamic property, which is related with the other thermodynamic quantities via

$$\epsilon + P = T\mathfrak{s} - \mu n \quad \text{and} \quad d\epsilon = Td\mathfrak{s} + \mu dn \ . \tag{2.21}$$

where, $\mathfrak{s}$ is the entropy density. The equilibrium entropy four-vector is deined as

$$S^\alpha = \mathfrak{s}u^\alpha \ . \tag{2.22}$$

The second law of thermodynamics demands,

$$\partial_\alpha S^\alpha \geq 0. \tag{2.23}$$

Considering the chemical potential to be zero and applying Eq. (2.21), Eq. (2.15) and (2.22), we get

$$\partial_\alpha S^\alpha = u^\alpha \partial_\alpha \mathfrak{s} + \mathfrak{s}\, \partial_\alpha u^\alpha = \frac{1}{T}\left[\zeta\, (\nabla_\alpha u^\alpha)^2 + 2\eta\sigma^{\alpha\beta}\sigma_{\alpha\beta}\right] \geq 0. \tag{2.24}$$

Since viscous coefficients are positive, $\eta \geq 0, \zeta \geq 0$, and RHS is the sum of two positive square, therefore $\partial_\alpha S^\alpha \geq 0$.

2.2.4 Acausal behavior of first-order hydrodynamics

It has been pointed out that the first-order gradient expansion violates the causality. This can be understand by perturbing the energy density and fluid velocity at rest frame as [175]

$$\epsilon = \epsilon_0 + \delta\epsilon(t, \vec{x}), \quad u^\mu = u^\mu_0 + \delta u^\mu(t, \vec{x}) \tag{2.25}$$

where $u^\mu_0 = (1, 0, 0, 0)$. Here we focus on the only spatial coordinate, y and using the relativistic hydrodynamics equation, so we get a diffusion kind of equation as

$$\frac{\partial}{\partial t}\delta u^\mu(y) - \frac{\eta_0}{\epsilon_0 + P_0}\frac{\partial}{\partial x^2}\delta u^\mu(y) = O(\delta^2) \tag{2.26}$$

Assume solution of the form, $\delta u^\mu(y) = f_{\omega,k}\, e^{-i\omega t + i\vec{k}\cdot\vec{x}}$ in Eq. (2.26), we get

$$\omega = \frac{\eta_0}{\epsilon_0 + P_0}\, k^2 \quad \text{and} \quad v_T = \frac{d\omega}{dk} = \frac{2\eta_0}{\epsilon_0 + P_0}\, k \ . \tag{2.27}$$

where v_T is the diffusion speed. From above equation, it can be seen that $v_T \propto k$, and therefore for a large k, the diffusion speed will be larger than the speed of light. This violate the causality. Therefore it implies that the relativistic Navior-Stokes equation holds for the large wavelength scale.

2.2.5 Causal hydrodynamics: Muller-Israel-Stewart (MIS) theory

A possible way to restore the causality is *Maxwell-Cattanio law*, given by [178] [175]

$$\tau_\pi \frac{\partial}{\partial t}\left(T^{xy}_{\text{visc}}\right) + T^{xy}_{\text{visc}} = \eta_0 \frac{\partial}{\partial x}\delta u^\mu(y) \tag{2.28}$$

where τ_π is the time scale, known as the relaxation time. Although the above equation solves the causality problems but the origin of this equation from first principal is not very clear.

The other possibility is related to the definition of entropy. In the equilibrium, the entropy is defined through the Eq. (2.22); however, in case of away from the equilibrium, entropy may not be limited to this but also contain the other term related with the dissipative part of the energy-momentum. The non-equilibrium entropy current is defined as [179] [174]

$$S^\mu = su^\mu - \frac{\beta_0}{2T}\Pi_B^2\, u^\mu - \frac{\beta_2}{2T}\Pi_{\alpha\beta}\Pi^{\alpha\beta}\, u^\mu + O(\Pi_B^2) \tag{2.29}$$

where β_0 and β_2 indicate the deviation of the entropy current from the equilibrium. Using the condition $\partial_\mu S^\mu \geq 0$, one can find the new expression for the shear and the bulk stress [175]. For $\beta_0 = \beta_2 = 0$, these reduces in to the relativistic Navier-Stokes equation. Furthermore, $\beta_0 = \tau_B/\zeta$ and $\beta_2 = \tau_\pi/\zeta$, the equation reduces in similar to *Maxwell-Cattanio law* (Eq. 2.28). The expression of entropy given in Eq. (2.29) respect the causality, see Ref. [175].

The entropy four-vector (Eq. (2.29)) consists of the second-order of the viscous terms, so the MIS theory corresponds to the second-order hydrodynamics. Therefore we see that the second-order hydrodynamics solves the causality problems.

2.3 Relativistic kinetic theory

In kinetic theory formalism, the thermodynamics quantity is defined in term of the particle distribution function, $f(x^\mu, p^\mu)$. In this theory, it is assumed that the system is close to the local thermal equilibrium, so the variation of distribution function is slow in both space and time. Therefore, one can assign the thermodynamic quantities such as temperature and energy to the system locally. The evolution of the distribution function is governed through the Boltzmann equation [36],

$$\hat{L}[f_p] = C[f_p] \ , \tag{2.30}$$

where, $\hat{L}$ represents the Lioville operator and $C[f_p]$ is the collisional term. In presence of the gravity, $\hat{L}$ is given by

$$\hat{L} = p^\mu \frac{\partial}{x^\mu} - \Gamma^\mu_{\nu\alpha} p^\nu p^\alpha \frac{\partial}{p^\mu} \tag{2.31}$$

For the flat space-time, $\hat{L} = p^\mu \frac{\partial}{x^\mu}$. At the equilibrium, f_p reduces to the its equilibrium value, i.e., $f(x^\mu, p^\mu) \equiv f_p^0$, and collisional term vanishes, $C[f_p] = 0$.

The equilibrium thermodynamic quantities can be written by using the moment of the distribution function. The 0−th moment provides the the number density as

$$n = \int \frac{d^3p}{(2\pi)^3} f_p^0 \ . \tag{2.32}$$

Also the first moment defines the four-current density of the particles as

$$J^\mu = \int \frac{d^3p}{(2\pi)^3} \frac{p^\mu}{E_p} f_p^0 \ . \tag{2.33}$$

where $J^\mu = (n, \vec{j})$ and $\mathbf{v}_p = \mathbf{p}/E_p$ is a single particle velocity. Furthermore, the second-moment represent energy momentum tensor, given as

$$T^{\mu\nu} = \int \frac{d^3p}{(2\pi)^3} \frac{p^\mu p^\nu}{E_p} f_p^0. \tag{2.34}$$

The average energy density can evaluate the T^{00} of the above equation as

$$T^{00} = \epsilon = \int \frac{d^3p}{(2\pi)^3} E_p \, f_p^0 \ . \tag{2.35}$$

Also, the (T^{0i}) component of Eq. (2.34) represent the momentum density as

$$T^{0i} = \int \frac{d^3p}{(2\pi)^3} p^i \, f_p^0. \tag{2.36}$$

Futher, component of the Eq. (2.34) represents the momentum density as

$$T^{ij} = \int \frac{d^3p}{(2\pi)^3} \frac{p^i p^j}{E_p} f_p^0. \tag{2.37}$$

For a homogenous and isotropic system, the average pressure of the system is given as

$$P = \frac{1}{3} T^i_i = \frac{1}{T} \int \frac{d^3p}{(2\pi)^3} \left[\frac{p^2}{3E_p}\right] f_p^0 \ . \tag{2.38}$$

In a thermodynamic equilibrium, one can also obtain the entropy density, $\mathfrak{s}$ of the viscous fluid medium, via the thermodynamic relation as

$$\mathfrak{s} = \frac{\epsilon + P}{T} = \frac{1}{T} \int \frac{d^3p}{(2\pi)^3} \left[E_p + \frac{p^2}{3E_p}\right] f_p^0 \ . \tag{2.39}$$

where, ϵ and P are the average energy density and average pressure.

Furthermore, when fluid departs from the local thermal equilibrium, then the distribution function changes, and hence EM tensor also changes. We assume that change that the system is slightly away from the equilibrium (nearly in local equilibrium), into the distribution function is of the linear order, thus

$$f'_p = f^0_p + \delta f_p + ... \tag{2.40}$$

where the first term f^0_p is the equilibrium distribution function, and the second term δf_p is the first order deviation from the equilibrium. Therefore upto first order of the distribution function expansion, the total non-equilibrium EM tensor is given by

$$T^{\mu\nu} = \int \frac{d^3p}{(2\pi)^3} \frac{p^\mu p^\nu}{E_p} f'_p = \int \frac{d^3p}{(2\pi)^3} \frac{p^\mu p^\nu}{E_p} (f^0_p + \delta f_p). \tag{2.41}$$

Furthermore, it is good to rewrite the non-equilibrium EM tensor as

$$T^{\mu\nu} = T^{\mu\nu}_0 + \int \frac{d^3p}{(2\pi)^3} \frac{p^\mu p^\nu}{E_p} \delta f_p \ , \tag{2.42}$$

where the first and second term in RHS corresponds for the ideal (given in Eq. (2.34)) and dissipative part. Therefore ij-component of the energy-momentum tensor of the dissipative term using the kinetic theory is given as

$$T^{ij}_{\text{dissK}} = \int \frac{d^3p}{(2\pi)^3} \frac{p^i p^j}{E_p} \delta f_p. \tag{2.43}$$

2.4 Calculation of bulk and shear viscosity using kinetic theory formalism

After being equipped with hydrodynamical and relativistic formalism, we will now calculate the shear and bulk viscosity by comparing the stress-energy tensor of the kinetic and hydrodynamic theory. To do so, firstly, we estimate the change of distribution function using the relaxation time approximation. Here we will briefly discuss the calculation, but for more details, see [180] [181] [182].

The evolution of the distribution function of the particles can be obtained by using the Boltzmann equation, given by Eq. (2.30). For simplicity, here we assume that

the particles are spinless, interacting, and there is no external force acting on them, $dp/dt = 0$. Therefore the Boltzmann equation is written as

$$p^{\mu}\frac{\partial}{x^{\mu}}f_p = \frac{\partial f_p}{\partial t} + v_p^i\frac{\partial f_p}{\partial x^i} = C[f_p] \ . \tag{2.44}$$

Here we are interested in $2 \leftrightarrow 2$ elastic collision, so $C[f_p]$ describe the rate of change of f_p due to collisions between the particles. It is also assumed that the collisions are effective in bringing the system to local equilibrium

To study the evolution of f_p, one needs to provide the form of $C[f_p]$, which crucially depends on the particle interaction. Here we approximate the $C[f_p]$, using the *relaxation time approximation*. The system comes in the local equilibrium exponentially in characteristic time, called relaxation time (τ), which is an order of the collision time of the particles. The value of τ provides us information about how much time is needed for the system to obtain the equilibrium.

Under the above assumptions, the collision term can be approximated by the linearized form [180]

$$C[f_p] \simeq -\frac{(f_p - f_p^0)}{\tau} = -\frac{\delta f_p}{\tau}, \tag{2.45}$$

where, $\delta f_p \equiv (f_p - f_p^0)$ is the deviation of distribution function from the equilibrium distribution function, f_p^0. The negative sign indicate that the non-equilibrium distribution function is decaying to its equilibrium value. In a general consideration, τ can be a function of energy, ie., $\tau \equiv \tau(E_p)$. However for calculation puposes, we assumed τ to be independent on energy. Thus, applying Eq. (2.45) and Eq. (2.44), we get

$$\delta f_p = -\tau(E_p)\left(\frac{\partial f_p^0}{\partial t} + v_p^i\frac{\partial f_p^0}{\partial x^i}\right). \tag{2.46}$$

Thus using δf_p from Eq. (2.46), we get the $T^{ij}_{\rm dissK}$ as

$$T^{ij}_{\rm dissK} = -\int \frac{d^3p}{(2\pi)^3}\,\tau(E_p)\,v^i p^j\left(\frac{\partial f_p^0}{\partial t} + v_p^l\frac{\partial f_p^0}{\partial x^l}\right). \tag{2.47}$$

The above $T^{ij}_{\rm dissK}$ corresponds to the dissipative part of the energy-momentum tensor, which is derived from kinetic theory. Therefore this form must be consistent with the $T^{ij}_{\rm dissH}$, as obtained from the hydrodynamics.

Further, in order to calculate the η and ζ, we need to compare Eq. (2.20) and Eq. (2.47). For this, we assume the fluid motion along, say, x axis with fluid velocity $u_x(y)$,

i.e. $\mathbf{u} = (u_x(y), 0, 0)$. In this case, Eq. (2.20) reduces to

$$T^{xy} = -\eta \frac{\partial \mathrm{u_y}}{\partial x} \ . \tag{2.48}$$

Furthermore, to simplify the Eq. (2.47), we consider the equilibrium distribution function of the form $f_p^0 = \exp(-p^\mu u_\mu / T)$. Then assuming $\partial f_p^0 / \partial t = 0$, one can get T^{xy} using Eq. (2.47) as

$$\eta = -\frac{1}{T} \int \frac{d^3p}{(2\pi)^3} \tau(E_p) \left(\frac{p_x p_y}{E_p} \right)^2 f_p^0 \left(\frac{\partial \mathrm{u_y}}{\partial x} \right) \ . \tag{2.49}$$

Thus using Eq. (2.48), Eq. (2.49) and after some simplification, we get [180] [182]

$$\eta = \frac{1}{15T} \int \frac{d^3p}{(2\pi)^3} \tau(E_p) \frac{p^4}{E_p^2} f_p^0 \ . \tag{2.50}$$

To calculate the bulk viscosity, we need to take the trace of Eq. (2.20), which gives as

$$T_i^i = -3\zeta \frac{\partial u^i}{\partial x^i} \ , \tag{2.51}$$

and compare with trace of Eq. (2.47). Further, using the conservation of stress energy tensor $T^{\mu\nu}_{\ ,\nu} = 0$ and after some manipulations, one can obtain the expression for the bulk viscosity as [180] [182]

$$\zeta = \frac{1}{T} \int \frac{d^3p}{(2\pi)^3} \tau(E_p) \left[E_p C_n^2 - \frac{p^2}{3E_p} \right]^2 f_p^0 \ , \tag{2.52}$$

where, $C_n = \left. \frac{\partial P}{\partial \epsilon} \right|_n$ is the speed of sound at constant number density. Eq. (2.50) and (2.52) are relativistic expression for the shear bulk viscosity from kinetic theory.

Therefore in order to estimate the viscosity we need to provide the energy dependent relaxation time. For the scattering process $a(p_a) + b(p_b) \leftrightarrow c(p_c) + d(p_d)$, $\tau(E_p)$ is defined as

$$\tau^{-1}(E_p) = \sum_{bcd} \int \frac{d^3p_b}{(2\pi)^3} \frac{d^3p_c}{(2\pi)^3} \frac{d^3p_d}{(2\pi)^3} W(a, b \to c, d) f_b^0 \ , \tag{2.53}$$

where, $W(a, b \to c, d)$ is related with the transition amplitute, $|\mathcal{M}|^2$ by

$$W(a, b \to c, d) = (2\pi)^4 \frac{\delta(p_a + p_b - p_c - p_d)}{(2E_a)(2E_b)(2E_c)(2E_d)} |\mathcal{M}|^2 \ . \tag{2.54}$$

In this work, we approximate the relaxation time to the thermal average relaxation time, $\tilde{\tau}$. For the scattering process $a(p_a) + b(p_b) \leftrightarrow c(p_c) + d(p_d)$, $\tilde{\tau}_a$ is defined as

$$\tilde{\tau}_a^{-1} = \sum_b n_b \langle \sigma_{ab} v_{ab} \rangle, \tag{2.55}$$

where n_b represents the number density of particle b, which is given by

$$n_b = \int_0^\infty \frac{d^3 p_b}{(2\pi)^3} f^0_{p_b} \ . \tag{2.56}$$

Further, $\langle \sigma_{ab} v_{ab} \rangle$ is the average velocity weighted cross-section, defined as

$$\langle \sigma_{ab} v_{ab} \rangle = \frac{\int d^3 p_a d^3 p_b \ \sigma \ v_{ab} \ \exp\left(\frac{-E_a}{T}\right) \exp\left(\frac{-E_b}{T}\right)}{\int d^3 p_a d^3 p_b \ \exp\left(\frac{-E_a}{T}\right) \exp\left(\frac{-E_b}{T}\right)} \ . \tag{2.57}$$

We see that the value of $\tilde{\tau}_a$ depends on the particle physics motivated model. Here we assume that the DM particles are colliding with themselves elastically and take $n_a = n$ and $\langle \sigma_{ab} v_{ab} \rangle = \langle \sigma v \rangle$.

2.5 Motivation of viscous cosmology

The Universe is homogeneous and isotropic on a large scale, typically greater than $\sim$ 100 Mpc. Therefore, the shear viscosity, which accounts for the fluid's anisotropy, is unfavored on large scales. Further, the shear viscosity is also considered unimportant at the early time of cosmic history, where the Universe was in linear regimes. However, at the late time of cosmic evolution, the perturbations become non-linear, and due to structure formation, the Universe becomes anisotropic at a small scale. Therefore at a late time, the contribution of the shear viscosity may be important and may not be neglected at present [92].

On the other hand, the bulk viscosity is consistent with the homogeneity and isotropy of the large scale of the Universe, and hence its effect can be explored throughout the cosmic evolution. In the presence of bulk viscosity, the energy-momentum tensor of the cosmic fluid is given as

$$T_{\mu\nu} = \rho u^\mu u^\nu + (P + \Pi_B)\Delta^{\mu\nu} \ , \tag{2.58}$$

where $P = (\gamma - 1)\rho$ (γ is constant) is the kinetic pressure and Π_B is the viscous pressure of the cosmic fluid. The energy density evolution of the bulk viscous fluid is obtained by using the continuity equation, $\Delta_\mu T^{\mu 0} = 0$ as

$$u^\mu \partial_\mu \rho + \Big(\epsilon + P + \Pi_B\Big) \nabla_\mu u^\mu = 0 \ . \tag{2.59}$$

For the flat FLRW metric and cosmic rest frame, $\nabla_\mu u^\mu = 3H$. So the above equation becomes

$$\dot{\rho} + 3H(\rho + P + \Pi_B) = 0 \ . \tag{2.60}$$

Therefore, in presence of the viscosity, the Eq. (1.10) and Eq. (1.12) gets modified as

$$H^2 = \frac{8\pi G}{3}\rho \ , \tag{2.61}$$

$$\frac{\ddot{a}}{a} = -\frac{4\pi G}{3}\left[\rho + 3\left(P + \Pi_B\right)\right] . \tag{2.62}$$

Eq. (2.61) and Eq. (2.62), indicate that the cosmic viscosity affects both the background expansion and also the rate of change of the cosmic expansion rate. For the flat FLRW metric and cosmic rest frame, $\Pi_B = -3\zeta H$ (using Eq. (2.12)). So the above equation becomes

$$\frac{\ddot{a}}{a} = -\frac{4\pi G}{3}\left[\rho + 3\left(P - 3\zeta H\right)\right] . \tag{2.63}$$

Thus, for a sufficiently large cosmic bulk viscosity, the total fluid pressure can be negative and leads to accelerated expansion.

Therefore at the very early time of the Universe, a large bulk viscosity in the cosmic medium can cause early cosmic acceleration (Inflation) [183–186]. Further using the same argument as above, it have been shown that the viscous cosmic fluid can also explain the currently observed acceleration of the Universe [79–92, 187]. Later, in Ref. [188], the authors have argued that the viscous dark matter can reduce the tension between the Planck and local measurements of the Hubble expansion rate.

However, it has been found that large shear and bulk viscosity can severely affect the cosmic evolution history. The viscosity can cause to decay of gravitational potential fluctuations and hence can affect the CMB power spectrum [90]. The bulk viscosity also reduces the growth of the density perturbation and therefore affects the structure formation [189][190]. The presence of cosmic shear viscosity can dampen the amplitude of the gravitational waves propagation [191–193]. In Refs.[194][88], the authors report that if the Universe is filled with the bulk viscous fluid, then the viscosity can reduce the age of the Universe. Therefore the DM viscosity is severely constrained from the different astrophysical and cosmological observations. For more recent work on the cosmic viscosity, see Refs. [195–199] and also a review [200].

We emphasize that the aforementioned constraints on the cosmic viscosity is considered on the different redshift of the cosmic evolution. Therefore depending on the strength of viscosity, the effect will be different. The modification in the background expansion requires large viscosity, $\tilde{\zeta} \sim 10^{-1}$ [190] whereas non-linear growth of the density perturbation needed small viscosity (existence of dwarf galaxies need $\tilde{\zeta} < 10^{-11}$, whereas presence of cluster halo requires $\tilde{\zeta} < 10^{-6}$), where $\tilde{\zeta} = \frac{24\pi G\zeta_0}{H_0}\left(3H_0^2/8\pi G\right)^{\nu}$ [190][189]. Hence at an early time of cosmic evolution, the viscosity should be small, and to produce the present accelerated expansion, the viscosity should be large. Therefore on the basis of the above discussion, we state that if the cosmic viscosity varies with the density, such as it is small at high redshift and large at low redshift, then the viscous dark matter can in principle account for the cosmic acceleration.

2.6 Validity of hydrodynamics for the DM particles

In this section, we discuss about the fluid validity for dark matter particles. As discussed previously, the hydrodynamic description of the dark matter particles will be held when the mean free path of the dark matter particles, $\lambda_{\rm SIDM}$ is less than the system size under consideration, i.e., $\lambda_{\rm SIDM} < L$. In the collisionless cold dark matter description, the DM particles do not interact within themselves; therefore, the MFP becomes large, and hence the fluid validity cannot establish like the interacting particles (where the scattering cause to establish the thermal equilibrium). However, the presence of non-linearities on small scales enables us to define an effective fluid description, which in turn can be used to define an effective MFP of the CDM particles [201]. In the effective theory of large scale structure, the fluid description of the dark matter particles is defined on $k_\Lambda \sim 1h$ Mpc^{-1} (or $L \sim 3$Mpc), and the description on the scale, $k_m \sim 0.5h$ Mpc^{-1} (or $L \sim 20$Mpc) includes the viscosity arising either from the coarse-graining scale $k_m < k < k_\Lambda$ or the fundamental viscosity arising from the dark matter microphysics [202]. For more discussion on fluid description for cold dark matter particles, see Refs. [202][203].

In case of collisional dark matter, collisions between the DM particles (like self-interacting dark matter) sets a MFP scale, $\lambda_{\rm mfp} = 1/\sqrt{2}n\sigma$, where n and σ represents

the density and interaction cross-section of the DM, respectively [204]. If $\lambda_{\rm mfp}$ becomes less than the length scale under consideration, then the hydrodynamics description will be valid. However, if one accounts the gravitational interaction along with the DM self-interaction, then the correct picture will be provided by the effective mean-free path. We will discuss this thing in more detail, in subsection 3.3.1.

Chapter 3

Viscous self-interacting dark matter and present cosmic expansion

3.1 Introduction

As discussed in chapter 1, that the ΛCDM model explains the CMB and the large scale observations CMB but is in conflict with some small scale observations. Here we will discuss the resolutions of these problems in the framework of self-interacting dark matter (SIDM) [156] and constrain the SIDM properties from the cosmological observations.

The self-interactions between the dark matter particles may lead to a modification in the evolution of the Universe. In Ref. [205], it has been argued that tightly bound DM and baryonic matter form the gravitating fluid and hence attribute to the thermodynamic properties. The collisional DM fluid's internal motion can source to the gravitational field and provide the extra energy (dark energy) required to flat the Universe [205]. This idea is further explored for polytropic DM model fluid and studied the cosmic acceleration and deceleration to the accelerated transition of the Universe [206].

In this chapter [207], we propose the viscous fluid description of the self-interacting dark matter particles and investigate their impact on the cosmological evolution history. We argue that a large self-interaction between the DM particles causes collisions between themselves and thermalizes the inner region of the halo; therefore, the SIDM

can be described as a fluid. The self-interaction between the DM particles causes to transfer of the energy and momentum between themselves. We propose that the scattering processes between SIDM particles would lead to the viscosity in SIDM fluid. To understand the scale at which the transport coefficients such as viscosity can be estimated, we calculate the mean free path of the DM particles. Taking the DM self-interaction and gravitational interaction into account, we report that the effective MFP of SIDM is an order of virial radius of the DM halo under consideration. Therefore we argue that for the SIDM scenario, the fluid description is valid from galaxy to a larger scale. Then assuming the velocity distribution of SIDM particles as Maxwellian, we estimate its shear and bulk viscosity using the kinetic theory framework. Further, the astrophysical data from the clusters scale suggest that at the present epoch, the SIDM viscosities are large; therefore, one may expect some cosmological consequence from viscous dissipation.

As an application of these results, we explore the scenario discussed in Ref. [92]. It was argued that the background quantities of cosmological fluid depend on the velocity gradient and viscosity (both shear and bulk viscosity) of the cosmic fluid via dissipation terms. If the backreaction from the local inhomogeneities is large, it modifies the solution to Einstein's equations and may explain the accelerated cosmic expansion. However, it remains unclear which kind of particles can produce such a large viscosity. We test this assertion using our Viscous Self-Interacting Dark Matter (VSIDM) model and estimate the dissipation term, which depends on the DM viscosity and spatial average of the fluid velocity gradient. The lower limit of the spatial average is the smallest scale over which the fluid description of SIDM is valid (i.e., a few times of MFP scales). The upper limit is taken to be a scale at which the Universe becomes homogeneous and isotropic (i.e., $\sim$ 100 Mpc).

Further, we calculate the dissipation term in our VSIDM model. The estimation of dissipation has been done using two different approaches. In the first approach, the spatial average of fluid velocity gradient is replaced by its average value, and in the second approach, fluid velocity gradient has been inferred from a realistic velocity power spectrum. In the first approach, we report that the dissipative effects of the SIDM obtained from the cluster scale DM halos are sufficiently large to account for

the present observed cosmic acceleration. We test our theoretical understanding using the astrophysical data and find that the data also points in the same direction.

In the second approach (using the velocity power spectrum), we find that the small scale predominantly contributes to cosmic dissipation, whereas the large scale contribution is very small. We also find that the non-linear velocity divergence power spectrum provides slightly smaller dissipation (i.e., $4\pi GD/3H^3 \approx 2.2$) in comparison with the required value for present cosmic acceleration (i.e.,$4\pi GD/3H^3 \approx 3.5$), where D is a dissipation term. However, we expect that the small value of the dissipation may be due to not incorporating the small-scale effect, which predominantly contributes to the dissipation. When appropriately considered, the dissipation term will increase. It can possibly lead to the correct value of cosmic dissipation, which is responsible for the present accelerated expansion of the Universe.

The organization of the chapter is as follows. In Section 3.2, we briefly analyze the resolution of the small-scale problems using the SIDM scenario and study its impact on the DM halo properties. In Section 3.3, we motivate the viscous self-interacting dark matter and calculate its bulk and shear viscosity using the kinetic theory. Further, in Section 3.4, we discuss the backreaction produced from the local inhomogeneities of viscous matter and its effect on cosmic evolution. In Section 3.5, using the VSIDM fluid model, we calculate the dissipation term and explore its contribution to the accelerated expansion of the Universe. Finally, in Section 3.6, we conclude our results.

3.2 Self-Interacting Dark Matter (SIDM)

The self-interacting dark matter is a lucrative solution to the small-scale issues discussed in chapter 1. The idea of SIDM was introduced to provide the solution for missing satellites, and core-cusp problems [156]. Since the velocity dispersion increases from the center to the outer region of the DM halo, therefore, a large DM self-interaction at the small scales causes the heat transfer between the inner and outer layers of the DM halo. This heated the central region of the halo; as a result, SIDM causes the core profile in the DM halo [208] [209][210].

One can understand the SIDM properties by analyzing the scattering rate of SIDM

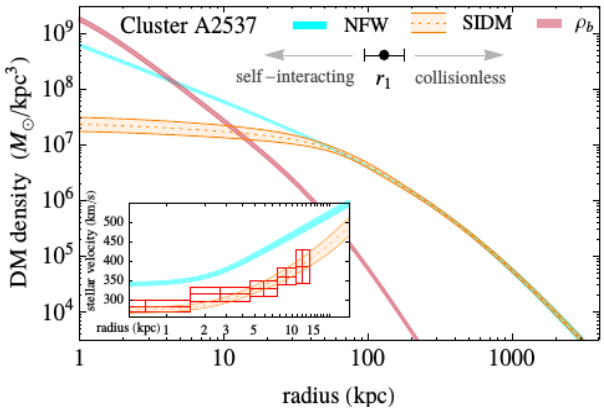

Figure 3.1: The plot of SIDM density as a function of distance for a cluster A2537. Fig. is taken from Ref.[7].

particles. Thes scattering rate is given by

$$R_{\rm scat} = \langle\sigma v\rangle \frac{\rho_{\rm DM}}{m} \approx 2.5\times10^{-8}\ {\rm Gyr}^{-1}\left(\frac{\rho_{\rm DM}}{{\rm M}_\odot{\rm kpc}^{-3}}\right)\left(\frac{v}{100{\rm kms}^{-1}}\right)\left(\frac{\sigma/m}{1{\rm cm}^2/{\rm g}}\right), \qquad (3.1)$$

where $\langle\sigma v\rangle$, $\rho_{\rm DM}$ and m, represents the velocity weighted self interacting cross-section, density, and mass of the dark matter particles, respectively. The number of times by which the DM particles scatter between themselves can be defined as, $N_{\rm scat} = R_{\rm scat}\times t_{\rm age}$, where $t_{\rm age}$ is a typical age of the DM halo. From the above equation, the behavior of the SIDM particles are interpreted as follows;

- At small scales $r \le r_1$, the DM density is large, and consequently the DM particles scatter with each other $N_{\rm scat} \ge 1$. As an example, for typical dwarf galaxies, $\rho_{\rm DM} \approx 10^8{\rm M}_\odot{\rm kpc}^{-3}, v = 50{\rm kms}^{-1}$, $\sigma/m \approx 1{\rm cm}^2/{\rm g}$ and in time scale of dwarf galaxies, $t_{\rm age} \sim 10$Gyr, we get $N_{\rm scat} = 1$ (also valid for for a typical cluster halo, $\rho \sim 2\times10^7$ M$_\odot$kpc^{-3}, $v \sim 2000$ km/s, $\sigma/m \sim 0.1$ cm^2/g and $t_{\rm age} \sim 5$Gyr) [7]. Therefore, inside the inner region of dark matter halo $N_{\rm scat} \ge 1$, so the DM behaves like a collisional dark matter.

- At a large scales $r > r_1$, the DM density falls rapidly, so the DM scattering rate becomes very small, $N_{\rm scat} < 1$. Therefore the dark matter approaches the standard collision-less CDM behavior (follow the NFW density profile) on large scales. Thus SIDM enjoys the success of the CDM on large scales.

The above properties of the SIDM halo is shown for the cluster halo in Fig. 3.1.

Further, as we discussed before, the non-linear region is well described by the numerical simulations. In order to study the SIDM properties two different simulations methods have been adopted. First, when the SIDM particles MFP is larger than the typical DM cores, $\lambda_{\rm mfp} > L_{\rm halo}$ (optically thin region) [208] [209][210][211] and second , when the SIDM mean free path is less than the DM galaxy cores scale $\lambda_{\rm MFP} < L_{\rm halo}$ (optically thick region) ie., fluid picture [212] [213][214].

It is found that in fluid discription leads to isothermal profile, which suggest a increasing density towards inner rigion of the DM halo $\rho \propto r^{-2}$ [213] [215] and core collapse [211][214]. However, in Ref. [216] it has been shown that for the present halo, the core collapse time is larger than Hubble time; therefore, the existence of the core profile is in agreement with the SIDM and gravothermal fluid model. Further, in a recent work [217], authors argued that the gravothermal collapse along with the velocity dependent cross-section can lower the subhalo density profile and explain the TBTF problems.

3.2.1 SIDM on the galactic scale

It has been found that $\sigma/m \approx 0.5 - 50$ cm^2/g produces DM halo core of size 300 – 600 pc and may solves the core-cusp and TBTF problems without any fine-tuning [218] (see also Ref. [219]). Further, including the baryons with SIDM for a given value of the DM mass halo, the DM velocity dispersion varies in the galaxies' inner region. Therefore the SIDM also explains the diverse velocity rotation curve of the spiral galaxies [220]. The presence of DM self-interactions may also suppress the halo mass function, but this is not enough to explain the missing satellite problems [208] [221].

3.2.2 SIDM with baryons and impact on the small scale cosmology

Since the real Universe also consists of the baryons. Therefore, including the baryonic contribution in the numerical simulations can shed light on the DM properties and may revise the SIDM constraints. The presence of baryons decreases the core radius but increases the inner density [222]. The hydrodynamical simulation of the dwarf galaxies (DM dominated) also indicates that the inner region of the SIDM is mildly

affected by the baryons [223]. It is because here, star formation was smooth, not bursty.

Recent numerical simulation using the baryons [224] shows that if the central region of the galaxy is steller dominated, then the SIDM halo is denser compared with the CDM-only simulation. In other cases, when the interior is DM dominated, the density profile becomes less concentrated w.r.t. the CDM-only simulations [224]. For the recent SIDM simulations, see Refs. [225][226].

To study the impact of the baryons on the DM halos, the analytical tool using the SIDM and baryonic potentials (neglecting the contribution of the feedback process) has also been developed [7][220][222]. In Ref. [222], the authors have studied the equilibrium solutions of the density profile analytically and found that the inner region follows the isothermal distribution, and the size of the DM halo is smaller compared with the SIDM-only simulations.

3.2.3 SIDM on the cluster scale

The colliding galaxy cluster also constraint the non gravitational interaction between the DM particles. The numerical simulations of the merging galaxy cluster 1E 0657-56 demands $\sigma/m < 1.25$ cm^2/g for 68% confidence limit (for null offset in subclusters) and $\sigma/m < 0.7$ cm^2/g (subclusters of equal mass to light ratio pror to merger) [227]. For more references on bullet cluster constraints, please see Refs. [228] [229] [230].

Numerical simulations suggest that the SIDM also reduce the DM density profile inside the cluster scale halo [212][231] [232]. Since the core size of the cluster scale ($\mathcal{O}$ (10 kpc)) is larger than the galaxy scale core ($\mathcal{O}$ (kpc)). Therefore, one would expect that the σ/m on the cluster scale should be small compared to the galaxy scale. The earlier investigations indicate that a velocity independent self-interaction can possibly ameliorate some of the galactic scales' small scales issues. Ref. [233] argued that for $\sigma/m = 1$ cm^2/g, the SIDM particles cannot reproduce the required core inferred from the galaxy scale (LSB and dSph) to cluster scale observations. However, for slightly small $\sigma/m = 0.1$ cm^2/g, the SIDM can produce a unified explanation of the aforementioned data without any velocity-dependent cross section [234].

The cluster scale constraints such as radial arcs and giant arcs also demands small

amount of the DM self-interaction, $\sigma/m = 0.1\text{cm}^2/\text{g}$ [235], (see also a review [236]). In the presence of scattering between the DM particles, the shape of the halo is expected to be spherical; however, many observations indicate that majority of the cluster DM halo is elliptical. Therefore, the halo's ellipticity may be used to constrain the SIDM properties of [237].

However, recent studies on cluster scale disfavor the velocity independent cross-section and demands the mild velocity-dependent cross-section. Using semi numerical method, in Ref. [7] the authors have argued that for the mild velocity-dependent self interacting cross-section, $\sigma(v)$ a variation of $\sigma/m \approx 2$ cm^2/g - 0.1 cm^2/g from galactic to cluster scale are consistent with the data.

3.2.4 Particle physics models for SIDM

The velocity dispersion of the DM particles increases from the small scale (dwarf galaxies) to a large scale (cluster). So the DM halo can act as the collider for the DM particles. It allows us a possibility to explore the theory of DM microphysics, which is valid on both scales. As inspired by the Ref. [7] (i.e., $\sigma/m \approx 2$ cm^2/g on galactic scale and $\sigma/m \approx 0.1$ cm^2/g on cluster scale), the unified explanation of galaxy and cluster demands the dependency of the DM self-interacting cross-section on to the relative velocity of the DM particles [7].

A simple model of the SIDM can be obtained by extending the SM sector with a stable real scalar having quadratic potential [238][239]. Nevertheless, this model provides a constant σ over all scales, therefore disfavored from the galactic and cluster scale data [7]. Another possibility is an exchange of the weakly coupled charged particles interacted with the DM, which can be obtained when the DM particles in charged under $U(1)$ gauge symmetry (charge conservation provides stability to DM) [240][241] [242][243]. This can be described by the Yukawa potential in non-relativistic limit and studied in perturbative [244] and non-perturbative regions [242]. The SIDM can also be a non-abelian gauge theory of the dark sector, which allows a large interaction; see review [245].

The SIDM can also be realized as a composite state like a dark atom that forms from the dark electron and dark protons. The self-interaction can arise with the scat-

tering between the dark atom and may be velocity-dependent [246]. Furthermore, the DM self-interaction may not be the elastic process. The dark sector can carry the ground states and the excited states. The DM self-interaction can cause to mediate the transition between these states, and their spectrum can be possibly detected in the DM searches [247].

3.3 Viscous Self-Interacting Dark matter

In the previous Section, we have discussed that the SIDM could ameliorate the small-scale issues faced by the CCDM. It requires a large scattering cross-section between the SIDM particles at small scales. The presence of DM-DM scattering thermalizes the halo's inner region; thus, the DM has a temperature. It is assumed that the SIDM fluid is slightly away from the local thermal equilibrium. Then the self-interaction between the DM particles causes to transfer of the energy and momentum between themselves and hence tries to attain the local thermodynamic equilibrium. Therefore one may expect that the scattering processes would lead to transport coefficients such as the thermal conductivity or the viscosity in SIDM fluid.

Here we assume that the SIDM is a viscous fluid (i.e., DM particle transfer momentum in scattering) and will not consider the thermal conductivity. Now on, we define the SIDM fluid having a viscosity as a Viscous Self Interacting Dark Matter (VSIDM), throughout our work.

3.3.1 Mean free path and validity of the fluid approximation

To evaluate the transport coefficients of the SIDM particles, we need to evaluate the mean free path (MFP) and define the scale over which the fluid description for the DM is valid. The MFP represents the average distance between the collision of particles. In our analysis, two length scales are important, firstly the microphysical scale associated with the scattering between the SIDM particles, $\lambda_{\rm SIDM}$ and secondly, is virial scale related to gravity. Here we will discuss both cases individually.

Mean free path only through SIDM microphysics

When gravity is unimportant, the hydrodynamic description for the SIDM particles will be valid when the mean free path of the dark matter particle, $\lambda_{\rm SIDM}$ is less than the typical length scale under consideration, i.e., $\lambda_{\rm SIDM} < L$. In the dilute gas approximation, the mean free path of the SIDM particle is given by [204]

$$\lambda_{\rm SIDM} = \frac{1}{\sqrt{2}}\left(\frac{1}{n\sigma}\right). \tag{3.2}$$

In a simplified manner, the expression for SIDM can be rewritten as

$$\lambda_{\rm SIDM} \sim 3\times 10^9 \left(\frac{m/\sigma}{\rm gm/cm^2}\right)\left(\frac{\rm M_\odot kpc^{-3}}{\rho}\right) \quad {\rm kpc}\,, \tag{3.3}$$

where m/σ and ρ should be taken in units of gm/cm^2 and M$_\odot$kpc^{-3}, respectively. In Ref. [207], λ_{SIDM} is estimated by approximating the dissipation term D as, $D \sim \eta(\vec{\nabla}\cdot\vec{v})^2$ and used the η with the expression for a dilute gas viz. $\eta = \rho v\lambda/3$ and then equating with Eq. (3.39). In this way, we get $\lambda_{SIDM} \sim 5(m/\rho\sigma)$. It suggest that the mean free path obtained by approximating D is larger in compare with the kinetic theory, i.e. $\frac{1}{\sqrt{2}}\frac{m}{\rho\sigma}$. Since, kinetic theory is more fundamental, therefore, in our calculation, we will use the MFP expression using the kinetic theory as given in Eq. (3.2).

The DM particles resides in the halos, named dark matter halos. To get a typical estimate of mean free path of SIDM particles at present, we use the peak central density of DM halos. for a galactic scale, following a Ref. [7], we assume $\sigma/m \sim 2$ cm^2/g. In case of large galaxy, *e.g* for a Milky way type, the DM densities are much lower and a typical estimates of density (assuming the NFW profile) are $\sim 10^6 - 10^7$ M$_\odot$kpc^{-3}[248], thus $\lambda_{\rm SIDM} \sim 1500$ kpc -150kpc, which are much larger than typical large galaxy scale (~ 30 kpc). Further, for LSB galaxies, the peak density for isothermal case are $\sim 10^7$ M$_\odot$kpc^{-3} [117], then $\lambda_{\rm SIDM} \sim 150$ kpc. For dwarf galaxies, the dark matter concentration can be a bit larger ($\sim 10^8$ M$_\odot$kpc^{-3}) [249], so $\lambda_{\rm SIDM} \sim 15$ kpc, but the typical sizes are smaller than 10 kpc. *However, we also point out that if explanation of the galaxy scale observations require large, σ/m ($\sim 10 - 50$ cm^2/g, see Refs. [218], [219]), then the MFP will be less than the size of galaxy scale, but here we will not consider these large σ/m values in our analysis.* Furthermore, for a cluster scale halos, $\sigma/m = 0.1$ cm^2/g [7], and using peak value of isothermal profile, $\rho \sim 2\times 10^7$ M$_\odot$kpc^{-3}

[7] [250, 251], $\lambda_{\rm SIDM} \sim 1$ Mpc, which is typically smaller than the typical cluster scale (~ 3 Mpc).

The above calculation suggests that for a given value of σ/m and ρ, the hydrodynamic description of SIDM particles do not valid on a galactic scale but on a cluster scale. However, we emphasize that the above MFP estimation has been performed using the peak value of the DM density and is not very correct.

Furthermore, to estimate the MFP of SIDM particles, we may apply the condition that to solve the core-cusp problem, DM particles should collide with each other at least once in the DM halo core time, see Ref. [7]. We also assume that one collision thermalizes the inner region of the SIDM halo and makes the inner profile core. In this scenario, SIDM halo (both galactic and cluster scale) may be divided into two different regions separated by length scale, r_1. The r_1 is defined in such a way that for $r \leq r_1$, SIDM particles interacts at least once, however for $r > r_1$, the SIDM particle collide less than once and behave like a collisionless dark matter, see Fig. 3.1. Since the dark matter (DM) collides at least once at $r = r_1$; therefore r_1 can be used to define a typical MFP scale, which is smaller than the virial radius of DM halos, i.e., $r_1 < \lambda_{\rm vir}$.

Since, in the SIDM description, the DM collides at least once in its halo formation, therefore, using this argument, we also define a typical MFP of the SIDM particles. The one collision in the time of halo age implies that

$$R_{\rm scat} \times t_{\rm age} \approx 1, \quad \text{or} \quad \frac{\rho\sigma}{m} v \times t_{\rm age} \approx 1. \tag{3.4}$$

where $R_{\rm scat} = (\rho\sigma v/m)$ and $t_{\rm age}$ represent the DM collision rate and the typical halo time, respectively. Further, characterizing, $\sqrt{2}\rho\sigma/m = 1/\lambda_{\rm SIDM}$ (Eq.(3.2)), the above equation can be rewritten as

$$\frac{1}{\sqrt{2}\lambda_{\rm mfp}} v \times t_{\rm age} \approx 1 \ , \tag{3.5}$$

This provide us

$$\lambda_{\rm SIDM} = \frac{v \times t_{\rm age}}{\sqrt{2}} \ . \tag{3.6}$$

For a typical galactic scale halo, $t_{\rm gal} = 10$ Gyr, and $v_{\rm gal} = 100$ Km/sec, which gives us $\lambda_{\rm gal} = 724$ kpc. Further, for a typical cluster scale halo, $t_{\rm cl} = 5$ Gyr, $v_{\rm cl} = 1000$ Km/sec, us provide $\lambda_{\rm cl} = 3.6$ Mpc.

Mean free path with gravity and SIDM microphysics

In the presence of self-interaction between SIDM particles and the gravity, effective MFP is calculated as [252]

$$\frac{1}{\lambda_{\rm eff}} = \frac{1}{\lambda_{\rm SIDM}} + \frac{1}{\lambda_{\rm vir}} \ . \tag{3.7}$$

To calculate, $\lambda_{\rm eff}$, we assume the virial radius of the galaxy (MW kind) and cluster are 30 kpc and 1 Mpc, respectively. Therefore, the effective MFP of SIDM on the galaxy and cluster scale is given by 28 kpc and 0.78 Mpc. Here we find that effective mean free path of both galaxy and cluster scale halos are smaller than their respective virial radius, i.e., $\lambda_{\rm eff} < \lambda_{\rm vir}$. *Therefore, basis on this, one can argue that the hydrodynamic description is valid from galactic to large scale.*

However, in our work, for mathematical simplicity, we assume the fluid validity starts from the cluster to a larger scale (see Section 3.4). *Hence, throughout our discussion, we consider that the cluster scale is the smallest scale from which the fluid picture of the SIDM particles can be applied unless otherwise specified explicitly.* Therefore, the length scale, where viscosity estimation has to be done, should be at least cluster or larger scales (i.e., supercluster scale); see also Refs. [207][253].

3.3.2 Calculation of bulk and shear viscosity of SIDM

Now, we will calculate the SIDM viscosity in the kinetic theory framework using the relaxation time approximation. In order to estimate the bulk and shear viscosity of the SIDM, we follow the expressions (given by Eq. (2.50) and Eq. (2.52)) derived in chapter 2. We assume that the DM is non-relativistic and follow the Maxwell-Boltzmann distribution [254]. This implies that

$$E_p \sim m + \frac{p^2}{2m} \quad \text{and} \quad f_p^0 = \exp\left(p^\mu u_\mu / T\right), \tag{3.8}$$

where p^μ and u_μ represents the four momentum and four-velocity of the SIDM particle. Further, we also assume that the sound speed of DM fluid is constant. In the DM rest frame ($u^\mu = (1,0,0,0)$), integration of Eq.(2.52) provides us an expression for the bulk viscosity as

$$\zeta = \frac{m}{12\langle\sigma v\rangle}\left[12C_n^4\left(\frac{m}{T}\right) + 5(4+9C_n^4)\left(\frac{T}{m}\right) + (-2+3C_n^2)\left\{12C_n^2 + 70\left(\frac{T}{m}\right)^2\right\} + 315\left(\frac{T}{m}\right)^3\right], \tag{3.9}$$

where, $C_n = \left.\frac{\partial P}{\partial \epsilon}\right|_n$. Also, using the same assumptions as discussed above, we can also estimate the shear viscosity from Eq.(2.50) as

$$\eta = \frac{m}{\langle\sigma v\rangle}\left(\frac{T}{m}\right)\left[1 - 7\left(\frac{T}{m}\right) + \frac{63}{4}\left(\frac{T}{m}\right)^2\right]. \tag{3.10}$$

Further, from Eq.(2.39) the expression for entropy density is obtained as

$$\mathfrak{s} = \left(\frac{m^2}{2\pi}\right)^{\frac{3}{2}}\left(\frac{T}{m}\right)^{\frac{1}{2}}\left[2 + 5\left(\frac{T}{m}\right) - 15\left(\frac{T}{m}\right)^2\right]. \tag{3.11}$$

From above equations (3.9), (3.10) and (3.11), we see that the viscous coefficients (η, ζ) and entropy density depends on the ratio of SIDM temperature to its mass (T/m) and its higher orders $O\left[(T/m)^2, ...\right]$. We assume that the VSIDM behaves like cold dark matter, hence $T/m \sim v_{\rm vd}^2 \ll 1$, where $v_{\rm vd}$ is the DM velocity dispersion on the scale of our interest. The VSIDM model respect the DM coldness criteria since from cluster to supercluster scale T/m varies from 10^{-5} to 10^{-4}. Thus, to a good approximation it is sufficient to put the linear term in T/m and neglect the higher order term in the expressions of Eq.(3.9), Eq.(3.10) and Eq.(3.11).

Therefore, in the cold dark matter approximation, the simplified form of the shear and bulk viscosity is written as

$$\eta = \frac{m}{\langle\sigma v\rangle}\left(\frac{T}{m}\right) \ , \tag{3.12}$$

$$\zeta = \frac{m}{\langle\sigma v\rangle}\left(\frac{T}{m}\right)\left[\frac{5}{3}\left(1 + \frac{9}{4}C_n^4\right) - 2C_n^2\left(1 - \frac{3}{2}C_n^2\right)\left(\frac{m}{T}\right) + C_n^4\left(\frac{m}{T}\right)^2\right] \ . \tag{3.13}$$

Here we find that the shear and bulk viscosities depend on the DM mass (m), temperature (T), velocity average scattering cross-section $(\langle\sigma v\rangle)$. We also point out that along with the above, ζ also depends on sound speed, C_n. It can also be emphasized that the above expression for shear and bulk viscosity is quite general and can be applied to the non-relativistic fluid, which follows the Maxwellian distribution and validates the relaxation time approximation.

However, we further point out that the viscosity calculation has been done in a model-independent way, so our whole calculation does not rely on any specific particle motivated model of SIDM. The viscosity calculation can be extended for a specific model (model-dependent) of SIDM. For specific particle physics model of SIDM, please see Section 3.2.

Since we can assign local thermal equilibrium in dark matter halos, we can use equipartition of energy to relate root mean square velocity with the temperature T i.e. $\frac{1}{2}m\langle v^2\rangle = \frac{3}{2}T$. Also using Maxwellian velocity distribution, the average velocity relates to the root mean square (r.m.s) velocity as

$$\sqrt{\langle v^2\rangle} = 1.085\langle v\rangle \ . \tag{3.14}$$

Thus, using above equation, Eq. (3.12) simplifies as

$$\eta = \frac{1.18}{3}\left(\frac{m}{\langle\sigma v\rangle}\right)\langle v\rangle^2 \ . \tag{3.15}$$

Further, repeating a similar exercise for Eq. (3.13), the expression of bulk viscosity is given by

$$\zeta = \frac{1.18}{3}\frac{m}{\langle\sigma v\rangle}\langle v\rangle^2\left[\frac{5}{3}\left(1+\frac{9}{4}C_n^4\right) - 5.1\left(\frac{C_n}{\langle v\rangle}\right)^2\left(1-\frac{3}{2}C_n^2\right) + 6.5\left(\frac{C_n}{\langle v\rangle}\right)^4\right] . \tag{3.16}$$

Assuming the sound speed to be zero, i.e., $C_n = 0$, the bulk viscosity is written as

$$\zeta = \frac{5.9}{9}\left(\frac{m}{\langle\sigma v\rangle}\right)\langle v\rangle^2 \ . \tag{3.17}$$

From Eq. (3.15) and Eq. (3.16), it is clear that the viscous coefficient η and ζ depend on the DM mass m, its velocity weighted average cross-section $\langle\sigma v\rangle$, and on $\langle v\rangle$. As the shear and bulk viscosity of the SIDM fluid is inversely proportional to $\langle\sigma v\rangle$, so for the non self-interacting particles $\sigma = 0$ the viscosities becomes infinitely large. In this case, the MFP, $\lambda_{\rm SIDM} \to \infty$; hence, in the lifetime of the Universe, the thermalization through the DM self-scattering never happens. Therefore, the fluid concept is not valid, so the notion of viscosity is not appropriate for such a system. Therefore for the truly non-interacting particles, the viscosities are not clearly defined. Furthermore, the interaction between the particles causes a decrease in the MFP, and the thermalization becomes possible on a scale larger than the MFP length. Therefore the fluid validity and hence the fluid properties such as viscosity can be defined.

We can now estimate the values of shear and bulk viscosity for cluster size dark matter halos. If we take $\langle\sigma v\rangle/(\langle v\rangle m)$ as an estimation of σ/m at a given scale, then η and ζ (for $C_n = 0$) are given as

$$\eta = 3.9\times10^5\left(\frac{m/\sigma}{\rm gm/cm^2}\right)\left(\frac{\langle v\rangle}{10^5{\rm m/s}}\right)\left[\frac{\rm kg}{\rm m-s}\right] \ , \tag{3.18}$$

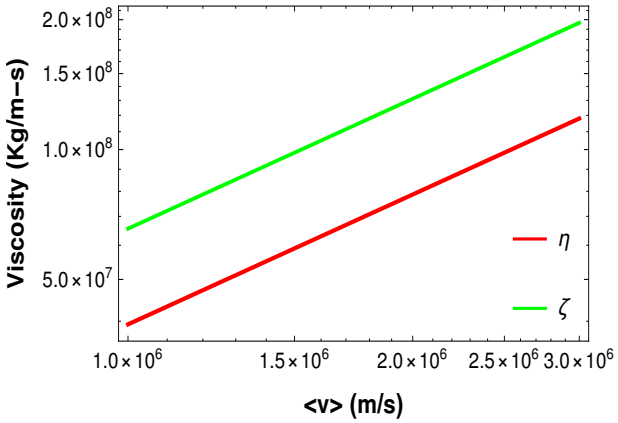

Figure 3.2: The plots of shear viscosity, η and bulk viscosity, ζ as a function of average velocity $\langle v \rangle$ at cluster scale. The ζ is estimated for vanishing sound speed limit, i.e., $C_n = 0$.

$$\zeta = 6.6 \times 10^5 \left(\frac{m/\sigma}{\mathrm{gm/cm^2}}\right)\left(\frac{\langle v \rangle}{10^5 \mathrm{m/s}}\right)\left[\frac{\mathrm{kg}}{\mathrm{m-s}}\right]. \tag{3.19}$$

In Fig. 3.2 we plot η and ζ as functions of average DM velocity $\langle v \rangle$ for different values of σ/m. Here we consider $\sigma/m \approx 0.1$ cm^2/g and average velocity varies from 10^3 kms^{-1} to 2×10^3 kms^{-1}. We note that the bulk viscosity contribution is slightly larger than the shear contribution.

As clear from the above discussion that at a late time, the contribution of shear and bulk viscosity is sufficiently large; therefore, it becomes important to study its impact on the evolution of the Universe. We will explore this in Section 3.4. To proceed further, we check whether the relaxation time approximation is valid for the SIDM halos or not.

3.3.3 Validity of relaxation time approximation for SIDM

In the previous subsection, the expression of bulk and shear viscosity of the SIDM fluid is obtained in the relaxation time approximation. This approximation assumes that the system is slightly away from the local equilibrium and acquires the equilibrium condition typically in the relaxation time. Therefore it is crucial to check the validity of the relaxation time approximation for the SIDM halos.

For this pupose, we should compare the relaxation time ($\tilde{\tau}$) with the age of the DM halo , t_{age}. The relaxation time approximation will only hold, when the DM particle

scatters with each other at least once in the DM halo formation time $t_{\rm halo}$, i.e. $t_{\rm halo}/\tilde{\tau} \approx 1$. In case of small DM halo age, $t_{\rm halo}/\tilde{\tau} < 1$, the relaxation time approximation fails to hold and one cannot apply it for the viscosity estimation. Furthermore, using Eq. (3.1) and (2.55), we infer that, $\tilde{\tau}^{-1} = R_{\rm scat}$. Therefore, using Eq. (3.1), the condition $t_{\rm age}/\tilde{\tau} \approx 1$, translates to

$$R_{\rm scat} \times t_{\rm age} = 2.4 \times 10^{-8} \left(\frac{\rho_{\rm DM}}{\rm M_\odot kpc^{-3}}\right)\left(\frac{v}{100 \rm kms^{-1}}\right)\left(\frac{\sigma/m}{1 \rm cm^2/g}\right)\left(\frac{t_{\rm age}}{\rm Gyr}\right) \approx 1. \tag{3.20}$$

We consider the age of cluster size halo to be 5 Gyr, respectively [7]. For a typical cluster size SIDM halo, core density $\rho \sim 2 \times 10^7$ $\rm M_\odot kpc^{-3}$ [7] (slightly large for the NFW profile, see Refs. [255, 256]), $v \sim 2000$ km/s and $\sigma/m \sim 0.1$ $\rm cm^2/g$ [7], thus $R_{scat} \times t_{age} \approx 2$. Therefore, the above calculations suggest that the relaxation time approximation is valid at the cluster size DM halo and hence we may assume that the DM halo are in local thermal equilibrium.

3.4 Backreaction produced from the viscous DM and its effect on cosmic evolution

In this section, we present a mathematical description of the backreaction produced from the local inhomogeneity of the Universe. Further, we explore the condition under which the backreaction produced from the inhomogeneous distribution of matter will be important and can produce the accelerated expansion of the Universe.

3.4.1 Backreaction produced from inhomogeneity of the Universe

The observations indicate that the Universe is homogeneous and isotropic on large scales, described by the FLRW metric. This is specifically true in a statistical sense. However, on a small scale, Universe is dominated by structures such as galaxies, clusters of galaxies and is inhomogeneous in nature [257]. Therefore, the FLRW metric will be perturbed.

In the standard cosmology, the evolution of the Universe is governed through Einstein's equation, which is non-linear. Therefore, the perturbation can non-linearly backreact on the background expansion. The structure formation has been studied by

considering some perturbation over the FLRW background. At the time of linear structure formation, the perturbation is small; hence do not modify the average expansion rate of the Universe. However, when structures become non-linear, the inhomogeneity becomes large (due to the structures), and hence perturbation may possibly affect the local evolution of the Universe.

The impact of inhomogeneity resulted from the geometry and matter sector of Einstein equations onto the background expansion, i.e., *backreaction effect* have been discussed in Refs. [93][258][259][260][261] [262] [263] and references therein. The backreaction effect due to metric and their impact on the cosmic evolution has been debated in the literature. In Refs. [93][94] it was reported that the local inhomogeneities are large enough to modify the background expansion and lead to the accelerated expansion. However, the authors of Refs. [95][96] argued that within the general relativity, backreaction from the local inhomogeneities is not sufficient to change the cosmic evolution and also can not account for the accelerated expansion of the Universe. For the debate on the backreaction effect, see Refs. [264] [265] [266]. However, this issue is not completely settled, and for other discussions, please see [267].

Here, our aim is to explore the backreaction generated from the matter side of Einstein equations and investigate their effect on the cosmic evolution. In this scenario, we focus on viscous dark matter and study their backreaction effect on the background evolution.

For this purpose, we apply the covariant conservation of energy-momentum and number density, given as $\nabla_\mu T^{\mu\nu} = 0$, $\nabla_\mu N^\mu = 0$. These are given by Eq. (2.15), Eq.(2.16), and Eq. (2.19). These equations involve the fluid velocity, and covariant derivative of the quantities; therefore, their estimation demands the specification of the metric tensor. Here, we assume only the scalar metric perturbation, given as

$$ds^2 = a^2(\tau)\left[-(1+2\psi(\tau,\vec{x}))d\tau^2 + (1-2\phi(\tau,\vec{x}))d\vec{x}\cdot d\vec{x}\right] \ , \tag{3.21}$$

and neglect the vector and tensor perturbations. In the above equation, $a(\tau)$ is scale factor and ψ, ϕ are the potentials, respectively. We also point out that since we are interested in the bacreaction from small scales, therefore we may also use inhomogeneous metric in our calculation. Further, using scalar metric perturbation Eq. (3.21),

the four velocity is obtained as

$$u^{\mu} = \frac{dx^{\mu}}{(-ds^2)^{\frac{1}{2}}} \equiv (\gamma, \gamma v^i) \ , \tag{3.22}$$

$$\text{where,} \quad \gamma \equiv \frac{1}{a(\tau)\left[(1+2\psi(\tau,\vec{x})) - (1-2\phi(\tau,\vec{x}))\delta_{ij}v^i v^j\right]^{1/2}} \ . \tag{3.23}$$

Here, $v^i = \dfrac{dx^i}{d\tau}$ represents the peculiar velocity. Therefore using Eq.(3.22) and upto linear order of potentials, we get

$$\nabla_\mu u^\mu = \frac{1}{a}\left(\vec{\nabla}\cdot\vec{v} + 3\frac{1}{a}\frac{da}{d\tau} + \psi\vec{\nabla}\cdot\vec{v} - 3\frac{1}{a}\frac{da}{d\tau}\psi - 3\frac{d\phi}{d\tau} - 3\vec{v}\cdot\vec{\nabla}\phi\right). \tag{3.24}$$

Now we focus on the situation at the late time of the cosmic evolution. Following a Ref. [92], we consider that at the late time of the cosmological evolution, perturbations are small, $\phi, \psi \ll 1$ and varring slowly with the time, $d\phi/d\tau \sim \mathcal{H}\phi$ (also $d\psi/d\tau \sim \mathcal{H}\psi$), where $\mathcal{H} = da/ad\tau = aH$. The one of the reason behind this assumption lies in the fact that to form the cold dark matter halos one requires $\phi > T_\chi/m_\chi$, where T_χ and m_χ represent the temperature and mass of the DM respectively [156]. This suggest, $\phi > v_{\rm vd}^2/3$, where $v_{\rm vd}^2 = 3T_\chi/m_\chi$ is the velocity dispersion of the DM particles. For the scale of our interest (cluster to large scales), $v_{\rm vd}^2 < 10^{-4}$ [7], therefore $\phi > 10^{-4}$. In our work, for simplicity, we have assumed $\phi \sim 10^{-4} \ll 1$.

Further, we also assume small fluid velocity $\vec{v}^2 \ll 1$, which is relevant for cosmological purposes. So with these assumptions, Eq. (3.24) simplifies as $\nabla_\mu u^\mu \approx \dfrac{1}{a}\left(\vec{\nabla}\cdot\vec{v} + 3\mathcal{H}\right)$, which is free from the potential terms. Therefore using Eq. (3.26), the evolution equation for energy density is given by

$$\frac{d\epsilon}{d\tau} + \vec{v}\cdot\vec{\nabla}\epsilon + (\epsilon+P)\left[3\mathcal{H} + \vec{\nabla}\cdot\vec{v}\right] = \frac{\zeta}{a}\left[3\mathcal{H} + \vec{\nabla}\cdot\vec{v}\right]^2 + \frac{\eta}{a}\left[\partial_i v_j + \partial_j v_i - \frac{2}{3}\left(\vec{\nabla}\cdot\vec{v}\right)^2\right] \ . \tag{3.25}$$

Furthermore, taking the spatial average of Eq. (3.25) and throwing out the surface terms, one can get the average energy density evolution equation as [92]

$$\frac{1}{a}\frac{d\langle\epsilon\rangle_s}{d\tau} + 3H\left[\langle\epsilon\rangle_s + \langle P\rangle_s - 3\langle\zeta\rangle_s H\right] = D \ , \tag{3.26}$$

where, the D term is given by

$$D = \frac{1}{a^2}\left\langle\eta\left[\partial_i v_j\partial_i v_j + \partial_i v_j\partial_j v_i - \frac{2}{3}\partial_i v_i\partial_j v_j\right]\right\rangle_s + \frac{1}{a^2}\left\langle\zeta[\vec{\nabla}\cdot\vec{v}]^2\right\rangle_s + \frac{1}{a}\left\langle\vec{v}\cdot\vec{\nabla}(P - 6\zeta H)\right\rangle_s \ . \tag{3.27}$$

and $\langle A\rangle_s$ is the spatial average of quantity A. In the above equation, the D term represents the backreaction originated from the matter side, which affects the evolution of the background quantity, average energy density ($\langle\epsilon\rangle_s$). It is evident that in the RHS of Eq. (3.27), the shear and bulk viscosity contribution are positive, so the first and second terms in D corresponds to the gain in internal energy on the cost of fluid velocity gradient dissipation. The third term indicates the energy generation due to the pressure gradient.

The dissipative strength by which the $\langle\epsilon\rangle_s$ modifies will depend on the viscosity, fluid velocity gradient, and equation of state of the DM fluid. At earlier times (when Universe was in a linear regime), the cosmic viscosity and velocity gradient were small, so one expects the dissipation effect was small. However, at the late time of cosmic evolution, non-linear structure formation takes place; therefore, the dissipation may be important and possibly show a sizable effect. Here it is important to mention that throughout the cosmic evolution, the average number density does not depend on the dissipation term D and changes only through the Hubble dilution [92].

In addition to Eq. (3.26), we also need Einstein's equation to get the equation for the Hubble expansion rate. For this purpose, we use the spatial average of the trace of Einstein equation $\langle G^{\mu}_{\mu}\rangle_s = -8\pi G\langle T^{\mu}_{\mu}\rangle$ and find as [92]

$$\frac{1}{a^3}\frac{d^2a}{d\tau^2} = \frac{1}{a}\frac{dH}{d\tau} + 2H^2 = \frac{4\pi G\langle\epsilon\rangle_s}{3}\Big(1 - 3\hat{w}_{\rm eff}\Big), \tag{3.28}$$

where, $\hat{w}_{\rm eff}$ represents effective equation of state (EoS), defined as

$$\hat{w}_{\rm eff} = \frac{\langle P\rangle_s + \langle\Pi_B\rangle_s}{\langle\epsilon\rangle_s} \ . \tag{3.29}$$

To study the evolution equation for VSIDM fluid, we need to solve the coupled differential equations (3.26) and (3.28) along with the average velocity evolution equation obtained using Eq. (2.16). But here, we are interested in the present epoch; therefore, we will not worry about the velocity equation and put their value using the present observation whenever it is required.

3.4.2 Criteria for the cosmic acceleration

Furthermore, our interest is to study the behavior of decelerated to accelerated transition in the light of cosmic dissipation arises due to the VSIDM. This requires to derive

the equation for deceleration parameter (related with the Hubble expansion rate as, $q = -1 - \frac{1}{aH^2}\frac{dH}{d\tau}$), which can be obtained by using Eq. (3.26) and Eq. (3.28) as [92]

$$-\frac{dq}{d\ln a} + 2(q-1)\left[q - \frac{(1+3\hat{w}_{\rm eff})}{2}\right] = \frac{4\pi GD}{3H^3}(1-3\hat{w}_{\rm eff}) \ . \tag{3.30}$$

This indicates that the evolution of the deceleration parameter depends on the DM dissipation and its effective EoS. For the dissipationless DM fluid, $\eta = \zeta = \partial v = 0$ (i.e., $D = 0$) and cold dark matter fluid, $\hat{w}_{\rm eff} = 0$. Furthermore, in the assumption of $dq/d\ln a = 0$, Eq. (3.30) provides $q = 1/2$. It suggests that that the Universe is in the decelerating phase. Clearly, this phase corresponds to the matter-dominated phase, and structure formation has not taken place. In this case, the cosmological evolution is governed by the CDM.

Further, using Eq. (3.30) and in the assumption $|dq/d\ln a| \ll 1$, one can obtain the criteria for the accelerated expansion of the Universe ($q < 0$) as

$$\frac{4\pi GD}{3H^3} > \frac{1+3\hat{w}_{\rm eff}}{1-3\hat{w}_{\rm eff}} \ . \tag{3.31}$$

From the above equation, it is clear that sufficiently large and positive D can lead to the accelerated expansion, provided $\hat{w}_{\rm eff} \neq 1/3$. So we may expect that this can be only possible at the late time of the cosmic evolution because, at a late time, the non-linear structure formation takes place. As a consequence, the viscosity and fluid velocity gradients acquire large values, and consequently, the dissipative term becomes important. Therefore for the cold SIDM fluid, $\hat{w}_{\rm eff} \ll 1$, one can therefore writes condition for accelerating Universe using Eq. (3.31), to be

$$\frac{4\pi GD}{3H^3} > 1 \ . \tag{3.32}$$

From the present epoch observations, $q \approx -0.6$ [268]. So in assumption of $\hat{w}_{\rm eff} = 0$ and $|dq/d\ln a| \ll 1$, a typical value of $4\pi GD/3H^3$ at present is $4\pi GD/3H_0^3 \approx 3.5$ [92].

3.5 Present accelerated expansion of the Universe in VSIDM model

Here, using the formalism developed above, we explore the effect of VSIDM on the evolution of the Universe. For this, we will calculate the dissipation term that requires

an estimation of spatial averaging. To do so, firstly, we need to define the scale between which spatial average has to be calculated.

Scale of the spatial averages

Below we discuss the small and large relevant scales considered in this analysis.

- **Large scales, $k_{\rm min}$:** The upper limit of the spatial average will be the largest size of the Universe up to which casual physics works, i.e., the size of the horizon at present. Therefore, $k_{\rm min} = k_H = 2\pi/L_H$, where L_H is the length scale corresponding to the horizon scale. However in our case we consider the homogeneity scale as a large scale, so $k_{\rm min} = \dfrac{2\pi}{100{\rm Mpc}}$. It is because our interest is to estimate the effect of the local inhomogeneities on the background quantities such as Hubble expansion rate and deceleration parameter, which is defined on the homogeneity scale.

- **Small scale, $k_{\rm max}$:** The lower limit of the spatial average is defined on the scale from which the DM fluid description starts. We have seen that the fluid description of the DM particle is valid on the scale cluster to a larger scale; therefore, we consider $k_{\rm max} = 2\pi/L_C$, where L_C is the value of typical cluster length scale.

Furthermore, to see the strength of the dissipative effect of SIDM on the evolution of the Universe, we need to provide an estimation of D. From equation (3.27), we see that the term D crucially depends on the spatial average of the velocity gradient and viscosities. Thus its calculation demands the explicit estimation of the spatial averages of quantities involved. To do so, we will follow two different approaches, first using a simplified approach where the velocity gradient is assumed to be a constant and second, through more rigorous analysis considering a more realistic velocity profile.

3.5.1 Dissipation estimation - a simplified approach

In this approach, without going into the detailed calculation of the spatial averages, we will approximate the dissipation term D using the following simplifying assumptions:

(1) We confine our analysis at the present epoch, thus we set $H = H_0$ and scale factor $a \equiv a_0 = 1$.

(2) We assume that η, ζ are do not vary over the spatial region, therefore we assume i.e, $\langle\eta\rangle_s = \eta$ and $\langle\zeta\rangle_s = \zeta$ [92]. We point that the viscosity should depend on the density for a realistic calculation of the term like $\left\langle\zeta[\vec{\nabla}\cdot\vec{v}]^2\right\rangle_s$. The, estimation of this term using the density dependence viscosity, i.e., $\zeta \propto \rho^\alpha$ is a numerically challenging task and will leave it for the future.

(3) The gradients and curls of velocity fields are prominent at a scale L, which we approximate as $\partial \sim 1/L \equiv 1/(R_H\alpha)$, where $R_H = H^{-1}$ is the Hubble size and $\alpha = L/R_H = LH$ is the fraction of Hubble size where the derivatives are prominent.

(4) We replace the spatial averages of the velocity gradient by its average value between the fluid element scale to homogeneity scale, viz 3 Mpc $\leq L \leq$ 100 Mpc. Therefore we approximate $\langle\vec{\nabla}\cdot\vec{v}\rangle_s \sim \langle v\rangle_s/L$, where $\langle v\rangle_s/L$ represents the spatial average velocity gradient.

Furthermore, before estimating the typical value of average velocity gradient, firstly, we argue that the small length scale physics is contributing significantly to the viscosity contribution and hence in the velocity gradient estimation. The scale from which the viscosity effect becomes prominent can be inferred from the Navier-Stokes equation, given by [172]

$$\rho\left(\partial_t u^i + u^j\cdot\nabla_j u^i\right) = -\frac{\partial P}{\partial x^i} - \frac{\partial}{\partial x^j}\left[-\eta\left(\frac{\partial u^i}{\partial x^j} + \frac{\partial u^j}{\partial x^i} - \frac{2}{3}\frac{\partial u^k}{\partial x^k}\delta^{ij}\right) - \zeta\frac{\partial u^k}{\partial x^k}\delta^{ij}\right] \quad . \tag{3.33}$$

Now since the viscous coefficient is proportional to the mean free path, $\eta = \rho v\lambda_{\rm mfp}/3$, therefore if we compare the second or third term on the right-hand side with the last term on the left-hand side, we find that as the length scale increases the viscous contribution decreases and hence can be ignored. Thus we may conclude that the major contribution from the viscous term comes from the smaller length scales. Since the smallest length scale at which we can apply the hydrodynamic approximation is larger than the mean free path (comparable to the cluster scales). Therefore the viscous term dominates around the cluster scale.

Furthermore, to estimate the representative value of the average velocity gradient, we do a rough calculation using the dimensional analysis. We divide the Universe into two different regions, first, small scale, where the inhomogeneity is large (cluster size scale to a few times higher than this, viz, 3 Mpc $\leq L \leq$ 20 Mpc) and second, large scale, where the Universe is less inhomogeneous or homogeneous, i.e., 20 Mpc $<$

$L \leq 100$ Mpc. On a small scale, due to the presence of inhomogeneity, the velocity gradient is influenced by the local dynamics. For typical cluster scale $L \sim 3$ Mpc, fluid velocity $\langle v\rangle_s \sim 1000$ km/sec, so $\langle v\rangle_s/L \sim 10^{-17}$ sec^{-1} and for large scale $L \sim 20$ Mpc and $\langle v\rangle_s \sim 6000$ km/sec so $\langle v\rangle_s/L \sim 9 \times 10^{-18}$ sec^{-1}. This suggests that the velocity gradient decreases but in a first approximation, we treat the velocity gradient as a constant on these scales.

However, as the scales become large and approach towards homogeneity viz 20 Mpc $< L \leq 100$ Mpc, the fluid velocity gradient decreases significantly, and they do not contribute much in dissipation. Furthermore, a more accurate estimation of the dissipation (as discussed in the next subsection 3.5.2) also validates our assumption.

(5) We assume SIDM is cold, therefore $\hat{w}_{\rm eff} = \langle P\rangle_s + \langle \Pi_B\rangle_s = 0$. Therefore

$$\langle P\rangle_s = -\langle \Pi_B\rangle_s = \zeta\left[\langle \nabla\cdot\vec{v}\rangle_s + 3H\right] = \zeta\left[\left(\frac{H\langle v\rangle_s}{\alpha}\right) + 3H\right]. \tag{3.34}$$

Using above approximations, first and second term of Eq. 3.27 simplifies as

$$\frac{4\eta}{3a^2}\left(\frac{\langle v\rangle_s}{L}\right)^2 \quad \text{and} \quad \frac{\zeta}{a^2}\left(\frac{\langle v\rangle_s}{L}\right)^2 \ . \tag{3.35}$$

Whereas the last term in Eq. (3.27) can be approximated as

$$\langle \vec{v}\cdot\vec{\nabla}(P - 6\zeta H)\rangle_s \sim \zeta\left(\frac{H\langle v\rangle_s}{\alpha}\right)^2\left[1 - 3\,\frac{\alpha}{\langle v\rangle_s}\right] \ . \tag{3.36}$$

Therefore in above approximations, D term given in Eq. (3.27) can be written as

$$D = \left(\frac{H\langle v\rangle_s}{\alpha}\right)^2\left[\frac{4}{3}\eta + \zeta\left(2 - 3\,\frac{\alpha}{\langle v\rangle_s}\right)\right] \ . \tag{3.37}$$

We point out for the length scale over which we are interested, i.e, galactic and cluster scale, $\alpha/\langle v\rangle_s < 1$. For example, a typical cluster size halo $L = 3$ Mpc, $\alpha = 7 \times 10^{-4}$ and $\langle v\rangle_s = 1000$ km-sec^{-1}, so $\alpha/\langle v\rangle_s = 0.2$. So one can neglect the last term of RHS in Eq. (3.37). With these assumptions, D terms simplify as

$$D = (1+z)^2\left(\frac{\langle v\rangle_s}{L}\right)^2\left[\frac{4}{3}\eta + 2\zeta\right] \ . \tag{3.38}$$

Furthermore using Eqs. (3.15), (3.16) in Eq. (3.38), we get the form of dissipation term at present epoch as

$$D = \frac{16.32}{9}\langle v\rangle_s^2\langle v\rangle^2\left(\frac{m}{\langle\sigma v\rangle}\right)\left(\frac{H}{\alpha}\right)^2. \tag{3.39}$$

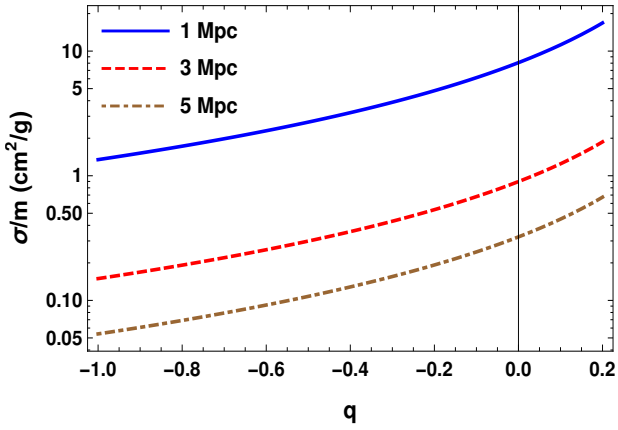

Figure 3.3: The plot between σ/m vs q for different $\langle v\rangle$ and α cluster scale. It suggest that the larger negative value of q is supported by smaller values of σ/m.

Hence to estimate the strength of the dissipative effect, we need to provide the $\langle\sigma v\rangle/m$, $\langle v\rangle$, $\langle v\rangle_s$ and the scale of the spatial average, (α/H).

Furthermore, now our main interest is to study the DM properties and their impact on the accelerated expansion of the Universe. This can be obtained by applying Eq. (3.30) and Eq. (3.39) as

$$\frac{\langle\sigma v\rangle}{m} = \frac{65.28\pi}{27H_0^3 m_{pl}^2}\left(\frac{H}{\alpha}\right)^2\left[\frac{\langle v\rangle_s^2\,\langle v\rangle^2}{(q-1)(2q-1)+dq/d\ln a}\right]. \tag{3.40}$$

where $m_{pl}^2 \equiv 1/G$. In the assumptions, $\langle\sigma v\rangle \sim \sigma\langle v\rangle$ and $dq/d\ln a \ll 1$ at present, the above equation simplifies as

$$\frac{\sigma}{m} = 4.8\times10^{-3}\left(\frac{\text{Mpc}}{L}\right)^2\left[\frac{1}{(q-1)(2q-1)}\right]\left[\frac{\langle v\rangle_s^{2/3}\langle v\rangle^{1/3}}{100\text{Km sec}^{-1}}\right]^3 \quad \frac{\text{cm}^2}{\text{g}}. \tag{3.41}$$

where, the velocities and length scale should be written in units of the Km-sec^{-1} and Mpc, respectively. This equation suggests that the σ/m depends on the fluid length scale, corresponding velocity, and deceleration parameter.

For simplicity, we consider that both the average dark matter particle velocity and fluid velocity is same, i.e., $\langle v\rangle \sim \langle v\rangle_s$. In this approximation, we estimate the fluid velocity gradient on the cluster to larger scales. The above approximation is based on the fact that the viscosity contribution is dominated by only the smallest scale, which is the cluster scale here. The theoretical behavior of σ/m as a function of $\langle v\rangle$ for galactic and cluster size DM halos are presented in figure 3.3. For plotting, we choose $\langle v\rangle$ to be $\langle v\rangle \sim 10^3$ kms^{-1} for a cluster size halo as a representative number. The above figures

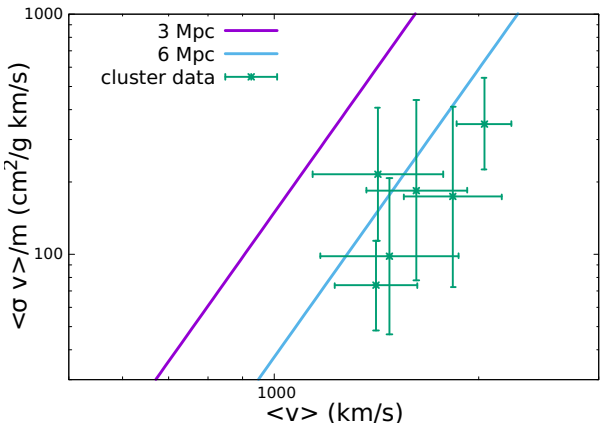

Figure 3.4: Plot of $\langle\sigma v\rangle/m$ *vs* $\langle v\rangle$ for cluster size dark halo for $q = -0.6$. The cluster data points are taken from Ref. [7].

indicate that the larger negative values of q are preferred by the smaller values of σ/m and vice versa. It is evident that the present observed deceleration parameter ($q \simeq -0.6$) can be obtained for a dark matter halo of roughly 5 Mpc size with $\sigma/m \sim 0.1$ cm^2/g.

Furthermore, to confirm our results, we also plot $\langle\sigma v\rangle/m$ a function of $\langle v\rangle$, at cluster scales along with the numerical simulated astrophysical data points inferred from the [7] in figure 3.4. Here, we have taken 6 relaxed cluster data (MS2137, A611, A963, A2537, A2667 and A2390), which are appropriate for spherical modelling [251][250]. Here the lines corresponds for present cosmic acceleration, i.e., $q = -0.6$. From Fig. 3.4, it becomes clear that the scale larger than the cluster scale $\sim$ 6 Mpc fit the data. This result also supports our theoretical estimate that the accelerated expansion of the Universe can be possibly realized by SIDM viscosity with the averaging scale larger than the cluster scale.

3.5.2 Dissipation estimation - a more realistic approach

In earlier case, the dissipation term has been calculated after replacing the , that velocity gradient is c, i.e., $\langle\vec{\nabla}\cdot\vec{v}\rangle_s \sim \langle v\rangle_s/L$. However, to estimate the D term more accurately, one needs to consider the realistic model of velocities. Here we have considered the velocity gradient information using the power spectrum as discussed in the literature.

To start with, firstly we simplify the dissipation term (defined in Eq. (3.27)), by decomposing the velocity gradients in term of the divergence, $\theta = \vec{\nabla}\cdot\vec{v}$, and curl of

the velocity vector, $\vec{w} = \vec{\nabla} \times \vec{v}$. Further, considering η and ζ as a constant in space, i.e, $\langle \eta \rangle_s = \eta$ and $\langle \zeta \rangle_s = \zeta$, the dissipation term (given in Eq. (3.27)) simplifies in Fourier space of $\theta, \vec{w}$ and P (defined by $\theta(\vec{x}) = \int \bar{\theta}(\vec{k})\, e^{i\vec{k}\cdot\vec{x}} d^3k$) as

$$D = \frac{1}{a^2}\left(\zeta + \frac{4}{3}\eta\right)\int P_{\theta\theta}(\vec{k})\, d^3k + \frac{\eta}{a^2}\int (P_w)_{ij}\,(\vec{k})\, d^3k - \frac{1}{a}\int P_{\theta p}(\vec{k})\, d^3k \ , \tag{3.42}$$

where the different power spectra are defined by

$$\langle \bar{\theta}(\vec{k}_1)\bar{\theta}(\vec{k}_2)\rangle = \delta^{(3)}(\vec{k}_1 + \vec{k}_2) P_{\theta\theta}(\vec{k}_1) \ ,$$

$$\langle \bar{w}_i(\vec{k}_1)\bar{w}_j(\vec{k}_2)\rangle = \delta^{(3)}(\vec{k}_1 + \vec{k}_2)\,(P_w)_{ij}\,(\vec{k}_1) \ ,$$

$$\langle \bar{\theta}(\vec{k}_1)\bar{P}(\vec{k}_2)\rangle = \delta^{(3)}(\vec{k}_1 + \vec{k}_2) P_{\theta P}(\vec{k}_1) \ .$$

In the assumption of $P_{\theta P}(\vec{k}) = 0$ and irrotational flow, i.e., $\vec{w} = 0$ (and hence, $(P_w)_{ij}\,(\vec{k}) = 0$), dissipation term can be approximated as

$$D = \frac{1}{a^2}\left(\zeta + \frac{4}{3}\eta\right)\int_{k_{\rm min}}^{k_{\rm max}} P_{\theta\theta}(\vec{k})\, d^3k \ , \tag{3.43}$$

where the integration limit, $k_{\rm min}$ and $k_{\rm max}$ corresponds for the minimum and maximum values of the wavenumber between which the averaging should be estimated. We focus our analysis on the dimensionless dissipation term, $\bar{D}$ defined as

$$\bar{D} = \frac{4\pi G D}{3H^3} = \frac{4\pi G}{3H}\left(\zeta + \frac{4}{3}\eta\right)\int_{k_{\rm min}}^{k_{\rm max}} P_{\theta\theta}(\vec{k})\, d^3k \ . \tag{3.44}$$

From the above equation, we see that to estimate the dissipation, we have to evaluate velocity divergence power spectrum, $P_{\theta\theta}(\vec{k})$.

Velocity divergent power spectrum (VDPS)

From the above discussion, it is clear that the calculation of dissipation term requires the spatial average of $P_{\theta\theta}(k)$ from cluster to a larger scale. The velocity divergence and density perturbations equations are coupled via the Einstein equations and energy-momentum conservation equations. Therefore $P_{\delta\delta}(k)$ and, $P_{\theta\theta}(k)$ are related with each other.

To proceed further, firstly, we estimate the matter power spectrum for SIDM particles. Fig. 3.5 shows the linear matter power spectrum for the SIDM and CDM particles. It suggests that the linear power spectrum of the SIDM matches with the ΛCDM

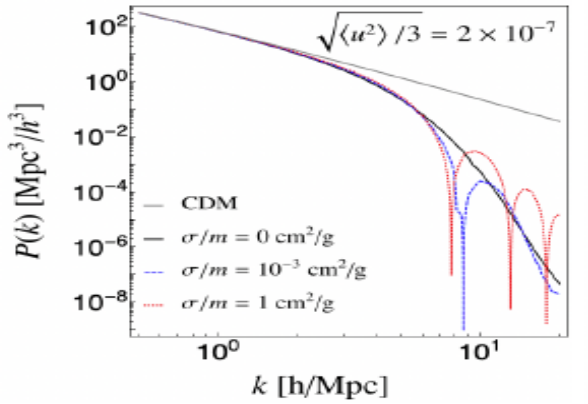

Figure 3.5: The linear matter power spectrum is plotted for the SIDM and CDM particles (Fig. is taken from Ref.[8]). The SIDM power spectrum matches the CDM prediction up to $k < 2h$ Mpc^{-1}.

model for $k < 2h$ Mpc^{-1}. Therefore we safely apply the LMPS of CDM for SIDM up to the scale, $k < 2$ Mpc^{-1}.

In this work, we will use the formalism of Ref. [9] to calculate $P_{\theta\theta}(k)$. In this formalism, the dimensionless velocity divergence power spectrum, $P_{\tilde{\theta}\tilde{\theta}}(k)$, has been fitted with the matter density power spectrum, $P_{\delta\delta}(k)$ via [9]

$$P_{\tilde{\theta}\tilde{\theta}}(z,k) = g[P_{\delta\delta}(z,k)] = \frac{\alpha_0 \sqrt{P_{\delta\delta}(z,k)} + \alpha_1 P^2_{\delta\delta}(z,k)}{\alpha_2 + \alpha_3 P_{\delta\delta}(z,k)} \ , \tag{3.45}$$

where $\tilde{\theta}$ is the dimensionless quantity given by

$$\tilde{\theta} = \frac{\vec{\nabla}\cdot\vec{v}}{aHf} = \frac{\theta}{aHf} \ , \quad \text{where} \quad f = \frac{d\ln\delta}{d\ln a} \ , \tag{3.46}$$

where, $\delta(z,\vec{k}) = \left(\epsilon(z,\vec{k}) - \bar{\epsilon}\right)/\bar{\epsilon}$ represents the density perturbations, and $\bar{\epsilon}$ is the background energy density. Here, $P_{\delta\delta}(z,k)$ represent the matter power spectrum and f describes the growth of density perturbation. Further, $\alpha_0 = -12480.5$, $\alpha_1 = 1.824$, $\alpha_2 = 2165.87$, $\alpha_3 = 1.796$.

Furthermore, using Eq. (3.45) and Eq. (3.46), we get

$$P_{\theta\theta}(z,k) = (aHf)^2 \ P_{\tilde{\theta}\tilde{\theta}}(z,k) \ . \tag{3.47}$$

Here f describes the growth of density perturbations and is cosmological model dependent quantity. Further, we estimate $P_{\tilde{\theta}\tilde{\theta}}(z,k)$, using the linear and non-linear matter power spectrum, $P_{\delta\delta}(z,k)$ of CDM from the *CLASS* code [5].

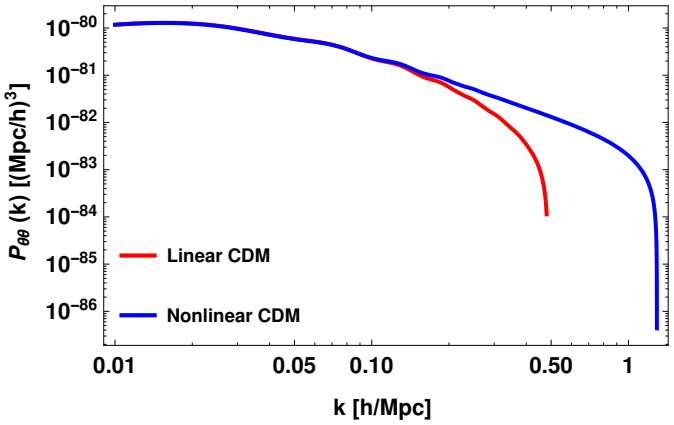

Figure 3.6: The plot of linear and nonlinear velocity divergence power spectrum of CDM using the *CLASS* code [5] and the fitting formula developed in Ref.[9].

In Fig. 3.6, we plot the $P_{\tilde{\theta}\tilde{\theta}}(z=0,k) = P_{\theta\theta}(k)$ as a function of the scale, k. We point out that, for some large k, $P_{\theta\theta}(k)$ becomes negative for both linear and non-linear power spectrum of CDM. It happens when $k > 0.48h$ Mpc^{-1} for LMPS and $k > 1.25h$ Mpc^{-1} for NLMPS. In the light of this, we assume that the fitting function for $P_{\tilde{\theta}\tilde{\theta}}(z,k)$ is valid on the scale upto which it is positive, i.e., $P_{\tilde{\theta}\tilde{\theta}}(z,k) > 0$. Therefore, our estimation of the $P_{\theta\theta}(k)$ is valid only upto $k = 0.48h$ Mpc^{-1} for LMPS, and $k = 1.25h$ Mpc^{-1} for NLMPS of CDM.

Estimation of the dissipation term

Here, we investigate the dependency of cosmic dissipation on the scale, k. For this purpose, we plot the dimensionless dissipation term, $\bar{D}$ as a function of k in Fig. 3.7. We consider $f = [\Omega_M(0)]^{0.6}$ and $k_{\rm min} = 10^{-3}h$ Mpc^{-1}, where, $\Omega_M(0)$ is the ratio of matter density to critical energy density at present. From Fig. 3.7, it is clear that the highest contribution in the dissipation comes from the largest k (smallest scale), and the small k (large scale) contribution is insignificant. This result also supports our expectation that the velocity gradient will be large on a small scale where the inhomogeneities are large, but on the large scales where the Universe is homogeneous and isotropic, the velocity gradients should be small. Therefore the contribution of small k should be very insignificant in the dissipation estimation.

As the small scale contributes predominantly in dissipation, therefore, we are interested in estimating the dissipation term on the largest k (smallest scale), which is

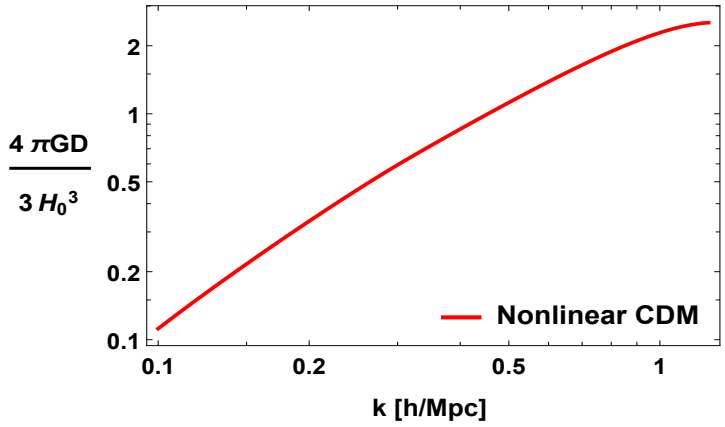

Figure 3.7: The plot of dimensionless dissipation term for non-linear CDM as a function of the k, where $k_{\rm min} = 10^{-3}h$ Mpc^{-1} and $k = k_{\rm max}$.

defined on the scale from where the SIDM fluid validity starts. We assume that the fluid description is defined on the length scale larger than two times of the mean free path of SIDM particles. This implies, $L \geq 2L_{\rm mfp}$, or equivalently $k_{\rm max} \leq k_{\rm mfp}/2$, where $k_{\rm mfp} = 2\pi/L_{\rm mfp} = 4.5h$ Mpc^{-1}. As the dominant contribution in the dissipation comes via the smallest scales, therefore to calculate the correct value of the dissipation term, we need to provide $P_{\theta\theta}(k)$ on $k = k_{\rm max} = k_{\rm mfp}/2$.

Nevertheless, our study of $P_{\theta\theta}(k)$ is limited only for $k_{\rm max} = 0.48h$ Mpc^{-1} for LMPS, and $k_{\rm max} = 1.25h$ Mpc^{-1} for NLMPS of CDM. This provides us, $\bar{D} = 0.55$ and $\bar{D} = 2.52$ corresponding to velocity divergence power spectrum estimated using the LMPS and NLMPS. Furthermore, it is important to point out that the value of the dissipation term calculated here, i.e., $\bar{D} = 2.52$ is slightly smaller than the required values corresponding to the present cosmic acceleration, i.e., $\bar{D} = 3.5$. This may possibly happen because, in our analysis, we are limited up to $k = 1.25h$ Mpc^{-1} (for NLMPS); therefore we cannot calculate the correct value of dissipation.

However, we hope that using the correct form of $P_{\theta\theta}$ at $k_{\rm max} = k_{\rm mfp}/2$, the dissipation term will increase, and one may get the sufficient dissipation that causes to the current accelerated expansion of the Universe.

3.5.3 VSIDM coldness paradigm

As we have discussed above, the viscous dissipation required for the present cosmic acceleration must be obtained from the cluster scale. To arrive at this conclusion, we assume the DM as cold fluid, for which the effective equation of state. $\hat{w}_{\rm eff} \approx 0$. Here, we estimate $\hat{w}_{\rm eff}$ on the cluster scale, where the dissipation is important. For a non-relativistic Maxwell-Boltmann distribution, one can write the relationship between the kinetic pressure and the number density as $P = nT$. Using equipartition arguments, this can be rewritten as $P = \epsilon\langle v\rangle^2/3$. For the cluster size DM halo, $\langle v\rangle \sim 10^{-3}$, so this provide, $\langle P\rangle_s/\langle\epsilon\rangle_s \sim 10^{-6}$. The second term in $\hat{w}_{\rm eff}$ is bulk pressure and given by, $\langle\Pi_B\rangle_s = -\zeta(\langle\nabla\cdot\vec{v}\rangle_s + 3H_0)$. To estimate gradients we approximate $\partial \sim 1/L$ where L is the size of the DM halo. For core density, $\epsilon \sim 5\times10^{-1}$ $\mathrm{M_\odot pc^{-3}}$ [250, 251] and $L \sim 1$ Mpc on the cluster DM halo, we find $\langle\Pi_B\rangle_s/\langle\epsilon\rangle_s \sim -10^{-7}$. Hence we find $\hat{w}_{\rm eff} \ll 1$ on the cluster DM halo and hence the coldness paradigm is valid for the SIDM fluid.

Limitations of our analysis

Our estimation of dissipation is based on the assumption that the SIDM power spectrum matches the ΛCDM prediction for $k \leq 2h$ $\mathrm{Mpc^{-1}}$. However, on a small scale, i.e., $k > 2h$ $\mathrm{Mpc^{-1}}$ SIDM power spectrum starts deviating from the ΛCDM model prediction. It has also been found that the effect of SIDM viscosity becomes important on the small scales, which effectively slows down the growth of density perturbations and hence dampens the structure formation. Therefore SIDM viscosity will modify both growth factor, f and the velocity divergence power spectrum, $P_{\theta\theta}$. Furthermore, we have also ignored the contribution of $(P_w)_{ij}(\vec{k})$ and $P_{\theta P}(\vec{k})$ in the dissipation estimation. However it is found in Ref. [269], that on the small scale, the contribution of $(P_w)_{ij}(\vec{k})$ may not be negligible. Therefore, to obtain the actual value of the cosmic dissipation, one needs to incorporate the SIDM physics on small scales. Inclusion of the SIDM properties in the non-linear power spectrum (both the density and velocity) is a numerically challenging task. I would like to pursue this in the future.

3.6 Conclusions

This chapter discussed the viscous self-interacting dark matter and explored its effect on the late time of cosmic evolution. To investigate the scale over which the transport coefficient, such as bulk and shear viscosity of SIDM, should be estimated, we calculate the MFP of SIDM particles. We report that for SIDM, the fluid description is valid from scale larger to galactic size DM halo. However, for mathematical simplicity, we assume fluid validity on a scale larger than cluster size. We have calculated the shear and bulk viscosity due to dark matter self-interactions using the kinetic theory formalism. The estimation of viscosity is performed at the late time of cosmic evolution when structures such as galaxies and clusters of galaxies have been formed.

The estimates suggest that bulk viscosity, ζ is larger than the shear viscosity η. Since the astronomical observations suggest a large SIDM viscosity, therefore one may expect some of the consequences arising due to the viscous energy dissipation at the present time. Furthermore, we explore the impact of these viscous effects on the cosmic evolution of the Universe.

To investigate the effect of SIDM viscosity on cosmological evolution, we estimate the dissipation term that depends on the DM viscosity and spatial average of the fluid velocity gradient. The lower and upper limit of the spatial average is defined on the DM fluid scale and homogeneity scale of the present Universe, respectively. The dissipation term has been estimated using two different approaches. In the first approach, the spatial average of fluid velocity gradient is replaced by its average value, and in the second approach, a realistic velocity power spectrum has been considered. In the first approach (approximating the fluid velocity gradient to its average velocity gradient value), we find that the dissipation term is large enough to account for the present observed cosmic acceleration. We test our theoretical understanding using the astrophysical data and find that the data also points in the same direction.

In the second approach, using the more realistic velocity power spectrum, we find that the small scale dominantly contributes to cosmic dissipation, whereas the large scale does not. Further, we report that our analysis for $P_{\theta\theta}(k)$ is only valid for $k_{\rm max} = 0.48h$ Mpc^{-1} for linear matter power spectrum, and $k_{\rm max} = 1.25h$ Mpc^{-1} for non-linear matter power spectrum of CDM. This provides us, $\bar{D} = 0.55$ and $\bar{D} = 2.52$

corresponding to velocity divergence power spectrum estimated using the LMPS and NLMPS. We also report that the velocity power spectrum estimated from the non-linear matter power spectrum provides slightly smaller dissipation (i.e., $4\pi GD/3H^3 \approx 2.2$) in comparison with the required value needed for present cosmic acceleration (i.e.,$4\pi GD/3H^3 \approx 3.5$). However, we expect that the small value of the dissipation may be the result of our limitation of not considering the small-scale contribution. When the small-scale contributions are appropriately considered into analysis, the dissipation term will increase and may lead to the correct value of cosmic dissipation.

We point out that in VSIDM fluid model, the cause of present accelerated expansion arising from its shear and bulk viscosity manifests at the late time of cosmic evolution. Therefore the cosmological constant is not needed here to explain the cosmic acceleration. The dissipative effect is prominent only at low redshift; hence this model does not face the coincidence problem. Thus, we conclude that the VSIDM can unify the dark sector of the Universe, i.e., dark matter and dark energy.

Chapter 4

VSIDM cosmology at the late time

4.1 Introduction

In the previous chapter, we discussed the possibility of present cosmic acceleration in the viscous SIDM framework. There we had assumed that the VSIDM mainly dominates the Universe without any extra dark energy component. In this chapter, we extend our previous study and investigate the late time of cosmic evolution, specifically $0 \leq z \leq 2.5$ within the framework of VSIDM cosmology [253]. For this purpose, we calculate the form of the dissipation term as a function of redshift. In order to calculate the dissipation term, we consider a power-law parameterization of average velocity gradient on the redshift and strict our estimates the viscosity of SIDM for vanishing sound speed, $C_n = 0$ [207]. Then we set up the first-order differential equations for the Hubble expansion rate $H(z)$ and deceleration parameter $q(z)$.

To extract the best fit values of the model parameters, power-law exponent, and length scale, we apply the χ^2 analysis method using the cosmic chronometer data and find that the best fit values explain the supernova data correctly. The best fit values also dictate that the SIDM dissipation term was smaller at earlier times, consistent with the expectation that the gradients become prominent only at late times. Further, in the VSIDM model, we also study the epoch of the deceleration-acceleration transition of the Universe. We find that for the best-fit values of model parameters, the value of deceleration parameter approaches $q \sim 0.5$, in the matter-dominated era, which agrees with the ΛCDM model prediction.

This chapter's arrangement is as follows: In Section 4.2, we approximate the form of dissipation term D following some simplifying assumptions. Then using D, we derive the coupled differential equation for the Hubble expansion rate and deceleration parameter. In Section 4.3, we estimate the best fit model parameter of the viscous SIDM model from χ^2 analysis with the cosmic chronometer data. In Section 4.4, we present our results. Using the best fit values, we fit the supernova data and also discuss the evolution of the deceleration parameter and dissipation due to viscous effects. In the last Section 4.5, we summarize the results and conclude our work.

4.2 VSIDM cosmology at low redshift

In this Section, we expand the ideas discussed in chapter 1 and estimate the dissipation of D. Later, we set up the coupled equations in $H(z)$ and $q(z)$ and then solve to get the evolution of the Universe.

4.2.1 Estimation of the dissipation tem, D

As we have seen in Section 3.4, that the dissipation term involves the spatial averages of the fluid velocity gradients and viscosities. Therefore to study the cosmic evolution on large redshift, the evolution of these quantities with redshift should be adequately taken into account. To do that, one needs to solve the viscosity and velocity evolution equation. However, in first approximation to get rid of the above difficulty, we use the following simplifying assumptions:

(i) Here, we focus our analysis in the redshift range, $0 \leq z \leq 2.5$. It is because, for $z > 2.5$, the relaxation time approximation will not be valid.

(ii) The viscous coefficients η and ζ are constant in space, i.e, $\langle\eta\rangle_s = \eta$ and $\langle\zeta\rangle_s = \zeta$. Further we also assume these to be constant in redshift range, $0 \leq z \leq 2.5$.

(iii) We assume that velocity derivatives evolve with redshift at a length scale of L, which is larger than the scale on which the hydrodynamic description is valid. Since we assume $\lambda_{\rm eff} \sim$ cluster scale, thus in principle, L, can be any scale between the cluster to the homogeneity scale ($\sim$ 100 Mpc) where cosmic expansion becomes prominent.

(iv) For simplicity, we replace the peculiar velocity gradient ∂v by its average spa-

tial value, i.e. $\partial v \sim \langle \partial v \rangle_s$. As earlier discussed, the velocity gradients evolve during the cosmic evolution, so instead of solving the space average velocity evolution equation (given in Eq. (2.16), we make an ansatz for it. We assume that over the low redshift ($0 \leq z \leq 2.5$), the $\langle \partial v \rangle_s$ follow a power-law form as

$$\langle \partial v \rangle_s \sim \frac{v_0}{L} (1+z)^{-n} \ , \tag{4.1}$$

where $n \geq 0$ is the free parameter. At present $\langle \partial v \rangle_s (z=0) \sim v_0/L$. Here, v_0 is the fluid velocity, which is defined on the scales larger than the cluster scale.

Thus in the light of above assumptions, we may approximate D, using Eq. (3.27), as

$$D = \left(\frac{v_0}{L}\right)^2 \left(\frac{4}{3}\eta + 2\zeta\right)(1+z)^{2-n} \ . \tag{4.2}$$

Here, we see that D depends on the length scale (L) and also its velocity dispersion at the same scale L (v_0), viscous coefficients (η, ζ) and redshift (z). It is clear from Eq.(4.2) that in the dissipation term D, the contribution from the smaller scale (where the Universe is inhomogeneous) is large, whereas the contribution from the larger scale (where Universe is more or less homogeneous) is small. For very large averaging length scale ($L \to \infty$) or vanishing bulk and shear viscosity ($\eta = 0, \zeta = 0$), D term vanishes and the VSIDM fluid behaves like a dissipationless fluid.

4.2.2 Estimation of Hubble rate and deceleration parameter

We now derive the evolution equations of Hubble expansion rate and deceleration parameter in VSIDM cosmology. The deceleration parameter q is given by

$$q(z) = -1 + (1+z)\frac{H'}{H} \ . \tag{4.3}$$

Using above Eq. (4.3), the differential equation for Hubble rate is written as

$$\frac{d\bar{H}}{dz} = \frac{(q+1)\bar{H}}{(1+z)} \ , \tag{4.4}$$

where, $\bar{H} = H/H_0$ is the dimensionless parameter, and H_0 is the present value of Hubble parameter, i.e., $H_0 = H(z=0)$. In order to solve the Eq. (4.4), we need to provide the expression for the deceleration parameter, which has been given in Eq. (3.30). To simplify the the equation, we assume VSIDM as a cold fluid, this provides

us $\hat{w}_{\rm eff} \sim 0$. So, the evolution equation for $q(z)$, can be written in term of the redshift as

$$\frac{dq}{dz} + \frac{(q-1)(2q-1)}{(1+z)} = \frac{4\pi G D}{3(1+z)H^3} \ , \tag{4.5}$$

where, D is given by Eq. (4.2). Further, using the dimensionless parameter $\bar{H}$, the above equation can be rewritten as

$$\frac{dq}{dz} + \frac{(q-1)(2q-1)}{(1+z)} = \beta\left(\frac{1+z}{\bar{H}^3}\right). \tag{4.6}$$

where,

$$\beta = \frac{4\pi G}{3H_0^3}\left(\frac{4}{3}\eta + 2\zeta\right)\left(\frac{v_0}{L(1+z)^n}\right) \tag{4.7}$$

Using the Eqns. (3.15) and (3.16), the dissipation parameter, β can be re-written in standard astrophysical units as

$$\beta = 3.88\times 10^{13}\left[\frac{100h \text{ km/(sec Mpc)}}{H_0}\right]^3\left[\frac{(\text{cm}^2/\text{gm})\text{ km/sec}}{\langle\sigma v\rangle/m}\right]\left(\frac{\langle v\rangle}{c}\right)^2\left(\frac{\text{Mpc}}{L}\right)^2\left(\frac{v_0}{(1+z)^n}\right)^2 \tag{4.8}$$

From Eq. (4.6) it is clear that the evolution of q depends on the new dissipation parameter, β. Here $H_0 = 100h$ km/(sec-Mpc), c is speed of light, and $h = 0.715$. To estimate β, we consider $\frac{\langle v\rangle}{c} = \frac{10^{-2}}{3}$ (for cluster scale), $v_0 = 2\times 10^{-2}$ and refer $\langle\sigma v\rangle/m \sim 100$ cm^2/gm km/sec from the Ref. [7].

As we can see that Eqs. (4.4) and (4.6) are coupled differential equation in $q(z)$ and $\bar{H}(z)$, and their solutions depend on two free parameters n and L. Since the analytical solution of the above equations are difficult to ontain, therefore to study the behaviour of solution, we need to solve them numerically. The initial condition for the equation is considered at present, given by $\bar{H}(z=0) = 1$ and $q_0 = -0.60$ [268].

4.3 Estimation of model parameters using cosmic chronometer data

As we have seen in Section 4.2.2, the solution for $\bar{H}(z)$ and $q(z)$, depends on two free model parameters n and L. In this section, we will estimate the best fit value of model parameters n and L using the method of χ^2 minimization.

Table 4.1: The best fit model parameter

Data set	1-σ	χ^2_{min}	$\chi^2_{\text{d.o.f}}$	Best fit parameters
Chronometer	$0.5083 \leq 0.5770 \leq 0.6513$	22.0207	0.6116	$n = 0.5770$
	$19.8002 \leq 20.1265 \leq 20.4416$			$L = 20.1265$ Mpc

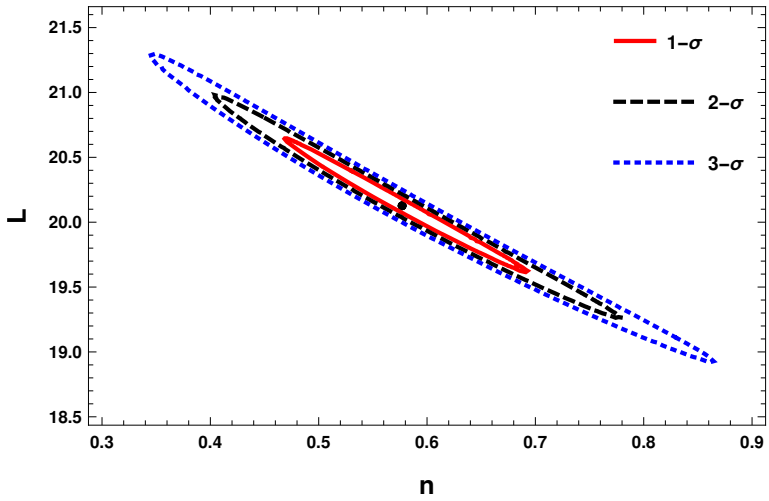

Figure 4.1: The joint confidence region of model parameters n and L have been plotted. The region correspond to 68.3%, 95.4% and 99.73% confidence limits. The best fit value is shown as a point.

The χ^2 is defined as

$$\chi^2(z, n, L) = \sum_{i=1}^{N} \left[\frac{H_{obs}(z_i) - H_{th}(z_i, n, L)}{\sigma_i} \right]^2, \tag{4.9}$$

where $H_{obs}(z_i)$ and $H_{th}(z_i, n, L) \equiv H_0 \bar{H}_{th}(z_i, n, L)$ represents ith observational Hubble parameter data and the theoretically predicted value for Hubble parameter, respectively. Here N is the total number of cosmic chronometer data points and σ_i^2 is the variance associated with the ith data points. The theoretical model of the Hubble rate for VSIDM cosmology is given by the coupled differential Eqs. (4.4) and (4.5). The observational data points for the Hubble expansion rate have been taken from the cosmic chronometer data set given in Ref. [270] and reference therein.

The χ^2 per degree of freedom, $\chi^2_{\text{d.o.f}}$, is given by $\frac{\chi^2_{\text{min}}}{N - M}$, where M is the number of parameters in the model. In our case $N = 38$ and $M = 2$. To understand the allowed parameters range, we have plotted the contour plot of joint confidence region of model parameters n and L corresponding to 68.3%, 95.4% and 99.73% in the Fig. 4.1. The

best fit values of the model parameters are represented as a point. Furthermore, in the table 4.1, we provide the best fit value of model parameters, $\chi^2_{\rm d.o.f}$ and 1-σ confidence region values.

The χ^2 minimization method provides us the best fit values are $n = 0.5770$ and $L = 20.1265$ Mpc for the power-law exponent and the gradient length scale. The significant digits of the best fit model have no physical meaning, but its approximate value $L \sim 20$ Mpc corresponds to the fluid length scale. The value suggests that the spatial averaging should be done on approximately one order of magnitude larger than the cluster size scale ($\sim$ 1 Mpc). Further, the positive value of the n implies that the velocity gradient should increase.

4.4 Results

In this Section, using the best fit model parameters, we show our results. Further, we will also compare our results with the ΛCDM model and also with the constant dissipation, $n = 0$ case.

4.4.1 Evolution of the dissipation parameter (β)

Here we will study the evolution of the dissipation parameter β, which provides us the information on how the dissipative effect of viscous SIDM due to dark matter self-interactions changes with time. To see the variation of dissipative effects, in Fig. 4.2 we plot the dissipation parameter as a function of redshift.

We see that for the $n = 0$ case, the velocity gradient and also the viscous coefficients (η, ζ) are constant, and hence β does not vary with the redshift. As a consequence, the dissipation parameter remains prominent even at the large redshift. For the case of the best fit value of model parameters, the velocity gradient and hence β decreases sharply on large redshifts. This behavior is expected because in the past, when structures were being formed, the average peculiar velocity gradients were small, and consequently, the dissipation term was ineffective. However, as the structure formation proceeds, the density perturbations start growing which increases the average peculiar velocity gradient and makes the dissipation term important at small redshifts. Hence the best fit

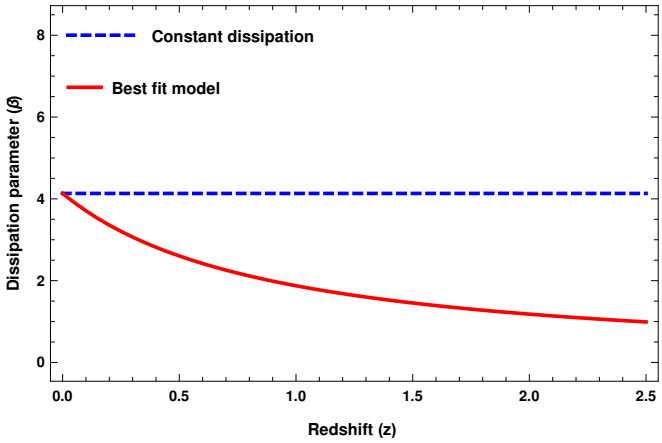

Figure 4.2: The plot of the dissipation parameter, β obtained from best fit model parameters ($n = 0.5770$) and also for constant dissipation model ($n = 0$).

model parameters suggest that the contribution of viscous effects becomes important only at a late time, not in the early time of a cosmic evolution history.

Furthermore, it is very important to estimate the magnitude of the dissipation parameter at the present time, i.e., $z = 0$. From eq. (4.6) and (4.8), and using the constraints on the SIDM properties, we find that at present epoch, $\beta = 4\pi GD/3H_0^3 \sim 4.1$. However, we see that our present estimated value differs from the value $4\pi GD/3H_0^3 \sim 3.5$ reported in earlier work [92]. It is important to mention that in work [92], the authors have assumed that at the present epoch, the variation of deceleration parameter with respect to the redshift is very small, i.e., $dq/dz \ll 1$, and hence neglected in their estimation. But in this work, by using the simplified assumptions as discussed in section 4.2.1, we infer $dq/dz = 0.61$. Hence by incorporating this contribution, we can address the discrepancy between the β values as mentioned above.

4.4.2 Hubble expansion rate

To see the cosmic evolution in the VSIDM model, we plot the Hubble expansion rate using the best-fit values of model parameters (solid red line) in 4.3. We also compare it with the case of constant dissipation, $\alpha = 0$ (blue dashed line), and standard ΛCDM model (black dotted line).

We see that the constant dissipation case explains the small redshift data, i.e., $z \leq 0.7$, but on the large redshift, due to constant viscous dissipation contribution,

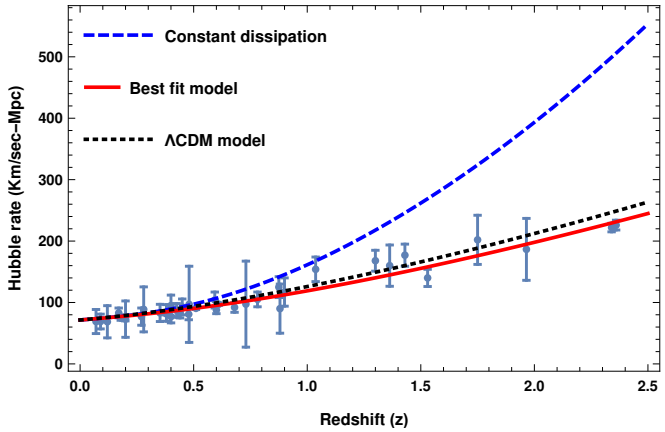

Figure 4.3: Plot of the Hubble expansion rate for the best fit value along with the case of constant dissipation is plotted. We also compare it with the ΛCDM model.

the Hubble rate starts increasing drastically. As a result, this model fails to fit the chronometer data on a large redshift. However, in the case of the best fit VSIDM, where the dissipation decreases with the redshift, and ΛCDM model explains the Hubble data very well in the entire redshift range. We point out that the best fit value has been obtained from the same cosmic chronometer data. Thus, we find that the constant dissipation case doesn't explain the right expansion rate of the Universe.

4.4.3 Fitting of Supernovae Ia data

The quantity measured in supernova observations is distance modulus μ, which is defined as the difference between the apparent and absolute magnitude of type Ia supernovae, i.e., $\mu(z) \equiv m - M$. The distance modulus is related with the luminosity distance, in the following manner,

$$\mu(z) \equiv m - M = 5 \log_{10} \left[\frac{\bar{d}_{\rm L}(z)}{\rm Mpc} \right] + 25, \tag{4.10}$$

where $\bar{d}_{\rm L}(z)$ is dimensionless distance modulus quantity, which is related with the distance modulus via $\bar{d}_{\rm L}(z) \equiv H_0 d_{\rm L}(z)$. The luminosity distance is calculated using the Hubble expansion rate as

$$d_{\rm L}(z) = \frac{(1+z)}{H_0} \int \frac{dz}{\bar{H}(z)}. \tag{4.11}$$

Further, using Eq. (4.10), we plot the distance modulus as a function of redshift for the best fit value of model parameters (solid red line) along with the SNe Ia data in

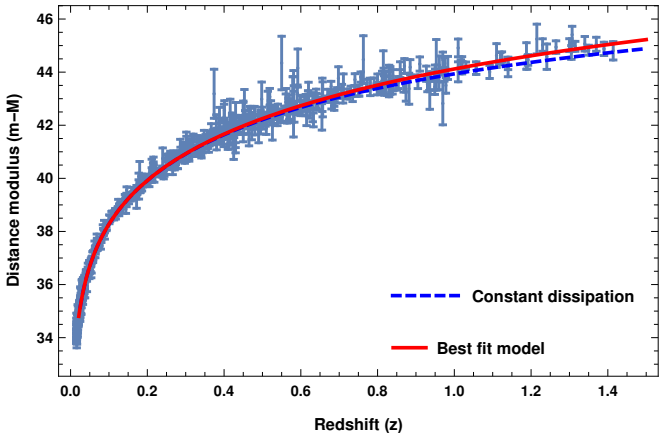

Figure 4.4: The distance modulus $(m - M)$ obtained from best fit model parameters and also for constant dissipation have been plotted along with the supernovae Ia data.

Fig. 5.3. We take Union 2.1 compilation SNe Ia data from the Refs.[271, 272], which consists of 580 SNe data. For comparison, we also, plot the distance modulus obtained for the case of constant dissipation (blue dashed line), where the velocity gradient is constant with the redshift.

From Fig. 5.3 we see that on the small redshift ($z < 1$), the best fit and the constant dissipation model matches with each other quite well, but at large redshift ($z \geq 1$), the difference between the above two become prominent. This is expected because, on the large redshifts, the contribution of cosmic dissipation is different in both cases. We thus conclude that the decreasing dissipation term with the redshift can explain both the cosmic chronometer and the supernova data while the constant dissipations fail to do so.

4.4.4 Deceleration parameter (q)

In this subsection, we study the epoch of decelerated to accelerated phase transition (i.e., the epoch of transition from $q > 0$ to $q < 0$) of the Universe in the VSIDM model. In Fig. 5.4, we plot $q(z)$ obtained from the best fit value of the model parameters (solid red line) and compare with the standard ΛCDM model (black dotted line) and constant dissipation model (blue dashed line).

We see that the transition point for best fit model parameters and ΛCDM model, corresponds for $z =$, and $z_{\rm tr} \sim 0.7$, respectively. In constant dissipation case the transi-

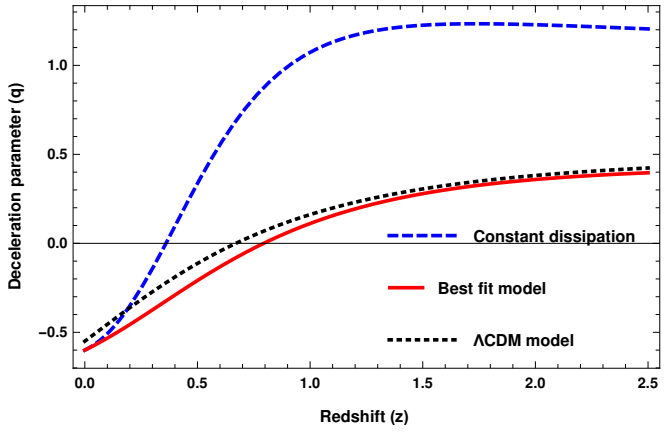

Figure 4.5: The plot of deceleration parameter, q obtained from the best fit model parameters along with the ΛCDM and constant dissipation case.

tion point is $z_{\rm tr} \sim 0.3-0.4$ which is later in comparison with the above two models. We see that for a constant dissipation model, the deceleration parameter firstly increases drastically and later settles around $q \sim 1.2$ for higher redshift. This is quite in contrast with our expectation that q should approach 0.5 in the matter-dominated era. On the other hand, the value of the deceleration parameter for best fit model parameters saturates at $q \sim 0.4$, which is approximately the same as the predicted value from the ΛCDM model.

Thus in the light of the above discussions, we may conclude that the constant velocity gradient model in which the dissipation term remains fixed is surely not the case to appropriately describe the cosmic evolution. The best fit model predicts the decreasing velocity gradient, and consequently, the cosmic dissipation can explain the low redshift observations and also matches with the ΛCDM prediction.

4.5 Summary and Conclusion

In this chapter, we have explored the evolution of the VSIDM dissipation in light of the low redshift observations. To study this, we assume the viscous coefficients are constant over the redshift of our interest ($0 \leq z \leq 2.5$). Then considering the spatial-averages of velocity gradients a power-law dependence on redshift, we set up the equations governing the Hubble expansion rate and deceleration parameter. We see that the solution depends on two free model parameters, n and L. The values of the parameters

provide us the information about the evolution of the velocity gradients and the scale of the averaging. To estimate the best fit model parameters, (n, L) we use the χ^2 minimization method and obtain $n = 0.5770$ and $L = 20.1265$ Mpc. This implies that the velocity gradient should decrease with redshift, and the average length scale should be approximately an order of magnitude larger than the typical cluster size DM halo.

The best fit model predicts that the velocity gradient hence the cosmic dissipation is large at present and decreases on earlier times (on large redshifts). This supports our expectation that the cosmic dissipation should decrease at higher redshift and becomes important at late times in order to explain the present observed cosmic acceleration. In this model, the epoch of decelerated to accelerated transition $z_{\rm tr} \sim 0.8$, which is earlier than the ΛCDM model. Furthermore, we find the best-fit parameters explain the low redshift observations such as cosmic chronometer, supernovae data and also attain the appropriate value of deceleration parameter in a matter-dominated era. However, in contrast with the best fit model, the constant velocity gradient, does not explain the low redshift data and also does not obtain the correct q value.

Chapter 5

Study of SIDM properties from KSS bound and low redshift observations

5.1 Introduction

In the previous chapter 3, we estimate the shear viscosity and entropy density of the SIDM fluid medium. It is expected that for a classical ideal fluid, both the shear and bulk viscosities should be zero, i.e., $\eta = \zeta = 0$. It has been found that it is true for the bulk viscosity case, which vanishes in the extreme relativistic and non-relativistic case for a gas [273]. However, this may not be correct when quantum effects become important. In the famous paper, [10], Kovtun, Son, and Starinets have conjectured a universal lower bound on the ratio of shear viscosity to entropy density. $\eta/\mathfrak{s} = 1/4\pi$ using the techniques of quantum field theories.

In this chapter, we study the SIDM properties such as its mass, evolution of its viscosity in the light of KSS, and late-time cosmological observations [274]. To investigate how perfect is the SIDM fluid, we check the KSS bound in this model. Using the constraints on σ/m inferred from the cluster scale observations, we see that the SIDM mass larger than the sub-GeV scale violates the lower limit of the $\eta/\mathfrak{s}$. In light of this, we discuss two possibilities; first, the VSDIM fluid violates the KSS lower bound, which can be confirmed when the dark matter searches will report the larger DM mass as inferred from the $\eta/\mathfrak{s}$ bound. Second, the VSIDM model respects the KSS bound, so using this one can explore the DM properties. Here using the $\eta/\mathfrak{s}$ bound we

derive an upper limit on the DM self-interaction cross-section to its mass ratio. Since the issues on a small scale demand a limit on the σ/m, therefore, using the σ/m bound on the cluster scale and $\eta/\mathfrak{s}$ upper limit, we constrain the SIDM mass. We argue that the allowed SIDM particle mass is sub-GeV.

In previous chapter 2, we have studied the cosmic evolution assuming that, on low redshift $0 \leq z \leq 2.5$, the SIDM viscosities are constant and velocity gradients larger to cluster scales varies with the redshift. However, here we explore the possibility that the viscous coefficients of SIDM fluid may vary with the redshift and constrain their evolution using the late-time observations. In order to study the evolution of cosmic dissipation, we consider the power-law form for bulk viscosity $\zeta(a) = \zeta_0 (a/a_0)^\alpha$ and shear viscosity $\eta(a) = \zeta_0 (a/a_0)^\alpha$. After that, we calculate the Hubble expansion rate, $H(z)$ and deceleration parameter, $q(z)$ applying the Einstein field equations, and energy-momentum conservation equations.

Considering the length scale of spatial averages larger than the typical cluster scale, we estimate the best fit value of the model parameter, α using the cosmic chronometer data, and the correct value of deceleration parameter in the matter-dominated era. The best fit parameter indicates decreasing DM viscosity on the larger redshift and explains the low redshift cosmological observations. In this model, the age of the Universe is smaller than the age obtained from the CMB anisotropy [61] but larger than the age of globular cluster [275].

The arrangement of our work is as follows: In Section 5.2, we discuss the $\eta/\mathfrak{s}$ bound violation in VSIDM fluid model. Later respecting the $\eta/\mathfrak{s}$ bound, we derive an upper limit on σ/m and also constraint on SIDM mass. In Section 5.3, using the Einstein equations and energy-momentum conservation equations, we set up the coupled differential equations for the Hubble expansion rate and deceleration parameter. In Section 5.4, we estimate the best-fit values of the model parameter and discuss the results. In the last Section 5.5, we conclude our work.

5.2 Fundamental properties of SIDM from $\eta/\mathfrak{s}$ bound

In this Section, we study the $\eta/\mathfrak{s}$ bound [10] for the VSIDM fluid model. Then applying the σ/m constraint obtained from the cluster scales, the upper limit on SIDM mass is estimated. To start with, we assume that the Universe is mainly dominated by the VSIDM fluid with no extra dark energy component. The important quantity which provides the information about the viscous medium is the ratio of shear viscosity to entropy density, $\eta/\mathfrak{s}$. In VSIDM model, this can be given by using Eq. (3.10) and Eq. (3.11) as

$$\frac{\eta}{\mathfrak{s}} = \frac{1}{2}\left(\frac{2\pi}{m^2}\right)^{\frac{3}{2}}\left(\frac{m}{\langle\sigma v\rangle}\right)\left(\frac{T}{m}\right)^{\frac{1}{2}} . \tag{5.1}$$

Here we see that $\eta/\mathfrak{s}$ depends on the velocity average self-interacting cross section $\langle\sigma v\rangle$, temperature, T and the mass of SIDM particle. After approximating, $\langle\sigma v\rangle \sim \sigma\langle v\rangle$ and $\langle v\rangle \sim (3T/m)^{\frac{1}{2}}$, in Eq. (5.1), we get that $\eta/\mathfrak{s}$ depends on the mass and σ/m value of SIDM particles.

It is important to ask a question how much perfect a SIDM fluid can be? In a seminal work [10], Kovtun-Son-Starinets (KSS) have conjectured a universal bound on shear viscosity to entropy density ratio $\eta/\mathfrak{s}$, as

$$\frac{\eta}{\mathfrak{s}} \geq \frac{1}{4\pi} . \tag{5.2}$$

This bound is also famously known as KSS bound. The lower bound on $\eta/\mathfrak{s}$, i.e. $\frac{\eta}{\mathfrak{s}} = \frac{1}{4\pi}$, may be applied various classes of quantum field theories. The success of the viscosity bound lies in the fact that no experiment has yet confirmed its violation. However, there are some theoretical studies where the violation from the KSS bound has been reported, see Refs. [276–279] and also status report [280].

Further, we check the applicability of this bound in our VSIDM model. As discussed above the $\eta/\mathfrak{s}$, depends on σ/m, and mass of the DM. The value of σ/m is given from the constraint obtained from the small-scale observations, which requires the DM self-interactions. The merging cluster IE 0657-56, provides the strong upper limit on the σ/m on cluster scale DM halo, which require $\sigma/m < 1.25$ cm^2/gm [227]. However the consistent explanation of the small scale observations varies from the galactic to cluster scale prefer the mild velocity dependent scattering cross-section. This requires slightly smaller value of σ/m on cluster scale given by $\sigma/m \approx 0.1$ cm^2/gm [7].

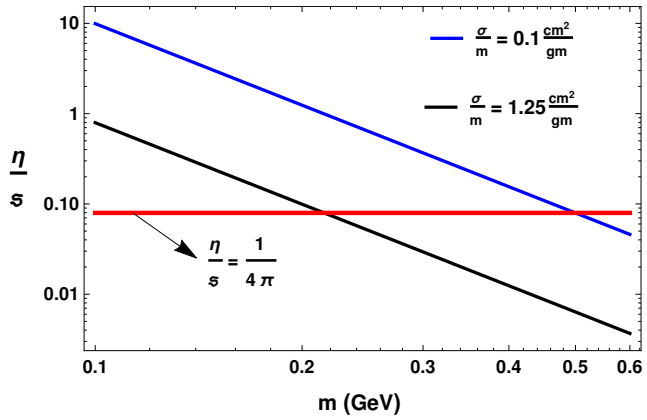

Figure 5.1: The ratio of shear viscosity to entropy density, $\eta/\mathfrak{s}$ is plotted as a function of DM mass. The red line represents the KSS lower bound, i.e., $\frac{\eta}{\mathfrak{s}} = \frac{1}{4\pi}$ [10].

Therefore the $\eta/\mathfrak{s}$, only depends on DM mass.

In Fig.5.1, using Eq. (5.1), $\eta/\mathfrak{s}$ has been plotted as a function of DM mass for the different values of σ/m for cluster scale halo at present $z = 0$. Here solid black and solid blue lines corresponds for $\sigma/m = 1.25\text{cm}^2/\text{gm}$ and $\sigma/m = 0.1\text{cm}^2/\text{gm}$, respectively. The red solid line corresponds for $\eta/\mathfrak{s} = 1/4\pi$. Since $\eta/\mathfrak{s} \propto m^{-3}$ (see Eq. (5.1)), so this decreases with the DM mass, therefore we may ecpect that for large DM mass, $\eta/\mathfrak{s}$ will be smaller than KSS lower bound (solid red line). From Fig. 5.1, it is evident that larger is the σ/m, smaller is the DM mass over which the $\eta/\mathfrak{s}$ for VSIDM model becomes smaller than the KSS lower bound. For example, for $\sigma/m = 1.25$ cm^2/gm , $m = 0.21$ GeV and for $\sigma/m = 0.1\text{cm}^2/\text{gm}$, $m = 0.5$ GeV.

Based on the above discussion, it becomes clear that the VSIDM model either violates or respects the KSS lower bound. In case the VSIDM obeys the $\eta/\mathfrak{s} = 1/4\pi$ bound, it can constraint the SIDM properties. We will discuss both the possibilities in upcoming subsections.

5.2.1 KSS lower bound violation in VSIDM fluid

Since in Fig.5.1, the $\eta/\mathfrak{s}$ comes below the KSS lower bound, thus in this case, one may assume that the VSIDM fluid violate the $\eta/\mathfrak{s} = 1/4\pi$ bound. This happens at a particular DM mass, which depends on the σ/m value. The $\eta/\mathfrak{s}$ bound violation can be confirmed when the DM detection experiments will detect the larger mass of DM

particle inferred from the KSS lower bound. It is worthwhile to mention that in the above, the violation of KSS bound and any characteristic inferred is at a phenomenological level only. The violation of KSS bound in a consistent field theory description of VSIDM would need to be studied carefully, and such a study may bring very different surprises while inferring the same characteristics in comparison to what can be simply concluded.

5.2.2 Constraining the SIDM properties from KSS bound

In this case, we assume that the KSS lower bound is universal; therefore, it allows us to explore the SIDM microphysics, such as its self scattering cross-section and mass. This assumption is based on the fact that no experiment has reported the violation of KSS bound in any fluid, viz superfluid Fermi gas [281], Quark-Gluon liquid [282]; therefore, this bound is well established by the experiment up to their current precision. It has been found that the KSS bound has been respected for the strongly interacting system [10][282]. The microphysics description of the SIDM particles is not clearly known, but only the constraint on $\sigma/m \sim 1\text{cm}^2/\text{g}$ is reported from the astrophysical observations, which is an order of the typical neutron-proton scattering cross-section. In case the SIDM microphysics is described by the strongly interacting particles (like a Quantum Chromodynamics (QCD) nature but in the dark sector), then due to the nature of strong interaction, the DM fluid may respect the KSS lower bound. In literature, considering the KSS bound, the properties of dark sectors, viz dark matter [283] and dark energy [279] has also been investigated. Since the nature of DM particles is not clear, therefore, we have used KSS bound to explore the DM properties.

Using Eq. (5.1) and Eq. (5.2), we obtain the constraint on $\langle\sigma v\rangle/m$, given by

$$\frac{\langle\sigma v\rangle}{m} \leq (2\pi)^{\frac{5}{2}} \left(\frac{1}{m}\right)^3 \left(\frac{T}{m}\right)^{\frac{1}{2}} . \tag{5.3}$$

We see that the constraint on $\langle\sigma v\rangle/m$ only depends on the SIDM mass and the temperature of the SIDM fluid. We emphasize that limit derived from the thermalized and non-relatistic VSIDM fluid, hence is quite general, and can be used to contrain the model parameters of various particle physics motivated model of SIDM.

The limit given in Eq. (5.3) can be manifest in term of σ/m using the approximations $\langle\sigma v\rangle \sim \sigma\langle v\rangle$ and $\langle v\rangle \sim (3T/m)^{\frac{1}{2}}$ as

$$\frac{\sigma}{m} \leq 1.2 \times 10^{-2} \left(\frac{\text{GeV}}{m}\right)^3 \left[\frac{\text{cm}^2}{\text{gm}}\right]. \tag{5.4}$$

The above equation implies that the σ/m constraint only depends on the SIDM mass and is independent of the DM temperature.

Furthermore, we also point out that the small scale observations provides a constraint on σ/m value. Therefore, this allows us to explore the available parameter space for the DM mass. This can be obtained via applying Eq. (5.4) as

$$m \leq 0.23 \left(\frac{m/\sigma}{\text{gm/cm}^2}\right)^{\frac{1}{3}} \text{ GeV}. \tag{5.5}$$

It is also clear that for small σ/m value, large DM mass range is allowed. For $\sigma/m = 1.25\text{cm}^2/\text{gm}$ (upper limit obtain from the cluster merger), $m \leq 0.21$ GeV and for $\sigma/m = 0.1\text{cm}^2/\text{gm}$ (required to explain the cluster scale issues for mild velocity dependent σ), we get slightly larger DM mass, $m \leq 0.5$ GeV.

It is important to mention that in the rest of our analysis, we will mainly focus on the second aforementioned possibility where we consider that the VSIDM model respects the KSS bound. Therefore, in light of the above discussion, we may conclude that the KSS lower bound severely constrains the DM mass range and permit the sub-GeV SIDM mass particles. The bound on the DM mass only depends on the σ/m value, so it will be improved for more precise astrophysical observations on σ/m in the future.

The recent direct detection DM searches have almost failed to detect the famous particle DM candidate, known as the Weakly-interacting massive particles (WIMP), for which the mass range varies from $\sim$ GeV to TeV scale. Therefore, our result suggests a new DM mass window that is crucial for future dark matter search experiments. We refer Ref. [284] for details of the experiment, which will probe the sub-GeV DM mass range.

5.3 Background cosmology in VSIDM model

In chapter 2, we have studied the cosmic evolution, in the assumptions that the SIDM viscosity as a constant and velocity gradients varies with redshift for $0 \leq z \leq 2.5$. But here, we consider the variation of viscosity with the redshift and discuss the evolution of the Universe. As we have seen from chapter 3 that to study the cosmic evolution, we need to simplify the expression of D given in Eq. (3.27), which basically needs to evaluate the spatial averages involved for the viscosity and velocity gradients. Instead of calculating the spatial averages, we consider the following approximations to estimate D :

(*i*) We assume that the length scale equal to or larger than the cluster scale, the spatial average peculiar velocity gradient $\langle \partial v \rangle_s$ is constant on the redshift of our interest $0 \leq z \leq 2.5$, i.e., $\langle \partial v \rangle_s \sim constant$. Therefore, we can approximate

$$\langle \partial v \rangle_s \sim v_0/L \ , \tag{5.6}$$

where v_0 and L represents the peculiar velocity and comoving length scale. Our assumption indicate that, for length scale cluster to larger, the peculiar velocity and comoving length scale varies in such a way so that the ratio of these two becomes constant for the low redshift.

(*ii*) The viscosity coefficients ζ, η depend on the thermal distribution of the dark matter [253], thus are independent with space. In order to study the evolution of the viscous coefficient ζ and η, we use the expression, given from equations (3.15) and (3.16) (in the case, where the sound speed vanishes, ie., $C_n = 0$). To see the redshift dependency of viscosities, we need to understand the evolution of the $m/\langle \sigma v \rangle$ and $\langle v \rangle$ with redshift individually, which is crucially dependent on the particle physics model of the SIDM. To keep discussion model independent, also for simplicity, we attribute all the redshift dependency as a power of form in scale factor. Thus in this assumption, the bulk and shear viscosities of the SIDM fluid can be given as

$$\zeta(z) = \zeta_0 \left(\frac{a}{a_0}\right)^{\alpha} = \zeta_0 \left(\frac{1}{1+z}\right)^{\alpha} , \tag{5.7}$$

$$\eta(z) = \eta_0 \left(\frac{a}{a_0}\right)^{\alpha} = \eta_0 \left(\frac{1}{1+z}\right)^{\alpha} . \tag{5.8}$$

Here, α is the viscosity parameter and $\frac{a}{a_0} = \frac{1}{1+z}$, where $a_0 = 1$ is the present value of the scale factor. Further, $\zeta_0 = \zeta(z=0)$ and $\eta_0 = \eta(z=0)$ represents the present values of bulk and shear viscosity, respectively. Their values are estimated from the equations (3.15) and (3.16) at the cluster scale, and we take cluster scale velocity, $\langle v \rangle \sim 1000$ km/sec and cluster scale $\frac{\langle \sigma v \rangle}{m} \sim 100$ (cm^2/gm)(km/sec) from Ref. [7].

In general, the viscosity of a fluid depends on its energy density. Therefore inspired by this fact, we assume that the DM viscosity depends on its energy density as a power-law form, i.e., $\eta, \zeta \propto \rho^k$, in a very simplified scenario. This kind of form of viscosity is widely used in cosmological studies (Ref.). Since $\rho \propto (1+z)^{-3}$, therefore, viscous coefficients, $\eta, \zeta \propto (1+z)^{-3k} \equiv (1+z)^{-\alpha}$, where $\alpha = 3k$.

Thus, using the approximations as discussed above, one can estimate D using Eq. (3.27), given by

$$D = \left(\frac{v_0}{L}\right)^2 \left(\frac{4}{3}\eta + 2\zeta\right)(1+z)^{2-\alpha}. \tag{5.9}$$

As we have assumed, v_0/L is constant, so η_0 and ζ_0 is fixed at present; therefore, the evolution of D will depend only on α parameter.

Thus, equipped with the simplified expression of D, now, we will set up the differential equations for the Hubble expansion rate and deceleration parameter. To obtain the equation for q, we consider VSIDM fluid to be cold, i.e. $\hat{w}_{\rm eff} \approx 0$ and using Eq. (5.9) in Eq. (4.3), and obtain

$$\frac{dq}{dz} + \frac{(q-1)(2q-1)}{(1+z)} = \beta\left(\frac{1+z}{\bar{H}^3}\right), \tag{5.10}$$

where, β is dissipation parameter, which is defined as

$$\beta = \frac{4\pi G}{3H_0^3}\left(\frac{4}{3}\eta_0 + 2\zeta_0\right)\left(\frac{v_0}{L}\right)^2 (1+z)^{-\alpha}\,. \tag{5.11}$$

The dissipation term, β, depends on exponent power, α and averaging length scale, L. The evolution equation for the Hubble expansion rate is given by Eq. (4.4) as

$$\frac{d\bar{H}}{dz} = \left(\frac{q+1}{1+z}\right)\bar{H}\,. \tag{5.12}$$

These coupled differential equations (5.10) and (5.12) can be solved numerically by using the initial conditions at present, given as $\bar{H}(z=0) = 1$ and $q(z=0) = -0.60$ [268]. Here we see that the solution of $q(z)$ and $\bar{H}(z)$ depends on two free parameters

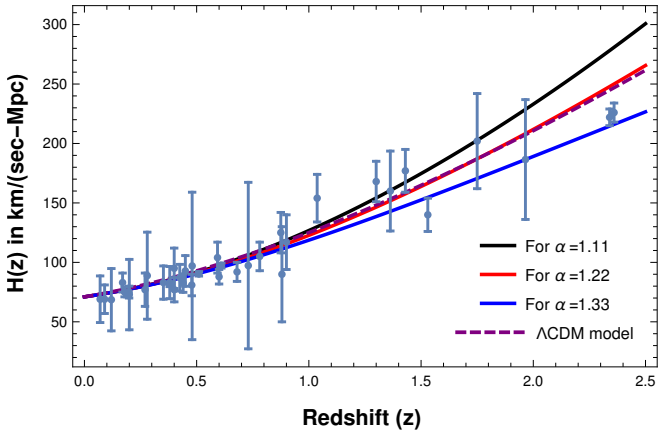

Figure 5.2: The Hubble expansion rate, $H(z)$ obtained from VSIDM model and ΛCDM model have been plotted as a function of redshift along with the cosmic chronometer data.

α and L, i.e. $q(z, \alpha, L)$ and $\bar{H}(z, \alpha, L)$. In this work, we take $L \sim 20$ Mpc, which is estimated in Ref. [253]. So finally, the solutions for q and $\bar{H}$ depend only on one free parameter, α.

5.4 Analysis and Results

In this Section, we will first estimate the value of the free parameter, α, using the low redshift. Then, using the best fit value of α, we will explore the evolution of viscosity and bulk viscous EoS of the VSIDM fluid.

5.4.1 Hubble expansion rate

In Fig. 5.2, the Hubble expansion rate, $H(z)$ we has plotted as a function of redshift for different values of model parameters α with the cosmic chronometer data taken from the Ref. [270]. Here the black, red and blue solid lines corresponds for $\alpha = 1.11$, $\alpha = 1.22$ and $\alpha = 1.33$, respectively. To compare the VSIDM model with the standard cosmology, we have also plotted the Hubble expansion rate derived from the ΛCDM model as a purple dashed line. From Fig. 5.2, we see that the expansion of the Universe depends on the dissipative strength of the dark matter; large is dissipation, larger will be the Hubble rate. However, on small redshift, all three viscous models contribute

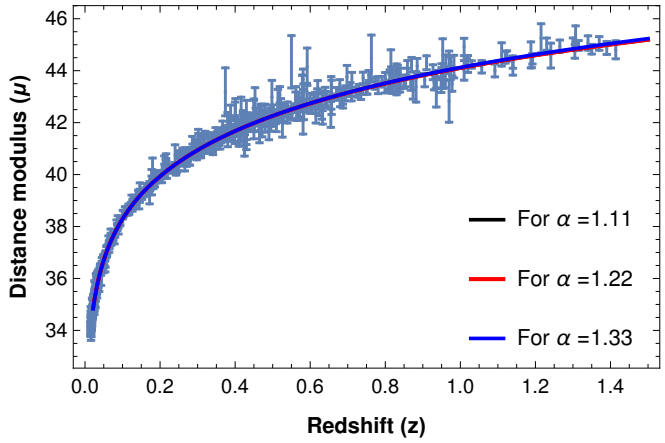

Figure 5.3: The distance modulus, $\mu(z)$ estimated from VSIDM model have been plotted with the Union 2.1 SNe Ia data for three different values of viscosity parameter, α.

equally to the Hubble expansion rate, but on the large redshift, due to differences in the dissipation term, all models contribute unequally in the $H(z)$. So as a consequence, all VSIDM models start deviating from each other on large redshift.

We see that for the $\alpha = 1.11$ case, the $H(z)$ increases quickly and becomes very large at large redshift and does not fit the Hubble data. In comparison with the $\alpha = 1.11$ case, for $\alpha = 1.33$ case, $H(z)$ increases slowly and does not fit the large redshift Hubble data. But for $\alpha = 1.22$ case, $H(z)$ increases moderately and explains the cosmic chronometer data, and also matches with the standard cosmology.

5.4.2 Fitting of Supernovae data

In Fig. 5.3, using Eq. (4.10), we plot the distance modulus as a function of redshift for different values of α along with the SNe Ia data. Here, we take Union 2.1 SNe Ia data compiled in Refs.[271, 272], which consists of 580 SNe data. The plot indicates that all values of the α considered here, i.e., $\alpha = 1.11, 1.22$, and $\alpha = 1.33$, fit the SNe Ia data well. Thus we conclude that the fitting of SNe Ia data cannot suggest the correct evolution of the SIDM viscosity, i.e., α value.

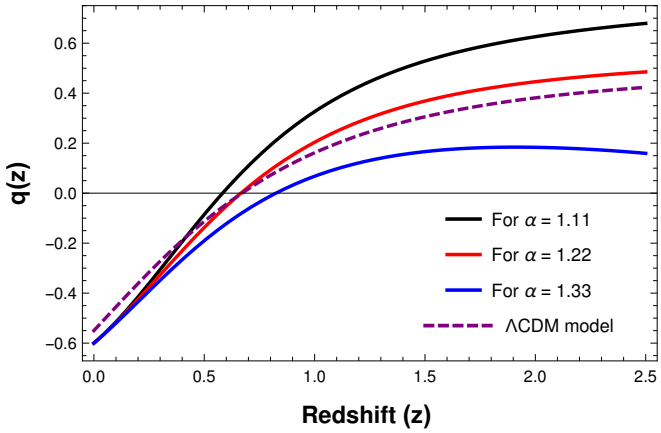

Figure 5.4: Deceleration parameter, $q(z)$ obtained from the VSIDM model parameters have been plotted with the ΛCDM model prediction.

5.4.3 Deceleration parameter q

The deceleration parameter (q) defined in the Eq. (4.5) provides the information, whether the Universe is in the accelerating (for $q > 0$) or in the decelerating phase (for $q < 0$). In order to see the epoch of decelerated to accelerated phase transition z_{tr} (i.e. epoch of $q > 0$ to $q < 0$) in our VSIDM model, we plot the $q(z)$ for different values of α, as a function of redshift in Fig. 5.4. The black, red and purple solid lines corresponds for $\alpha = 1.11, \alpha = 1.22$ and $\alpha = 1.33$, respectively. The green dashed line corresponds for ΛCDM prediction. We can see that for large α, the transition point is earlier (on large redshift). For $\alpha = 1.11,\ 1.22$ and $\alpha = 1.33$, the transition points are $z_{tr} = 0.58,\ z_{tr} = 0.66$ and $z_{tr} = 0.81$, respectively. The transition point corresponding to $\alpha = 1.22$ matches with the ΛCDM model prediction.

We point out from Fig. 5.4 that for $\alpha = 1.11$ case, the deceleration parameter increases and settles around $q \sim 0.7$ for large redshift. This is quite in contrast with our expectation that q should approach 0.5 in the matter-dominated era. Also, it does not explain the large redshift Hubble data correctly; see 5.4.1. For $\alpha = 1.33$ case, at higher redshift, q is decreasing and approaching towards $q \sim 0.16$, which is below the expected value of $q = 0.5$ in matter-dominated era. We may thus safely conclude that the case for $\alpha = 1.11$ or $\alpha = 1.33$ is surely not the case to describe the cosmic evolution appropriately.

Furthermore, from Fig. 5.4 we can see that for $\alpha = 1.22$ case, the deceleration

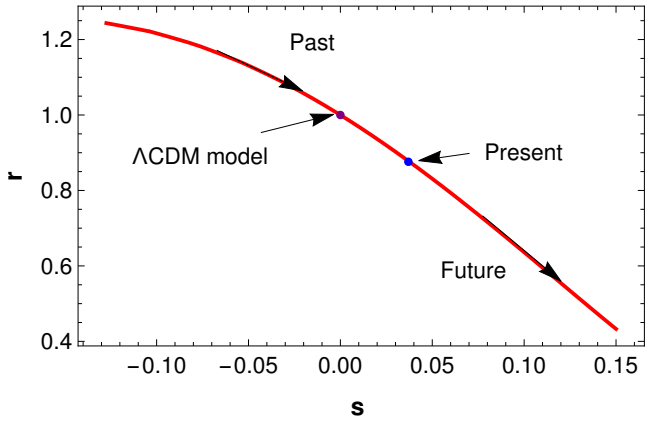

Figure 5.5: The Statefinder pair (r, s) evolution for the best fit model parameter $\alpha = 1.22$ in the VSIDM model of the Universe.

parameter saturates around $q \sim 0.49$, which is very close to our expectation and slightly different from the ΛCDM model q prediction. The important feature of this model is that the $H(z)$ obtained from it overlaps with the ΛCDM expectation of the Hubble parameter and explains the cosmic chronometer data correctly. Hence assuming $C_n = 0$, $\alpha = 1.22$ is the most intriguing possibility to explain the Hubble data and q value and matches with some of the ΛCDM prediction.

5.4.4 Statefinder technique

As we have seen in the previous subsection that the best fit value of the model parameter for VSIDM matches with the ΛCDM model prediction. To see the deviation of the VSIDM model with the Λ CDM model, we adopt a geometric diagnostic approach discussed in Ref. [285], which was introduced to differentiate between the different dark energy models. In this approach, one calculates a Statefinder parameter pair $\{r, \mathrm{s}\}$, which is related to the higher-order derivative of the Hubble expansion rate. In terms of the redshift, the Statefinder parameters are defined as

$$r(z) = 1 - 2(1+z)\left(\frac{H'}{H}\right) + (1+z)^2\left[\left(\frac{H'}{H}\right)^2 + \frac{H''}{H}\right] , \tag{5.13}$$

$$\text{and} \qquad \mathrm{s}(z) = \frac{1}{3}\left(\frac{r(z)-1}{q(z)-\frac{1}{2}}\right) . \tag{5.14}$$

The idea lies in the fact that $\{r, s\}$ pair is a fixed point given by $\{1, 0\}$ for ΛCDM model, and may varies for the other models. In Figure 5.5, we plot the evolution of $r - \mathrm{s}$ plane

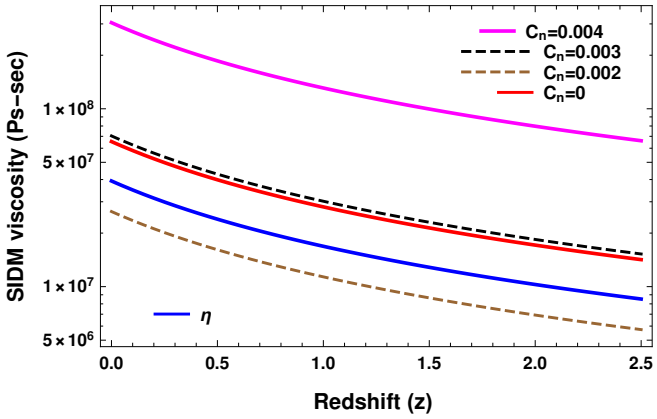

Figure 5.6: The bulk viscosity (ζ) and shear viscosity (η) of VSIDM have been plotted as a function of redshift for the best fit model parameter, $\alpha = 1.22$. Blue line corresponds for shear viscosity and the rest of the lines corresponds for bulk viscosity at the different sound speeds.

for the best fit value of the parameter α. We find that for our VSIDM model the pair lies on the second quadrant of $r - s$ plane in the past and evolve towards the first quadrant. The present value of pair in VSIDM model $\{r, s\}$ is $\{0.87, 0.03\}$ which clearly implies that the VSIDM model is different from the ΛCDM model.

5.4.5 Evolution of VSIDM viscosity on small redshift

In Fig. 5.6, using given equations (3.15) and (3.16), we plot η and ζ as a function of redshift for the best fit values of the viscosity parameter, i.e. $\alpha = 1.22$. The blue line refers to the shear viscosity, and the rest of the other lines correspond to the bulk viscosity for different sound speed values. We see that the ζ and η are large at present, $z = 0$ and decreases on the larger redshift $z > 0$. This implies that at the earlier times when the halo starts forming, the SIDM viscosities were small, but at later times of cosmic evolution, when the DM halo becomes more or less virialized, the viscosities contribute more. We also find that for low sound speed, $C_n < 0.027$, negative term in Eq. (3.13) becomes large and decreases ζ in comparison with the $C_n = 0$ counterpart. But for large sound speed, $C_n > 0.027$, the positive term in Eq. (3.13) becomes large and increases ζ.

Further, we emphasize that the value of the VSIDM viscosity obtained here can

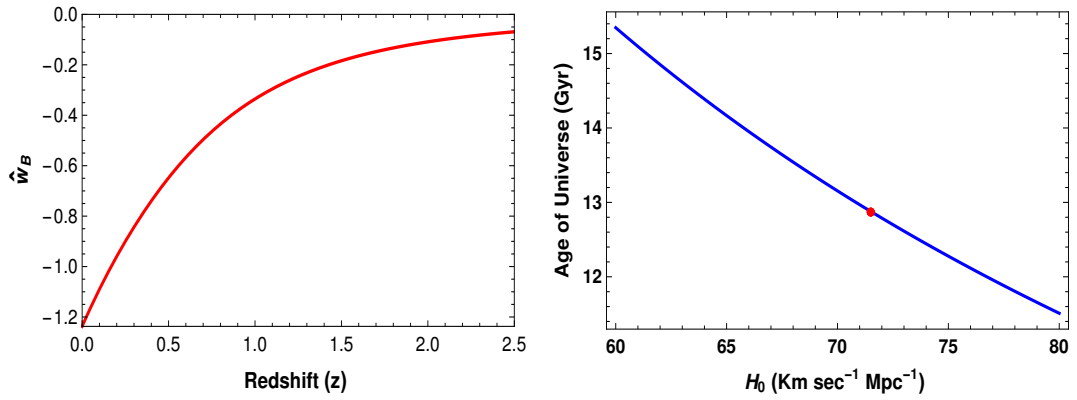

(a) (b)

Figure 5.7: In Fig. 5.7(a) equation of state, $\hat{w}_B$ of VSIDM model is plotted as a function of redshift for best fit model parameter. In Fig. 5.7(b), the age of the Universe is plotted as a function of the Hubble expansion rate. The red point corresponds for $t_{\rm U} = 13$ Gyr and $H_0 = 71.5$ Km sec^{-1}Mpc^{-1} obtained from the best fit model parameter.

only be possible at the late times when the non-linear structure formation occurs and collapse objects are formed. Because a large DM viscosity at earlier times may wash out the density perturbation, and non-linear structure formation will not be possible [189, 190].

As we have discussed above, at present ($z = 0$), the viscous contribution from the bulk as well as shear DM viscosity increases on low redshift; thus, we may expect some consequences. In the Ref. [207], we have shown that at present, $z = 0$, the viscous effects of VSIDM are large and can explain the present observed acceleration. Further, these results also provide the physical basis of the cosmic acceleration and also why it starts at a late time (low redshift), not at a very early time (large redshift).

5.4.6 Bulk viscosity EoS

In this subsection, we show the evolution of EoS of VSIDM fluid on small redshift. In Fig. 5.7(a), we plot the equation of state corresponding the SIDM bulk viscosity, $\hat{w}_B$ as a function of the redshift for the best fit value of viscosity parameter, i.e. $\alpha = 1.22$. We see that on the small redshift $\hat{w}_B$ subsequently becomes more negative and at present, $\hat{w}_B(z = 0) = -1.2$. On the large redshift, $\hat{w}_B$ increases (becomes less negative) and

approaches towards $\hat{w}_B \sim 0$.

5.4.7 Age of Universe

The age of Universe at any redshift, $t_{\rm U}(z)$ is obtained from the Hubble expansion rate as

$$t_{\rm U}(z) = \int_z^\infty \frac{dz}{(1+z)H(z)} \ . \tag{5.15}$$

In this work, we have assumed that the SIDM viscosity becomes effective only at late time $z \leq 2.5$ and consequently, the viscous effect modifies the evolution of the Universe only at a late time. At early time $z > 2.5$, the evolution of the Universe is governed via standard cosmology. Thus we consider

$$H(z) = \begin{cases} H_{\rm visc} & \text{if } z \leq 2.5 \ , \\ H_{\Lambda\rm CDM} & \text{if } z > 2.5 \ , \end{cases} \tag{5.16}$$

where $H_{\rm visc}$ is obtained from the Eqs. (5.10) and (5.12). Also, the Hubble expansion rate in matter dominated era is given by

$$H_{\Lambda\rm CDM} \approx H_0[\Omega_B(z) + \Omega_\chi(z)]^{1/2}. \tag{5.17}$$

Thus, using the best fit value of α, we get the age of the Universe

$$t_{\rm U} \sim \frac{0.974}{H_0} \ . \tag{5.18}$$

In Fig. 5.7(b), we plot the age of the Univere, $t_{\rm U}$ in the VSIDM model as a function of the Hubble expansion rate. We see that as the H_0 increases, $t_{\rm U}$ decreases. In VSIDM model, using the best fit value of model parameter, $\alpha = 1.22$, $t_{\rm U} = 13$ Gyr. Our estimation of $t_{\rm U}$ is slightly small in comparison with the age of the Univere (13.76 Gyr) obtained in the CMB anisotropy data [61] and larger than the age of globular cluster (12.9 Gyr) [275].

5.5 Conclusion

In this chapter, we study the SIDM properties using the KSS bound, $\eta/\mathfrak{s} \geq 1/4\pi$, and explore the evolution of the SIDM viscosity using the low redshift observations. We

calculate the $\eta/\mathfrak{s}$ in the framework of the VSIDM model, and then using the constraint on σ/m inferred from the astrophysical observations, we show that the SIDM fluid violates the KSS lower bound. It will be confirmed when the future DM detection experiment detects a larger DM mass as provided by KSS bound. Further, in the assumption that the SIDM fluid respects the $\eta/\mathfrak{s} = 1/4\pi$ bound, we report that the KSS bound allowed a sub-GeV ($\mathcal{O}(0.1)$ GeV) mass of the SIDM particles. This limit on the DM mass is conservative, which will further be improved for a more precise estimation of σ/m in the future.

To understand the evolution of SIDM viscosity at the redshift of our interest, we assume the power law form of bulk $\zeta(z) = \zeta_0 (a/a_0)^\alpha$ and shear viscosity $\eta(z) = \eta_0 (a/a_0)^\alpha$. Then inspired from the observational evidence that velocity gradient is constant on typical cluster and supercluster scale at the present time, we assume it to be constant on the low redshift interval $0 \leq z \leq 2.5$.

Further, we calculate the Hubble expansion rate and deceleration parameter and find that these depend on the viscosity parameter, α, and the length scale, L. We assume $L = 20$ Mpc, which is larger than the typical cluster size DM halo. Further, using the cosmic chronometer data points and the correct value of the deceleration parameter at the matter-dominated era, we obtain $\alpha = 1.22$. The best fit values of model parameter shows that the viscous coefficients, η and ζ are large at present, $z = 0$ and decrease at earlier time $z > 0$. The deceleration to an acceleration transition point in this model is $z_{\rm tr} = 0.66$, which matches with the ΛCDM model. We find that the VSIDM model fits with the supernovae data very well. Although our VSIDM model matches the ΛCDM prediction at a late time, but using the Statefinder technique, we report that the VSIDM model is different from the ΛCDM model. Also, in our model, the age of the Universe is 13 Gyr, which is smaller than the age inferred from the CMB anisotropy data (13.8 Gyr) but larger than the globular cluster age.

Thus in light of the small redshift observations, we conclude the VSIDM model may be a possible alternative theory of the standard model of cosmology. Our result also provides a new DM mass range, which will be crucial for future particle dark matter searches.

Chapter 6

Lightning the DM from its viscosity and imlication for 21-cm signal

In our previous chapters, we have studied the effect of DM viscosity, specifically in the SIDM framework, on the small redshift, $0 \leq z \leq 2.5$. We considered that the DM is interacting with themselves elastically and interacts with the standard model particles via gravity. In this chapter, we will not assume any specific cause of DM viscosity like previously it was DM self-interaction. Further, we investigate the effect of DM viscosity on comparably large redshift, $10 \leq z \leq 1300$, and also assume non-gravitational interaction between the DM and the SM particles. In this work [286], we propose the possibility of the observational signal generated from the viscous DM energy dissipation. In particular, we study the visible photons (standard model photon) production from the viscous DM dissipation.

It has been found that the viscosity contributes to the entropy production and energy dissipation in the cosmic medium [12]. The produced energy depends on the viscosity parameters and can increase the fluid temperature. We apply this idea in the viscous dark matter framework and calculate the analytic expression for the viscous DM fluid temperature and check its dependency on its mass and viscosity parameters. We find that for large DM mass and viscosity, its temperature becomes large and can conflict with the DM coldness criteria, as discussed in Ref. [287]. Further, to keep the cold dark matter paradigm successful, we derive the condition on the DM viscosity parameters, which respects the DM coldness criteria.

We explore a possible effect of viscous energy dissipation and its impact on the evolution history of the Universe. We propose that viscous energy dissipation produces visible particles, particularly the photons (different from the CMB photons). Photon production is considered in two different ways. Firstly, when the DM dissipates directly into the photons, and secondly, when the dark matter dissipates into the dark radiation (DR), which can generate the visible photons via a kinetic mixing. We find that in both cases, the generated photons crucially depend on the DM temperature (which depends on the DM mass and its viscosity parameters) and increase as the temperature increases. Due to the presence of the DM viscosity, the DM temperature, and consequently, photon generation increases at low redshift. Thus it is crucial to explore the effect of these produced photons on the small redshift.

Recently, the EDGES collaboration [162] has announced to detect the global signal of the 21-cm line at $z \sim 17$ and reported an anomaly in it. A possible explanation of this anomaly requires a large number of photons in the Rayleigh-Jeans limit of the CMB spectrum [11, 164–167]. Using the viscous DM framework, we try to check the possibility of whether the photons generated via the viscous energy dissipation can address the EDGES anomaly in the 21 cm signal or not.

For this purpose, we calculate the number density of RJ photons produced from the viscous energy dissipation. We find that when the DM directly dissipates into the photons, it does not produce sufficient RJ photons and hence fails to explain the EDGES anomaly. However, in the case when the photons production takes place through the kinetic mixing, it can significantly increase the number density of photons in the RJ limit and hence address the EDGES anomaly. Further, we constrain the parameter space for the mixing parameter, DM mass, dark radiation mass, and DM viscosity parameters, which can explain the reported EDGES anomaly.

The arrangement of this chapter is as follows: In Section 6.1, assuming a power-law from its bulk viscosity, we calculate the expression of the DM temperature as a function of the redshift. Further, we derive the condition on the DM viscosity that respects the DM coldness criteria. In Section 6.2, we discuss the two different mechanisms for the photon generation from the viscous DM energy dissipation. Then in Section 6.3, the 21-cm anomaly reported by the EDGES experiment is explained using these excess RJ

photons. Later, we also explored the parameter space for DM mass, mixing parameter, viscosity parameter in the light of the EDGES explanation. Lastly in Section 6.4, we discuss and conclude our results.

Note that, throughout our discussion, we use the terms visible photon and photon interchangeably unless specified explicitly.

6.1 Viscous dark matter cosmology

As discussed earlier, in the standard model of cosmology (ΛCDM model), DM is considered to be cold and an ideal fluid (with no viscosity). In this chapter, we assume that dark matter is a bulk viscous fluid, consistent with the homogeneity and isotropy of the Universe. The possibility that DM fluid has shear viscosity can be ruled out from the large scale's homogeneity and isotropy.

In this Section, we will investigate the energy dissipation from the viscous DM and also explore the DM temperature evolution. Further, using the coldness criteria of the DM fluid, we will constrain the DM viscosity.

6.1.1 Viscous dark matter and energy dissipation

The origin of the bulk viscosity is a relaxation phenomenon and is related to its microscopic properties. Thus the expression of viscosity is dependent on the model of DM under consideration. Here for simplicity, we assume that the bulk viscosity depends only on the energy density of the DM. We consider bulk viscosity as a power-law in its energy density as [288]

$$\zeta_\chi(z) = \zeta_0 \left(\frac{\rho_\chi(z)}{\rho_{\chi 0}}\right)^\alpha , \tag{6.1}$$

where, $\rho_\chi(z)$ and $\rho_{\chi 0}$ represent the DM energy density at any redshift, z and at present, $z = 0$, respectively. Here ζ_0 and α are the viscosity parameters, and their values can be decided using the observations. For $\alpha = 0$, the DM viscosity becomes independent of its energy density and remains constant throughout the cosmic evolution.

In literature, the power law form of bulk viscosity has been widely used to study of the cosmic evolution. Murphy, in Ref. [289], assuming the bulk viscosity of form $\zeta = \kappa\rho$ ($\alpha = 1$), has find that viscous model can avoid the singularity of the spacetime.

Furthermore, the above form of viscosity, has also been used to explore the cosmic evolution (using $\alpha \geq 1$ and also $\alpha < 1$), the large scale structure formation [189] [190] ($\alpha = 0, 1/4$), 21-cm cosmological signal [274] ($\alpha = 0$ and $-1/2$). However, α values considered in the above studies were phenomenological. In chapter 3, considering the evolution of the bulk viscosity as, $\zeta = \zeta_0(1+z)^{\alpha}$ ($\alpha = -1.22$), we find that VSIDM cosmology can explain the low redshift observations. In Refs.[80][290], considering the DM decay in light relativistic particles, the bulk viscosity of cosmic fluid has been estimated, and reported that the viscosity is linearly proprtional in its energy density, i.e $\zeta \propto \rho$ ($\alpha = 1$). Thus inspired by both the cosmological and DM microphysics arguments as discussed above, we assume $\alpha = 1$ as a representative value for viscosity evolution.

Further, the presence of the dark matter viscosity causes energy injection in the cosmic medium and hence modifies the temperature evolution. In order to study the viscous dark matter temperature evolution, we need to estimate the energy generation due to the DM viscosity. For this purpose, firstly, we calculate the entropy production due to the DM viscosity. S. Weinberg, in Ref. [12], estimated the entropy generation due to the viscous fluid in the expanding Universe using the thermodynamics and Einstein equations. We apply this formalism to the viscous DM and obtain the entropy generation per unit volume due to the dark matter bulk viscosity as [273] [12]

$$\nabla_\mu S^\mu = \frac{\zeta_\chi}{T_\chi}\left(\nabla_\mu u^\mu\right)^2 \ , \tag{6.2}$$

where, T_χ is DM temperature, and S^μ is the entropy four-vector, which is defined by

$$S^\mu = n_\chi s_\chi u^\mu \ . \tag{6.3}$$

Here, s_χ , n_χ and u^μ represents the entropy per unit particle, number density and the four-velocity of the dark matter, respectively. Furthermore, applying the Second Law of Thermodynamics, one can estimate the heat energy per unit time per unit volume generated by the dark matter viscosity is given by

$$\frac{dQ_{\rm v}}{dVdt} = T_\chi \nabla_\mu S^\mu \ . \tag{6.4}$$

In order to estimate the heat energy production, we consider the homogeneous and isotropic expansion of the Universe, given by the flat FLRW metric as

$$ds^2 = -dt^2 + a^2(t)\delta_{ij}dx^i dx^j \ , \tag{6.5}$$

where $a(t)$ is the scale factor of the Universe. In the comoving frame, where the spatial component of the four-vector vanishes, $u^\mu = (1, 0, 0, 0)$, the above Eq. (6.4) simplifies as

$$\frac{dQ_{\rm v}}{dVdt} = 9\zeta_\chi H^2 \ . \tag{6.6}$$

In terms of redshift, the dissipated energy density by viscous DM from Eq. (6.6) is given by

$$q_{\rm vis}(z_{\rm s} \to z_{\rm e}) = \int_{z_{\rm s}}^{z_{\rm e}} \left(\frac{dQ_{\rm v}}{dVdz}\right) dz = -9 \int_{z_{\rm s}}^{z_{\rm e}} \zeta_\chi(z) \, \frac{H(z)}{(1+z)} \, dz \ . \tag{6.7}$$

Here $z_{\rm s}$ and $z_{\rm e}$ represent the starting and ending redshift between which the DM dissipates its energy. After integrating Eq. (6.7), we get

$$q_{\rm vis}(z_{\rm s} \to z_{\rm e}) = 5.36 \times 10^{-43} \left(\frac{H_0 \, m_{Pl}^2}{24\pi}\right)\left(\frac{\bar{\zeta}}{2\alpha+1}\right)\left[(z_{\rm s}+1)^{3(\alpha+\frac{1}{2})} - (z_{\rm e}+1)^{3(\alpha+\frac{1}{2})}\right]. \tag{6.8}$$

Thus the dissipated energy density depends on the dark matter viscosity parameters, $\bar{\zeta}$ and α. Also, the viscous DM dissipation becomes prominent when the viscosity is large. From Eq. (6.8), it is clear that $\alpha \neq -0.5$, otherwise the expression on RHS will blow. We point out that the viscous energy dissipation becomes large at a late time and increases with the DM viscosity.

6.1.2 DM temperature evolution due to its viscosity

As the presence of the DM viscosity causes the energy dissipation in the cosmic medium and hence viscosity can modify the DM temperature evolution equation. The temperature of the viscous dark matter evolves as [274]

$$\frac{dT_\chi}{dz} = 2\,\frac{T_\chi}{1+z} - \frac{2}{3(1+z)H}\left(\frac{m_\chi}{\rho_\chi}\right)\left(\frac{dQ_{\rm v}}{dVdt}\right) \ , \tag{6.9}$$

where m_χ, ρ_χ represents the mass and energy density of the DM, respectively. The first term in Eq. (6.9) corresponds to the Hubble dilution factor, which basically decreases the DM temperature as the universe expands. Further, the second term in Eq. (6.9) is due to the DM viscous energy dissipation, and its negative sign indicates that due to the viscosity, the dark matter temperature increases.

To calculate the DM temperature, we should provide the expression for the Hubble rate. In our work, we are interested in the matter-dominated era in which the Hubble

expansion rate is given by

$$H(z) \approx H_0 \, (\Omega_{M0})^{1/2} \, (1+z)^{3/2} \quad , \tag{6.10}$$

where, Ω_{M0} and H_0 ($H_0 = 100h$ km-s^{-1}MPc^{-1}) correspond to the present value of total matter content (DM and baryon) and the Hubble expansion rate, respectively. Here, we consider the values of the cosmological parameters, $h = 0.674$, $\Omega_{B0}h^2 = 0.0224$, $\Omega_{M0}h^2 = 0.142$ from the recent Planck 2018 data [20].

Furthermore, using Eq. (6.9), one can obtain the analytic solution for the DM temperature as

$$T_\chi(z) = A(1+z)^2 - \frac{4.2}{24\pi}\left(\frac{H_0^2\, m_{\rm Pl}^2}{\rho_c}\right)\left(\frac{m_\chi\, \bar{\zeta}}{\alpha - 1.16}\right)[1+z]^{3(\alpha-\frac{1}{2})} \quad , \tag{6.11}$$

where A and $\rho_c = 3H_0^2/8\pi G$ represent the constant of integration and the present critical energy density of the Universe, respectively. Further, $\bar{\zeta}$ is a dimensionless viscosity parameter and $m_{\rm Pl}$ is the Planck mass, defined by

$$\bar{\zeta} = \frac{24\pi G \zeta_0}{H_0} \quad \text{and} \quad m_{\rm Pl} = \frac{1}{\sqrt{G}} \quad . \tag{6.12}$$

From the equation (6.11), it is clear that the DM temperature depends on its mass and the viscosity parameters, $\bar{\zeta}$ and α. We also point out that DM temperature is non-singular at $\alpha = 1.16$. To calculate A, we need to provide the initial condition to the DM temperature. Since in our analysis, we assume the cold DM, we take the initial condition at the redshift, $z_{\rm i} \ll z_{\rm dec}$, where we assume $T_\chi(z_{\rm i}) = 0$. Here $z_{\rm dec}$ is the redshift where the DM kinetically decouples from the rest of the thermal. Therefore, using the above initial condition in Eq. (6.11), we obtain

$$A = \frac{4.2}{24\pi}\left(\frac{H_0^2\, m_{\rm Pl}^2}{\rho_c}\right)\left(\frac{m_\chi\, \bar{\zeta}}{\alpha - 1.16}\right)[1+z_{\rm i}]^{3\alpha-\frac{7}{2}} \, . \tag{6.13}$$

In particular, here, we assume the initial condition for DM temperature at $z_{\rm i} = 1300$. However, this initial condition does not carry a specific meaning. We also checked that while modifying the initial condition for DM temperature from 1300 to 1700 does not show any significant change in our results.

To see the effect of the DM viscosity parameters on its temperature evolution, in figure 6.1, we plot the DM temperature as a function of the redshift, for different values of the viscosity parameters. We fix $\bar{\zeta} = 10^{-15}, m_\chi = 0.1$ GeV and plot $T_\chi(z)$ for

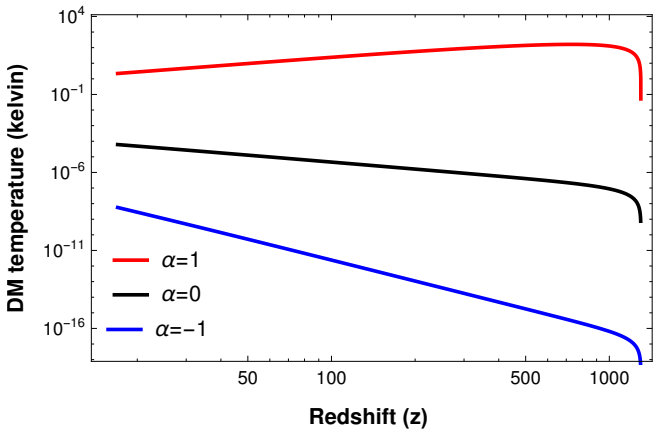

Figure 6.1: DM temperature evolution for different values of the DM viscosity for $\alpha = 1$ and $m_\chi = 0.1$ GeV.

$\alpha = 1$ (red line), $\alpha = 0$ (black line), $\alpha = -1$ (blue line). We see that for $\alpha = -1$, DM temperature also increases. This happens because the DM viscosity in inversly proprtional to the DM energy density, which decreases at late times (small redshift). Further, for $\alpha = 0$, the DM temperature increases at a small redshift but slightly lower rate in comparison with the $\alpha = -1$ case. But for $\alpha = 1$, the DM temperature firstly increases on large redshift and decreases below redshift ~ 500. Thus we conclude that for a fix value of $\bar{\zeta}$ and increasing the viscosity parameter α, causes to increases the DM temperature.

6.1.3 DM coldness criteria and constraints on its viscosity

Furthermore, as we have seen previously, as the DM viscosity increases, the DM starts heating up. In the case of sufficiently large DM viscosity, the DM temperature becomes high and may conflict with the DM coldness paradigm. In Ref. [287], using the CMB and LSS data, the authors have obtained an upper limit on the ratio of DM temperature to its mass at present.

The condition that DM will be cold in the redshift interval $z_{\rm dec} \geq z \gg 1$, is given by [287]

$$\frac{T_\chi}{m_\chi} \leq 1.07 \times 10^{-14}\,(1+z)^2 \ . \tag{6.14}$$

The above condition is explicitly applied for the linear regime, $z \gg 1$, where the structures are not in collapsed form. Therefore the above condition can be apply to

find a constraint on the DM viscosity parameters for which the DM behaves as cold. For this purpose, we use Eq. (6.11), to obtain the ratio of the viscous DM temperature to its mass, given as

$$\frac{T_\chi}{m_\chi} = \frac{A}{m_\chi}(1+z)^2 - \frac{4.2}{24\pi}\left(\frac{H_0^2\, m_{\rm Pl}^2}{\rho_c}\right)\left(\frac{\bar{\zeta}}{\alpha - 1.16}\right)[1+z]^{3(\alpha-\frac{1}{2})} \ , \tag{6.15}$$

where, A is given by Eq. (6.13). From above equation, we point out that, T_χ/m_χ is independent of the DM mass and only depends on the viscosity parameters, $\bar{\zeta}$ and α.

Furthermore, using Eq. (6.11) and Eq. (6.15), we derive the condition on the DM viscosity parameters. Thus the viscous DM behaves as a cold fluid at the redshift, $z_{\rm f}$, if

$$\bar{\zeta} \ \leq \ 1.92\times 10^{-13}\left(\frac{\rho_c}{H_0^2\, m_{\rm Pl}^2}\right)\Big(\alpha - 1.16\Big)\Big[(1+z_{\rm i})^{3\alpha-\frac{7}{2}} - (1+z_{\rm f})^{3\alpha-\frac{7}{2}}\Big]^{-1} \ , \tag{6.16}$$

where, $z_{\rm dec} \gg z_{\rm i} > z_{\rm f} \gg 1$. In case, the above inequality does not hold, then the viscous DM will no longer behaves as cold fluid. For example, for $\alpha = 1$, the maximum allowed bulk viscosity, which respect the DM coldness criteria at $z_{\rm f} = 17$, is given by $\bar{\zeta} \sim 10^{-14}$. We stress that the DM coldness criteria discussed above hold only for the linear regime of the structure formation and do not valid for the late time where the structures are formed and found in the form of the collapsed object (such as galaxies and clusters).

6.2 Production of visible photons from the viscous DM

In this Section, we discuss the production of visible photons from the dissipation of viscous DM fluid. In the previous Section, we have seen that the DM viscosity leads to energy dissipation in the cosmic medium. We make out an essential assumption that due to viscous energy dissipation, visible photons production may occur. *Here, we point out that the word visible photons (or photons) indicates to the produced standard model photons from the DM energy dissipation, and are different from the CMB photons*. Further, the photon generation can take place in two ways: (1) when the viscous DM directly dissipates into the visible photons and (2) when the DM firstly dissipates into the dark radiation (DR), which can further convert into the photons via a kinetic mixing between the DR and photons. We will discuss both the photon production mechanisms in subsequent subsections.

Furthermore, our analysis does not discuss the explicit particle physics motivated mechanism from which the viscous dissipation occurs and leaves it as a future exercise. However, for completeness, some of the possible models for the visible particle production via the DM energy dissipation can be found in the Refs. [11, 291–293].

6.2.1 When DM directly dissipates into photons

In this case, we assume that the viscous DM directly dissipates into visible photons. These photons are in thermal equilibrium with the DM and hence follow the Bose-Einstein distribution. So in terms of the distribution functions, the number density of generated photons from DM viscous dissipation is given as

$$n_{\chi\to A} = g_A \int_0^\infty \frac{d^3 p_A}{(2\pi)^3}\, f_A(p_A)\,, \tag{6.17}$$

where, p_A and $g_{A'}$ represents the momentum and relativistic degree of freedom of the photons, respectively. The photon distribution function is given as $f_A(p_A) = [\exp\left(\frac{\omega_A}{T_A}\right) - 1]^{-1}$, where $\omega_A = p_A$ is the energy associated with a photon. So, the number density of photons generated up to a small frequency limit, $\omega_{\rm max}$ is given as

$$n_{\chi\to A} = \frac{1}{\pi^2}\int_0^{\omega_{\rm max}} \frac{\omega_A^2}{\exp\left(\frac{\omega_A}{T_A}\right) - 1}\, d\omega_A\,. \tag{6.18}$$

In the low energy limit of the photon distribution, $\omega_A/T_\chi < 1$, so we can approximate, $e^{\frac{\omega_A}{T_\chi}} - 1 \approx \frac{\omega_A}{T_\chi}$. Furthermore, since photons are in thermal equilibrium with the DM, therefore they follow the dark matter temperature, ie., $T_A = T_\chi$. Thus in low energy limit, integration of Eq. (6.18), provide us

$$n_{\chi\to A} \approx \frac{\omega_{\rm max}^2}{2\pi^2}\, T_\chi. \tag{6.19}$$

The above equation shows that the number density of the produced low-energy photons is proportional to the DM temperature. The greater is the DM temperature, the larger is the low-energy photon production.

However, photon generation may change the cosmological evolution history. Since the photon production crucially depends on the DM temperature, so at large redshift (i.e., at the time of CMB release), due to small DM viscosity, the DM temperature was small, and hence the photons production was less. But at low redshift, due to increment

in the DM viscosity, the DM temperature becomes large and contributes more to the photons production rate. Therefore, at the time of photon decoupling, for sufficiently large DM viscosity, the photons generation will be large, which increases the radiation component and the Hubble expansion rate of the Universe. The increment in $H(z)$ modifies the baryon to photon ratio and also decreases the length of the sound horizon r_s, because $r_s \propto 1/H$ (see, Refs. [294] [295] and also references therein), which is well constraint from the CMB measurement [20].

Next, we estimate the above-discussed quantities and see whether the relativistic particles' production can create a problem for the cosmological observation or not? For this perpose, we calculate the effective degree of freedom $\Delta N_{\rm eff}$, which quantifies the energy contribution of extra radiation component in comparison with the CMB. The quantity, $\Delta N_{\rm eff}$ is defined as

$$\Delta N_{\rm eff} = \frac{\rho_{\rm REL}}{\rho_{\rm CMB}} \,. \tag{6.20}$$

Where, $\rho_{\rm REL}$ is the energy density of the extra radiation component (excluding the CMB and standard model neutrino) present in the Universe. The value of the $\Delta N_{\rm eff}$ decides whether the extra energy can be within the limit or modifies the cosmological observations. Here we use the Planck 2018 data to constraint the maximum energy contained in extra DR, which demands $\Delta N_{\rm eff} \leq 0.33$ [20]. Since, we consider that the viscous energy dissipation directly leads to the radiation component photon generation, hence one may assume

$$\rho_{\rm REL} = q_{\rm vis} \,. \tag{6.21}$$

For the viscosity parameters interested throughout in this work, given as $\alpha = 1$ and $\bar{\zeta} = 3 \times 10^{-15}$, the value of effective degree of freedom, $\Delta N_{\rm eff} = 10^{-15}$. This implies that the viscous energy dissipation is small in comaparision with the CMB radiation energy density. Therefore, the energy generated from the DM viscous dissipation into the photons is within the limits allowed from the Planck 2018 data (i.e. $\Delta N_{\rm eff} \leq 0.33$ [20]). Thus such a small energy density produced via the viscous dissipation will not affect H and also r_s.

6.2.2 When DM dissipates into DR which convert into photon via kinetic mixing

In this case, we assume that the DM dissipates into the dark radiation, A'. The produced DR is in thermal equilibrium with the DM and follows the Bose-Einstein distribution. Therefore in terms of distribution function, the number density of the produced dark radiation can be written as

$$n_{A'} = g_{A'} \int_0^\infty \frac{d^3 p_{A'}}{(2\pi)^3} f_{A'}(p_{A'}) \, . \tag{6.22}$$

where, $p_{A'}$ and $g_{A'}$ represents the momentum and relativistic degree of freedom of the dark radiation, respectively. The distribution function of the dark radiation is $f_{A'}(p_{A'}) = [\exp\left(\frac{\omega_{A'} - \mu_{A'}}{T'_A}\right) - 1]^{-1}$, where $\mu_{A'}$ represent the chemical potential of the dark radiation.. Further $\omega_{A'}$ is the energy associated with DR, given by $\omega_{A'} = (m^2_{A'} + p^2_{A'})^{\frac{1}{2}}$, where $m_{A'}$ is the mass of the dark radiation. So, after simplification, the above equation modifies as

$$n_{A'} = \frac{g_{A'}}{2\pi^2} \int_{m_{A'}}^\infty \frac{\omega_{A'}}{\exp\left(\frac{\omega_{A'} - \mu_{A'}}{T_{A'}}\right) - 1} \left(\omega^2_{A'} - m^2_{A'}\right)^{\frac{1}{2}} \, d\omega_{A'} \, , \tag{6.23}$$

Since the produced dark radiation is in thermal equilibrium with the DM, therefore $T_{A'} = T_\chi$. Thus considering $\mu_{A'} = 0$, the differential number density of the DR is given as

$$\frac{dn_{A'}}{d\omega_{A'}} = \frac{g_{A'}}{2\pi^2} \frac{\omega_{A'}}{\exp\left(\frac{\omega_{A'}}{T_\chi}\right) - 1} \left(\omega^2_{A'} - m^2_{A'}\right)^{\frac{1}{2}} \, . \tag{6.24}$$

Furthermore, as discussed in subsection 6.2.1, here we also point out that the production of extra relativistic particles may increase the Hubble expansion rate and can create problems at decoupling. Here, we consider that the viscous energy dissipation to the dark radiation generation, hence one can assume $\rho_{\rm REL} = q_{\rm vis}$. Thus for $\alpha = 1$ and $\bar{\zeta} = 3 \times 10^{-15}$, and using Eq., we get (6.20) $\Delta N_{\rm eff} = 10^{-15}$. Therefore, we find that dark radiation production does not affect the CMB observations for the redshift range of our interest.

We further make an important assumption that the dark radiation can generate the visible photons through a kinetic mixing, in a similar way as the standard model neutrinos change their flavors [296]. Therefore, the Lagrangian density of the DR-photon

system can be written as

$$\mathcal{L}_{\mathcal{A}'\mathcal{A}} = -\frac{1}{4}F_{\mu\nu}F^{\mu\nu} - \frac{1}{4}F'_{\mu\nu}F'^{\mu\nu} - \frac{\epsilon}{2}F_{\mu\nu}F'^{\mu\nu} + \frac{1}{2}m^2_{A'}A'_{\mu}A'^{\mu} \ . \tag{6.25}$$

Here, the first and second term corresponds to the kinetic term for photon and DR. The third term represents the interaction between the DR and visible photon, and ϵ is the kinetic mixing parameter. Further, the last term corresponds to the dark radiation mass.

The probability of conversion of DR to photons becomes maximum at the time of resonance, for which the DR mass is equal to the photon plasma mass, i.e.,

$$m_{A'} = m_A(z) \ . \tag{6.26}$$

Here, $m_A(z)$ is the plasma mass of the photon at redshift z, which is defined as [297, 298]

$$m_A(z) \simeq 1.7 \times 10^{-21} \ (1+z)^{3/2} \ x_e^{1/2}(z) \ \text{GeV} \ , \tag{6.27}$$

where $x_e(z)$ is the electron fraction which is calculated from the `RECFAST` code [299] using `CAMB` [300]. The resonance condition can happen for a range of DR mass between, $10^{-23} - 10^{-18}$ GeV. The conversion probability of DR (A') into the SM photon (A) at the resonance is given by [297]

$$P_{A\longrightarrow A'} = P_{A'\longrightarrow A} = \frac{\pi\epsilon^2 m^2_{A'}}{\omega_{A'}} \left|\frac{d\log m_A^2}{dt}\right|^{-1}_{t=t_{\rm res}} \ , \tag{6.28}$$

where $t_{\rm res}$ is the time at which the resonance can takes place. In terms of the redshift, the conversion probability can be rewritten as

$$P_{A'\longrightarrow A} = \frac{\pi\epsilon^2 m^2_{A'}}{\omega_{A'}} \left|(1+z)\,H(z)\,\frac{dm_A^2}{dz}\right|^{-1}_{z=z_{\rm res}} \ . \tag{6.29}$$

where, $z_{\rm res}$ is the redshift corresponds for resonance time, $t_{\rm res}$. As for the low energy photons, the free-free (bremsstrahlung) absorption effect should be taken into consideration. Then the above probability should be multiplied by the photon survival probability, $P_S(x,z) \approx e^{-\tau(x,z)}$, where $\tau(x,z)$ is the optical depth of the plasm medium, which depends on the position and the redshift. Hence for low energy photon case, the conversion probability modifies and given as, $P_{A\to A'} \longrightarrow P_{A\to A'}\,P_S(x,z)$. However, it has been found that the absorption of the low energy photons in the cosmic plasma becomes effective for $z > z_{\rm abs} = 1700$ [301]. Since here we are interested in relatively

low redshift $z < z_{\rm abs}$, so the photon absorption factor will not be necessary. Therefore we can neglect the photon survival factor in our analysis.

Therefore, the differential number density of the visible photon produced from the viscous dissipation of DM into DR and further to photons is given by

$$\frac{dn_{A'\to A}}{d\omega_{A'}} = \left(\frac{dn_{A'}}{d\omega_{A'}}\right) P_{A'\to A} \ . \tag{6.30}$$

Thus using the Eq. (6.24) and Eq. (6.29) in Eq. (6.30), we obtain

$$n_{A'\to A} = \frac{\pi\epsilon^2 g_{A'} m_{A'}^2 T_\chi}{2\pi^2} \left|(1+z)\, H\, \frac{dm_A^2}{dz}\right|^{-1}_{z=z_{\rm res}} \int_{m_{A'}}^{\infty} \frac{\sqrt{\omega_{A'}^2 - m_{A'}^2}}{\omega_{A'}}\, d\omega_{A'} \ . \tag{6.31}$$

The number density of the photons lies in the low energy limit $\omega_{A'}/T_\chi < 1$, is estimated by integrating Eq. (6.31) up to a small frequency limit, $\omega_{\rm max}$. This gives us

$$n_{A'\to A} = \frac{\pi\epsilon^2 g_{A'} m_{A'}^2 T_\chi}{2\pi^2} \left[\sqrt{\omega_{\rm max}^2 - m_{A'}^2} + m_{A'} \tan^{-1}\left(\frac{m_{A'}}{\sqrt{\omega_{\rm max}^2 - m_{A'}^2}}\right) - \frac{\pi m_{A'}}{2}\right] \times \left|(1+z)\, H(z)\, \frac{dm_A^2}{dz}\right|^{-1}_{z=z_{res}} \ , \tag{6.32}$$

where, $g_{A'} = 2$. The above equation shows that the number density of the produced photons depend on the DM temperature, DR mass, and the mixing parameter.

Thus, from the above discussion, we conclude that in both cases (i.e., indirect conversion or via kinetic mixing), the photons' production via viscous dissipation does not modify the CMB and LSS observations. Therefore, we explore the effect of these photons in the light of the recent cosmological signal of 21-cm observed by the EDGES collaboration. The next Section is devoted to the basics of the 21-cm cosmological signal and associated anomaly reported by EDGES.

Comment on thermal dark radiation and photons from viscous dark matter

In our work, we assume that the system of DM-DR (or photons) is thermalized. The DM couples with the photons (direct coupling of the DM with photons is not necessary) and continuously dissipates its energy into the photons throughout the cosmic evolution. Further, we also consider that the DM-photons system is in quasi thermal equilibrium and do not very far from the local thermal equilibrium. Therefore in this

crude approximation, the system is in equilibrium, therefore, follows the same temperature. Due to common temperature, the system of DM-photons follows the same temperature evolution until the equilibration is maintained. Further, on the same basis, for the case of DM dissipation into the dark radiation, we consider the DM-DR system is in quasi-equilibrium and shares the same temperature. In this system, photon production takes place from the kinetic mixing between the DR and photons.

In the expanding Universe, the thermalization of viscous dark matter with the DR (or photons) is possible when the DM scattering rate with the DR (or photons) is larger than the Hubble expansion rate, $\Gamma_{\chi A',\chi A} > H$, where $\Gamma_{\chi A'}$ and $\Gamma_{\chi A}$ represent the DM scattering rate with the DR and photons, respectively. However, if $\Gamma_{\chi A',\chi A} < H$, then the production takes place at out of equilibrium and hence DM and DR (or photons) do not share the common temperature. Therefore the process by which the system is thermalized depends on the particle model of the DM dissipation.

We emphasize that in our work, the word photons represent the produced photons (from the DM energy dissipation), which are different from the CMB photons. Our analysis relies on the assumption that the system of DM-DR (or photons) is thermalized and constraints are valid when the above condition is met. In this case, due to a common temperature (thermalization), a system of DM-DR (or photons) does not redshift differently. To explore the particle physics model of the DM dissipation and non-thermal production of the photons and DR from DM is my future goal.

6.3 VDM explanation of EDGES anomaly

In Section1, we have seen that the standard model of cosmology can not explain the anomaly observed in the 21-cm signal reported by the EDGES collaboration. Therefore it explanation may require a new physics. In this direction, many efforts have been made and found that the EDGES anomaly can be addressed via the DM-baryon interaction [157] or by increasing the photons in the low-frequency limit of the CMB, tail [11, 164–167], etc. For other possible EDGES explanations, see Refs. [168–171].

In this work, we focus on the explanation of the EDGES anomaly that requires an increase in the photons in the Rayleigh-Jeans limit of the CMB radiation. The photons

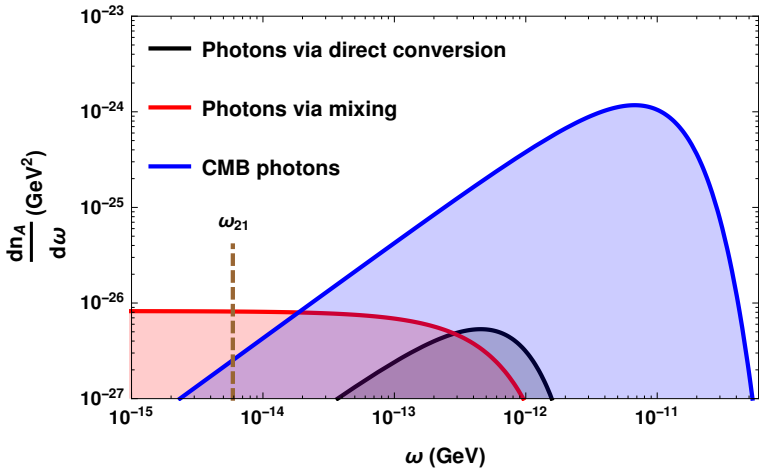

Figure 6.2: The spectrum of the photons produced by the viscous dissipation and the CMB radiation at the redshift, $z = 17$. We fix $\alpha = 1$, $\bar{\zeta} = 1.5 \times 10^{-14}$, $m_\chi = 0.1$ GeV and $\epsilon = 2.1 \times 10^{-7}$ [11].

in the low energy limit of the RJ tail of the CMB radiation, i.e., $\omega/T_{\rm CMB} < 1$, is given by

$$n_{\rm RJ} = \frac{g_{\rm CMB}}{2\pi^2} \int_0^{\omega_{\rm max}} \frac{1}{\exp\left(\frac{\omega}{T_{\rm CMB}}\right) - 1} \omega^2 \, d\omega \approx \frac{\omega_{\rm max}^2}{2\pi^2} T_{\rm CMB} \ , \tag{6.33}$$

where, $g_{\rm CMB} = 2$. Here, we propose a new mechanism to explain the EDGES anomaly by the viscous DM dissipation into the photons. As we have seen in the previous Section that the viscous dissipation leads to photon production and can increase the photon number density in the RJ frequency limit of the CMB radiation. Here we inquire whether the produced photons are sufficient enough to address the anomaly or not.

6.3.1 Production of visible photons from the viscous dissipation

In this subsection, we study the photon production via the DM energy dissipation and compare it with the CMB photons using formalism, as discussed in Section 6.2. In Figure 6.2, we plot the differential number density of the photons obtained from the direct dissipation of the dark matter (black region), through kinetic mixing with the DR (red region), and from the CMB (blue region). To generate the plot, we fix the DM viscosity parameters, $\alpha = 1, \bar{\zeta} = 10^{-15}$, DM mass, $m_\chi = 0.1$ GeV and kinetic mixing parameter, $\epsilon = 2.1 \times 10^{-7}$ [11].

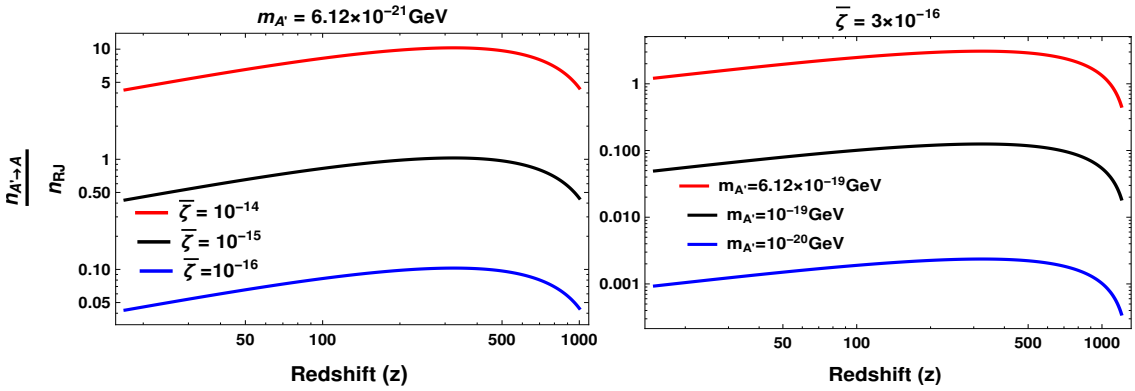

(a) (b)

Figure 6.3: Plot of the ratio of photons number density obtained from viscous dissipation to the CMB photon in the RJ limits. We consider, $\epsilon = 2.1 \times 10^{-7}$ [11] and $\alpha = 1$.

From Fig. 6.2, we see that the photons obtained from the kinetic mixing (red region) can significantly increase the number density of photons in the RJ region of CMB radiation. However, this does not alter the number density of high-frequency photons by an appreciable amount. For the case of directly produced photons (black region), there is an increase in the CMB photons only at higher frequency regions. Since the explanation of EDGES anomaly demands a large number of photons at RJ of CMB radiation. Therefore, one can find that photons generated via kinetic mixing may explain, but directly produced photons can not address the EDGES anomaly. Here, our focus is to explain the EDGES anomaly, so the case where the photons generate through kinetic mixing is interesting. Thus the rest of our analysis, we will discuss this case only.

Further, we also check the dependency of the photon production through the kinetic mixing on the DM viscosity. In Fig. 6.3(a), we plot the $n'_{A'\to A}/n_{RJ}$ and (6.33)) as a function of the redshift for different values of the DM viscosity. In this plot the red line, black line and blue line correspond to $\bar{\zeta} = 10^{-14}$, $\bar{\zeta} = 10^{-15}$ and $\bar{\zeta} = 10^{-16}$, respectively. We take $\epsilon = 2.1 \times 10^{-7}$ [11], $\alpha = 1$ and $m_{A'} = 6.12 \times 10^{-19}$ GeV (for this DR mass the resonant condition happens at $z_{\rm res} = 1268$). From Fig. 6.3(a), we see that increasing the DM viscosity increases the photon production rate.

Then we also explore the dependency of DR production on its mass. For this

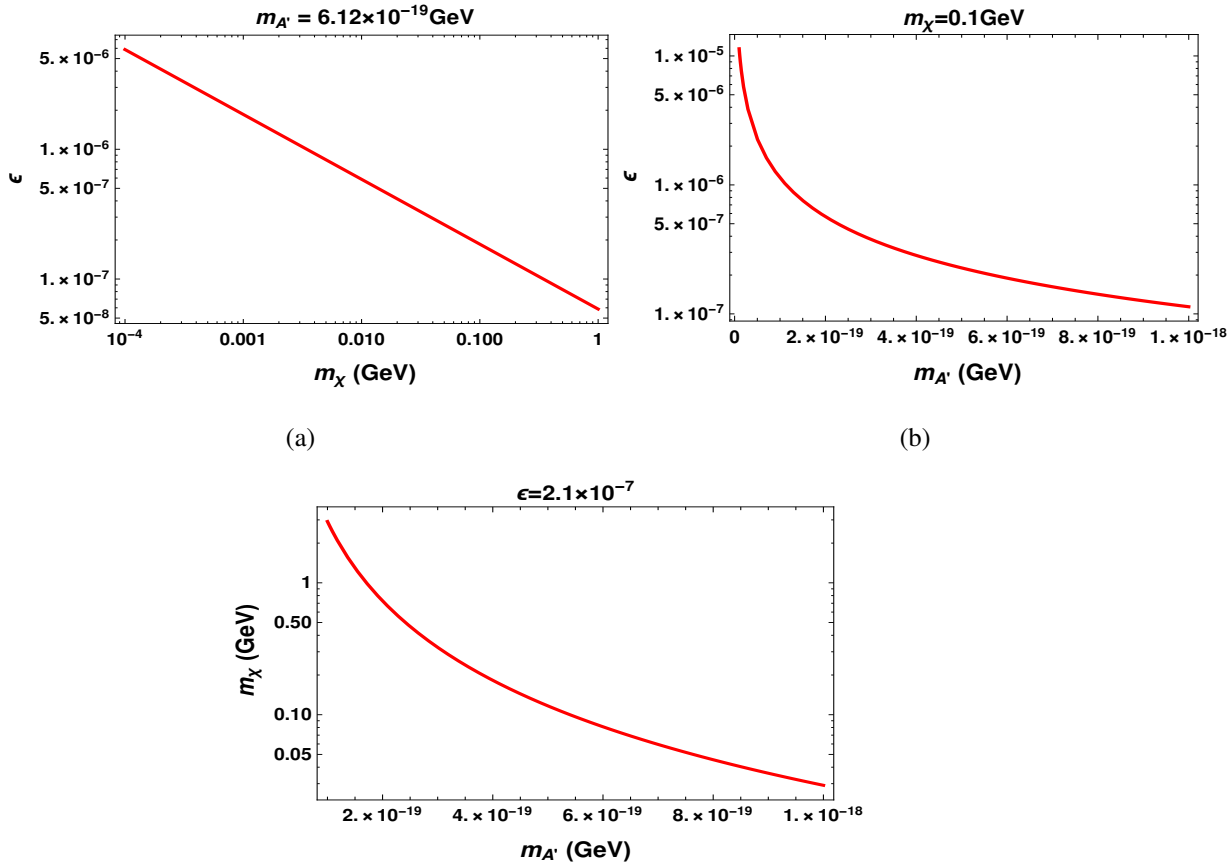

Figure 6.4: Contraining the parameters that explain the EDGES observed 21 cm signal, i.e. $n'_{\chi\to A}/n_{RJ} = 1$ [11]. We assume $\alpha = 1$ and $\bar{\zeta} = 3 \times 10^{-15}$.

purpose, we plot $n'_{A'\to A}/n_{RJ}$ as a function of redshift for different values of the DR mass in Fig. 6.3(b). Here, blue, black and red line represents the DR masses 10^{-20} GeV , 10^{-19} GeV and 6.12×10^{-19} GeV, which correspond to the resonance redshift $z_{\rm res} = 637, 973, 1268$, respectively.

From Fig. 6.3(b) we point out that the photon number density increases as the DR mass, $m_{A'}$ increases. It is because for a large $m_{A'}$, the resonance condition is met earlier (i.e., at large redshift), and hence the probability of conversion of DR to photon becomes large. Therefore we conclude that photon production increases as the DM viscosity and DR mass increase.

6.3.2 Constraining the parameter space for ϵ, $m_{A'}$ and m_χ

In this subsection, we will constrain the range of parameter space for ϵ, $m_{A'}$ and m_χ, which is consistent with the explanation of the global 21-cm signal reported by EDGES. In order to address the EDGES anomaly the number density of produced photon requires, $n'_{\chi\to A}/n_{RJ} = 1$ [11]. In Fig. 6.4, to study the constraint on the parameters involved, we take $\alpha = 1$ and $\bar{\zeta} = 10^{-7}$.

In Fig. 6.4(a), we fix $m_{A'} = 6.12 \times 10^{-19}$ GeV and plot kinetic mixing parameter, ϵ as a function of DM mass, m_χ that satisfy the condition $n'_{\chi\to A}/n_{RJ} = 1$. We see that as m_χ increases, ϵ decreases. In Fig. 6.4(b), on fixing $m_\chi = 0.1$GeV, we plot ϵ as a function of dark radiation mass, $m_{A'}$. Here also, we find that ϵ decreases as $m_{A'}$ increases. Therefore, we find that to address the EDGES anomaly from the small DM or DR mass, the mixing parameter should be sufficiently large and vice-versa.

Further, in Fig. 6.4(c) on fixing $\epsilon = 2.1 \times 10^7$, we plot DM mass, m_χ as function of dark radiation mass, $m_{A'}$, that explain the explain the EDGES anomaly. We see that in order to produce the sufficient photons that satisfy the condition $n'_{\chi\to A}/n_{RJ} = 1$, a large m_χ prefer small $m_{A'}$ and vice-versa.

6.3.3 Constraint on the DM viscosity parameters

Here, we explore the parameter space for the DM viscosity that may address the EDGES anomaly and also respect the DM coldness condition. In Fig. 6.5, keeping $m_\chi = 1$ GeV, $\epsilon = 2.1 \times 10^{-7}$ and $m_{A'} = 6.12 \times 10^{-19}$ GeV fixed, we plot the $\bar{\zeta} - \alpha$ plane. The the blue region explains the EDGES anomaly and the red region represents the region which is ruled out from the DM coldness paradigm. From Fig. 6.5, we infer that the small value of α (more negative α value) needs large $\bar{\zeta}$ and large value of α (for less negative α value) requires small $\bar{\zeta}$. Futhernore, the parameter space towards the large α values is prohibited due to the cold dark matter criteria, but corresponding to a small α values, a large parameter space is still allowed.

Here, it is important to highlight that the DM viscosity parameters $(\bar{\zeta}, \alpha)$ discussed during our analysis, $(3 \times 10^{-15}, 1)$ at $z = 17$, is less than the maximum limit allowed from the DM coldness condition (given in Eq. (6.16), i.e. $(5 \times 10^{-15}, 1)$. Therefore, we conclude that the viscous effect of the DM considered here is not large, and hence the

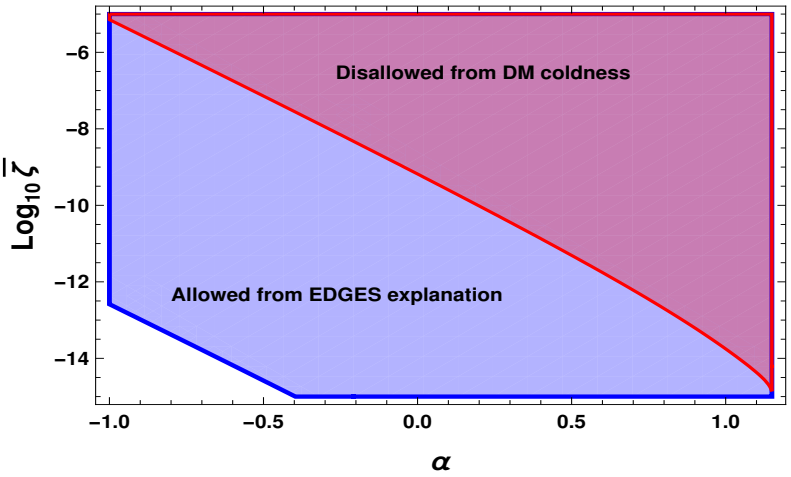

Figure 6.5: The DM viscosity parameter space that explain the EDGES 21 cm anomaly and consistent with the DM coldness. We fix $m_\chi = 1$ GeV, $\epsilon = 2.1 \times 10^{-7}$ and $m_{A'} = 6.12 \times 10^{-19}$ GeV.

DM is cold.

We also calculate the energy dissipation from the viscous DM fluid that is needed to explain the EDGES anomaly. We estimate the ratio of DM dissipational energy which produces the required number density of the photons, $q_{\rm vis}$ from Eq. (6.8) to the present DM energy density, $\rho_{\chi 0}$. In our analysis, we have considered $z_{\rm s} = 1300$ and $z_{\rm e} = 15$. For the viscosity parameters, $\alpha = 1$ and $\bar{\zeta} = 3 \times 10^{-15}$, we get $q_{\rm vis}/\rho_{\chi 0} \sim 10^{-17}$, which implies that only a small part of the total DM dissipates into the visible photons.

6.4 Conclusion

In this work, we study the DM temperature evolution in the presence of viscosity and explore its implication on cosmic evolution. We show that the presence of the viscosity in DM fluid leads to energy dissipation and raises its temperature. This effect becomes important at the late time of cosmic evolution. The DM temperature depends on its mass and viscosity. In case the DM viscosity is large, its temperature becomes high, so the DM fluid may no longer behave like a cold fluid. We have derived the condition on the DM viscosity parameters for which the DM behaves like a cold fluid.

The viscous effect of DM can be realized when DM produces an observable signal. In this study, we have proposed one of the possible scenarios where the DM viscosity

leads to the generation of visible photons. We consider visible photon production in two ways. First, when the dark matter dissipates directly to the visible photons, and second when the dark matter dissipates into the dark radiation, which can further lead to the visible photons through the kinetic mixing.

Further, the production of extra relativistic particles such as the photons or dark radiation from the DM viscous dissipation may affect the cosmological observations. In the case of small DM viscosity, the relativistic particles do not affect the cosmic evolution, but for sufficiently large DM viscosity, it can increase the Hubble expansion rate and create problems at decoupling. We show that for the DM viscosity parameters considered in this work, the production of the relativistic particles is not large enough (lie within the limit allowed from the Planck 2018 observations) to increase the Hubble expansion rate. Hence it will not modify the CMB observations.

We find that the photons produced via the DM viscous dissipation populate the low-frequency range of the CMB radiation and explain the 21 cm anomalous signal reported by the EDGES collaboration. In particular, we point out that the resonantly produced photons increase the number density of the RJ tail of the CMB radiation and are sufficient to explain the reported EDGES anomaly, but the directly produced photons fail to do so. We also explore the range of the mixing parameter values, ϵ, the DM mass, m_χ, the DR mass, $m_{A'}$, and DM viscosity parameters in the light of EDGES 21 cm anomaly. These parameter spaces can further provide a useful probe for DR and DM viscosity from the upcoming precise 21 cm cosmological observations. However, in this analysis, it is important to point out that we have not discussed the explicit particle physics motivated mechanism from which the viscous dissipation and photon production occurs and leaves it as a future exercise.

Chapter 7

Viscous DM-baryon interaction and EDGES anomaly

7.1 Introduction

In the previous chapter, we study the EDGES anomaly's explanation by photon production via the DM viscosity. However, one of the other explanations demands a smaller baryonic temperature in comparison with the value quoted using the standard cosmological calculation. Since at the time of cosmic dawn, the DM was much colder than the baryons, so a promising way to reduce the baryon temperature could be an interaction between the baryons, and the dark matter [157, 158]. For a sufficient baryonic cooling, the preferable form of DM-baryon scattering is assumed as $\sigma = \hat{\sigma} v_{\rm rel}^{-4}$, where $v_{\rm rel}$ represents the relative velocity between DM and baryons [302–304].

Furthermore, it has been found that in order to explain the EDGES observation due to DM-baryon interaction, the DM mass should be sub GeV scale, $m_\chi \leq 1$ GeV [157, 158]. The widely favored DM candidate, known as weakly interacting massive particles (WIMPs), which fits the Planck observational data well, has a mass range of $\sim$ few GeV to TeV. However, the non-observation of WIMP in the direct detection experiments like XENON100 [305], LUX [306] and LHC, have excluded large parameter space of the DM mass. The direct detection experiments are highly sensitive around DM masses of 30 GeV and less sensitive for DM mass below 10 GeV due to the small nuclear recoil energy. Therefore, the low mass DM particles (i.e., $m_\chi \leq 1$ GeV), which

is required to explain the EDGES observation, can evade the direct detection DM mass constraints.

The observation 21-cm signal reported by the EDGES collaboration provides an opportunity to understand the dark matter's microscopic properties and the thermal plasma at the cosmic dawn era. Any kind of energy dissipation leads to the energy injection into the cosmic medium and, hence, modifies the temperature evolution of the DM, CMB, and baryon. This led to a change in the Brightness temperature and the strength of the 21-cm signal. In Refs. [307, 308], the EDGES observation has been used to estimate the constraints on dark matter annihilation and decay rates. Later, in Ref. [309], authors argued that the interaction between the DM and lighter degree of freedom could delay the 21-cm absorption signal due to collisional damping, and hence the EDGES absorption signal put a strong bound on DM-interaction with the light Standard model particles. Further, in Ref.[310] using the EDGES observation, the authors have been constraint the kinematic mixing strength between the photon and hidden photon in the ultra-light hidden photon DM model. In Ref. [311, 312], the authors have constrained the strength of the magnetic field using the EDGES signal and further explained the EDGES anomaly due to the Alpha-effect properties of the magnetic fields [313].

In this chapter [314], we study the DM properties within the viscous DM-gas interaction framework in the light of the reported 21 cm absorption signal. Inspired by the large-scale homogeneity and isotropy of the Universe, we assume the bulk viscosity in the DM fluid. To explore the impact of the DM viscosity onto the cosmic evolution, we consider a its form power law as $\zeta_\chi = \zeta_0 \left(\frac{\rho_\chi(z)}{\rho_\chi(0)}\right)^\gamma$. We mention that to be consistent with our paper notation, we assume the exponential power parameter is γ. Then using the energy-momentum conservation equation, we derive the DM and gas energy density evolution in the presence of the viscous DM-gas interaction and the relative velocity between them. It is pointed out that for the values of bulk viscosity considered here, the Hubble expansion rate does not show any significant change compared to the ΛCDM model. Therefore, the viscous DM model does not change the cosmic evolution.

Furthermore, we set up the temperature evolution equations for the viscous dark

matter and gas in the presence of DM-gas interaction. Then, we check the dependency of DM and gas temperature on the DM viscosity and its mass and the DM-gas interaction cross-section. We find that in the case of the low DM viscosity, the energy dissipation is small, and hence the DM temperature does not increase appreciably. But, if the DM viscosity is sufficiently large, it increases the DM temperature and the gas temperature through the DM-baryon scattering at the low redshift. We also find that the DM and gas heating depends on the DM mass and increases for higher DM masses.

However, the gas can be cooled by either increasing the DM-gas interaction or decreasing the DM mass. It allows us to put new limits on the DM mass, bulk viscosity, and the DM-gas interaction cross-section. We argue that explaining the EDGES absorption signal in the light of the viscous DM scenario requires a larger DM-gas cross-section and a smaller DM mass in comparison with the ideal DM fluid.

We find that the EDGES global 21-cm observation allows a large DM viscosity, which is approximately 10^4 (for a constant viscosity) to 10^7 (for a variable viscosity) times larger in comparison with the limit obtained from the structure formation. Furthermore, the cold dark matter paradigm (that explains the CMB observations) enables us to put another constraint on the DM viscosity, which is an order of magnitude (for constant viscosity case) smaller than the limit obtained on the DM viscosity from the structure formation. To the best of our knowledge, this is the stringent bound on the DM viscosity.

The organization of this chapter is as follows: In Section 7.2, Assuming the viscous DM-gas interaction, we derive the background cosmology and then set up the temperature evolution equations of the dark matter and baryons. Further, in Section 7.3, we show our results and put constraints on the DM mass and DM-baryon scattering using the EDGES observational signal. We also put two independent constraints on DM viscosity; one is coming from the EDGES observation, and another is coming from the coldness of the dark matter. Finally, we discuss and conclude our work in Section 7.4.

7.2 Viscous DM-gas interaction cosmology

In our viscous DM model, we consider that the Universe consists of radiation (R), baryon (B), viscous cold dark matter (χ), and cosmological constant (Λ). Unlikely previous chapters, here we focus on a comparably larger redshift range, $15 \leq z \leq 1100$, where the larger non-linear structures have not been formed (structure like the first stars are forming, and below the above redshift, a reionization occurs).

In this work, we make an important assumption that DM is bulk viscous fluid and interacting with the gas elastically. Since, at the time of our interest, the gas is hotter in comparison with the DM, therefore, due to elastic scattering, the gas cools by transferring the heat energy to the DM. In order to have a sufficient cooling of the gas at the cosmic dawn era, the interaction between the DM and gas must be sufficiently large. This can be done by considering the DM-gas interaction of the Rutherford type $\sigma = \hat{\sigma} v_{\rm rel}^{-4}$ [302, 303], where $v_{\rm rel}$ is the relative velocity between DM and gas.

7.2.1 Energy evolution of viscous DM-gas interaction

In the presence of the viscous DM-gas interaction, the energy density of the viscous dark matter and gas can be obtained by applying the energy conservation equation. Here, we approximated the total energy associated with the DM and gas as the sum of their rest mass energy, thermal energy, and fluid kinetic energy, respectively. Thus the equation for the energy density of viscous DM (ϵ_χ) and gas (ϵ_G) is given by

$$\frac{d\epsilon_\chi}{dt} + 3H(\epsilon_\chi + P_\chi - 3\zeta_\chi H) = n_\chi \left(\frac{dQ_\chi}{dt}\right) + \frac{\rho_\chi \rho_G}{\rho_M} v_\chi \, D(v_{\rm rel}) \ , \tag{7.1}$$

$$\frac{d\epsilon_G}{dt} + 3H\left(\epsilon_G + P_G\right) = n_G \left(\frac{dQ_G}{dt}\right) - \frac{\rho_\chi \rho_G}{\rho_M} v_G \, D(v_{\rm rel}) \ , \tag{7.2}$$

where, ϵ_χ and ϵ_G represents the total energy of the DM and gas, respectively. n_G, corresponds to the number density of the gas. In our notation, the ρ_χ, ρ_G, and $\rho_M \approx \rho_\chi + \rho_G$ represents the rest mass-energy density of the DM, gas and total matter content (that is the sum of the DM and gas, rest mass energy density), respectively.

Further, the term $\frac{dQ_G}{dt}$ in Eq. (7.2) represents the heat transfer rate by gas to DM due to DM-baryon interaction. For Rutherford type of DM-gas scattering cross section,

the heat transfer rate by baryons to DM is given by Refs. [302–304] as

$$\frac{dQ_G}{dt} = \sum_I \sqrt{\frac{2}{\pi}} \left(\frac{\mu_I}{m_I + m_\chi}\right) \left[x_I \frac{e^{-r_I^2/2}}{u_{\rm th}^3}\right] \Big[T_\chi - T_G\Big] n_\chi \hat{\sigma}_I \; + \; \frac{\rho_\chi \mu_I}{\rho_M} \, v_{\rm rel} \, D(v_{\rm rel}) \;\; , \tag{7.3}$$

where $\hat{\sigma}_I$ is the DM-gas scattering cross-section and ρ_M is the total matter density. Here $I = (e, p, H, He)$ are the species with which the DM can interact. The different quantities in Eq. (7.3) are defind by

$$\mu_I = \frac{m_\chi m_I}{m_\chi + m_I}, \;\; x_I = \frac{n_I}{n_H}, \; r_I = \frac{v_{\rm rel}}{u_{\rm th}^I} \;\; \text{and} \;\; u_{\rm th}^I = \left(\frac{T_G}{m_I} + \frac{T_\chi}{m_\chi}\right)^{\frac{1}{2}} \;\; . \tag{7.4}$$

If the DM is interacting with the Hydrogen only then $m_I = m_H$ and $x_I = 1$. The second term, $\dfrac{dQ_\chi}{dt}$ in Eq. (7.1) represents the heat absorption rate by the dark matter particles, which can be obtained by replacing the gas by DM, i.e. $G \leftrightarrow \chi$ into the Eq. (7.3). Also, the $D(v_{\rm rel})$ is related with the DM-gas interaction, given by

$$D(v_{\rm rel}) \equiv -\frac{dv_{\rm rel}}{dt} = \sum_I \frac{\rho_I}{\rho_B} \left(\frac{\rho_m \hat{\sigma}_I}{m_I + m_\chi}\right) \left(\frac{1}{v_{\rm rel}^2}\right) F(r_I) \;\; , \tag{7.5}$$

and the function $F(r_I)$ is given by

$$F(r_I) \equiv {\rm Erf}\left(\frac{r_I}{\sqrt{2}}\right) - \sqrt{\frac{2}{\pi}} \, r_I \, e^{-r_I^2/2} \tag{7.6}$$

From the heat transfer rate (for both the baryon and DM) Eq. (7.3), we can explain the two term as follows:

- The first term is the heat transfer term due to the temperature difference between the DM and gas. This term causes cooling when $T_G > T_\chi$ and heating when $T_G < T_\chi$ and vanishes when both DM and gas temperature becomes same, i.e, $T_G = T_\chi$.

- The second term corresponds to the drag term, which arises due to the fluid velocity difference between the gas and the DM. In comparison with the temperature difference term, this term is small for the sub-GeV DM mass ($m_\chi < 1$GeV). For relatively larger DM mass ($m_\chi > 1$GeV), the contribution of the drag term becomes prominent and will heat both the DM and gas irrespective of their temperatures [303].

Here we emphasize that, we are interested in DM mass range less than GeV, i.e. $m_\chi \leq 1$ GeV, hence the friction term in heat transfer rate Eq. (7.3) (second term) contribution becomes small in comparison with the temperature difference proportional term (first term) [303]. In the same way, the second term in the r.h.s of energy equations for DM (Eq. (7.1)) and gas (Eq. (7.2)) becomes subdominent in contrast with the term proportional to the temperature difference. Thus we see that in the energy evolution equation for the DM and gas, we are only left with temperature difference proportional term in RHS.

In order to solve the energy equation, we need to provide the evolution equations for the DM and gas velocity. Considering the homogeneity and isotropy of the Universe, the DM and gas velocity equation can be written as

$$\frac{\partial v_\chi}{\partial t} + v_\chi\left(\frac{\partial v_\chi}{\partial r}\right) + Hv_\chi = \frac{\rho_G}{\rho_M} D(v_{\rm rel}) + \frac{\zeta_\chi}{\rho_\chi}\left(\frac{\partial^2 v_\chi}{\partial r^2}\right) , \tag{7.7}$$

$$\frac{\partial v_G}{\partial t} + v_G\left(\frac{\partial v_G}{\partial r}\right) + Hv_G = -\frac{\rho_\chi}{\rho_M} D(v_{\rm rel}) . \tag{7.8}$$

Here the first term in the r.h.s. of both the DM and gas velocity corresponds for the Hubble dilution and the second term corresponds for the DM-gas interaction. The positive and negative sign before the second term in the Eq. (7.7) and Eq. (7.8) implies that due to DM-gas interaction, the velocity of DM increases and the gas velocity decreases. Further, we are interested in the linear regime of the structure formation, where the fluid velocity is small. Therefore keeping a linear order in velocity and neglect the higher order in the velocity, we get

$$\frac{\partial v_\chi}{\partial t} + Hv_\chi = \frac{\rho_G}{\rho_M} D(v_{\rm rel}) , \tag{7.9}$$

$$\frac{\partial v_G}{\partial t} + Hv_G = -\frac{\rho_\chi}{\rho_M} D(v_{\rm rel}) . \tag{7.10}$$

We also point that all the differential equations discussed above depends on the relative velocity of DM and gas. Therefore, for all calculation purposes, instead of the considering the individual velocity evolution of DM and gas, we only need the knowledge of relative velocity evolution with redshift. This can be obtained using Eq. (7.10) and Eq. (7.9). Thus in the presence of DM-gas interaction, the DM-gas relative velocity evolves as [303, 304]

$$\frac{dv_{\rm rel}}{dz} = \frac{v_{\rm rel}}{(1+z)} + \frac{D(v_{\rm rel})}{(1+z)H} , \tag{7.11}$$

where, $D(v_{\rm rel})$ is given in Eq. (7.5). The first term of Eq. (7.11) represents the dilution due to expansion of the Universe, whereas the second term is a result of DM and gas interaction. Since $D(v_{\rm rel}) > 0$, therefore it is clear from the Eq. (7.11) that in presence of DM-gas interaction the relative velocity decreases on low redshift.

Furthermore, after addition of Eq. (7.1) and Eq. (7.2), we get

$$\frac{d}{dt}\left(\epsilon_\chi + \epsilon_G\right) + 3H(\epsilon_\chi + P_\chi - 3\zeta_\chi H + \epsilon_G + P_G) = n_\chi \frac{dQ_\chi}{dt} + n_G \frac{dQ_G}{dt} - \frac{\rho_\chi \rho_G}{\rho_M}\, v_{\rm rel}\, D(v_{\rm rel}) \ . \tag{7.12}$$

Further, using Eq. (7.3), Eq. (7.9) and Eq. (7.10), we get

$$n_\chi \frac{dQ_\chi}{dt} + n_G \frac{dQ_G}{dt} - \frac{\rho_\chi \rho_G}{\rho_M}\, v_{\rm rel}\, D(v_{\rm rel}) = 0 \ . \tag{7.13}$$

Since the r.h.s of the above equation (7.14) vanishes, (also, see Ref.[303]), therefore this equation simplifies as

$$\frac{d}{dt}\left(\epsilon_\chi + \epsilon_G\right) + 3H(\epsilon_\chi + P_\chi - 3\zeta_\chi H + \epsilon_G + P_G) = 0 \ . \tag{7.14}$$

The above equation indicates that the DM-gas are coupled tightly to each other and combinedly follow a single fluid description.

7.2.2 Temperature evolution of viscous DM-gas interaction

In this subsection, we will set up the basic differential equations to study the baryon and DM temperature evolution in the presence of the DM viscosity and DM-gas interaction. Considering the viscous effect of dark matter and DM-baryon interaction, the temperature of gas and dark matter evolve as

$$\frac{dT_G}{dz} = 2\frac{T_G}{(1+z)} + \frac{\Gamma_C}{(1+z)H}(T_G - T_{\rm CMB}) - \frac{2}{3(1+z)H}\left(\frac{dQ_G}{dt}\right) \ , \tag{7.15}$$

$$\frac{dT_\chi}{dz} = 2\frac{T_\chi}{(1+z)} - \frac{2}{3(1+z)H}\left(\frac{dQ_\chi}{dt}\right) - \frac{6}{(1+z)H}\left[\frac{m_\chi \zeta_\chi H^2}{\rho_\chi}\right]. \tag{7.16}$$

Here Γ_C is the Compton scattering rate, which is given by

$$\Gamma_C = \frac{8\sigma_T a_r}{3m_e}\left(\frac{x_e}{1 + x_{He} + x_e}\right) T^4_{\rm CMB}(z) \ , \tag{7.17}$$

where $\sigma_T = 6.65 \times 10^{-25}{\rm cm}^2$ is the Compton scattering cross section, and $a_r = 7.5657 \times 10^{-16}$Joule m^{-3} K^{-4} is the radiation constant. Here the electron fraction,

$x_e = n_e/n_H$ and the helium fraction, $x_{He} = n_{He}/n_H$ =, where n_e, n_{He} and n_H represents the electron, helium and hydrogen number density respectively. The CMB temperature at any redshift is given by $T_{\rm CMB}(z) = T_0(1+z)$, where $T_0 \sim 2.72$ K. From the DM and gas evolution equations, we point out the following results;

- In gas temperature evolution (7.15), we see that there are two energy dissipation mechanisms;first compton scattering which arises due to CMB and electron scattering and tries to equiliberate

- In DM temperature evolution (7.16), we have seen that there is two heating mechanism for the DM: first coming from the baryonic heating (second term) and second coming from the viscous heating (third term) in the Eq.(7.16). The magnitude of the viscosity parameter at which the viscous dissipation becomes important in the dark sector can be obtained by comparing the viscous heating and baryonic heating. To quantify the relative strength of the two competing heating mechanism of dark sector, we define a quantity, Υ which is the magnitude of ratio of baryonic heating to DM viscous heating as

$$\Upsilon = \frac{1}{\bar{\zeta}} \frac{\hat{\sigma}_I m_\chi^5}{H_0 m_{\rm Pl}^2} \frac{\mu_I}{m_I + m_\chi} \left[\frac{n_I n_\chi}{m_\chi^5 H^2} \left(\frac{\rho_{\chi 0}}{\rho_\chi} \right)^{+\gamma} \left\{ \sqrt{\frac{2}{\pi}} \frac{x_I e^{-r_I^2/2}}{u_{\rm th}^3} \left| T_G - T_\chi \right| + \frac{m_I F(r_I)}{v_{\rm rel}} \right\} \right] . \tag{7.18}$$

  The term inside the square bracket decreases with the cosmic evolution, and the term before the square bracket is independent of the redshift, and its value will decide the strength of Υ. The condition that the viscous heating of DM will be prominent over the baryonic heating is $\Upsilon \ll 1$ and the baryonic heating dominant over the viscous DM heating when $\Upsilon \gg 1$.

To solve the DM and gas temperature evolution, we need to provide an equation for the electron fraction, $x_e(z)$, which tells us about how the neutral hydrogen atoms are formed during the cosmic evolution. This can be written as [315]

$$\frac{dx_e}{dz} = \frac{1}{H(1+z)} \frac{\frac{3}{4}R_{Ly\alpha} + \frac{1}{4}\Lambda_{2s,1s}}{\beta_B + \frac{3}{4}R_{Ly\alpha} + \frac{1}{4}\Lambda_{2s,1s}} \left[n_H x_e^2 \alpha_B(T_B) - 4(1-x_e)\beta_B e^{-E_{21}/T_{\rm CMB}} \right] . \tag{7.19}$$

In this equation, we summarise the different envolved terms as follows;

- Here α_B is the case-B recombination coefficient and can be given by the numerically fitting function as

$$\alpha_B = 10^{-19}\left(\frac{at^b}{1+ct^d}\right)\ \mathrm{m}^3\ \mathrm{sec}^{-1}, \tag{7.20}$$

with a=4.309, b=-0.6166, c=0.6703, d=0.5300 and $t = \frac{T_B}{10^4 K}$ [299, 316].

- The β_B corresponding to photoionization rate, which is given by

$$\beta_B = \frac{2\pi\mu_e T_{\rm CMB}}{4h^3}\,\alpha_B(T_B = T_{\rm CMB})\,e^{E_2/T_{\rm CMB}}\ , \tag{7.21}$$

where, $E_2 = 3.4eV$ is the energy of the hydrogen in quantum number $n = 2$.

- The $R_{Ly\alpha}$ is the photon escape life and defined by

$$R_{Ly\alpha} = \frac{8\pi H}{3n_H(1-x_e)\lambda^3_{Ly\alpha}}\ . \tag{7.22}$$

where, $\lambda_{Ly\alpha} = 121.5682$ nm is the rest wavelength of Lymann-alpha line. The H two photon decay rate is $\Lambda_{2s,1s} = 8.22\ \mathrm{sec}^{-1}$ and E_{21} is the rest energy corresponding to Lyα wavelength [299, 316].

Furthermore, to close the above differential equations, we also need to estimate the expansion rate of the Universe. For this purpose, we calculate the energy density associated with the DM and gas. For simplicity, here we consider the dominant term (rest mass energy term) in the total energy of the DM and gas, hence $\epsilon_\chi \simeq \rho_\chi$ and $\epsilon_G \simeq \rho_G$. Thus in this approximation, the Hubble expansion rate in the viscous DM model is given by

$$H = H_0\Big[\Omega_{R0}(1+z)^4 + \Omega_B(z) + \Omega_\chi(z) + \Omega_\Lambda\Big]^{1/2}. \tag{7.23}$$

Here $\Omega_{\rm i}(z) = \frac{4\pi G\rho_{\rm i}(z)}{3H_0^2}$, where $i = R, B, \chi, \Lambda$ and $\Omega_\chi(0) = \Omega_{\chi_0}$. In the Eq. (7.23), the subscript, 0 represents the present values of the respective quantities, which have been taken from the Planck 2015 results [317]. From the above equation, we point out that the DM viscosity does not only affect the DM temperature, but in the case of a large viscosity, it can also affect the background expansion of the Universe.

To check whether the DM viscosity parameters used in this work can change the Hubble rate with respect to standard cosmological prediction or not, we plot the $H(z)$

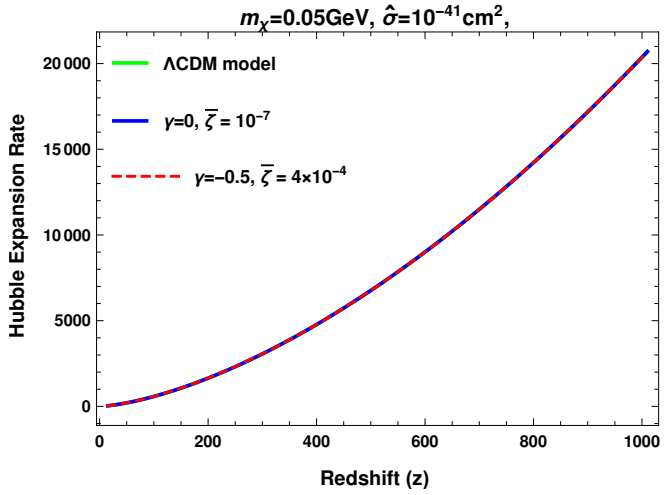

Figure 7.1: The Hubble expansion rate for the viscous DM is plotted as a function of redshift along with the ΛCDM model prediction.

obtained from the viscous DM and ΛCDM model, in Fig. 7.1. Here we see that, throughout the redshift interval of our interest ($15 \leq z \leq 1100$), the value of DM viscosity parameter used in our analysis, the Hubble expansion rate does not change in comparison with the ΛCDM model. Thus we conclude that the viscous DM model does not modify the background cosmology.

After being equipped with the necessary equations, we further explore the evolution of the gas and dark matter fluid temperature. This can be obtained by solving the coupled differential equations. Eq.(7.16), Eq.(7.15), Eq.(7.11) and Eq.(7.19). We consider the initial conditions at the redshift $z = 1010$. Here we assume that the DM temperature is zero, $T_\chi(1010) = 0$, the gas follow the CMB temperature, $T_G(1010) = 2.35 \times 10^{-10}$ GeV, the electron fraction, $x_e(1010) = 0.057$ [316], the relative velocity, $v_{\rm rel}(1010) \sim 29$ Km/sec $\sim 10^{-4}$ [318], $\Omega_\chi(1010) = 10^{-38}$ [317] and $\Omega_G(1010) = 1.873 \times 10^{-39}$ [317].

7.3 Results and discussions

In this section, we discuss the DM and viscous DM temperature evolutions. Then we constraint the DM properties such as its mass, interaction cross-section with the gas, and viscosity in the light of the anomaly observed in the 21-cm signal by EDGES

collaboration. Here in our analysis, we will consider that the DM is interacting with the hydrogen only, and at last, we will generalize our analysis for the other components of the gas like Helium, electron, and proton in subsection 7.3.3.

7.3.1 Evolution of DM and baryon temperature

In this subsection, we will study the effects of the viscosity parameters $(\gamma, \bar{\zeta})$, DM mass (m_χ) and the DM-gas interaction cross-section $(\hat{\sigma})$ onto the temperature evolution of DM and gas.

Temperature dependency on DM viscosity, $\bar{\zeta}$ and DM mass, m_χ

Fig.(7.2) shows the temperature evolution of dark matter and baryons as a function of redshift for different viscosity parameters. The upper Figures 7.2(a) and 7.2(b) are the plots for which the viscosity is constant with the redshift, i.e. $\gamma = 0$ and the lower Figures 7.2(c) and 7.2(d) are the plots for which the viscosity varies with the redshift, i.e. $\gamma = -0.5$. In all the figures, the solid blue line represents the evolution of baryon temperature where the dark matter-baryon interaction and the DM viscosity vanishes. In Fig. 7.2(a), we see that for the viscosity parameter, $\bar{\zeta} = 10^{-12}$, both the dark matter and baryon temperature evolution follow the same behavior as the DM has no viscosity (see, also Fig.1 of Ref.[303]). This suggests that this amount of the DM viscosity is too small to change the DM and baryon temperature. In this case, throughout the cosmic evolution, $\Upsilon \gg 1$, and hence the heating corresponding to DM-baryon interaction dominant over the viscous energy dissipation. But for higher DM viscosity $\bar{\zeta} = 10^{-8}$, see Fig. 7.2(b), the dissipation becomes prominent and hence increases both the DM and gas temperature. In this case, $\Upsilon \ll 1$, hence the heating due to the large viscosity of dark matter, dominates over the heating due to the DM-baryon interaction. Consequently, the DM temperature increases sharply and becomes greater than the baryon at low redshift.

A similar argument can be given for the varying viscosity case, as plotted in the Figures 7.2(c) and 7.2(d). However, here, the value of viscosity parameter up to which the DM and gas follow the same temperature evolution behavior such that the DM viscosity is $\bar{\zeta} \sim 10^{-11}$. This value is an order of magnitude larger than the value

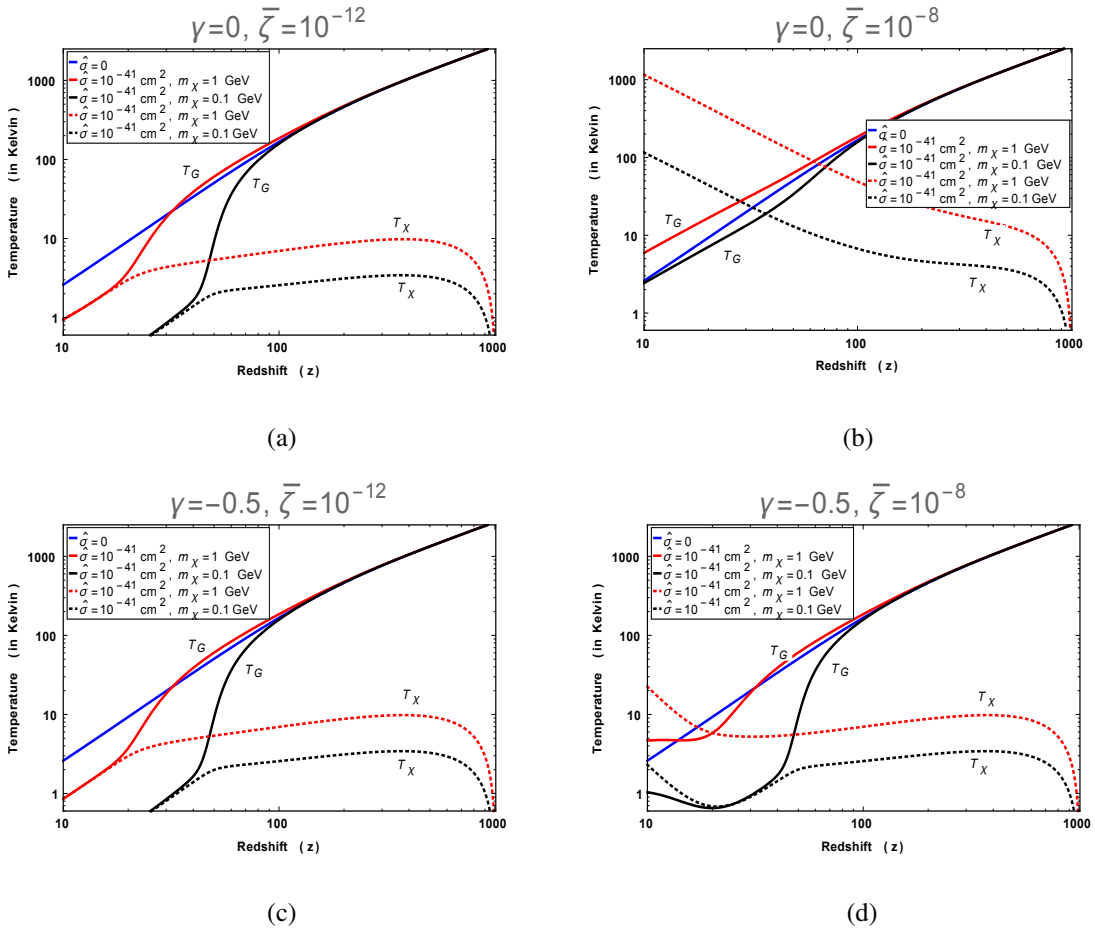

Figure 7.2: The temperature evolution of baryon and DM with redshift for different viscosity parameter, DM mass, and DM baryon cross-section. The solid blue line represents $\hat{\sigma} = 0$ and $\bar{\zeta} = 0$ in all figures. The red and black solid curves correspond to gas temperature whereas the red-dashed and black-dashed curves corresponds for VDM temperature.

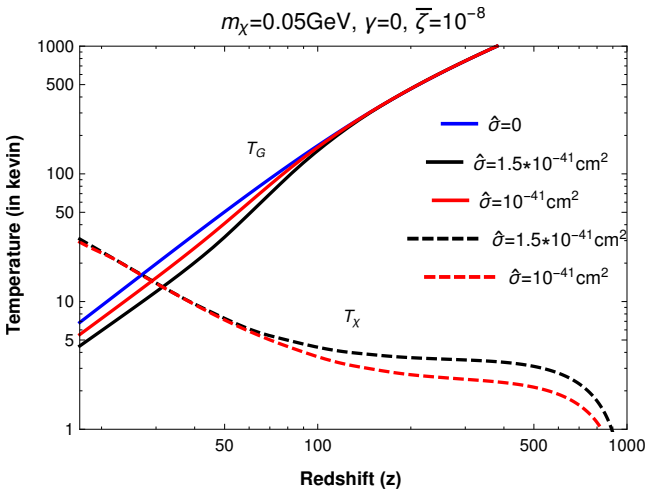

Figure 7.3: The temperature evolution of the gas (solid lines) and DM (dashed lines) is plotted as a function of redshift for different values of DM-gas scattering cross-section, $\hat{\sigma}$. At low redshift, plot indicate that as $\hat{\sigma}$ increases, the DM temperature increases but the gas temperature decreases.

obtained from the constant viscosity case. From Fig. 7.2(c) and Fig. 7.2(d), we point out that at small redshift, for a fix value of DM viscosity parameter $\bar{\zeta} = 10^{-8}$, the DM temperature corresponding to a constant viscosity ($\gamma = 0$) is larger than the varying viscosity ($\gamma = -1/2$) during the evolution of the Universe. This happens because, in the cosmic evolution history, dissipation corresponding to a constant viscosity case is larger than the varying viscosity case.

Furthermore, in Fig. 7.2, we may also investigate the effect of DM mass on the temperature evolution of the DM and gas. Analyzing the upper Figures 7.2(a) and 7.2(b), we see that while increasing the DM mass, from 0.1 GeV to 1 GeV, the viscous energy dissipation increases, and therefore the DM and gas temperature becomes high onto large DM mass. In light of the above discussion, we conclude that increasing the DM viscosity and its mass causes more heating in both the DM and baryon. Therefore to cool the gas efficiently, the DM mass and its viscosity should not be large.

Temperature dependency on DM-baryon scattering cross-section, $\hat{\sigma}$

In Fig. 7.3, we plot the temperature of gas as a function of redshift for different values of the DM-baryon interaction cross-section, $\hat{\sigma}$. To obtain this, we fix the DM viscosity

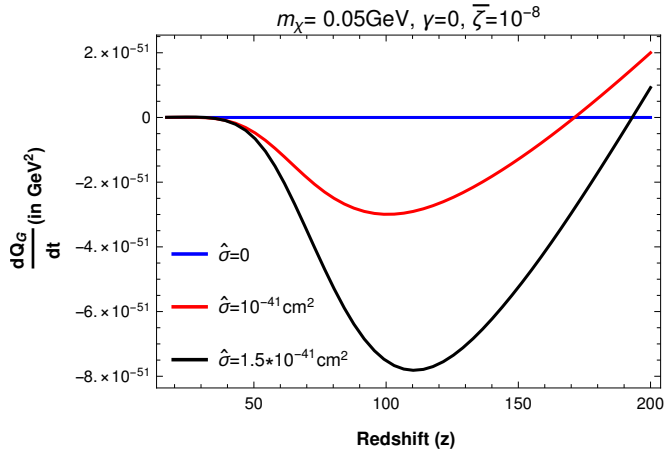

Figure 7.4: The heat transfer rate from gas to DM has been plotted as a function of the redshift for different DM-gas scattering cross-section values, $\hat{\sigma}$.

parameters, $\gamma = 0$, $\bar{\zeta} = 10^{-8}$ and its mass, $m_\chi = 0.05$ GeV. The blue line represents the gas temperature for $\hat{\sigma} = 0$ and $\bar{\zeta} = 0$. For $T_G > T_\chi$, the interaction between the DM and gas causes to transfers energy from the gas to DM, and therefore cools the gas. We see that for $\hat{\sigma} = 10^{-41}$ cm^2 (red thick line), the baryon temperature at $z = 17$ is ~ 5.4 K, which is smaller in comparison with the standard cosmological prediction. But as the $\hat{\sigma}$ increase from $\hat{\sigma} = 10^{-41}$ cm^2 to $\hat{\sigma} = 1.5 \times 10^{-41}$ cm^2, due to the increament, the cooling of the gas and also the heating of the DM starts comparatively at earlier times. Therefore it reduces the gas temperature at low redshifts.

Furthermore, in order to understand the cooling of gas on the larger DM-gas scattering cross-section values, we plot the heat transfer rate by the gas to DM, dQ_G/dt given in Eq. (7.3), as a function of redshift for the different values of the $\hat{\sigma}$ in Fig. 7.4. Here we have considered the same values of parameters, which we have taken to plot Fig. 7.3. The blue line corresponds to the heat tranfer rate when there is no DM-gas scattering, i.e. $\hat{\sigma} = 0$, so $dQ_G/dt = 0$. Hence in this case, there is no heat tranfer takes place between the DM and gas. For $\hat{\sigma} = 10^{-41}$ cm^2 (red line), then the heat transfer rate, dQ_G/dt is small, but as $\hat{\sigma}$ increases to $\hat{\sigma} = 1.5 \times 10^{-41}$ cm^2(red line), then dQ_G/dt start growing more fastly in comparison with the $\hat{\sigma} = 10^{-41}$ cm^2 case at the large redshift. Also, it is clear from Fig. 7.4 that the cooling of the gas for larger $\hat{\sigma}$ is comparatively more and as a result T_G decreases at a low redshift.

However, on the small redshifts, when $T_\chi > T_G$ makes the heat transfer rate posi-

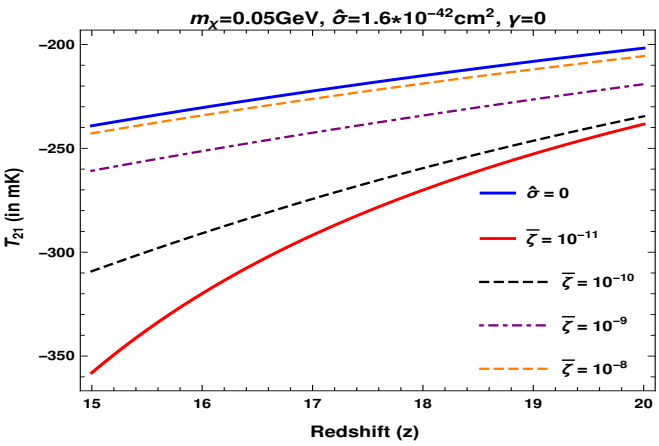

Figure 7.5: The plot of brightness temperature, T_{21} as a function of redshift for the different values of viscosity. The blue line represents the standard scenario with no DM-Hydrogen interaction ($\hat{\sigma} = 0$) and also no viscosity. For the other curves $\hat{\sigma} = 1.6 \times 10^{-42}$ cm^2 and viscosity is constant, $\gamma = 0$. As the DM viscosity increases, the strength of the absorption signal decreases, i.e brightness temperature, T_{21} increases.

tive, i.e. $\frac{dQ_G}{dt} > 0$. This indicates that instead of the gas being cooled, the DM starts heating the gas by transferring its energy. It is important to mention that although the temperature of gas starts increasing at low redshifts, but the overall effect of increasing $\hat{\sigma}$ is cooling of the gas. This conclusion is only valid for small DM viscosity and low DM mass, $m_\chi < 0.3$ GeV. We have checked that for a fixed DM viscosity and large DM mass, i.e., $m_\chi > 0.3$ GeV, increasing the $\hat{\sigma}$ causes more energy transfer from the gas to DM at the high redshifts, but the resultant effect at small redshift will be heating to the gas. Thus, from the above discussions, it becomes clear that for the sufficiently large DM bulk viscosity and DM mass, the gas cannot be cool using a large DM-gas scattering cross-section.

7.3.2 Brightness Temperature

After investigating the term that affects the DM and gas temperature, here we study the effect of DM viscosity onto the brightness temperature, given in Eq.(7.3). For this, we plot T_{21} as a function of redshift for the different values of viscosities in Fig. 7.5. To do so, we assume that between the redshift of our interest, i.e., $15 \leq z \leq 20$, the spin temperature tightly couples with the gas temperature, therefore $T_S = T_G$. We also fix

$\hat{\sigma} = 1.6 \times 10^{-41}$ cm^2 and DM mass $m_\chi = 0.05$ GeV. In Fig. 7.5, the thick blue line corresponds to the brightness temperature, when DM-gas interaction and DM viscosity are zero, and the rest of the lines show the behavior of T_{21} in the presence of DM-gas interaction and DM viscosity.

It is evident from Fig. 7.5 that when the viscosity is small, $\bar{\zeta} = 10^{-11}$ (red line), the gas can cool efficiently through the DM interaction and alter the brightness temperature T_{21} towards the more negative value, and as a consequence explain the EDGES observation. However, as the DM viscosity increases from the $\bar{\zeta} = 10^{-10}$ to $\bar{\zeta} = 10^{-9}$ (black dashed and purple dot-dashed lines, respectively), due to DM-gas interaction, the gas temperature starts growing. This, in turn, starts diminishing the absorption signal. For a sufficient large DM viscosity $\bar{\zeta} = 10^{-8}$ (orange dashed line), the signal strength becomes very small and will be unable to address the EDGES anomaly. Therefore, we see that in order to explain the EDGES signal, the DM viscosity should not be large.

7.3.3 Constraints on DM-baryon interaction and DM mass

In the previous subsection 7.3.1, we have analyzed the effect of the model parameters such as the $\bar{\zeta}, m_\chi$ and DM and gas temperature. We now constrain these parameters using the requirement of the observed 21-cm signal reported by the EDGES collaboration. In order to get the constraint, we focus on the upper limit of the reported EDGES absorption signal at $z = 17$ during our analysis. This requires the gas temperature, $T_G = 5.20$ K. Furthermore, in subsection 7.3.3, we discuss the qualitative constraints on the model parameters using the lower limit observed by EDGES.

In Fig.(7.6), we plot the DM-baryon scattering cross-section as a function of DM mass for the different viscosity parameters. Here all the lines correspond to $T_G = 5.20$ K at $z = 17$, which explains the upper limit of the EDGES absorption signal. The solid lines correspond to $T_\chi < T_G$, and the dot-dashed lines correspond to $T_\chi > T_G$. We find that to explain the EDGES observation, the upper limit on the DM mass corresponding to DM viscosity parameter, $\bar{\zeta} = 10^{-11}$ is the same as for the ideal DM case, but at this time, the scattering cross-section has been increased comparatively (See Fig.1 of Ref. [158]). Furthermore, as we increase the DM viscosity from $\bar{\zeta} = 10^{-11}$ to $\bar{\zeta} = 10^{-7}$, the DM temperature grows, and therefore it opposes the heat transfer rate

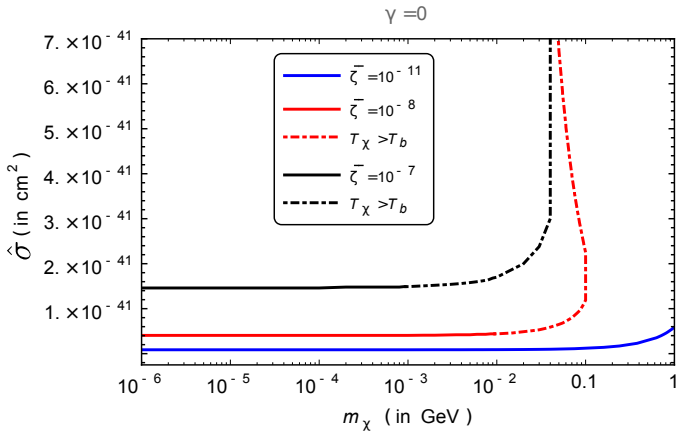

Figure 7.6: The DM-Hydrogen scattering cross section vs DM mass needed to fit the EDGES absorption signal are plotted for three constant viscosity $\bar{\zeta}$=10^{-11} (blue line), 10^{-8} (red line) and 10^{-7}(black line). The solid lines corresponds to $T_\chi < T_G$ and dot dashed lines corresponds to $T_\chi > T_G$. The cross-section corresponds to the brightness temperature $T_{21} = -300$ mK ($T_\chi = 5.20$ K at $z = 17$).

from the baryons to DM. So this implies that the baryon temperature necessary for addressing the EDGES observation cannot be achieved with the above-given mass and cross-section.

However, to obtain $T_G = 5.20\,\mathrm{K}$ (upper limit of EDGES absorption signal) for the viscosity parameter, $\gamma = 0$, $\bar{\zeta} = 10^{-8}$, either we need to decrease the DM mass or increase the DM-baryon interaction or maybe the combination of both. From Fig. (7.6), it can be recognized that while increasing the viscosity, $\bar{\zeta}$ from 10^{-11} to 10^{-7}, the DM-baryon scattering cross-section has increased from 8.5×10^{-43} cm^2 to 1.5×10^{-41} cm^2 and also the DM mass range have been decreased.

In Fig.(7.6), we also point out that for a large DM viscosity ($\bar{\zeta} > 10^{-11}$) and after a certain DM mass, the DM temperature becomes higher than the baryon temperature (here $T_G = 5.20$ K). The red dot-dashed and blue dot-dashed line in Fig.(7.6) corresponds to $T_\chi > T_G$ for the $\bar{\zeta} = 10^{-8}$ and 10^{-7}, respectively. But as soon as the DM temperature increases above the baryon temperature, it heats the baryons due to its coupling and may erase the excess dip in the 21-cm absorption signal. Hence in order to cool the gas further, the energy transfer between the DM and gas must be increased.

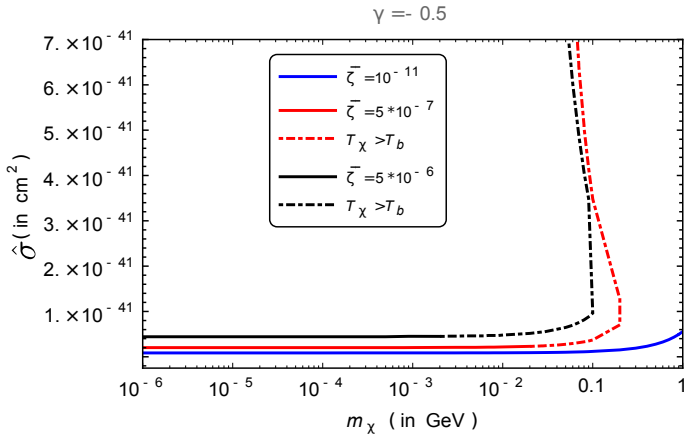

Figure 7.7: The DM-Hydrogen scattering cross section vs DM mass needed to fit the EDGES absorption signal are plotted for three varying viscosity parameters $\bar{\zeta}$=10^{-11} (blue line), 5×10^{-7} (red line) and 5×10^{-6} (black line). The solid lines corresponds to $T_\chi < T_G$ and dot dashed lines corresponds to $T_\chi > T_G$. The cross-section corresponds to the brightness temperature $T_{21} = -300$ mK ($T_\chi = 5.20$ K at $z = 17$).

This can be obtained via an enhancement in the DM-gas interaction cross-section. The DM mass scale over which the $\hat{\sigma}$ increases sharply can put an upper bound on the DM mass. We find that corresponding to DM viscosities $\tilde{\zeta} = 10^{-8}$ and 10^{-7}, the upper limit on the DM masses are 0.1 GeV and 0.02 GeV, respectively.

Similarly, in Fig.(7.7), we plot the DM-baryon scattering cross-section as a function of the DM mass for varying viscosity with the redshift ($\gamma = -1/2$). Here also all the lines corresponds to the gas temperature $T_G = 5.20$ K at $z = 17$, in which the solid line represents to $T_\chi < T_G$ and dot-dashed line corresponds to $T_\chi > T_G$. In this case, also we find that to explain the EDGES observation, the maximum limit for the DM mass corresponds to DM viscosity, $\bar{\zeta} = 10^{-11}$ is the same as the ideal DM case, but the cross-section has been increased comparatively (See Fig.1 of Ref. [158]). Also while increasing the viscosity parameter, $\bar{\zeta}$ from 10^{-11} to 5×10^{-6} and in order to keep the baryon temperature at $5.20K$, the DM-baryon scattering cross section, $\hat{\sigma}$ increases from 8.5×10^{-43} cm^2 to 4.42×10^{-42} cm^2. In this case the upper limits on DM masses are 0.2 GeV and 0.1 GeV corresponding to DM viscosity 5×10^{-11} and

5×10^{-6} respectively.

7.3.4 Constraint on dark matter viscosity

In the above subsection 7.3.3, we have derived the upper limit on DM mass for a given DM viscosity using the EDGES observation. Here, we derive the constraint on the DM viscosity from two different ways: first, from the EDGES absorption signal and using the upper limit obtained on $\hat{\sigma}$ from the Planck observation, see Ref. [319] and second, from the requirement of the DM coldness criteria. Further, we also compare the above limits with the viscosity constraints obtained from the structure formation.

In Ref. [319] using the the Planck temperature, polarization and lensing measurements, it has been found a constraint on the DM-baryon interaction, $\hat{\sigma}$, which varies with the DM masses. For the DM of masses $m_\chi \leq 0.1$ GeV, the maximum upper limit on $\hat{\sigma}$ is 1.7×10^{-42} cm^2. Here, we point out that for a constant viscosity of 10^{-8} and 10^{-7}, the value of DM-baryon interaction cross-section, $\hat{\sigma}$ for the allowed DM mass range are 4×10^{-42} cm^2 and 1.5×10^{-41} cm^2 (see, Figure,7.6) which are the within the 95% confidence limit of allowed $\hat{\sigma}$ obtained from the Ref. [319]. If we increase the viscosity from 10^{-7} to larger, then it further reduces the allowed DM mass range and increases $\hat{\sigma}$ in order to explain the 21 cm observation. Consequently, after sufficiently large value of DM viscosity, the $\hat{\sigma}$ will be greater than the maximum limit i.e. 1.7×10^{-42}cm^2 for $m_\chi \leq 0.1$ GeV as obtained in Ref. [319]. Thus the upper limit on $\hat{\sigma}$ can use to constrain the DM viscosity. Here we find that for constant viscosity ($\gamma = 0$), the maximum limit on the viscosity is $\bar{\zeta} \sim 10^{-7}$, which is one order of magnitude higher than the limit obtained from the structure formation. For the variable viscosity case ($\gamma = -1/2$), the maximum limit on viscosity is $\bar{\zeta} \sim 4 \times 10^{-4}$, which is approximately ~ 3 orders of magnitude larger in comparison with the constant viscosity limit.

Although the EDGES observation can allow a large viscosity in the dark matter but the presence of such a large viscosity heats the DM and increases its temperature, see Fig. 7.2(b) and Fig. 7.2(d). If the dark matter temperature is sufficiently high, then it will no longer behave like a cold dark matter, and hence the coldness criteria can be used to constraint the DM viscosity. As discussed in chapter 6, the DM to be cold the

at any redshift, $z_{\rm dec} \geq z \gg 1$ the ratio of DM temperature to DM mass should obey $T_\chi/m_\chi \leq 1.07\times10^{-14}(1+z)^2$ [287]. At the redshift of reported 21-cm signal at EDGES $z = 17$, the limit becomes, $T_\chi/m_\chi \leq 3.46 \times 10^{-12}$. Therefore, considering the upper limit obtained on $\hat{\sigma}$ from Ref. [319] and using the constraint on T_χ/m_χ from Eq. (6.14), we can estimate the upper limit on the viscosity at the redshift of EDGES observation. For a constant DM viscosity case the limit is $\bar{\zeta} = 6 \times 10^{-10}$ and for a variable DM viscosity case the limit is $\bar{\zeta} = 7.5\times10^{-8}$. We also find that while varying the DM mass and DM-baryon interaction will not create a significant change in the limit on the DM viscosity.

We also point out that the DM viscosity parameters have also been constraint from the structure formation. The presence of viscosity dilutes the density perturbations' growth rate and, hence, delays the structure formation. In Ref. [190], the authors have argued that in order to match with predictions from the standard cosmology but sightly suppressed growth of smallest structures like galaxies, the DM viscosity, $\bar{\zeta}$ should not be larger than 10^{-8}. Otherwise, the larger viscosity will sharply decrease the growth of structures, which is ruled out from the current observations [190].

Thus from the above discussion, we find that the recent EDGES observation allows a large DM viscosity, which is many orders of magnitude larger than the viscosity inferred from the structure formation ($\bar{\zeta} \sim 10^{-8}$). However, the viscosity obtained from the DM coldness criteria is smaller than the allowed from the EDGES explanation. Therefore, we conclude that the DM coldness paradigm's requirement put a stringent constraint on the DM viscosity.

7.3.5 Generalisation to Helium, proton and electron parameters

Throughout our analysis, we consider the interaction of the DM with the hydrogen in order to derive the constraints on the DM viscosity, ($\bar{\zeta}$) DM mass (m_χ) and DM-gas interaction cross-section, $\hat{\sigma}$. But instead of hydrogen if DM interacts with the other species in the gas like helium, electron or proton, then the constraints on the above parameters will change. For the DM with no viscosity and in the approximation $m_\chi \ll 1$ GeV and cooling energy rate $\dfrac{dQ_I}{dt}$ to be fixed, the DM-gas interaction cross-section $\hat{\sigma}^I$ ($I = He, e, p$) will increase in compared with cross-section with the hydrogen $\hat{\sigma}^H$

by [158]

$$\frac{\hat{\sigma}^I}{\hat{\sigma}^H} = \frac{1}{x^I}\left(\frac{m_I + m_\chi}{m_p + m_\chi}\right)^2 \left(\frac{m_p}{m_I}\right)^{\frac{5}{2}}. \tag{7.24}$$

Within the redshift of our interest $15 \leq z \leq 200$, we can consider $x_{\rm He} \sim \frac{1}{13}$ and $x_{\rm e} \sim 10^{-4}$. Considering the DM mass of order of sub GeV, for example $m_\chi = 0.05$ GeV, we get $\hat{\sigma}^{He} \sim 6\hat{\sigma}^H$. For other species of the gas like electron and proton, the scattering cross-section with the DM is larger in comparison with the $\hat{\sigma}^H$. The higher value of the cross-section suggests that to explain the EDGES absorption signal in the presence of DM viscosity, the upper limit on the DM viscosity would be achieved for comparatively lower values of $\bar{\zeta}$ than the value obtained in the case of DM-Hydrogen interaction.

We point out that in our previous analysis, we have taken the upper bound of the reported EDGES absorption signal, $T_G = 5.20$ K, to get the parameter space for $\hat{\sigma}$ and DM mass. Further, if we consider the lower bound of the reported EDGES signal, $T_G = 1.68$K, then we need to increase the DM-gas scattering cross-section for a given viscosity parameter. Thus in Fig. (7.6) and (7.7), all the curvey will shift upward in the $\hat{\sigma}$-axis. In this case (when $T_G = 1.68$K), the constraint on the DM viscosity will decrease compared to the constraint on the DM viscosity obtained from the upper bound of EDGES absorption signal (when $T_G = 5.20$K).

7.4 Conclusion

The EDGES detection of 21 cm absorption signal in the cosmic dawn era opens a new and unique window to study and test the DM properties. In the standard cosmology, the DM is assumed to be ideal, but if it is a viscous fluid and interacting with the gas, it can modify the gas temperature and hence may affect the EDGES observation. In this work, we have studied the properties of DM in the framework of VDM-gas interaction using the observation of EGDES anomaly.

To study the effect of the DM bulk viscosity, we consider its form as power law, $\zeta_\chi = \zeta_0 \left(\frac{\rho_\chi(z)}{\rho_{\chi_0}}\right)^\gamma$. Further, assuming the viscous DM-gas interaction and friction between the DM and gas fluid, we derive the equation for the energy density and temperature of the DM and gas. We then check the dependency of the gas temperature on the

viscosity parameters ($\gamma, \bar{\zeta}$), DM mass (m_χ) and DM-gas interaction cross section ($\hat{\sigma}$).

We point out that for the DM bulk viscosity $\bar{\zeta} < 10^{-12}$ (for the constant viscosity, $\gamma = 0$) and $\bar{\zeta} < 10^{-11}$ (for a varying viscosity, $\gamma = -1/2$), the DM viscous dissipation does not play a significant role in temperature evolution and DM behaves like an ideal fluid. For such small viscosities, the dark matter heating due to DM-gas interaction is dominant over the DM viscous heating. Nevertheless, for larger DM viscosity, the DM dissipation becomes prominent, and the viscous heating starts dominating over the gas heating into the DM fluid. This leads to an increase in the temperature of the DM, also the gas via the DM-gas interaction. The heating of the cosmic fluid (both DM and gas) also depends on the DM mass and increases the DM and gas temperature efficiently for the higher DM masses ($m_\chi \sim 0.1 - 1$ GeV). Also, for a sufficiently large DM viscosity and DM mass, the DM temperature rises sharply and becomes larger than the baryon temperature on a small redshift. We find that for a given viscosity, the gas temperature can be reduced by either decreasing the DM mass (m_χ) or increasing the DM-gas interaction cross-section ($\hat{\sigma}$).

In order to explain the upper limit of EDGES absorption signal (which implies the temperature of gas is 5.20K at $z = 17$), we obtained the constraints on the DM viscosity ($\bar{\zeta}$), DM mass (m_χ) and DM-baryon scattering cross-section ($\hat{\sigma}$). We find that a low value of viscosity, $\bar{\zeta} = 10^{-12}$ is not sufficient enough to heat the DM and baryons hence constraints obtained on DM mass are the same as the case when the DM has no viscosity. Further, increasing the DM viscosity causes more heating in the dark sector and, consequently, in the baryonic sector through the DM-baryon interaction. This implies that in order to maintain the gas temperature of 5.20K at $z = 17$, the DM-baryon scattering cross-section should increase, and the upper limit on the DM mass should decrease. In the case of constant DM viscosities, $\bar{\zeta} = 10^{-8}$ and $\bar{\zeta} = 10^{-7}$, the upper limit on DM masses are 0.1 GeV and 0.02 GeV respectively. For varying DM viscosity corresponds to $\bar{\zeta} = 10^{-8}$ and $\bar{\zeta} = 10^{-7}$, the upper limits on DM masses are obtained as 0.2 GeV and 0.1 GeV respectively.

In our work, we have obtained two independent constraints on the DM viscosity. The first constraint on the DM viscosity has obtained using the EDGES 21 cm absorption line, which is $\bar{\zeta} \sim 10^{-7}$ for a constant viscosity case and $\bar{\zeta} \sim 4 \times 10^{-4}$ for varying

viscosity case. This implies that the EDGES observation can allow a large viscosity in the dark matter, which is many orders of magnitude larger than the maximum allowed DM viscosity ($\bar{\zeta} \sim 10^{-8}$) reported from the structure formation.

Further, we have obtained the second constraint on the DM viscosity in order to preserve the coldness of the dark matter paradigm. We see that the presence of the DM viscosity increases the DM temperature, and if the viscosity is sufficiently large enough, it may increase the DM temperature so high that the DM will no longer follow the cold dark matter paradigm. Thus under the assumption of the coldness of the DM, the constraint on dark matter viscosity is $\bar{\zeta} = 6 \times 10^{-10}$ for constant DM viscosity case and $\bar{\zeta} = 7.5 \times 10^{-8}$ for a variable DM viscosity case. In this case, the allowed limit on the DM viscosity is smaller compared with the DM viscosity limit obtained from the structure formation and EDGES observation. Thus we find that the DM to be cold puts a stringent bound on the dark matter viscosity, which is, to the best of our knowledge is the tightest bound on the DM viscosity.

We point out that the constraint on DM viscosity from the EDGES signal is based on the assumption that the EDGES has discovered an anomaly in the 21-cm signal. However, if the EDGES anomaly is an artifact of incorrect estimation of the foreground radio emission from our galaxy, then the constraint on DM viscosity will no longer be valid. Therefore the constraint on DM viscosity is not fully established until the EDGES anomaly is confirmed by the other experiments.

Chapter 8

Summary and conclusions

In the ΛCDM model of cosmology, the dark matter is assumed to be cold, collisionless, and dissipationless fluid. This model successfully explains the CMB and large-scale structure observation. However, it faces difficulty to explain the physical origin of the Λ, the small scale structure observations and the signal of the 21-cm line reported by the EDGES collaboration, etc. These problems suggest us to extend the cosmological model beyond the ΛCDM and explore a new model that keeps the success of the ΛCDM model and addresses the above drawbacks.

In this thesis, we relax the dissipationless assumption and consider that the DM is a viscous fluid. The viscosity is a relaxation phenomenon, which can operate when the system gets slightly away from the equilibrium. The presence of viscosity tries to equilibrate the system at the cost of energy dissipation due to velocity gradients. Here, using the viscous dark matter framework, we have attempted to explain some of the major problems of the ΛCDM model, such as the dark energy, EDGES anomaly in the 21-cm signal. Further, we have also discussed the possible signals from the DM (visible photon production) and explored the DM properties, such as its mass (sub-GeV), which is relevant for particle DM searches.

In chapter 3, we have calculated the bulk and shear viscosity of the VSIDM fluid and studied their impact on the background expansion of the Universe. The constraint on the ratio of SIDM scattering cross-section to its mass (σ/m) inferred from the astrophysical observations indicates that the SIDM viscosity is large enough to explain the present cosmic acceleration. Further, the mean free path estimation suggests that

the contribution of the viscous dissipation relevant to cosmic acceleration should be manifested on a galactic to a larger scale. Therefore, the viscous SIDM fluid can unify the DM and the DE.

In chapter 4, we have explored the effect of VSIDM dissipation in the light of low redshift observations, $0 \leq z \leq 2.5$. It is assumed that the bulk and shear viscosity of SIDM is constant, but the velocity gradient varies with the redshift as a power-law form. The χ^2 minimization method suggests an averaging length scale $\approx$ 20 Mpc (larger than the typical cluster scale) and decreasing fluid velocity gradients. The best fit value of the model parameters suggests that the DM dissipation is significant at present, $z = 0$ but decreases on the low redshift interval. This explains the supernovae data and also the correct value of the deceleration parameter in the matter-dominated era. Therefore the VSIDM fluid model explains the late-time observations and can be a lucrative alternative to the ΛCDM model.

In chapter 5, we have constrained the SIDM microphysics and studied its viscosity evolution. It has been found that the $\eta/\mathfrak{s}$ decreases as the DM mass increases, therefore for a large DM mass ($\sim$ GeV scale), the SIDM fluid violates the KSS bound $\eta/\mathfrak{s} = 1/4\pi$. This can be tested if the DM searches detect SIDM with a mass above the value inferred from this bound. In the assumption that the SIDM fluid respects the KSS bound, we report that the mass of the SIDM particles should be sub-GeV. However, the limit on the DM mass is conservative and improves further with a more precise value of σ/m from observations. Furthermore, considering the power-law form of SIDM viscosity, we explore its evolution in the light of late-time observations. We find that the shear and bulk viscosity are large at present and decrease at an earlier time. In this model, the age of the Universe, t_{U} is slightly small in comparison with the age obtained in the CMB anisotropy data (13.76 Gyr) [61] and larger than the age of globular cluster (12.9 Gyr) [275].

In chapter 6, we have investigated the effect of viscosity on the DM temperature evolution and explored its possible signatures in the Universe. We focus our analysis between the redshifts, $15 \leq z \leq 1300$, where the matter decouples from the photons, and possibly the first star forms. Inspired by cosmological studies, we assume the bulk viscosity as a power-law form and derive the analytical expression of the DM

temperature. We find that the DM viscosity increases its temperature and is sensitive to its mass and viscosity parameters. For a large DM viscosity case, DM may no longer be treated as cold dark matter and challenged by the CMB and the large-scale observations. This led us to derive the condition on the viscosity parameters, which respect the DM coldness condition. Due to the presence of viscosity, DM dissipates the heat energy into the cosmic medium. We assume that the viscous energy dissipation may lead to visible photon generation. This mechanism has been hypothesized in two ways: first, when the photon is directly produced from the viscous energy dissipation, the second considers that the energy dissipation leads to dark radiation, which further converts into the visible photons via the kinetic mixing. We find that the photons obtained from the kinetic mixing are large enough to populate the Rayleigh-Jeans limit of the CMB radiation; hence can explain the EDGES anomaly. However, the directly converted photons fail to do so. Further, we have explored the parameter space for the DM mass, DM mixing strength with the photons, and dark radiation mass, which can be explored in future observations.

In chapter 7, we have studied the DM properties using the VDM-gas interaction and anomalous 21-cm absorption signal reported by the EGDES collaboration. The presence of the DM viscosity increases the DM and also the baryonic temperature via DM-baryon interaction. Consequently, DM viscosity decreases the energy transfer from the baryon to DM compared with what one would expect in an ideal DM case. For a large viscosity case, the DM temperature becomes large compared to the baryon and therefore heats the baryons. This scenario has been explored using the EDGES anomaly, which explanation demands a low baryonic temperature compared with the standard cosmological prediction. Therefore, the EDGES anomaly can constraint the mass, interaction cross-section with the baryons, and viscosity of the DM particles. We find that in the viscous DM scenario, the explanation of the EDGES absorption signal requires a larger DM-gas cross-section and a smaller DM mass compared to the ideal DM fluid. It has been found that the EDGES 21-cm observation allows a large DM viscosity, which is many orders of magnitude larger than the viscosity inferred from the structure formation. We also constrain the DM viscosity from the dark matter coldness paradigm (which is required to explain the CMB observation). The viscosity

obtained here is an order of magnitude smaller than the DM viscosity obtained from the structure formation. Thus we find that the condition for DM to be cold gives a stringent bound on the dark matter viscosity, which is, to the best of our knowledge, the tightest bound on the DM viscosity.

Future direction

In the thesis, we have investigated some possible signatures of the viscous dark matter such as cosmic acceleration, gas heating, and photon production (explain the EDGES anomaly). However, establishing this will require much further work, which is worth pursuing. Below, I discuss some of the possible directions which I would like to explore in the future.

We found that the viscosity of self-interacting dark matter fluid can be sufficient enough to explain the present cosmic acceleration. The effect of viscous SIDM physics governs through the dissipation term, estimated using some of the assumptions. In our calculation, for simplicity, we have assumed that fluid description for SIDM will be valid on a scale larger than cluster scale, but as we argued for the realistic scenario, one needs to include the fluid description from the galactic scale. Further, our estimation was done for a constant viscosity case, but one has to consider the density dependence case for realistic calculation.

Further, our estimation of dissipation has been based on the assumption that the SIDM power spectrum matches the ΛCDM prediction for $k \leq 2h$ Mpc^{-1} and has left the viscosity contribution in power spectrum calculation. Since the presence of viscosity damps the growth of density perturbations, therefore SIDM viscosity will modify both growth factor, f and the velocity divergence power spectrum, $P_{\theta\theta}$. Furthermore, in our analysis, we have also ignored the contribution of other terms like $(P_w)_{ij}(\vec{k})$ and $P_{\theta P}(\vec{k})$, but their effect will be non-negligible on a small scale. Furthermore, to study the evolution of the velocity gradient term, we assumed it form as a power law, but its actual evolution should be governed through the power spectrum obtained from Einstein's equation. Therefore, to obtain the actual value of the cosmic dissipation, one needs to incorporate the SIDM physics on small scales. Inclusion of the SIDM proper-

ties in the non-linear power spectrum (both the density and velocity) is a numerically challenging task. I would like to pursue these in the future.

Nevertheless, we have explored the dark radiation (visible photon) production in the viscous dark matter framework. There, we have investigated the thermal photon production from viscous energy dissipation; however, we have not discussed the particle physics model for dark matter thermalization with dark radiation (visible photons). My future goal is to explore the particle physics model of the DM dissipation and non-thermal production of photons and dark radiation from dark matter.

Bibliography

[1] https://en.citizendium.org/wiki/File:GalaxyRotationCurve.png.

[2] X-ray:NASA/CXC/CfA/M.Markevitchetal.;Optical:NASA/STScI; Magellan/U.Arizona/D.Cloweetal.;LensingMap:NASA/STScI; ESOWFI;Magellan/U.Arizona/D.Cloweetal.

[3] S. Giagu, *Wimp dark matter searches with the atlas detector at the lhc,* Frontiers in Physics **7**, 75 (2019).

[4] https://sci.esa.int/web/planck/-/51557-planck-new-cosmic-recipe.

[5] D. Blas, J. Lesgourgues, and T. Tram, *The cosmic linear anisotropy solving system (class). part ii: Approximation schemes,* Journal of Cosmology and Astroparticle Physics **2011**, 034034 (2011).

[6] J. R. Pritchard and A. Loeb, *21 cm cosmology in the 21st century,* Reports on Progress in Physics **75**, 086901 (2012).

[7] M. Kaplinghat, S. Tulin, and H.-B. Yu, *Dark Matter Halos as Particle Colliders: Unified Solution to Small-Scale Structure Puzzles from Dwarfs to Clusters,* Phys. Rev. Lett. **116**, 041302 (2016).

[8] D. Egana-Ugrinovic, R. Essig, D. Gift, and M. LoVerde, *The Cosmological Evolution of Self-interacting Dark Matter,* (2021).

[9] E. Jennings, *An improved model for the non-linear velocity power spectrum,* Monthly Notices of the Royal Astronomical Society: Letters p. nono (2012).

[10] P. Kovtun, D. T. Son, and A. O. Starinets, *Viscosity in strongly interacting quantum field theories from black hole physics,* Phys. Rev. Lett. **94**, 111601 (2005).

[11] M. Pospelov, J. Pradler, J. T. Ruderman, and A. Urbano, *Room for New Physics in the Rayleigh-Jeans Tail of the Cosmic Microwave Background,* Phys. Rev. Lett. **121**, 031103 (2018).

[12] S. Weinberg, *Gravitation and Cosmology: Principles and Applications of the General Theory of Relativity* (John Wiley and Sons, New York, 1972).

[13] C. W. Misner, K. S. Thorne, and J. A. Wheeler, *Gravitation* (1973).

[14] F. Zwicky, *Die Rotverschiebung von extragalaktischen Nebeln,* Helv. Phys. Acta **6**, 110–127 (1933). [Gen. Rel. Grav.41,207(2009)].

[15] S. Smith, *The mass of the virgo cluster,* The Astrophysical Journal **83**, 23 (1936).

[16] F. Zwicky, *On the masses of nebulae and of clusters of nebulae,* The Astrophysical Journal **86**, 217 (1937).

[17] V. C. Rubin and J. F. W. Kent, *Rotation of the andromeda nebula from a spectroscopic survey of emission regions,* The Astrophysical Journal **159**, 379 (1970).

[18] D. Clowe, A. Gonzalez, and M. Markevitch, *Weak lensing mass reconstruction of the interacting cluster 1E0657-558: Direct evidence for the existence of dark matter,* Astrophys. J. **604**, 596–603 (2004).

[19] S. Profumo, L. Giani, and O. F. Piattella, *An Introduction to Particle Dark Matter,* Universe **5**, 213 (2019).

[20] N. Aghanim *et al.*, *Planck 2018 results. VI. Cosmological parameters,* (2018).

[21] J. Einasto, *Dark matter,* Brazilian Journal of Physics **43**, 369–374 (2013).

[22] J. Einasto, *Dark matter,* (2009).

[23] S. Tulin and H.-B. Yu, *Dark Matter Self-interactions and Small Scale Structure,* Phys. Rept. **730**, 1–57 (2018).

[24] G. Jungman, M. Kamionkowski, and K. Griest, *Supersymmetric dark matter,* Physics Reports **267**, 195373 (1996).

[25] L. D. Duffy and K. v. Bibber, *Axions as dark matter particles,* New Journal of Physics **11**, 105008 (2009).

[26] A. Boyarsky, M. Drewes, T. Lasserre, S. Mertens, and O. Ruchayskiy, *Sterile neutrino dark matter,* Progress in Particle and Nuclear Physics **104**, 145 (2019).

[27] B. Carr, F. Khnel, and M. Sandstad, *Primordial black holes as dark matter,* Physical Review D **94** (2016).

[28] R. FOOT, *Mirror matter-type dark matter,* International Journal of Modern Physics D **13**, 21612192 (2004).

[29] E. Zackrisson, *Quasars and Low Surface Brightness Galaxies as Probes of Dark Matter,* Ph.D. thesis, Department of Astronomy and Space Physics, Uppsala University, Sweden (2005).

[30] J. L. Feng, *Dark matter candidates from particle physics and methods of detection,* Annual Review of Astronomy and Astrophysics **48**, 495–545 (2010).

[31] A. Peter, *Dark matter: A brief review, arxiv (2012),* arXiv preprint arXiv:1201.3942 .

[32] M. Lisanti, *Lectures on dark matter physics,* New Frontiers in Fields and Strings (2016).

[33] G. Bertone and D. Hooper, *History of dark matter,* Reviews of Modern Physics **90** (2018).

[34] T. Lin, *Tasi lectures on dark matter models and direct detection,* (2019).

[35] S. Profumo, L. Giani, and O. F. Piattella, *An introduction to particle dark matter,* (2019).

[36] E. W. Kolb and M. S. Turner, *The Early Universe*, vol. 69 (1990).

[37] P. Bode, J. P. Ostriker, and N. Turok, *Halo formation in warm dark matter models,* The Astrophysical Journal **556**, 93 (2001).

[38] M. Viel, G. D. Becker, J. S. Bolton, and M. G. Haehnelt, *Warm dark matter as a solution to the small scale crisis: New constraints from high redshift Lyman-α forest data,* Phys. Rev. D **88**, 043502 (2013).

[39] J. R. Primack and M. A. Gross, *Hot dark matter in cosmology,* pp. 287–308 (2000).

[40] M. W. Goodman and E. Witten, *Detectability of Certain Dark Matter Candidates,* Phys. Rev. D **31**, 3059 (1985).

[41] A. K. Drukier, K. Freese, and D. N. Spergel, *Detecting cold dark-matter candidates,* Phys. Rev. D **33**, 3495–3508 (1986).

[42] J. Lewin and P. Smith, *Review of mathematics, numerical factors, and corrections for dark matter experiments based on elastic nuclear recoil,* Astropart. Phys. **6**, 87–112 (1996).

[43] D. Akerib *et al.*, *Improved Limits on Scattering of Weakly Interacting Massive Particles from Reanalysis of 2013 LUX Data,* Phys. Rev. Lett. **116**, 161301 (2016).

[44] E. Aprile *et al.*, *Dark Matter Results from 225 Live Days of XENON100 Data,* Phys. Rev. Lett. **109**, 181301 (2012).

[45] M. Klasen, M. Pohl, and G. Sigl, *Indirect and direct search for dark matter,* Prog. Part. Nucl. Phys. **85**, 1–32 (2015).

[46] T. Marrodn Undagoitia and L. Rauch, *Dark matter direct-detection experiments,* J. Phys. G **43**, 013001 (2016).

[47] M. Cirelli, *Indirect Searches for Dark Matter: a status review,* Pramana **79**, 1021–1043 (2012).

[48] J. Lavalle and P. Salati, *Dark Matter Indirect Signatures,* Comptes Rendus Physique **13**, 740–782 (2012).

[49] L. Evans and P. Bryant, *LHC machine,* Journal of Instrumentation **3**, S08001–S08001 (2008).

[50] B. Penning, *The pursuit of dark matter at colliders—an overview,* J. Phys. G **45**, 063001 (2018).

[51] A. Boveia and C. Doglioni, *Dark Matter Searches at Colliders,* Ann. Rev. Nucl. Part. Sci. **68**, 429–459 (2018).

[52] O. Buchmueller, C. Doglioni, and L. T. Wang, *Search for dark matter at colliders,* Nature Phys. **13**, 217–223 (2017).

[53] E. J. Copeland, M. Sami, and S. Tsujikawa, *Dynamics of dark energy,* Int. J. Mod. Phys. D **15**, 1753–1936 (2006).

[54] R. R. Caldwell and M. Kamionkowski, *The Physics of Cosmic Acceleration,* Ann. Rev. Nucl. Part. Sci. **59**, 397–429 (2009).

[55] J. Frieman, M. Turner, and D. Huterer, *Dark Energy and the Accelerating Universe,* Ann. Rev. Astron. Astrophys. **46**, 385–432 (2008).

[56] A. Silvestri and M. Trodden, *Approaches to Understanding Cosmic Acceleration,* Rept. Prog. Phys. **72**, 096901 (2009).

[57] S. Perlmutter *et al.*, *Measurements of* Ω *and* Λ *from 42 high redshift supernovae,* Astrophys. J. **517**, 565–586 (1999).

[58] A. G. Riess *et al.*, *Observational evidence from supernovae for an accelerating universe and a cosmological constant,* Astron. J. **116**, 1009–1038 (1998).

[59] R. Jimenez, P. Thejll, U. Jorgensen, J. MacDonald, and B. Pagel, *Ages of globular clusters: a new approach,* Mon. Not. Roy. Astron. Soc. **282**, 926–942 (1996).

[60] B. M. Hansen, J. Brewer, G. G. Fahlman, B. K. Gibson, R. Ibata, M. Limongi, R. Rich, H. B. Richer, M. M. Shara, and P. B. Stetson, *The white dwarf cooling sequence of the globular cluster messier 4,* Astrophys. J. Lett. **574**, L155–L158 (2002).

[61] M. Tegmark *et al.*, *Cosmological Constraints from the SDSS Luminous Red Galaxies,* Phys. Rev. **D74**, 123507 (2006).

[62] D. Spergel *et al.*, *Wilkinson Microwave Anisotropy Probe (WMAP) three year results: implications for cosmology,* Astrophys. J. Suppl. **170**, 377 (2007).

[63] R. Caldwell, R. Dave, and P. J. Steinhardt, *Cosmological imprint of an energy component with general equation of state,* Phys. Rev. Lett. **80**, 1582–1585 (1998).

[64] A. A. Starobinsky, *How to determine an effective potential for a variable cosmological term,* JETP Lett. **68**, 757–763 (1998).

[65] T. D. Saini, S. Raychaudhury, V. Sahni, and A. A. Starobinsky, *Reconstructing the cosmic equation of state from supernova distances,* Phys. Rev. Lett. **85**, 1162–1165 (2000).

[66] T. Chiba, T. Okabe, and M. Yamaguchi, *Kinetically driven quintessence,* Phys. Rev. D **62**, 023511 (2000).

[67] C. Armendariz-Picon, V. F. Mukhanov, and P. J. Steinhardt, *A Dynamical solution to the problem of a small cosmological constant and late time cosmic acceleration,* Phys. Rev. Lett. **85**, 4438–4441 (2000).

[68] C. Armendariz-Picon, V. F. Mukhanov, and P. J. Steinhardt, *Essentials of k essence,* Phys. Rev. D **63**, 103510 (2001).

[69] A. Sen, *Tachyon matter,* JHEP **07**, 065 (2002).

[70] T. Padmanabhan, *Accelerated expansion of the universe driven by tachyonic matter,* Phys. Rev. D **66**, 021301 (2002).

[71] J. Bagla, H. K. Jassal, and T. Padmanabhan, *Cosmology with tachyon field as dark energy,* Phys. Rev. D **67**, 063504 (2003).

[72] E. J. Copeland, M. R. Garousi, M. Sami, and S. Tsujikawa, *What is needed of a tachyon if it is to be the dark energy?* Phys. Rev. D **71**, 043003 (2005).

[73] R. Caldwell, *A Phantom menace?* Phys. Lett. B **545**, 23–29 (2002).

[74] A. Y. Kamenshchik, U. Moschella, and V. Pasquier, *An Alternative to quintessence,* Phys. Lett. B **511**, 265–268 (2001).

[75] M. Bento, O. Bertolami, and A. Sen, *Generalized Chaplygin gas, accelerated expansion and dark energy matter unification,* Phys. Rev. D **66**, 043507 (2002).

[76] R. Jackiw, *A Particle field theorist's lectures on supersymmetric, nonAbelian fluid mechanics and d-branes,* (2000).

[77] L. Amendola, F. Finelli, C. Burigana, and D. Carturan, *WMAP and the generalized Chaplygin gas,* JCAP **07**, 005 (2003).

[78] F. Salahedin, R. Pazhouhesh, and M. Malekjani, *Cosmological constrains on new generalized Chaplygin gas model,* Eur. Phys. J. Plus **135**, 429 (2020).

[79] J. C. Fabris, S. V. B. Goncalves, and R. de Sa Ribeiro, *Bulk viscosity driving the acceleration of the Universe,* Gen. Rel. Grav. **38**, 495–506 (2006).

[80] G. J. Mathews, N. Q. Lan, and C. Kolda, *Late Decaying Dark Matter, Bulk Viscosity and the Cosmic Acceleration,* Phys. Rev. **D78**, 043525 (2008).

[81] A. Avelino and U. Nucamendi, *Can a matter-dominated model with constant bulk viscosity drive the accelerated expansion of the universe?* JCAP **0904**, 006 (2009).

[82] S. Das and N. Banerjee, *Can neutrino viscosity drive the late time cosmic acceleration?* Int. J. Theor. Phys. **51**, 2771–2778 (2012).

[83] O. F. Piattella, J. C. Fabris, and W. Zimdahl, *Bulk viscous cosmology with causal transport theory,* JCAP **1105**, 029 (2011).

[84] H. Velten and D. J. Schwarz, *Constraints on dissipative unified dark matter,* JCAP **1109**, 016 (2011).

[85] J.-S. Gagnon and J. Lesgourgues, *Dark goo: Bulk viscosity as an alternative to dark energy,* JCAP **1109**, 026 (2011).

[86] B. D. Normann and I. Brevik, *General Bulk-Viscous Solutions and Estimates of Bulk Viscosity in the Cosmic Fluid,* Entropy **18**, 215 (2016).

[87] B. D. Normann and I. Brevik, *Characteristic Properties of Two Different Viscous Cosmology Models for the Future Universe,* Mod. Phys. Lett. **A32**, 1750026 (2017).

[88] N. D. J. Mohan, A. Sasidharan, and T. K. Mathew, *Bulk viscous matter and recent acceleration of the universe based on causal viscous theory,* Eur. Phys. J. **C77**, 849 (2017).

[89] N. Cruz, E. Gonzlez, S. Lepe, and D. Sez-Chilln Gmez, *Analysing dissipative effects in the ΛCDM model,* JCAP **1812**, 017 (2018).

[90] B. Li and J. D. Barrow, *Does Bulk Viscosity Create a Viable Unified Dark Matter Model?* Phys. Rev. **D79**, 103521 (2009).

[91] C. M. S. Barbosa, J. C. Fabris, O. F. Piattella, H. E. S. Velten, and W. Zimdahl, *Viscous Cosmology,* in "Proceedings, 12th International Conference on Gravitation, Astrophysics and Cosmology (ICGAC-12): Moscow, Russia, June 28-July 5, 2015," (2015).

[92] S. Floerchinger, N. Tetradis, and U. A. Wiedemann, *Accelerating Cosmological Expansion from Shear and Bulk Viscosity,* Phys. Rev. Lett. **114**, 091301 (2015).

[93] T. Buchert, *Dark Energy from Structure: A Status Report,* Gen. Rel. Grav. **40**, 467–527 (2008).

[94] E. W. Kolb, *Backreaction of inhomogeneities can mimic dark energy,* Class. Quant. Grav. **28**, 164009 (2011).

[95] A. Ishibashi and R. M. Wald, *Can the acceleration of our universe be explained by the effects of inhomogeneities?* Class. Quant. Grav. **23**, 235–250 (2006).

[96] S. R. Green and R. M. Wald, *How well is our universe described by an FLRW model?* Class. Quant. Grav. **31**, 234003 (2014).

[97] B. Paul, P. Debnath, and S. Ghose, *Accelerating universe in modified theories of gravity,* Physical Review D **79**, 083534 (2009).

[98] F. Sbis, *Modified Theories of Gravity,* Other thesis (2014).

[99] T. Clifton, P. G. Ferreira, A. Padilla, and C. Skordis, *Modified Gravity and Cosmology,* Phys. Rept. **513**, 1–189 (2012).

[100] S. Dodelson, *Modern Cosmology* (Academic Press, Amsterdam, 2003).

[101] T. Padmanabhan, *Structure Formation in the Universe* (1993).

[102] C.-P. Ma and E. Bertschinger, *Cosmological perturbation theory in the synchronous and conformal Newtonian gauges,* Astrophys. J. **455**, 7–25 (1995).

[103] C. Knobel, *An introduction into the theory of cosmological structure formation,* arXiv preprint arXiv:1208.5931 (2012).

[104] M. Stref, *Dark Matter on the Galactic Scale : from Particle Physics and Cosmology to Local Properties,* Ph.D. thesis, Montpellier U. (2018).

[105] W. H. Press and P. Schechter, *Formation of galaxies and clusters of galaxies by self-similar gravitational condensation,* The Astrophysical Journal **187**, 425 (1974).

[106] R. E. Smith, J. A. Peacock, A. Jenkins, S. D. M. White, C. S. Frenk, F. R. Pearce, P. A. Thomas, G. Efstathiou, and H. M. P. Couchmann, *Stable clustering, the halo model and nonlinear cosmological power spectra,* Mon. Not. Roy. Astron. Soc. **341**, 1311 (2003).

[107] R. Takahashi, M. Sato, T. Nishimichi, A. Taruya, and M. Oguri, *Revising the Halofit Model for the Nonlinear Matter Power Spectrum,* Astrophys. J. **761**, 152 (2012).

[108] S. Weinberg, *The cosmological constant problem,* Rev. Mod. Phys. **61**, 1–23 (1989).

[109] L. Lombriser, *On the cosmological constant problem,* Phys. Lett. B **797**, 134804 (2019).

[110] J. Dubinski and R. G. Carlberg, *The structure of cold dark matter halos,* The Astrophysical Journal **378**, 496 (1991).

[111] J. F. Navarro, C. S. Frenk, and S. D. M. White, *The structure of cold dark matter halos,* The Astrophysical Journal **462**, 563 (1996).

[112] J. F. Navarro, C. S. Frenk, and S. D. M. White, *A universal density profile from hierarchical clustering,* The Astrophysical Journal **490**, 493508 (1997).

[113] R. A. Flores and J. R. Primack, *Observational and theoretical constraints on singular dark matter halos,* The Astrophysical Journal **427**, L1 (1994).

[114] B. Moore, T. Quinn, F. Governato, J. Stadel, and G. Lake, *Cold collapse and the core catastrophe,* Monthly Notices of the Royal Astronomical Society **310**, 11471152 (1999).

[115] A. Burkert, *The Structure of dark matter halos in dwarf galaxies,* IAU Symp. **171**, 175 (1996).

[116] F. C. van den Bosch and R. A. Swaters, *Dwarf galaxy rotation curves and the core problem of dark matter halos,* Mon. Not. Roy. Astron. Soc. **325**, 1017 (2001).

[117] R. Kuzio de Naray, S. S. McGaugh, and W. J. G. de Blok, *Mass Models for Low Surface Brightness Galaxies with High Resolution Optical Velocity Fields,* Astrophys. J. **676**, 920–943 (2008).

[118] A. J. Maxwell, J. Wadsley, and H. Couchman, *The Energetics of Cusp Destruction,* Astrophys. J. **806**, 229 (2015).

[119] W. J. G. de Blok, *The core-cusp problem,* Advances in Astronomy **2010**, 114 (2010).

[120] D. J. Sand, T. Treu, and R. S. Ellis, *The dark matter density profile of the lensing cluster ms2137-23: a test of the cold dark matter paradigm,* Astrophys. J. Lett. **574**, L129–L134 (2002).

[121] D. J. Sand, T. Treu, G. P. Smith, and R. S. Ellis, *The dark matter distribution in the central regions of galaxy clusters: Implications for CDM,* Astrophys. J. **604**, 88–107 (2004).

[122] I. Babyk, I. Vavilova, and A. Del Popolo, *The Dark Matter Haloes of Chandra X-ray Galaxy Clusters and Baryons Effect,* Astron. Rep. **58**, 587 (2014).

[123] V. Springel, J. Wang, M. Vogelsberger, A. Ludlow, A. Jenkins, A. Helmi, J. F. Navarro, C. S. Frenk, and S. D. M. White, *The aquarius project: the subhaloes of galactic haloes,* Monthly Notices of the Royal Astronomical Society **391**, 16851711 (2008).

[124] B. Moore, S. Ghigna, F. Governato, G. Lake, T. R. Quinn, J. Stadel, and P. Tozzi, *Dark matter substructure within galactic halos,* Astrophys. J. Lett. **524**, L19–L22 (1999).

[125] A. A. Klypin, A. V. Kravtsov, O. Valenzuela, and F. Prada, *Where are the missing Galactic satellites?* Astrophys. J. **522**, 82–92 (1999).

[126] A. Kravtsov, *Dark matter substructure and dwarf galactic satellites,* Advances in Astronomy **2010** (2010).

[127] M. Boylan-Kolchin, J. S. Bullock, and M. Kaplinghat, *Too big to fail? the puzzling darkness of massive milky way subhaloes,* Monthly Notices of the Royal Astronomical Society: Letters **415**, L40L44 (2011).

[128] M. Boylan-Kolchin, J. S. Bullock, and M. Kaplinghat, *The milky ways bright satellites as an apparent failure of cdm,* Monthly Notices of the Royal Astronomical Society **422**, 12031218 (2012).

[129] E. J. Tollerud, M. Boylan-Kolchin, and J. S. Bullock, *M31 Satellite Masses Compared to LCDM Subhaloes,* Mon. Not. Roy. Astron. Soc. **440**, 3511–3519 (2014).

[130] S. Garrison-Kimmel, M. Boylan-Kolchin, J. S. Bullock, and E. N. Kirby, *Too big to fail in the local group,* Monthly Notices of the Royal Astronomical Society **444**, 222–236 (2014).

[131] R. A. Flores and J. R. Primack, *Observational and theoretical constraints on singular dark matter halos,* Astrophys. J. **427**, L1–4 (1994).

[132] B. Moore, *Evidence against dissipationless dark matter from observations of galaxy haloes,* Nature **370**, 629 (1994).

[133] K. A. Oman, J. F. Navarro, A. Fattahi, C. S. Frenk, T. Sawala, S. D. M. White, R. Bower, R. A. Crain, M. Furlong, M. Schaller, and et al., *The unexpected diversity of dwarf galaxy rotation curves,* Monthly Notices of the Royal Astronomical Society **452**, 36503665 (2015).

[134] J. F. Navarro, V. R. Eke, and C. S. Frenk, *The cores of dwarf galaxy halos,* Mon. Not. Roy. Astron. Soc. **283**, L72–L78 (1996).

[135] O. Y. Gnedin and H. Zhao, *Maximum feedback and dark matter profiles of dwarf galaxies,* Mon. Not. Roy. Astron. Soc. **333**, 299 (2002).

[136] H.-J. Mo and S. Mao, *Galaxy formation in pre-processed dark haloes,* Monthly Notices of the Royal Astronomical Society **353**, 829–840 (2004).

[137] J. I. Read and G. Gilmore, *Mass loss from dwarf spheroidal galaxies: the origins of shallow dark matter cores and exponential surface brightness profiles,* Monthly Notices of the Royal Astronomical Society **356**, 107–124 (2005).

[138] F. Governato *et al.*, *At the heart of the matter: the origin of bulgeless dwarf galaxies and Dark Matter cores,* Nature **463**, 203–206 (2010).

[139] H. Katz, F. Lelli, S. S. McGaugh, A. Di Cintio, C. B. Brook, and J. M. Schombert, *Testing feedback-modified dark matter haloes with galaxy rotation curves: estimation of halo parameters and consistency with λcdm scaling relations,* Monthly Notices of the Royal Astronomical Society **466**, 1648–1668 (2017).

[140] A. M. Brooks, M. Kuhlen, A. Zolotov, and D. Hooper, *A baryonic solution to the missing satellites problem,* The Astrophysical Journal **765**, 22 (2013).

[141] J. Peñarrubia, A. Pontzen, M. G. Walker, and S. E. Koposov, *THE COUPLING BETWEEN THE CORE/CUSP AND MISSING SATELLITE PROBLEMS,* The Astrophysical Journal **759**, L42 (2012).

[142] B. Moore, T. Quinn, F. Governato, J. Stadel, and G. Lake, *Cold collapse and the core catastrophe,* Monthly Notices of the Royal Astronomical Society **310**, 1147–1152 (1999).

[143] M. Leo, C. M. Baugh, B. Li, and S. Pascoli, *Nonlinear growth of structure in cosmologies with damped matter fluctuations,* JCAP **08**, 001 (2018).

[144] V. Avila-Reese, P. Colin, O. Valenzuela, E. D'Onghia, and C. Firmani, *Formation and structure of halos in a warm dark matter cosmology,* Astrophys. J. **559**, 516–530 (2001).

[145] M. R. Lovell, V. Eke, C. S. Frenk, L. Gao, A. Jenkins, T. Theuns, J. Wang, S. D. White, A. Boyarsky, and O. Ruchayskiy, *The haloes of bright satellite galaxies in a warm dark matter universe,* Monthly Notices of the Royal Astronomical Society **420**, 2318–2324 (2012).

[146] M. R. Lovell, C. S. Frenk, V. R. Eke, A. Jenkins, L. Gao, and T. Theuns, *The properties of warm dark matter haloes,* Mon. Not. Roy. Astron. Soc. **439**, 300–317 (2014).

[147] R. Kennedy, C. Frenk, S. Cole, and A. Benson, *Constraining the warm dark matter particle mass with Milky Way satellites,* Mon. Not. Roy. Astron. Soc. **442**, 2487–2495 (2014).

[148] F. Villaescusa-Navarro and N. Dalal, *Cores and Cusps in Warm Dark Matter Halos,* JCAP **03**, 024 (2011).

[149] V. Irˇ sič *et al.*, *New Constraints on the free-streaming of warm dark matter from intermediate and small scale Lyman-α forest data,* Phys. Rev. D **96**, 023522 (2017).

[150] M. Viel, G. D. Becker, J. S. Bolton, M. G. Haehnelt, M. Rauch, and W. L. Sargent, *How cold is cold dark matter? Small scales constraints from the flux*

power spectrum of the high-redshift Lyman-alpha forest, Phys. Rev. Lett. **100**, 041304 (2008).

[151] A. Schneider, D. Anderhalden, A. Maccio, and J. Diemand, *Warm dark matter does not do better than cold dark matter in solving small-scale inconsistencies,* Mon. Not. Roy. Astron. Soc. **441**, 6 (2014).

[152] J. Primack, *Cosmology: small scale issues revisited,* New J. Phys. **11**, 105029 (2009).

[153] M.-Y. Wang, A. H. G. Peter, L. E. Strigari, A. R. Zentner, B. Arant, S. Garrison-Kimmel, and M. Rocha, *Cosmological simulations of decaying dark matter: implications for small-scale structure of dark matter haloes,* Mon. Not. Roy. Astron. Soc. **445**, 614–629 (2014).

[154] K. J. Bae, A. Kamada, and H. J. Kim, *Decaying axinolike dark matter: Discriminative solution to small-scale issues,* Phys. Rev. D **99**, 023511 (2019).

[155] K. Choi, K.-Y. Choi, and C. S. Shin, *Dark radiation and small-scale structure problems with decaying particles,* Phys. Rev. D **86**, 083529 (2012).

[156] D. N. Spergel and P. J. Steinhardt, *Observational evidence for self interacting cold dark matter,* Phys. Rev. Lett. **84**, 3760–3763 (2000).

[157] R. Barkana, *Possible interaction between baryons and dark-matter particles revealed by the first stars,* Nature **555**, 71–74 (2018).

[158] R. Barkana, N. J. Outmezguine, D. Redigolo, and T. Volansky, *Strong constraints on light dark matter interpretation of the EDGES signal,* Phys. Rev. D **98**, 103005 (2018).

[159] R. Barkana, N. J. Outmezguine, D. Redigolo, and T. Volansky, *Strong constraints on light dark matter interpretation of the EDGES signal,* Phys. Rev. **D98**, 103005 (2018).

[160] G. B. Field, *Excitation of the hydrogen 21-cm line,* Proceedings of the IRE **46**, 240–250 (1958).

[161] S. A. Wouthuysen, *On the excitation mechanism of the 21-cm (radio-frequency) interstellar hydrogen emission line.* The Astronomical Journal **57**, 31 (1952).

[162] J. D. Bowman, A. E. E. Rogers, R. A. Monsalve, T. J. Mozdzen, and N. Mahesh, *An absorption profile centred at 78 megahertz in the sky-averaged spectrum,* Nature **555**, 67–70 (2018).

[163] P. Sikivie, *Axion dark matter and the 21-cm signal,* Physics of the Dark Universe **24**, 100289 (2019).

[164] A. Ewall-Wice, T.-C. Chang, J. Lazio, O. Dore, M. Seiffert, and R. Monsalve, *Modeling the Radio Background from the First Black Holes at Cosmic Dawn: Implications for the 21 cm Absorption Amplitude,* Astrophys. J. **868**, 63 (2018).

[165] S. Fraser *et al.*, *The EDGES 21 cm Anomaly and Properties of Dark Matter,* Phys. Lett. B **785**, 159–164 (2018).

[166] Y. Yang, *Contributions of dark matter annihilation to the global 21 cm spectrum observed by the EDGES experiment,* Phys. Rev. D **98**, 103503 (2018).

[167] T. Moroi, K. Nakayama, and Y. Tang, *Axion-photon conversion and effects on 21 cm observation,* Phys. Lett. B **783**, 301–305 (2018).

[168] G. Lambiase and S. Mohanty, *The 21-cm axion,* (2018).

[169] N. Houston, C. Li, T. Li, Q. Yang, and X. Zhang, *Natural Explanation for 21 cm Absorption Signals via Axion-Induced Cooling,* Phys. Rev. Lett. **121**, 111301 (2018).

[170] A. Auriol, S. Davidson, and G. Raffelt, *Axion absorption and the spin temperature of primordial hydrogen,* Phys. Rev. D **99**, 023013 (2019).

[171] J. C. Hill and E. J. Baxter, *Can Early Dark Energy Explain EDGES?* JCAP **08**, 037 (2018).

[172] L. Landau and E. Lifshitz, *Fluid Mechanics: Volume 6*, v. 6 (Elsevier Science, 1987).

[173] C. Eckart, *The thermodynamics of irreversible processes. iii. relativistic theory of the simple fluid,* Phys. Rev. **58**, 919–924 (1940).

[174] A. Muronga, *Causal theories of dissipative relativistic fluid dynamics for nuclear collisions,* Phys. Rev. C **69**, 034903 (2004).

[175] P. Romatschke, *New Developments in Relativistic Viscous Hydrodynamics,* Int. J. Mod. Phys. E **19**, 1–53 (2010).

[176] E. Andrej, *Investigation of Transition Between Kinetic Theory and Dissipative Hydrodynamic Formalisms,* Ph.D. thesis, Frankfurt U. (2011).

[177] D. H. Rischke, *Fluid dynamics for relativistic nuclear collisions,* Lect. Notes Phys. **516**, 21 (1999).

[178] J. C. Maxwell, *IV. on the dynamical theory of gases,* Proc. R. Soc. Lond. .

[179] W. Israel and J. Stewart, *Transient relativistic thermodynamics and kinetic theory,* Annals Phys. **118**, 341–372 (1979).

[180] S. Gavin, *Transport coefficients in ultra-relativistic heavy-ion collisions,* Nuclear Physics A **435**, 826 – 843 (1985).

[181] P. Chakraborty and J. Kapusta, *Quasi-Particle Theory of Shear and Bulk Viscosities of Hadronic Matter,* Phys. Rev. C **83**, 014906 (2011).

[182] G. P. Kadam and H. Mishra, *Dissipative properties of hot and dense hadronic matter in an excluded-volume hadron resonance gas model,* Phys. Rev. **C92**, 035203 (2015).

[183] T. Padmanabhan and S. M. Chitre, *Viscous universes,* Phys. Lett. **A120**, 433–436 (1987).

[184] O. Gron, *Viscous inflationary universe models,* Astrophys. Space Sci. **173**, 191–225 (1990).

[185] B. Cheng, *Bulk viscosity in the early universe,* Phys. Lett. **A160**, 329–338 (1991).

[186] W. Zimdahl, *Bulk viscous cosmology,* Phys. Rev. **D53**, 5483–5493 (1996).

[187] M. Szydlowski and A. Krawiec, *Interpretation of bulk viscosity as the generalized Chaplygin gas,* (2020).

[188] S. Anand, P. Chaubal, A. Mazumdar, and S. Mohanty, *Cosmic viscosity as a remedy for tension between PLANCK and LSS data,* JCAP **1711**, 005 (2017).

[189] H. Velten, D. J. Schwarz, J. C. Fabris, and W. Zimdahl, *Viscous dark matter growth in (neo-)Newtonian cosmology,* Phys. Rev. **D88**, 103522 (2013).

[190] H. Velten, T. R. P. Caramłs, J. C. Fabris, L. Casarini, and R. C. Batista, *Structure formation in a* Λ *viscous CDM universe,* Phys. Rev. **D90**, 123526 (2014).

[191] G. Goswami, G. K. Chakravarty, S. Mohanty, and A. R. Prasanna, *Constraints on cosmological viscosity and self interacting dark matter from gravitational wave observations,* Phys. Rev. **D95**, 103509 (2017).

[192] B.-Q. Lu, D. Huang, Y.-L. Wu, and Y.-F. Zhou, *Damping of gravitational waves in a viscous Universe and its implication for dark matter self-interactions,* (2018).

[193] I. Brevik and S. Nojiri, *Gravitational Waves in the Presence of Viscosity,* Int. J. Mod. Phys. **D28**, 1950133 (2019).

[194] A. Sasidharan and T. K. Mathew, *Bulk viscous matter and recent acceleration of the Universe,* Eur. Phys. J. C **75**, 348 (2015).

[195] R.-G. Cai, T.-B. Liu, and S.-J. Wang, *Gravitational wave as probe of superfluid dark matter,* Phys. Rev. **D97**, 023027 (2018).

[196] S. Anand, P. Chaubal, A. Mazumdar, S. Mohanty, and P. Parashari, *Bounds on Neutrino Mass in Viscous Cosmology,* JCAP **1805**, 031 (2018).

[197] S. B. Medina, M. Nowakowski, and D. Batic, *Viscous Cosmologies,* (2019).

[198] W. Yang, S. Pan, E. Di Valentino, A. Paliathanasis, and J. Lu, *Challenging bulk viscous unified scenarios with cosmological observations,* (2019).

[199] J. R. Bhatt, P. K. Natwariya, and A. K. Pandey, *Viscosity in cosmic fluids,* (2019).

[200] I. Brevik, . Grn, J. de Haro, S. D. Odintsov, and E. N. Saridakis, *Viscous Cosmology for Early- and Late-Time Universe,* Int. J. Mod. Phys. **D26**, 1730024 (2017).

[201] D. Baumann, A. Nicolis, L. Senatore, and M. Zaldarriaga, *Cosmological Non-Linearities as an Effective Fluid,* JCAP **07**, 051 (2012).

[202] S. Floerchinger, M. Garny, N. Tetradis, and U. A. Wiedemann, *Effective description of dark matter as a viscous fluid,* EPJ Web Conf. **125**, 03018 (2016).

[203] D. Blas, S. Floerchinger, M. Garny, N. Tetradis, and U. A. Wiedemann, *Viscous dark matter,* in "14th Marcel Grossmann Meeting on Recent Developments in Theoretical and Experimental General Relativity, Astrophysics, and Relativistic Field Theories," (2017).

[204] C. C. Chapman S., Cowling T.G., *The Mathematical Theory of Non-uniform Gases: An Account of the Kinetic Theory of Viscosity, Thermal Conduction and Diffusion in Gases*, Cambridge Mathematical Library (Cambridge University Press, 1970), 3rd ed.

[205] K. Kleidis and N. K. Spyrou, *A conventional approach to the dark-energy concept,* Astron. Astrophys. **529**, A26 (2011).

[206] K. Kleidis and N. K. Spyrou, *Polytropic dark matter flows illuminate dark energy and accelerated expansion,* Astron. Astrophys. **576**, A23 (2015).

[207] A. Atreya, J. R. Bhatt, and A. Mishra, *Viscous Self Interacting Dark Matter and Cosmic Acceleration,* JCAP **1802**, 024 (2018).

[208] R. Dave, D. N. Spergel, P. J. Steinhardt, and B. D. Wandelt, *Halo properties in cosmological simulations of selfinteracting cold dark matter,* Astrophys. J. **547**, 574–589 (2001).

[209] C. Firmani, E. D'Onghia, V. Avila-Reese, G. Chincarini, and X. Hernandez, *Evidence of self-interacting cold dark matter from galactic to galaxy cluster scales,* Mon. Not. Roy. Astron. Soc. **315**, L29 (2000).

[210] A. Burkert, *Self-interacting cold dark matter halos,* (2000).

[211] A. Burkert, *The Structure and evolution of weakly selfinteracting cold dark matter halos,* Astrophys. J. Lett. **534**, L143–L146 (2000).

[212] N. Yoshida, V. Springel, S. D. White, and G. Tormen, *Weakly self-interacting dark matter and the structure of dark halos,* Astrophys. J. Lett. **544**, L87–L90 (2000).

[213] N. Yoshida, V. Springel, S. D. White, and G. Tormen, *Collisional dark matter and the structure of dark halos,* Astrophys. J. Lett. **535**, L103 (2000).

[214] J. Koda and P. R. Shapiro, *Gravothermal collapse of isolated self-interacting dark matter haloes: N-body simulation versus the fluid model,* Monthly Notices of the Royal Astronomical Society **415**, 1125–1137 (2011).

[215] B. Moore, S. Gelato, A. Jenkins, F. Pearce, and V. Quilis, *Collisional versus collisionless dark matter,* Astrophys. J. Lett. **535**, L21–L24 (2000).

[216] S. Balberg, S. L. Shapiro, and S. Inagaki, *Selfinteracting dark matter halos and the gravothermal catastrophe,* Astrophys. J. **568**, 475–487 (2002).

[217] J. Zavala, M. R. Lovell, M. Vogelsberger, and J. D. Burger, *Diverse dark matter density at sub-kiloparsec scales in milky way satellites: Implications for the nature of dark matter,* Physical Review D **100**, 063007 (2019).

[218] O. D. Elbert, J. S. Bullock, S. Garrison-Kimmel, M. Rocha, J. Oorbe, and A. H. Peter, *Core formation in dwarf haloes with self-interacting dark matter: no fine-tuning necessary,* Mon. Not. Roy. Astron. Soc. **453**, 29–37 (2015).

[219] M. Vogelsberger, J. Zavala, and A. Loeb, *Subhaloes in self-interacting galactic dark matter haloes,* Monthly Notices of the Royal Astronomical Society **423**, 3740–3752 (2012).

[220] A. Kamada, M. Kaplinghat, A. B. Pace, and H.-B. Yu, *How the Self-Interacting Dark Matter Model Explains the Diverse Galactic Rotation Curves,* Phys. Rev. Lett. **119**, 111102 (2017).

[221] G. Despali, M. Sparre, S. Vegetti, M. Vogelsberger, J. Zavala, and F. Marinacci, *The interplay of Self-Interacting Dark Matter and baryons in shaping the halo evolution,* Mon. Not. Roy. Astron. Soc. **484**, 4563 (2019).

[222] M. Kaplinghat, R. E. Keeley, T. Linden, and H.-B. Yu, *Tying Dark Matter to Baryons with Self-interactions,* Phys. Rev. Lett. **113**, 021302 (2014).

[223] M. Vogelsberger, J. Zavala, C. Simpson, and A. Jenkins, *Dwarf galaxies in CDM and SIDM with baryons: observational probes of the nature of dark matter,* Mon. Not. Roy. Astron. Soc. **444**, 3684–3698 (2014).

[224] O. D. Elbert, J. S. Bullock, M. Kaplinghat, S. Garrison-Kimmel, A. S. Graus, and M. Rocha, *A testable conspiracy: simulating baryonic effects on self-interacting dark matter halos,* The Astrophysical Journal **853**, 109 (2018).

[225] V. H. Robles, J. S. Bullock, O. D. Elbert, A. Fitts, A. González-Samaniego, M. Boylan-Kolchin, P. F. Hopkins, C.-A. Faucher-Giguère, D. Kereš, and C. C. Hayward, *Sidm on fire: Hydrodynamical self-interacting dark matter simulations of low-mass dwarf galaxies,* Monthly Notices of the Royal Astronomical Society **472**, 2945–2954 (2017).

[226] A. Robertson, D. Harvey, R. Massey, V. Eke, I. G. McCarthy, M. Jauzac, B. Li, and J. Schaye, *Observable tests of self-interacting dark matter in galaxy clusters: cosmological simulations with SIDM and baryons,* Mon. Not. Roy. Astron. Soc. **488**, 3646–3662 (2019).

[227] S. W. Randall, M. Markevitch, D. Clowe, A. H. Gonzalez, and M. Bradac, *Constraints on the Self-Interaction Cross-Section of Dark Matter from Numerical Simulations of the Merging Galaxy Cluster 1E 0657-56,* Astrophys. J. **679**, 1173–1180 (2008).

[228] F. Kahlhoefer, K. Schmidt-Hoberg, M. T. Frandsen, and S. Sarkar, *Colliding clusters and dark matter self-interactions,* Mon. Not. Roy. Astron. Soc. **437**, 2865–2881 (2014).

[229] D. Harvey, R. Massey, T. Kitching, A. Taylor, and E. Tittley, *The nongravitational interactions of dark matter in colliding galaxy clusters,* Science **347**, 1462–1465 (2015).

[230] A. Robertson, R. Massey, and V. Eke, *What does the Bullet Cluster tell us about self-interacting dark matter?* Mon. Not. Roy. Astron. Soc. **465**, 569–587 (2017).

[231] C. Firmani, E. D'Onghia, G. Chincarini, X. Hernandez, and V. Avila-Reese, *Constraints on dark matter physics from dwarf galaxies through galaxy cluster haloes,* Mon. Not. Roy. Astron. Soc. **321**, 713 (2001).

[232] K.-J. Ahn and P. R. Shapiro, *Formation and evolution of the self-interacting dark matter halos,* Mon. Not. Roy. Astron. Soc. **363**, 1092–1124 (2005).

[233] M. Rocha, A. H. G. Peter, J. S. Bullock, M. Kaplinghat, S. Garrison-Kimmel, J. Onorbe, and L. A. Moustakas, *Cosmological Simulations with Self-Interacting Dark Matter I: Constant Density Cores and Substructure,* Mon. Not. Roy. Astron. Soc. **430**, 81–104 (2013).

[234] A. H. G. Peter, M. Rocha, J. S. Bullock, and M. Kaplinghat, *Cosmological Simulations with Self-Interacting Dark Matter II: Halo Shapes vs. Observations,* Mon. Not. Roy. Astron. Soc. **430**, 105 (2013).

[235] M. Meneghetti, N. Yoshida, M. Bartelmann, L. Moscardini, V. Springel, G. Tormen, and S. D. White, *Giant cluster arcs as a constraint on the scattering cross-section of dark matter,* Mon. Not. Roy. Astron. Soc. **325**, 435 (2001).

[236] M. Meneghetti, M. Bartelmann, H. Dahle, and M. Limousin, *Arc Statistics,* Space Sci. Rev. **177**, 31–74 (2013).

[237] J. Miralda-Escude, *A test of the collisional dark matter hypothesis from cluster lensing,* Astrophys. J. **564**, 60 (2002).

[238] M. Bento, O. Bertolami, R. Rosenfeld, and L. Teodoro, *Selfinteracting dark matter and invisibly decaying Higgs,* Phys. Rev. D **62**, 041302 (2000).

[239] J. McDonald, *Thermally generated gauge singlet scalars as self-interacting dark matter,* Physical Review Letters **88** (2002).

[240] J. L. Feng, M. Kaplinghat, and H.-B. Yu, *Halo Shape and Relic Density Exclusions of Sommerfeld-Enhanced Dark Matter Explanations of Cosmic Ray Excesses,* Phys. Rev. Lett. **104**, 151301 (2010).

[241] T. Lin, H.-B. Yu, and K. M. Zurek, *On Symmetric and Asymmetric Light Dark Matter,* Phys. Rev. D **85**, 063503 (2012).

[242] S. Tulin, H.-B. Yu, and K. M. Zurek, *Beyond Collisionless Dark Matter: Particle Physics Dynamics for Dark Matter Halo Structure,* Phys. Rev. **D87**, 115007 (2013).

[243] T. Hambye and L. Vanderheyden, *Minimal self-interacting dark matter models with light mediator,* JCAP **05**, 001 (2020).

[244] S. Tulin, H.-B. Yu, and K. M. Zurek, *Resonant Dark Forces and Small Scale Structure,* Phys. Rev. Lett. **110**, 111301 (2013).

[245] G. D. Kribs and E. T. Neil, *Review of strongly-coupled composite dark matter models and lattice simulations,* Int. J. Mod. Phys. A **31**, 1643004 (2016).

[246] J. M. Cline, Z. Liu, G. Moore, and W. Xue, *Scattering properties of dark atoms and molecules,* Phys. Rev. D **89**, 043514 (2014).

[247] K. K. Boddy, M. Kaplinghat, A. Kwa, and A. H. G. Peter, *Hidden Sector Hydrogen as Dark Matter: Small-scale Structure Formation Predictions and the Importance of Hyperfine Interactions,* Phys. Rev. D **94**, 123017 (2016).

[248] M. Weber and W. de Boer, *Determination of the local dark matter density in our galaxy,* Astronomy and Astrophysics **509**, A25 (2010).

[249] S.-H. Oh, W. J. G. de Blok, E. Brinks, F. Walter, and R. C. Kennicutt, *DARK AND LUMINOUS MATTER IN THINGS DWARF GALAXIES,* The Astronomical Journal **141**, 193 (2011).

[250] A. B. Newman, T. Treu, R. S. Ellis, D. J. Sand, C. Nipoti, J. Richard, and E. Jullo, *The Density Profiles of Massive, Relaxed Galaxy Clusters: I. The Total Density Over 3 Decades in Radius,* Astrophys. J. **765**, 24 (2013).

[251] A. B. Newman, T. Treu, R. S. Ellis, and D. J. Sand, *The Density Profiles of Massive, Relaxed Galaxy Clusters: II. Separating Luminous and Dark Matter in Cluster Cores,* Astrophys. J. **765**, 25 (2013).

[252] J. Pollack, D. N. Spergel, and P. J. Steinhardt, *Supermassive Black Holes from Ultra-Strongly Self-Interacting Dark Matter,* Astrophys. J. **804**, 131 (2015).

[253] A. Atreya, J. R. Bhatt, and A. K. Mishra, *Viscous Self Interacting Dark Matter Cosmology For Small Redshift,* JCAP **1902**, 045 (2019).

[254] M. Vogelsberger and J. Zavala, *Direct detection of self-interacting dark matter,* Monthly Notices of the Royal Astronomical Society **430**, 1722–1735 (2013).

[255] A. B. Newman, T. Treu, R. S. Ellis, D. J. Sand, C. Nipoti, J. Richard, and E. Jullo, *THE DENSITY PROFILES OF MASSIVE, RELAXED GALAXY CLUSTERS. i. THE TOTAL DENSITY OVER THREE DECADES IN RADIUS,* The Astrophysical Journal **765**, 24 (2013).

[256] A. B. Newman, T. Treu, R. S. Ellis, and D. J. Sand, *THE DENSITY PROFILES OF MASSIVE, RELAXED GALAXY CLUSTERS. II. SEPARATING LUMINOUS AND DARK MATTER IN CLUSTER CORES,* The Astrophysical Journal **765**, 25 (2013).

[257] R. Maartens, *Is the Universe homogeneous?* Phil. Trans. Roy. Soc. Lond. A **369**, 5115–5137 (2011).

[258] A. Paranjape, *The Averaging Problem in Cosmology,* Ph.D. thesis, TIFR, Mumbai, Dept. Astron. Astrophys. (2009).

[259] D. J. Schwarz, *Cosmological backreaction,* in "12th Marcel Grossmann Meeting on General Relativity," (2010), pp. 563–577.

[260] T. Singh, *The effect of cosmic inhomogeneities on the average cosmological dynamics,* in "Proceedings of the International Conference on Two Cosmological Models," (Plaza y Valdes, 2011), p. 259.

[261] C. Clarkson, G. Ellis, J. Larena, and O. Umeh, *Does the growth of structure affect our dynamical models of the universe? The averaging, backreaction and fitting problems in cosmology,* Rept. Prog. Phys. **74**, 112901 (2011).

[262] T. Buchert and S. Rsnen, *Backreaction in late-time cosmology,* Ann. Rev. Nucl. Part. Sci. **62**, 57–79 (2012).

[263] T. Buchert, P. Mourier, and X. Roy, *On average properties of inhomogeneous fluids in general relativity III: general fluid cosmologies,* Gen. Rel. Grav. **52**, 27 (2020).

[264] T. Buchert *et al.*, *Is there proof that backreaction of inhomogeneities is irrelevant in cosmology?* Class. Quant. Grav. **32**, 215021 (2015).

[265] S. R. Green and R. M. Wald, *Comments on Backreaction,* (2015).

[266] S. R. Green and R. M. Wald, *A simple, heuristic derivation of our 'no backreaction' results,* Class. Quant. Grav. **33**, 125027 (2016).

[267] K. Bolejko and M. a. Korzyński, *Inhomogeneous cosmology and backreaction: Current status and future prospects,* **1**, 602–621 (2017).

[268] P. A. R. Ade *et al.*, *Planck 2013 results. XVI. Cosmological parameters,* Astron. Astrophys. **571**, A16 (2014).

[269] D. Jeong, J.-O. Gong, H. Noh, and J.-c. Hwang, *General relativistic effects on non-linear power spectra,* Astrophys. J. **727**, 22 (2011).

[270] O. Farooq, F. R. Madiyar, S. Crandall, and B. Ratra, *Hubble Parameter Measurement Constraints on the Redshift of the Decelerationacceleration Transition, Dynamical Dark Energy, and Space Curvature,* Astrophys. J. **835**, 26 (2017).

[271] R. Amanullah *et al.*, *Spectra and Light Curves of Six Type Ia Supernovae at 0.511 ¡ z ¡ 1.12 and the Union2 Compilation,* Astrophys. J. **716**, 712–738 (2010).

[272] N. Suzuki *et al.*, *The Hubble Space Telescope Cluster Supernova Survey: V. Improving the Dark Energy Constraints Above z¿1 and Building an Early-Type-Hosted Supernova Sample,* Astrophys. J. **746**, 85 (2012).

[273] S. Weinberg, *Entropy generation and the survival of protogalaxies in an expanding universe,* Astrophys. J. **168**, 175 (1971).

[274] J. R. Bhatt, A. K. Mishra, and A. C. Nayak, *Viscous dark matter and 21 cm cosmology,* Phys. Rev. D **100**, 063539 (2019).

[275] E. Carretta, R. G. Gratton, G. Clementini, and F. Fusi Pecci, *Distances, ages and epoch of formation of globular clusters,* Astrophys. J. **533**, 215–235 (2000).

[276] T. D. Cohen, *Is there a most perfect fluid consistent with quantum field theory?* Physical Review Letters **99** (2007).

[277] M. Lublinsky and E. Shuryak, *How much entropy is produced in strongly coupled Quark-Gluon Plasma (sQGP) by dissipative effects?* Phys. Rev. C **76**, 021901 (2007).

[278] P. Romatschke and U. Romatschke, *Viscosity Information from Relativistic Nuclear Collisions: How Perfect is the Fluid Observed at RHIC?* Phys. Rev. Lett. **99**, 172301 (2007).

[279] S. Dutta and R. Biswas, *Violation of Universal Lower Bound for the Shear Viscosity to Entropy Density Ratio in Dark Energy Dominated Accretion,* Eur. Phys. J. **C79**, 545 (2019).

[280] A. Dobado, F. J. Llanes-Estrada, and J. M. T. Rincon, *The Status of the KSS bound and its possible violations: How perfect can a fluid be?* AIP Conf. Proc. **1031**, 221–231 (2008).

[281] G. Rupak and T. Schäfer, *Shear viscosity of a superfluid Fermi gas in the unitarity limit,* Phys. Rev. A **76**, 053607 (2007).

[282] H. Song, S. A. Bass, U. Heinz, T. Hirano, and C. Shen, *200 A GeV Au+Au collisions serve a nearly perfect quark-gluon liquid,* Phys. Rev. Lett. **106**, 192301 (2011). [Erratum: Phys.Rev.Lett. 109, 139904 (2012)].

[283] M. Rogatko and K. I. Wysokinski, *Viscosity bound for anisotropic superfluids with dark matter sector,* Phys. Rev. D **96**, 026015 (2017).

[284] T. Lin, *Dark matter models and direct detection,* PoS **333**, 009 (2019).

[285] V. Sahni, T. D. Saini, A. A. Starobinsky, and U. Alam, *Statefinder: A New geometrical diagnostic of dark energy,* JETP Lett. **77**, 201–206 (2003). [Pisma Zh. Eksp. Teor. Fiz.77,249(2003)].

[286] A. K. Mishra, *Lightening the Dark Matter from its Viscosity and Explanation of EDGES Anomaly,* JCAP **05**, 034 (2020).

[287] C. Armendariz-Picon and J. T. Neelakanta, *How Cold is Cold Dark Matter?* JCAP **03**, 049 (2014).

[288] W.-H. Huang, *Anisotropic cosmological models with energy density dependent bulk viscosity,* J. Math. Phys. **31**, 1456–1462 (1990).

[289] G. L. Murphy, *Big-bang model without singularities,* Phys. Rev. **D8**, 4231–4233 (1973).

[290] J. R. Wilson, G. J. Mathews, and G. M. Fuller, *Bulk Viscosity, Decaying Dark Matter, and the Cosmic Acceleration,* Phys. Rev. **D75**, 043521 (2007).

[291] R. Foot and S. Vagnozzi, *Dissipative hidden sector dark matter,* Phys. Rev. **D91**, 023512 (2015).

[292] R. Foot and S. Vagnozzi, *Diurnal modulation signal from dissipative hidden sector dark matter,* Phys. Lett. **B748**, 61–66 (2015).

[293] R. Foot and S. Vagnozzi, *Solving the small-scale structure puzzles with dissipative dark matter,* JCAP **1607**, 013 (2016).

[294] Z. Hou, R. Keisler, L. Knox, M. Millea, and C. Reichardt, *How Massless Neutrinos Affect the Cosmic Microwave Background Damping Tail,* Phys. Rev. **D87**, 083008 (2013).

[295] M. Archidiacono, E. Giusarma, S. Hannestad, and O. Mena, *Cosmic dark radiation and neutrinos,* Adv. High Energy Phys. **2013**, 191047 (2013).

[296] T.-K. Kuo and J. T. Pantaleone, *Neutrino Oscillations in Matter,* Rev. Mod. Phys. **61**, 937 (1989).

[297] A. Mirizzi, J. Redondo, and G. Sigl, *Microwave Background Constraints on Mixing of Photons with Hidden Photons,* JCAP **03**, 026 (2009).

[298] K. E. Kunze and M. . Vzquez-Mozo, *Constraints on hidden photons from current and future observations of CMB spectral distortions,* JCAP **12**, 028 (2015).

[299] S. Seager, D. D. Sasselov, and D. Scott, *How exactly did the universe become neutral?* Astrophys. J. Suppl. **128**, 407–430 (2000).

[300] A. Lewis, A. Challinor, and A. Lasenby, *Efficient computation of CMB anisotropies in closed FRW models,* Astrophys. J. **538**, 473–476 (2000).

[301] J. Chluba, *Green's function of the cosmological thermalization problem – II. Effect of photon injection and constraints,* Mon. Not. Roy. Astron. Soc. **454**, 4182–4196 (2015).

[302] H. Tashiro, K. Kadota, and J. Silk, *Effects of dark matter-baryon scattering on redshifted 21 cm signals,* Phys. Rev. D **90**, 083522 (2014).

[303] J. B. Muoz, E. D. Kovetz, and Y. Ali-Hamoud, *Heating of Baryons due to Scattering with Dark Matter During the Dark Ages,* Phys. Rev. D **92**, 083528 (2015).

[304] J. B. Muoz and A. Loeb, *A small amount of mini-charged dark matter could cool the baryons in the early Universe,* Nature **557**, 684 (2018).

[305] E. Aprile *et al.*, *First Dark Matter Search Results from the XENON1T Experiment,* Phys. Rev. Lett. **119**, 181301 (2017).

[306] C. F. P. da Silva, *Dark Matter Searches with LUX,* in "Proceedings, 52nd Rencontres de Moriond on Very High Energy Phenomena in the Universe: La Thuile, Italy, March 18-25, 2017," (2017), pp. 199–209.

[307] H. Liu and T. R. Slatyer, *Implications of a 21-cm signal for dark matter annihilation and decay,* Phys. Rev. **D98**, 023501 (2018).

[308] G. D'Amico, P. Panci, and A. Strumia, *Bounds on Dark Matter annihilations from 21 cm data,* Phys. Rev. Lett. **121**, 011103 (2018).

[309] L. Lopez-Honorez, O. Mena, and P. Villanueva-Domingo, *Dark matter microphysics and 21 cm observations,* Phys. Rev. **D99**, 023522 (2019).

[310] E. D. Kovetz, I. Cholis, and D. E. Kaplan, *Bounds on ultralight hidden-photon dark matter from observation of the 21 cm signal at cosmic dawn,* Phys. Rev. D **99**, 123511 (2019).

[311] J. R. Bhatt, P. K. Natwariya, A. C. Nayak, and A. K. Pandey, *Baryon-Dark matter interaction in presence of magnetic fields in light of EDGES signal,* (2019).

[312] T. Minoda, H. Tashiro, and T. Takahashi, *Insight into primordial magnetic fields from 21-cm line observation with edges experiment,* Monthly Notices of the Royal Astronomical Society **488**, 20012005 (2019).

[313] P. K. Natwariya and J. R. Bhatt, *EDGES signal in presence of magnetic fields,* (2020).

[314] A. K. Mishra, *Exploring the Self Interacting Dark Matter Properties From Low Redshift Observations,* (2020).

[315] Y. Ali-Haimoud and C. M. Hirata, *HyRec: A fast and highly accurate primordial hydrogen and helium recombination code,* Phys. Rev. D **83**, 043513 (2011).

[316] S. Seager, D. D. Sasselov, and D. Scott, *A new calculation of the recombination epoch,* Astrophys. J. **523**, L1–L5 (1999).

[317] P. A. R. Ade *et al.*, *Planck 2015 results. XIII. Cosmological parameters,* Astron. Astrophys. **594**, A13 (2016).

[318] D. Tseliakhovich and C. Hirata, *Relative velocity of dark matter and baryonic fluids and the formation of the first structures,* Phys. Rev. D **82**, 083520 (2010).

[319] K. K. Boddy, V. Gluscevic, V. Poulin, E. D. Kovetz, M. Kamionkowski, and R. Barkana, *Critical assessment of CMB limits on dark matter-baryon scattering: New treatment of the relative bulk velocity,* Phys. Rev. D **98**, 123506 (2018).

List of Publications

Thesis related Publications

1. **A. K. Mishra**, *Exploring the Self Interacting Dark Matter Properties From Low Redshift Observations, arXiv:2002.11652 [astro-ph.CO]*
   (In communication with EPJC).

2. ***A. K. Mishra**, Lightening the Dark Matter from its Viscosity and Explanation of EDGES Anomaly, JCAP **05**, 034 (2020), [arXiv:1907.04238 [astro-ph.CO]].*

3. *J. R. Bhatt, **A. K. Mishra** and A. C. Nayak, Viscous dark matter and 21 cm cosmology, Phys. Rev. D **100**, no. 6, 063539 (2019), [arXiv:1901.08451 [astro-ph.CO]].*

4. *A. Atreya, J. R. Bhatt and **A. K. Mishra** Viscous Self Interacting Dark Matter Cosmology For Small Redshift, JCAP **02**, 045 (2019), [arXiv:1810.11666 [astro-ph.CO]].*

5. *A. Atreya, J. R. Bhatt and **A. Mishra**, Viscous Self Interacting Dark Matter and Cosmic Acceleration, JCAP **02**, 024 (2018), [arXiv:1709.02163 [astro-ph.CO]].*

Other publication

(a) ***A.K. Mishra**, J.R. Bhatt and A. Atreya, Late Time Cosmology with Viscous Self Interacting Dark Matter; Springer Proc. Phys. **261**, 299-305 (2021).*

(b) ***A.K. Mishra**, Viscous dark matter and its implication for 21-cm signal, Springer Proc. Phys. **248**, 321-327 (2020).*